European windstorm losses under current and future climate conditions

Zur Erlangung des akademischen Grades eines
DOKTORS DER NATURWISSENSCHAFTEN (Dr. rer. nat.)
von der KIT-Fakultät für Physik des
Karlsruher Instituts für Technologie (KIT)

genehmigte

DISSERTATION

von

M.Sc. Inovasita Alifdini
aus Bengkulu, Indonesien

Tag der mündlichen Prüfung:	14.02.2025
Referent:	Prof. Dr. Joaquim G. Pinto
Korreferent:	Prof. Dr. Andreas H. Fink

Karlsruher Institut für Technologie

“We can’t change the wind, but we can set the sails differently.”
(Aristotle)

Abstract

European windstorms pose a major risk for insurance companies due to their potential for widespread and costly damage. Metrics to quantify these losses range from a simple loss index to complex insurance loss models. Comparing these metrics is crucial for ensuring effective risk assessment and impact forecasting. Furthermore, estimating the losses associated with European windstorms under climate change is challenging due to uncertainties in general circulation model and regional climate model projections, as well as changes at the regional level, such as changes in the structure of population and infrastructure. In addition, the occurrence of multiple storms within a single season is of significant concern to insurers owing to their potential to cause substantial economic losses.

Firstly, windstorm losses are analyzed using the Loss Index (LI) and compared with losses obtained from the European Windstorm Model of Aon Impact Forecasting. To test the sensitivity of LI to different meteorological input data, LI derived from calculations using the ERA5 reanalysis dataset is compared with that derived from its predecessor, ERA-Interim. Focus is given to investigating the similarities and differences between the datasets in terms of loss values and storm rankings for specific storm events within the common reanalysis period across 11 European countries. Findings indicate that ERA5 shows higher LI values compared to ERA-Interim across Europe, attributed to ERA5's higher spatial resolution. Storm rankings are comparable in Western and Central European countries for both reanalyses. While LI from ERA5 ranks storms similarly to Aon's Impact Forecasting model, it struggles to differentiate between extreme windstorms with high losses and those with moderate losses. Despite this limitation, LI remains a simple and effective method for estimating impacts and ranking storm events.

Secondly, this study presents novel insights into the potential impacts of climate change on windstorm losses in Europe using the LI method. A large EURO-CORDEX multi-model ensemble at 12 km resolution with 20 different general circulation model to regional climate model (GCM-RCM) chains following the historical plus RCP8.5 scenario is considered. The use of these datasets allows for an enhanced representation of regional weather conditions, enabling a more precise evaluation of the regional impact of windstorms. A comparison between the simulated historical 10 m wind gusts and ERA5 reanalysis reveals substantial model biases. An empirical quantile mapping method is employed to bias-correct the daily maximum wind gust speeds, leading to the effective reduction of these biases. Considering different global warming levels (GWLs), this study shows an increase in windstorm intensity for Central and Eastern Europe in a warming world and a general decrease of windstorm frequency for large parts

of Europe. While the ensemble mean changes are mostly moderate for a +2°C world, signals are more pronounced for +3°C. The projected changes in windstorm losses are small and mostly non-robust, generally showing negative trends for Central Europe and positive trends for Eastern Europe. For the most extreme loss events, the EURO-CORDEX ensemble projects shorter return periods for Eastern Europe independent of the GWLs, while no clear trends for Central Europe emerge. The results show a large spread between the individual ensemble members, without a clear dominance of a single GCM or RCM. The projected changes in windstorm losses are subtle but important, particularly for Central and Eastern Europe, which should be considered in the mid- and long-term planning of the insurance industry.

Lastly, seasonal loss clustering (the occurrence of multiple windstorm losses in a season) in a warming climate is investigated. Seasonal loss clustering is identified by examining the Occurrence Exceedance Probability (OEP) to Annual Exceedance Probability (AEP) ratio, which reflects the significant role of multiple storms in contributing to the total seasonal loss. ERA5 wind gust data is used to investigate seasonal loss clustering under the current climate condition, while previously bias-corrected EURO-CORDEX data is employed to examine changes in seasonal loss clustering under GWL2 and GWL3 compared to the historical period. Seasonal loss clustering occurs in seasons with an OEP/AEP ratio below the first tercile of the climatology for years characterised by a high (top 25%) AEP value and is more frequent in Central Europe than in Eastern Europe. Central Europe also shows larger AEP and OEP values with shorter return periods compared to Eastern Europe. The impact of climate change on the overall patterns of the OEP/AEP ratio is small, with a large spread in model ensembles, thereby hampering robust conclusions on the possible changes in seasonal loss clustering. For AEP and OEP, the impact of global warming in Central Europe is unclear, while Eastern Europe consistently faces higher risks of severe AEP and OEP for longer return periods under both GWLs.

This study provides novel and innovative contributions towards attaining a thorough comprehension of European windstorm losses in the context of both current and future climate conditions. While the findings are particularly useful for insurance companies to evaluate catastrophe models and ensure premium values are aligned with the risks, this study also potentially provides significant benefits for a wide range of stakeholders. These include policymakers, urban planners, and other professionals working in risk mitigation and climate adaptation, enabling them to better anticipate and address potential changes in windstorm impacts in the future.

Zusammenfassung

Windstürme in Europa stellen ein erhebliches Risiko für Versicherungsunternehmen dar, da sie weitreichende und kostenintensive Schäden verursachen können. Zur Bestimmung dieser Schäden werden verschiedene Methoden genutzt, von einfachen Schadenindizes bis hin zu komplexen Schadensmodellen der Versicherungswirtschaft. Ein Vergleich dieser Methoden ist unerlässlich, um eine effektive Risikobewertung und Vorhersage der Auswirkungen zu gewährleisten. Darüber hinaus gestaltet es sich schwierig, den Einfluss des Klimawandels auf die von Windstürmen verursachten Schäden abzuschätzen. Das liegt zum einen an Unsicherheiten in den Projektionen von globalen und regionalen Klimamodellen, und zum anderen an möglichen Veränderungen in der Bevölkerungs- und Infrastruktur auf der regionalen Skala. Zudem ist das Auftreten mehrerer Stürme innerhalb einer einzigen Saison für Versicherer von großer Bedeutung, da dies zu erheblichen wirtschaftlichen Verlusten führen kann.

In einem ersten Schritt werden Sturmschäden mit Hilfe des sogenannten Loss Index (LI) analysiert und im Anschluss mit Schäden aus dem europäischen Sturmmodell von Aon Impact Forecasting verglichen. Außerdem wird die Sensitivität des LI gegenüber verschiedener meteorologischer Eingabedaten getestet, indem LI aus Reanalysedaten von ERA5 und dem Vorgänger ERA-Interim berechnet und verglichen wird. Der Schwerpunkt liegt auf der Untersuchung der Ähnlichkeiten und Unterschiede zwischen den Datensätzen in Bezug auf Schadenswerte und Sturmranglisten für bestimmte Ereignisse innerhalb des gemeinsamen Reanalysezeitraums in 11 europäischen Ländern. Die Ergebnisse zeigen, dass ERA5 im Vergleich zu ERA-Interim in ganz Europa höhere LI-Werte aufweist, was auf die höhere räumliche Auflösung von ERA5 zurückzuführen ist. Die Rangfolge der Stürme ist in den west- und mitteleuropäischen Ländern für beide Reanalysen vergleichbar. Während LI aus ERA5 die Stürme ähnlich einstuft wie das Impact Forecasting Modell von Aon, zeigen sich gleichzeitig große Schwierigkeiten bei der Unterscheidung zwischen extremen Stürmen mit hohen Schäden und solchen mit moderaten Schäden. Trotz dieser Einschränkung ist LI eine einfache und effektive Methode um die Auswirkungen von Stürmen abzuschätzen und Sturmranglisten zu erstellen.

Im zweiten Teil werden neue Erkenntnisse über die möglichen Auswirkungen des Klimawandels auf die Sturmschäden in Europa unter Verwendung der LI-Methode vorgestellt. Dazu wird ein umfangreiches EURO-CORDEX-Multimodel-Ensemble mit einer räumlichen Auflösung von 12 km und 20 verschiedenen global-regionalen Modellketten (GCM-RCM) herangezogen, basierend auf dem historischen und dem RCP8.5-Szenario. Die Verwendung dieser Datensätze ermöglicht eine verbesserte Darstellung der

regionalen Wetterbedingungen und somit eine genauere Bewertung der Auswirkungen von Stürmen auf der regionalen Skala. Ein Vergleich der 10m Windböen aus den historischen Simulationen mit denen aus ERA5 weist auf erhebliche Modellabweichungen hin. Diese Abweichungen können mithilfe einer Bias-Korrektur reduziert werden. Dazu wird die Empirical Quantile Mapping Methode auf die tägliche maximale Windböengeschwindigkeit angewendet. Für verschiedene globale Erwärmungsniveaus (GWL) zeigen die Ergebnisse eine Zunahme der Sturmintensität für Mittel- und Osteuropa in einer sich erwärmenden Welt und eine allgemeine Abnahme der Sturmhäufigkeit für große Teile Europas. Während die Änderungen im Ensemble- Mittel für eine +2°C-Welt meist moderat ausfallen, sind die Signale für +3°C stärker ausgeprägt. Die projizierten Veränderungen der Sturmschäden sind gering und meist nicht robust, wobei sie im Allgemeinen negative Trends für Mitteleuropa und positive Trends für Osteuropa aufweisen. Für die extremsten Schadensereignisse projiziert das EURO-CORDEX-Ensemble, unabhängig vom GWL, kürzere Wiederkehrperioden für Osteuropa, während für Mitteleuropa keine eindeutigen Trends erkennbar sind. Die Ergebnisse zeigen eine große Streuung zwischen den einzelnen Ensemblemitgliedern, ohne dass ein einzelnes GCM oder RCM eindeutig dominiert. Die projizierten Veränderungen der Sturmschäden sind zwar gering, aber dennoch wichtig, insbesondere für Mittel- und Osteuropa, und sollten bei der mittel- und langfristigen Planung der Versicherungswirtschaft berücksichtigt werden.

Im dritten Teil wird schließlich die saisonale Schadenshäufung (das Auftreten mehrerer Sturmschäden in einer Saison) in einem wärmeren Klima untersucht. Die saisonale Schadenshäufung wird durch die Untersuchung des Verhältnisses von Occurrence Exceedance Probability (OEP) zu Annual Exceedance Probability (AEP) ermittelt, welches die Rolle mehrerer Stürme für den gesamten saisonalen Schaden widerspiegelt. Um die saisonale Schadenshäufung für das derzeitige Klima zu untersuchen, werden ERA5-Windböendaten verwendet, während für Veränderungen in einem zukünftigen Klima die zuvor bias-korrigierte EURO-CORDEX-Daten verwendet werden. Saisonale Schadenshäufungen treten in Jahreszeiten mit einem OEP/AEP-Verhältnis unterhalb des ersten Terzils der Klimatologie für Jahre auf, die durch einen hohen AEP-Wert (obere 25%) gekennzeichnet sind. Diese sind in Mitteleuropa verbreiteter als in Osteuropa. In Mitteleuropa sind zudem größere AEP- und OEP-Werte mit kürzeren Wiederkehrperioden als in Osteuropa zu beobachten. Die Auswirkungen des Klimawandels auf das OEP/AEP-Verhältnis sind gering, da die große Streuung im Modell-Ensemble robuste Schlussfolgerungen zu möglichen Veränderungen in der saisonalen Schadenshäufung erschwert. Die Auswirkung der globalen Erwärmung auf AEP und OEP ist für Mitteleuropa nicht eindeutig, während sich für Osteuropa ein höheres Risiko für hohe AEP und OEP mit längeren Wiederkehrperioden zeigt.

Diese Arbeit liefert einen neuartigen und innovativen Beitrag zu einem umfassenderen Verständnis von Sturmschäden in Europa, sowohl unter aktuellen als auch zukünftigen Klimabedingungen. Die Ergebnisse sind dabei insbesondere für Versicherungsunternehmen wertvoll, um Katastrophenmodelle zu evaluieren und sicherzustellen, dass die Prämienwerte mit den Risiken übereinstimmen. Die Arbeit kann

aber auch weitere Interessengruppen, wie politische Entscheidungsträger, Stadtplaner und Experten im Bereich der Risikominderung und Klimaanpassung, unterstützen dadurch, dass sie mögliche künftige Veränderungen bei den Auswirkungen von Stürmen besser vorhersehen und so entsprechend reagieren können.

Preface

The PhD candidate confirms that the results included in this dissertation make significant scientific contributions by herself. Some materials have been reused from the following publications:

1. Moemken*, J., Alifdini*, I., Ramos, A. M., Georgiadis, A., Brocklehurst, A., Braun, L., and Pinto, J. G. 2024a. Insurance loss model vs. meteorological loss index – how comparable are their loss estimates for European windstorms?, Nat. Hazards Earth Syst. Sci., 24, 3445–3460. https://doi.org/10.5194/nhess-24-3445-2024.
*These authors contributed equally to this work.

The first manuscript was conceptualized and designed by Dr. Julia Moemken, Dr. Alexandre M. Ramos, and Prof. Joaquim G. Pinto. The candidate performed all the data analysis and made the figures with the help of Dr. Alexandros Georgiadis, Dr. Aidan Brocklehurst and Lukas Braun. Dr. Julia Moemken wrote the initial paper draft. All authors discussed the results and contributed with paper revisions. The colleagues from Aon IF provided training to the candidate on running insurance loss model of windstorm in Aon's loss modelling platform (ELEMENTS).

2. Alifdini, I., Moemken, J., Ramos, A. M., and Pinto, J. G. 2025. Future Changes of European Windstorm Losses in EURO-CORDEX Simulations. Tellus A: Dynamic Meteorology and Oceanography, 77(1), 20–37. https://doi.org/10.16993/tellusa.4094.

The second manuscript was conceived and designed by Dr. Julia Moemken and Prof. Joaquim G. Pinto. The candidate performed all the data analyses and made all the figures. All authors discussed the results, wrote parts of the initial paper draft and contributed with manuscript revisions.

In the study of seasonal loss clustering, the candidate conducted all data analysis, with the concept developed together collaboratively with Aleksa Stankovic, Prof. Rodrigo Caballero, Dr. Julia Moemken, Dr. Alexandre M. Ramos, and Prof. Joaquim G. Pinto. Advices and corrections for this disertation were provided by Dr. Julia Moemken, Dr. Alexandre M. Ramos, Prof. Dr. Joaquim G. Pinto, and Prof. Dr.

Andreas H. Fink.

Chapters 1, 2, 3, 4, 5, abstract, and the appendix A reuse the material from Moemken et al. (2024a), with copyright CC BY 4.0. Chapters 1, 2, 3, 4, 6, abstract, and the appendix B reuse the material from Alifdini et al. (2025), with copyright CC BY 4.0.

The research has been funded by the European Union's Horizon 2020 research and innovation programme under the Marie Skłodowska-Curie grant agreement No 956396 (EDIPI). The results from publication (1) were achieved through collaborative efforts with colleagues from Aon Impact Forecasting (Dr. Alexandros Georgiadis, Dr. Aidan Brocklehurst, and Lukas Braun) during the candidate's first international secondment in Aon Impact Forecasting (IF) Prague. Publication (2) results were produced within IMKTRO KIT. The findings regarding seasonal loss clustering of windstorm were developed during the candidate's second international secondment while collaborating with colleagues from the Department of Meteorology at Stockholm University (MISU), specifically Prof. Rodrigo Caballero and Aleksa Stankovic.

We thank the German Climate Computer Centre (DKRZ, in Hamburg) for computer and storage resources. For the first manuscript, we thank Dr. Ting-Chen Chen for preparing the cyclone track data, Dr. Jisesh Sethunadh for discussion on LI calculations, and Federico Stainoh (all IMKTRO KIT) for discussion on statistical analysis methods. For the second manuscript, we thank Hendrik Feldmann (IMKTRO KIT) for discussion about EURO-CORDEX data. The candidate thanks Ines Dillerup (IMKTRO KIT) for reviewing the preliminary version of the German-language thesis abstract and to Dr. Julia Moemken (IMKTRO KIT) for the final reading and corrections.

Contents

1 Introduction **1**

2 Background theory **5**

2.1 European windstorms: Large-scale circulation, formation, tracks, and influencing factors . . . 5

2.2 Wind gust: Driver of windstorm damage . . . 10

2.3 Different methodologies to estimate windstorm losses . . . 13

2.3.1 Meteorological perspective . . . 13

2.3.2 Catastrophe model perspective . . . 15

2.4 Seasonal clustering of windstorm losses . . . 16

2.5 Climate models . . . 18

2.6 Climate variability and change in European windstorms and losses . . . 22

3 Main research questions **27**

4 Data and methods **31**

4.1 Data . . . 31

4.1.1 Reanalysis data . . . 31

4.1.2 Insurance data – PERILS . . . 32

4.1.3 EURO-CORDEX dataset . . . 33

4.2 Methods . . . 34

4.2.1 Loss index . . . 34

4.2.2 Aon Impact Forecasting European Windstorm Model . . . 36

4.2.3 Bias correction of wind gusts . . . 39

4.2.4 Seasonal loss clustering . . . 40

4.2.5 Return value analysis . . . 40

5 Insurance loss model vs meteorological loss index - How comparable are their loss estimates for European windstorms? **43**

5.1 Comparison between ERA5 and ERA-Interim . . . 44

5.1.1 Wind gust climatology . . . 44

5.1.2 Storm losses and storm ranking . . . 45

5.2 Comparison of loss estimates from LI ERA5 and Aon's IF Euro WS model 47
5.2.1 Case study – Storm Sabine 49
5.2.2 Windstorm loss 51
5.2.3 Storm ranking 51
5.3 Summary and discussion 55

6 Future changes of European windstorm losses in EURO-CORDEX simulations 59
6.1 Evaluation of historical simulations 60
6.2 Changes under future climate conditions 62
6.2.1 Changes in windstorm intensity 62
6.2.2 Changes in windstorm frequency 63
6.2.3 Changes in windstorm losses 65
6.2.4 Changes in rare extreme loss events 67
6.3 Summary and discussion 70

7 Seasonal loss clustering in a warming climate 73
7.1 Seasonal loss clustering in the historical period 74
7.1.1 Historical record and relationship analysis 74
7.1.2 Regional variability 78
7.1.3 Characteristics of high AEP season 80
7.2 Seasonal loss clustering under climate change 81
7.3 Summary and discussion 85

8 Discussion and conclusions 89
8.1 Overview and key findings 89
8.1.1 Insurance loss model vs. meteorological loss index 89
8.1.2 Future changes in European windstorm losses 90
8.1.3 Seasonal loss clustering in a warming climate 90
8.2 Discussion 91
8.3 Concluding remarks 95

A Appendix for Chapter 5 97

B Appendix for Chapter 6 105

C Appendix for Chapter 7 115

D Bibliography 117

E List of Figures 135

F List of Tables **145**

1. Introduction

European windstorms are powerful extratropical cyclones that significantly impact Europe. They typically occur during the extended winter months (October-March) (Pinto et al., 2007) and originate over the North Atlantic Ocean, intensifying as they move eastward and reach Europe. Prominent examples, such as the windstorms Anatol and Lothar in December 1999 (Ulbrich et al., 2001), windstorm Kyrill in 2007 (Fink et al., 2009), and windstorms Ciara and Dennis in 2020 (Jardine et al., 2023) illustrate the devastating impact of these natural hazards. For instance, windstorm Kyrill had a significant impact on Central Europe, resulting in insured losses of 6.7 billion USD (Roberts et al., 2014) and considerable damage to infrastructure (Figure 1.1). In 2022, European windstorms reached the highest aggregated insured losses since 2013 with about $5.7 billion, which is above the long-term (2000-2021) averages of $3.2 billion (Aon, 2023).

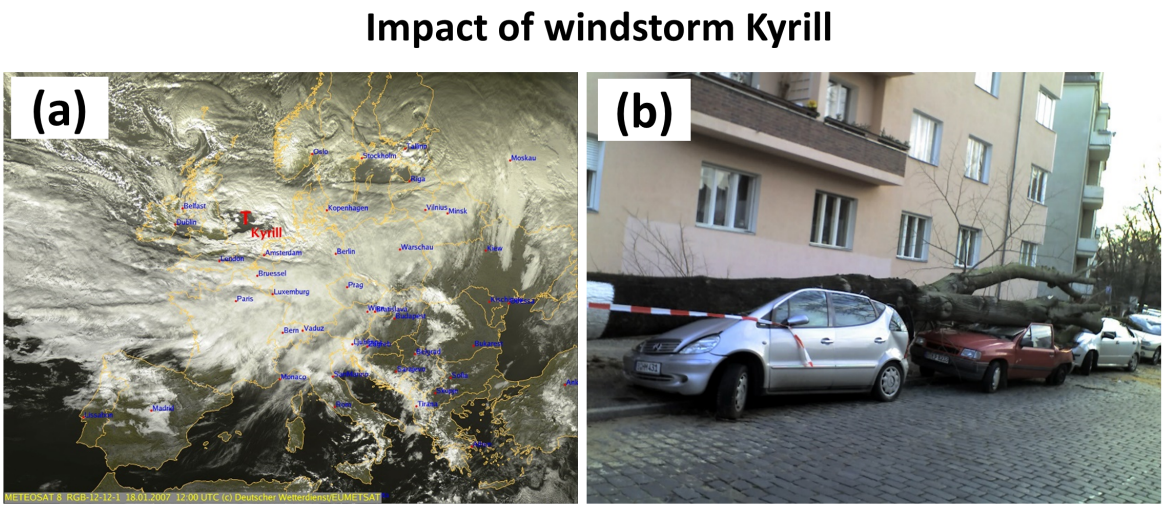

Figure 1.1.: Impacts of windstorm Kyrill in January 2007. (a) The satellite image of windstorm Kyrill from Meteosat-8 RGB at 12 PM on January 18, 2007. (b) Storm Kyrill 2007 damaged cars in Berlin-Lichterfelde after the heavy storm. The figure (a) is reprinted from the press release by Deutscher Wetterdienst (DWD) (2017), with ©Deutscher Wetterdienst/EUMETSAT (used with permission). Figure (b) is reprinted from Krueger-Krusche (2007) under ©CC BY-SA 3.0 Unported.

In general, quantifying windstorm losses or damages involves assessing three components: the windstorm itself (the hazard), the location, attributes, and value of assets (the exposure), and the likelihood of those assets being affected when exposed to the hazard (the vulnerability) (Pörtner et al., 2022). Based on these components, indices and methodologies have been developed to quantify losses caused

by European windstorms on a district or country level. There are various methods to estimate European windstorm loss from different perspectives. For instance, one approach is to estimate windstorm loss from a meteorological perspective, which considers only wind speed and population density data (Klawa and Ulbrich, 2003; Leckebusch et al., 2008; Pinto et al., 2012). In this context, when high-speed windstorms reach densely populated areas, larger losses are typically caused compared to when the same wind speeds affect less densely populated areas. Another approach involves using storm damage functions (Prahl et al., 2016) in catastrophe models, which are typically employed by insurance companies for pricing purposes but are not publicly available. The various methods used to estimate windstorm impacts can result in differing loss values (Moemken et al., 2024b). A recent review paper by Gliksman et al. (2023) highlights the lack of a clearly defined methodology for selecting the most appropriate index to evaluate windstorm losses. Furthermore, the accuracy of loss estimates is influenced by uncertainties in wind speed data (Moemken et al., 2024a), which can vary due to differences in data resolutions.

In recent decades, climate change has become a key concern regarding its influence on the frequency and intensity of European windstorms (e.g., Catto et al. 2019). Understanding these changes is crucial for predicting how windstorms might affect us in the future. To study the influence of climate change on windstorms, climate models are commonly used. These models simulate the complex interactions among the atmosphere, oceans, land surfaces, and other components of the Earth's climate system (Edwards, 2011). However, because these models are based on predictions, uncertainties arise (e.g., Foley 2010, Knutti and Sedláček 2013, Qian et al. 2016). These uncertainties arise from differences in how climate models handle essential components, including spatial resolution, model parameterizations, and the assumptions made in defining boundary conditions. The uncertainty in climate models leads to uncertainty in windstorm projections, making it challenging to accurately predict the impact of climate change on European windstorm losses (e.g., Spinoni et al. 2020).

Regarding the projection of the impact of climate change on European windstorms, the latest IPCC report highlights that there is low agreement on changes in extra-tropical cyclone track density in the North Atlantic by the end of the century. While it is projected that the frequency and intensity of windstorms will increase in Western and Central Europe, the low agreement among models indicates significant uncertainty in these projections (Pörtner et al., 2022). Regarding the projections of windstorm-related impacts in Europe, previous studies have analyzed it in terms of global climate projections (e.g., Leckebusch et al. 2007, Pinto et al. 2007, Schwierz et al. 2010, Donat et al. 2011, Karremann et al. 2014b, Little et al. 2023), but fewer have used regional climate projections (e.g., Bloomfield et al. 2018, Michel and Sorteberg 2023). More recently, Little et al. (2023) provided evidence that windstorm losses in Northern and Central Europe may significantly increase according to CMIP6 general circulation models (GCMs) under the high emission scenario SSP5-8.5 by 2100. However, substantial disparities between individual GCMs and scenarios were identified, highlighting the need for a detailed analysis using multi-model

ensemble of regional climate models (RCMs) at the European scale. The use of RCMs is crucial because they simulate climate at a finer resolution, allowing for a more accurate representation of physical processes at the regional scale (Feser et al., 2011; Iles et al., 2020). This, in turn, provides a better understanding of windstorm characteristics and improves the reliability of projections. For example, the use of regional climate models (RCMs) data, such as in the EURO-CORDEX initiative, which collaboratively generates detailed RCMs for Europe (Giorgi et al., 2009; Vautard et al., 2021), provides valuable insights for conducting comprehensive analyses of windstorm from a regional climate perspective which facilitates a better understanding of regional characteristics and enables investigations into the impact of extreme events (Iles et al., 2020).

In examining the impact of windstorms, it is essential not only to estimate the losses attributed to individual storms but also to explore the seasonal variation of cumulative losses resulting from multiple windstorms occurring within a single season. The North Atlantic winter cyclones tend to occur in groups (Dacre and Pinto, 2020). These groups of cyclones impact Europe and can lead to significant aggregated losses, as the occurrence of multiple cyclones in close succession can cause cumulative damage over a short period. As a result, this can pose challenges for insurance companies, as they may face a higher volume of claims in a short timeframe. This is known as seasonal loss clustering, which refers to the occurrence of multiple European windstorms within a single season, potentially resulting in significant aggregated losses (Priestley et al., 2018). Seasonal loss clustering is important for insurance companies under Solvency II, which is a set of rules that defines the capital and risk management requirements for insurers in the European Union (Parliament, 2009). Under Solvency II, insurers need to assess their ability to cover potential losses, including the combined impact of multiple events in a season, to ensure they have sufficient capital to cover expected seasonal losses. Moreover, under the future climate conditions, it is projected that the intensity of windstorms during clustering periods will increase for Western Europe (Pinto et al., 2013; Priestley et al., 2020; Karwat et al., 2024). Previous studies have investigated the loss caused by windstorm clustering under current climate conditions, focusing on seasonal variation (Priestley et al., 2018), and under future climate conditions, but have not specifically addressed seasonal variations (Karremann et al., 2014a,b). Those previous studies have relied on low-resolution reanalysis data or climate models that may not provide an accurate representation of regional climate conditions. Additionally, those studies have not investigated how losses resulting from seasonal windstorm clustering might vary under different global warming levels (GWLs) when compared to historical periods. Furthermore, the characteristics of seasons with high cumulative losses, particularly in terms of seasonal loss clustering, remain poorly defined.

Based on the research gaps mentioned above, the three key aspects require further investigation: Firstly, there is a need to compare loss estimates of European windstorms from different perspectives to evaluate the existing methods for estimating losses for extreme or rare storms. Secondly, using high-resolution

datasets is crucial for a better understanding of both the current and future impacts of windstorms. Thirdly, it is essential to enhance our understanding of regional differences in the characteristics of seasons associated with high cumulative losses. This understanding is vital for obtaining deeper insights into the degree of seasonal loss clustering that can result in substantial cumulative losses. To address those research gaps, this study primarily uses high-resolution reanalysis data (ERA5) and RCM data (EURO-CORDEX) to improve understanding of windstorm losses in a warming climate. Loss estimates from the meteorological perspective are used throughout the thesis, while the full insurance model of Aon Impact Forecasting is applied to estimate losses from the insurance perspective.

This thesis is organized as follows: Chapter 2 provides an overview of the background theory. Chapter 3 presents the research questions. Chapter 4 outlines the data and methods used. The results are presented across three chapters (Chapter 5 to Chapter 7). Chapter 5 discusses the comparison between loss estimates from a meteorological perspective and insurance loss estimates. Chapter 6 examines changes in windstorm loss under future climate conditions using the EURO-CORDEX dataset. Chapter 7 investigates seasonal loss clustering of windstorms in a warming climate. Finally, Chapter 8 presents the discussion and conclusions of the thesis.

2. Background theory

Intense wintertime European windstorms have caused significant damage and losses over the years, affecting infrastructure, disrupting transportation networks, and posing significant threats to life and property. To comprehensively understand the impact of European windstorms, this chapter examines the underlying theoretical framework. This chapter begins with exploring the fundamental theory underlying the general circulation of winds, leading into the generation of European windstorms. Subsequently, it delves into the mechanisms of wind-induced loss and methods for estimating such losses. An overview of seasonal loss clustering of windstorm is also provided. Additionally, the utilization of climate models to explore the impact of climate change on windstorm loss changes is presented.

2.1. European windstorms: Large-scale circulation, formation, tracks, and influencing factors

To introduce European windstorms, it is essential to first understand the basics of global wind circulation. The global wind circulation on a rotating Earth is driven by temperature differences between the equator and the poles, resulting in distinct high- and low-pressure zones (Figure 2.1; Tarbuck and Lutgens 2013). Near the equator, surface heating creates a low-pressure zone, causing warm air to rise until it reaches the tropopause. This air then moves toward the subtropics, where it cools, becomes denser, and sinks around 20-30° latitude, forming the Hadley cell circulation and creating a high-pressure region in 30° latitude known as the subtropical high. From this high-pressure zone, surface winds split into two branches: the westerlies, which flow poleward over the mid-latitudes, and the northeast trade winds, which flow equatorward. Due to Earth's rotation, the Coriolis effect deflects these winds to the right in the Northern Hemisphere, reinforcing the eastward flow of the westerlies at mid-latitudes.

The wind circulation in the mid-latitudes of the Northern Hemisphere is influenced by temperature and pressure gradients (baroclinicity) between cold polar air masses and warm subtropical air masses (Tarbuck and Lutgens, 2013). As the westerly winds transport air masses from the subtropical regions towards the poles, they encounter the contrasting cold air masses of the polar regions. The collision of these air masses with different temperatures leads to the formation of a low-pressure center, also known as a mid-latitude or extra-tropical cyclone (Bjerknes, 1922; Tarbuck and Lutgens, 2013; Schultz et al., 2019). In the early 20th century, Vilhelm Bjerknes and his son Jacob Bjerknes, Norwegian meteorol-

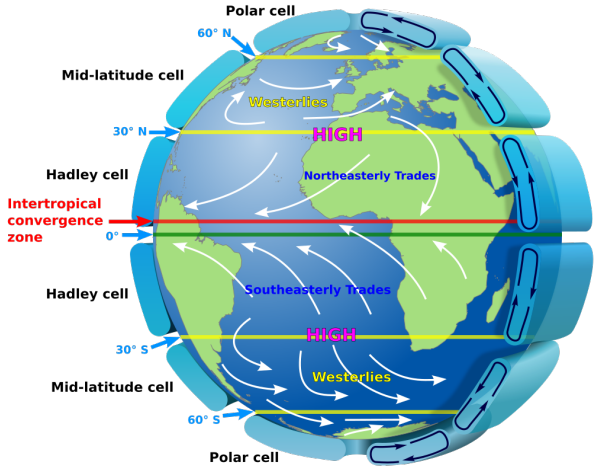

Figure 2.1.: Global wind circulation. The figure is reprinted from Kaidor (2013), via Wikimedia Commons. Copyright ©CC BY-SA 3.0

ogists, formulated the polar front theory, which provided a fundamental framework for comprehending the development and movement of extratropical cyclones. This theory explains how the polar front, a boundary where cold polar air masses meet warm subtropical air masses, acts as the primary zone for the development of extratropical cyclones. When these contrasting air masses collide, the warm, less dense air is forced to rise over the colder, denser air, creating a low-pressure system. This interaction, combined with the Earth's rotation and the Coriolis effect, leads to the development of a rotating weather system. As the cyclone intensifies, it forms warm, cold, occluded, and stationary fronts, which further enhance cyclonic circulation around the low-pressure center. In a low-pressure system, air close to the surface moves inward toward the center where pressure is lowest. As it converges, the Earth's rotation causes the Coriolis effect to deflect these inflowing winds, generating a counterclockwise rotation in the Northern Hemisphere. In low-pressure systems, when a cold air mass moves into a warm air region, friction near the surface slows it down, causing the cold front to become steeper. Because the cold front moves faster and is steeper than the warm front, it leads to more intense weather and heavier precipitation. The extratropical cyclones are more likely to occur in winter because of the strong temperature gradients in the midlatitudes, where cold polar air contrasts sharply with warmer air from lower latitudes. This creates strong westerlies and an enhanced jet stream—a narrow, high-speed air current in the upper atmosphere (200 to 300 hPa) flowing around the globe—which promotes the formation and intensification of extratropical cyclones, leading to more frequent and severe windstorms.

The cyclogenesis of extratropical cyclones in the Northern Hemisphere, including European windstorms, is described in the two most common conceptual models. Those are the Norwegian model and the Shapiro-Keyser model (Figure 2.2). The Norwegian cyclone model was developed by Norwegian meteorologists, Bjerknes (1919), while the Shapiro-Keyser cyclone model was proposed by Shapiro and

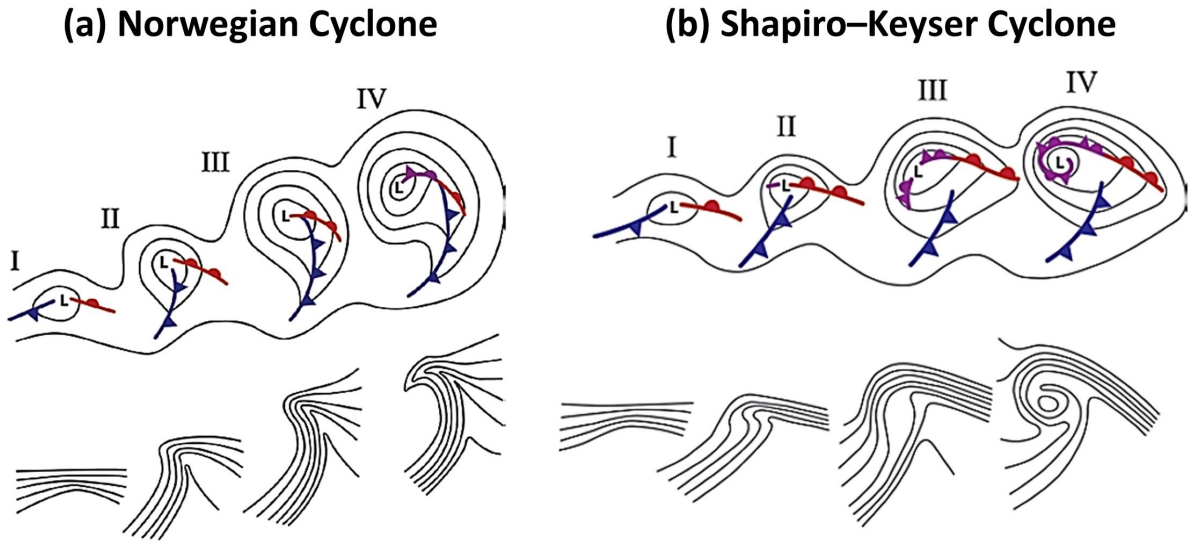

Figure 2.2.: Conceptual models of (a) Norwegian cyclone and (b) Shapiro-Keyser cyclone depict lower-tropospheric geopotential height and fronts (top) and lower-tropospheric potential temperature (bottom). In the top panels, blue indicates the cold front, red represents the warm front, and violet denotes the occluded front. The cyclone center, denoted as 'L,' progresses through stages separated by approximately 6 to 24 hours, with the distance from 'L' to the outermost contour in stage IV being 1000 km. The figures are reprinted from Figures 2 and 12 in Schultz and Vaughan (2011). © American Meteorological Society. Used with permission.

Keyser (1990). Both models are important for understanding cyclogenesis, and they each highlight different aspects of mid-latitude cyclone development and structure. The main difference between the Norwegian cyclone model and the Shapiro-Keyser cyclone model lies in the frontal structures they emphasize (Schultz and Keyser, 2021). The Norwegian cyclone model demonstrates the presence of a sharp angle between the cold and warm fronts, as the warm sector progressively converges and transforms into an occluded front during the cyclone's maturation. In contrast, the Shapiro-Keyser cyclone model emphasizes a perpendicular (T-bone) relationship between the cold and warm fronts, accompanied by the establishment of a warm-core seclusion of post-cold-frontal air. The process of cyclone formation according to the Norwegian model can be delineated into 4 phases:

1. Incipient frontal cyclone (phase I): The initial stage of cyclone formation in the Norwegian model involves the development of a cyclone characterized by the presence of both a warm front and a cold front.

2. Narrowing warm sector (phases II and III): Subsequently, as the cyclone matures, the warm sector of the cyclone undergoes a process of closure.

3. Occlusion (phase IV): During the subsequent stage, the cold front of the cyclone catches up to and merges with the warm front, resulting in the formation of an occluded front.

The Shapiro-Keyser cyclone model describes cyclone formation in 4 phases, with phase I being similar to the Norwegian cyclone model:

1. Incipient frontal cyclone (phase I): The cyclone begins with the formation of a cold front and a warm front.

2. Frontal fracture (phase II): The poleward portion of the cold front weakens near its intersection with the warm front.

3. Bent-back front and frontal T-bone (phase III): The warm-frontal zone extends around the low center, forming a bent-back front and a right angle (T-bone) between the cold and warm fronts.

4. Warm-core seclusion (phase IV): The bent-back front wraps around to form a warm-core seclusion of post-cold-frontal air.

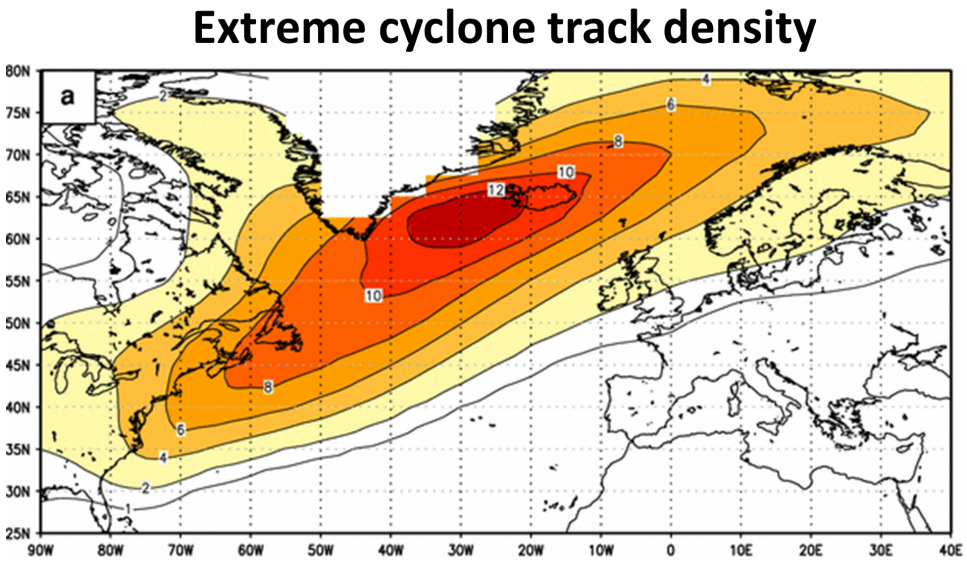

Figure 2.3.: Cyclone track density (cyclone days per winter) for the most intense 10% of cyclones, derived from NCEP reanalysis data (1958–1998). The figure is reprinted from Figure 4a in Pinto et al. (2009). Copyright © CC BY-NC 2.0

Over the North Atlantic, extratropical cyclones typically follow common paths known as the North Atlantic cyclone tracks or the extratropical cyclone tracks (Pinto et al., 2009; Shaw et al., 2016, Figure 2.3). Methods have been developed to track cyclones (Murray and Simmonds, 1991; Sinclair, 1994; Hodges, 1994, 1995; Pinto et al., 2005). Different tracking methods show significant variations, particularly in the count of extratropical cyclones (Neu et al., 2013). Different tracking methods in the Northern Hemisphere, using various parameters such as MSLP or vorticity, show differences in the number of cyclones of over 100% (Walker et al., 2020). Other than that, the choice of methods and variables can lead to variations in cyclone track statistics, particularly for weaker cyclones, but less so for stronger cyclones. Compared to the method using relative vorticity, the pressure-based methods for tracking cyclones often have a bias towards identifying certain types of cyclones, specifically the deeper and slower-moving ones (Sinclair, 1994). These methods may miss detecting other important cyclones, particularly those that

have pressure differences not just zonally but also meridionally. Vorticity-based methods, on the other hand, are not as influenced by these biases. They are better at detecting a broader range of cyclones, including those with pressure differences in different directions. Vorticity tracking tends to identify more extratropical cyclones compared to mean sea level pressure (MSLP) tracking, particularly evident at the initial and final time-steps due to its ability to capture small-scale features (Walker et al., 2020). This means they are more effective at capturing various types of cyclonic disturbances, providing a more comprehensive understanding of cyclone activity.

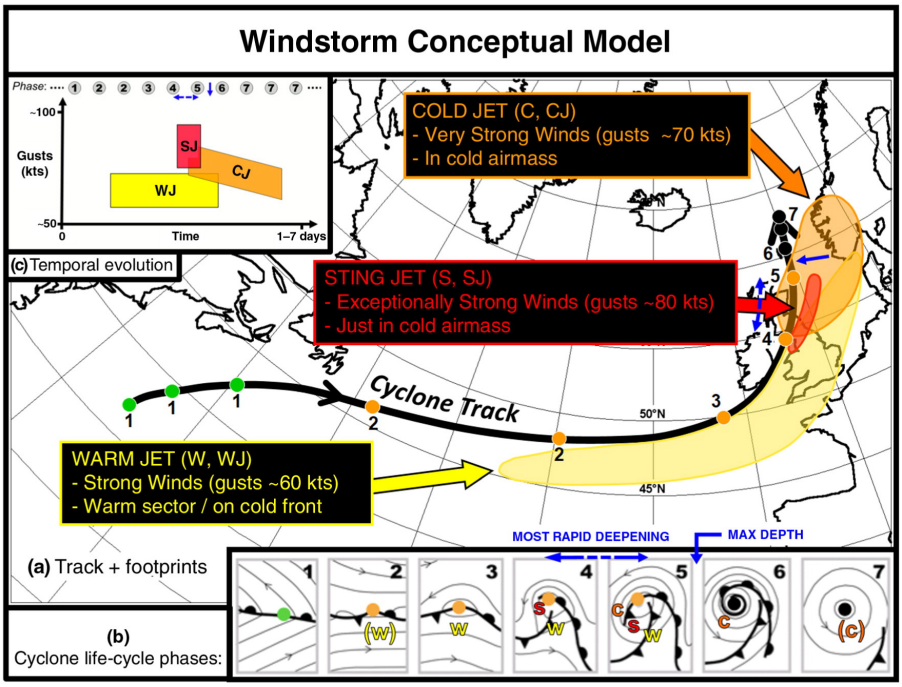

Figure 2.4.: Windstorm conceptual model of extratropical cyclone in the Northern Hemisphere, illustrating (a) the track of the cyclone (represented by a black dotted line) and the storm footprints caused by the warm jet (yellow), sting jet (red), and cold jet (orange). (b) The phases of the cyclone's life cycle, depicting the development of fronts and isobars, as well as the formation of jets. The small green dots represent a minor frontal wave, the orange dots represent a frontal wave cyclone, and the black dots represent a barotropic low. (c) The temporal evolution of the jets, displaying the corresponding wind gust magnitudes from phase 1 to 7. The dashed blue line represents the most rapid deepening, while the solid blue arrow indicates the maximum depth of the cyclone. This figure is reprinted from Figures 1 in Hewson and Neu (2015), with copyright CC BY 4.0.

Tracking the path of a cyclone is crucial for predicting which regions will be impacted. However, the impact of the storm is not only determined by its path but also by the different stages of its life cycle, which include intense wind phenomena. These intense wind phenomena include the warm jet, sting jet, and cold jet, as described in the windstorm conceptual model by Hewson and Neu (2015) (Figure 2.4). These jets can produce extremely strong winds that can cause significant damage. The warm jet represents the initial phase of warm conveyor belts, which are expansive streams of warm, moist air that ascend within an extratropical cyclone, transporting moisture and heat towards higher latitudes. This jet precedes the

cold front within a cyclone, typically occurs in the warm sector of the cyclone, and is known for causing wind damage and heavy precipitation (Catto, 2016). The sting jet refers to a relatively narrow and intense stream of descending air that can be found in certain mature extratropical cyclones (Clark and Gray, 2018). This jet is exclusively present in the Shapiro-Keyser cyclone model, specifically at the tip of the bent-back front during stage 4. It forms within the cloud head of the cyclone and descends rapidly, leading to exceptionally strong surface winds. Sting jets, despite their brief existence, cause severe and localized wind damage that surpasses the intensity caused by cold or warm jets, leaving significant destruction in their path. The cold jet denotes a fast-moving stream of cold air situated behind the cold front of an extratropical cyclone. It exhibits strong winds that commonly blow from the northwest to the southeast in the Northern Hemisphere. This jet is responsible for transporting cold air from polar regions towards the equator and is known to cause more prevalent wind damage across Europe compared to the warm and sting jets.

The position and intensity of extra-tropical cyclones are influenced by the interaction of several factors within synoptic-scale (large-scale) weather patterns. Firstly, the Sea Surface Temperature (SST) and its gradients play a crucial role, as warm SSTs provide the energy necessary for cyclone development, and the intensification of cyclones is more likely to occur over warmer waters (Bui and Spengler, 2021). Consequently, changes in SSTs have an impact on cyclone position and its intensity. Secondly, significant changes in baroclinic instability, which is crucial for extratropical cyclone development as they thrive on temperature gradients (baroclinicity), can promote the formation and movement of cyclones in regions with strong temperature contrasts (Holton and Hakim, 2012). Thirdly, the position and strength of the polar and subtropical jet streams determine both the location of cyclone formation and their subsequent movement (Shapiro and Keyser, 1990). A stronger jet stream tends to guide cyclones along specific paths. Fourthly, climate modes and oscillations also exert an influence on cyclone tracks. For instance, the North Atlantic Oscillation (NAO) affects the position and strength of the North Atlantic jet stream. Positive phases of NAO result in a more zonal (west-to-east) jet stream, therefore influencing cyclone tracks (Hanna and Cropper, 2017). Similarly, variations in the Arctic Oscillation (AO) impact the jet stream and cyclone paths (Thompson and Wallace, 2000), by the intensification of the meridional MSLP gradient aligned with the increase in winter storm frequency across Northern Europe (Bloomfield et al., 2018). Lastly, coastal features, including the Gulf Stream, can also influence cyclone tracks. The warmer waters of the Gulf Stream promote cyclone development and intensification (Palter, 2015).

2.2. Wind gust: Driver of windstorm damage

The primary source of wind damage is sudden, short bursts of increased wind speed, known as wind gusts, which are often followed by a period of decreased intensity (Brasseur, 2001; AMS, 2022). The

wind gust, as defined by the WMO, refers to the peak wind speed observed when averaging over 3-second intervals (World Meteorological Organization, 2014). Using wind gust data is suitable for investigating destructive windstorms because wind gusts represent the peak intensity of the winds experienced during a storm, providing a more accurate reflection of the strongest forces that infrastructure may encounter (Brasseur, 2001; Thalla and Stiros, 2018; Sheridan, 2018).

There are various methodologies available for estimating wind gusts, each with its own approach and appropriateness depending on the accessible data and specific requirements of the application. One such approach is the gust factor concept, initially proposed by Durst (1960), which involves quantifying the relationship between wind gusts and mean wind speed. The gust factor denotes the ratio between the peak wind gust and the mean wind speed over a specific time interval. It serves as an indicator of the variability or fluctuation in wind speed around the mean. The gust factor holds significant importance in the field of wind engineering as it assists engineers in evaluating the maximum wind loads that infrastructures may encounter during severe wind events.

In addition to the empirical estimation of wind gusts by Durst (1960), the estimation of wind gusts in numerical models is conducted through a more intricate approach known as wind gust parameterization. This method is used to represent the physical processes that contribute to gustiness in the atmosphere. In the review paper of Sheridan (2011), wind gust parameterizations for convective (i.e., thunderstorms) and non-convective gusts (i.e., windstorm) employed in various climate models are compiled into lists, and an examination of the similarities between these methods is conducted. Here, we specifically focus on the non-convective wind gust parameterization, which is primarily related to windstorm events. There are numerous methods available for the parameterization of non-convective wind gusts. For example, a widely used method is the Wind Gust Estimate (WGE) method by Brasseur (2001), which compares the vertical profiles of stability and turbulence (Figure 2.5). In the WGE method, the surface wind gusts are a consequence of the displacement of air parcels originating from higher regions within the boundary layer. These air parcels are subsequently transported towards the surface through the action of turbulent eddies. In essence, gusts manifest themselves as a result of downward redirection of air caused by turbulent motions. The WGE method considers both the mean wind components and the turbulent atmospheric structure. To estimate the wind gust using the WGE method, follow these steps:

1. Calculate the Turbulent Kinetic Energy (TKE): Determine the TKE profile in the boundary layer, typically averaged over a certain height from the surface.

2. Compute the Mean Wind Components: Calculate the mean wind components (U and V) in the x and y directions, respectively, within the boundary layer.

3. Estimate the Wind Gust: Use the equation 2.1 for different heights z_p satisfying the condition in Figure 2.5 when a parcel of air at a specific altitude descends to the surface and possesses a mean TKE that exceeds the buoyant energy between the surface and the parcel's altitude.

$$W_{\text{g\_estimate}} = \max\left[\sqrt{U^2(z_p) + V_p^2(z_p)}\right] \tag{2.1}$$

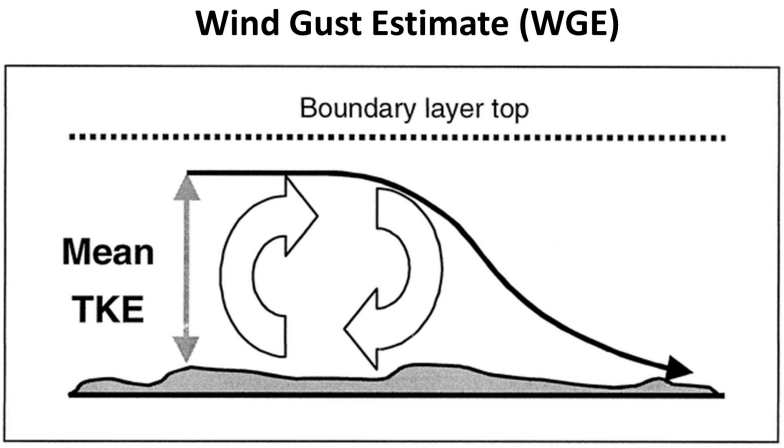

Figure 2.5.: The Wind Gust Estimate (WGE) method by Brasseur (2001) employs the utilization of turbulent kinetic energy (TKE) averaged over a specified depth within the boundary layer to determine the estimates of wind gust. The figures are reprinted from Figure 4 in Brasseur (2001). © American Meteorological Society. Used with permission.

The WGE method offers both a single estimated value for gust magnitudes and also calculates a bounding interval surrounding this estimate. The bounding interval serves as a representation of the probable range of gust magnitudes, taking into consideration the uncertainties inherent in the estimation process.

Another common method, such as employed in the COSMO-CLM regional climate model initially developed by the German Weather Service (DWD) and later by the European Consortium COSMO, involves interpolating wind speed from the lowest model level to 30 meters above ground (standard measurement height) and incorporating the friction velocity u_* (equation 2.2).

$$v_{\text{gust}} = |v_{\text{z=30}m}| + 3.0 \cdot 2.4 \cdot u_* \tag{2.2}$$

The values 3.0 and 2.4 in the equation 2.2 are determined by Prandtl-layer theory (Panofsky and Dutton, 1984), which draws support from various observation campaigns. For a more comprehensive explanation and assessment of this formula, please refer to Schulz (2008).

In the study conducted by Born et al. (2012) , which examines the performance of various parameterization approaches of wind gusts, it was found that the WGE method by Brasseur tends to overestimate

wind gust speeds over land compared to the sea, particularly in flatland and moderately hilly regions. It shows better performance in mountainous areas and under conditions of weaker winds. However, using the method of interpolating wind speed from the lowest model level to a height of 30 meters generally shows overall better performance. These results indicate that wind gusts are influenced by topography (roughness) and surface elevations, which create turbulent eddies and affect atmospheric turbulence. A key challenge in estimating wind gusts is that spatially distributed observations often lack enough data on atmospheric turbulence, making statistical calibration of the turbulence component of wind gust estimation difficult.

2.3. Different methodologies to estimate windstorm losses

There are various methods to quantify windstorm losses across Europe, ranging from meteorological to catastrophe model perspectives (see review in Gliksman et al. 2023). The meteorological perspective offers a simpler approach to estimating windstorm losses but does not directly translate into monetary terms. In contrast, the catastrophe model, commonly employed by insurance companies, focuses on estimating monetary damages, making it a more complex approach. The following subsections describe these different methods for estimating windstorm loss from both meteorological and catastrophe model perspectives.

2.3.1. Meteorological perspective

The quantification of windstorm losses from a meteorological perspective has been conducted over the last three decades. This method provides simple, non-monetary estimates, and focuses solely on the physical impact of storms. The physical impact refers to the direct effects of the severe wind gusts on the environment and infrastructure, such as measuring wind strength and determining the extent of the areas affected by the windstorm. Lamb and Frydendahl (1991) developed the first Storm Severity Index (SSI), which considers the observed peak wind over land, the storm duration, and the affected area. Later, Dorland et al. (1999) introduced the storm loss function, suggesting that damage or loss to buildings increases exponentially with wind speed. Subsequently, Klawa and Ulbrich (2003) developed an index that incorporates both meteorological variables and insurance factors to assess storm severity (equation 2.3). The loss is assumed to increase with the cube of the normalized gust intensity that exceeds the 98$^{\text{th}}$ percentile threshold.

$$\text{loss} = c \cdot \text{LOSSINDEX} = c \sum_{\text{district}} \text{pop}(\text{district}) \left(\frac{v_{\max(\text{district})}}{v_{98(\text{district})}} - 1 \right)^3 \tag{2.3}$$

The LOSSINDEX values computed daily (over 24-hour periods) are summed for each individual year, resulting in an annual loss index. The regression coefficient c represents the relationship between the

annual loss index and the actual annual loss from the German Insurance Association (GDV), serving as a scaling factor between the two time series. The pop(district) refers to the population count provided for a specific district. $v_{\max}$ is the daily maximum wind speed, and $v_{98\text{th}}$ is the 98$^{\text{th}}$ percentile of daily maximum wind speed for a given period. The cube of wind speed is proportional to the advection of kinetic energy. This means that as wind speed increases, the rate at which turbulent kinetic energy dissipates due to viscosity increases significantly (Businger and Businger, 2001). Nevertheless, the v^3 relationship between wind speeds and economic loss, which is commonly used in such investigations, is primarily supported by empirical evidence (MunichRe, 1993; Palutikof and Skellern, 1991; Lamb and Frydendahl, 1991).

Later, Leckebusch et al. (2008) further developed the method that was initially proposed by Klawa and Ulbrich (2003) by incorporating event tracking called event SSI to calculate losses over time and space. The event SSI was determined by summing the values of exceeded thresholds (from 90$^{\text{th}}$ to 98$^{\text{th}}$ percentiles) across all grid points accumulated over all time steps in which exceedances were observed (equation 2.4).

$$\text{SSI}_{T,K} = \sum_{t}^{T} \sum_{k}^{K} \left[\max \left(0, \frac{v_{k,t}}{v_{\text{perc},k}} - 1 \right)^3 * A_k \right] \tag{2.4}$$

t refers to a time index, k refers to the grid boxes, $v_{\text{k},t}$ is the daily maximum wind speed, and $v_{\text{perc},k}$ is defined by the local 90$^{\text{th}}$, 95$^{\text{th}}$, and 98$^{\text{th}}$ percentile values of the daily maximum wind speed, and A_{k} is the affected area. The use from 90$^{\text{th}}$ to the 98$^{\text{th}}$ percentiles is to understand the increasing severity of storms in different percentiles. Only tracks that last at least 24 hours are considered for the calculation of event SSI.

Furthermore, Pinto et al. (2012) compare windstorm severity using two indices: the meteorological index (MI) and the loss index (LI). The MI measures storm intensity over time across both land and sea, disregarding population factors, making it ideal for studying storms in isolation from social factors. In contrast, the LI focuses solely on land, incorporating population density to evaluate the societal impact of storms. These indices are calculated every 24 hours with a 6-hour moving window. Karremann et al. (2014a) subsequently refined the formulated index, originally known as LI3-D, by extending the observation period to 72 hours instead of 24 hours. This adjustment was made to account for the general lifetime period of cyclones (Hewson and Neu, 2015), thereby ensuring clearer differentiation between individual storms.

The rationale behind the utilization of the 98$^{\text{th}}$ percentile of the daily maximum wind gust, in the study conducted by Klawa and Ulbrich (2003), stems from the prevailing practice among insurance companies in Germany. The threshold for destructive windstorms in the insurance industry (Beaufort scale 8, or

17-20 m/s) (Berz and Smolka, 1988) roughly corresponds to the wind gusts that occur on the top 2% of all days Palutikof and Skellern (1991), which aligns with the 98th percentile. Consequently, the daily peak gusts are scaled using the local 98th percentile to account for these extreme, loss-inducing wind events. This definition is not only applicable to Germany but also to other countries in Western and Central Europe. However, the 98th percentile of daily maximum wind speed in other regions is considered too low to serve as a threshold for wind-induced damage, such as in countries located in Eastern Europe, the Iberian Peninsula, and Scandinavia (Karremann et al., 2014b). In cases where the 98th percentile is deemed insufficient, the threshold for wind speed causing damage is typically set at 9 m/s or wind gust speeds ranging from 20-25 m/s (Klawa and Ulbrich, 2003; Karremann et al., 2014b; Welker et al., 2021), depending on the datasets used, which corresponds to empirical evidence on when losses are expected to occur.

2.3.2. Catastrophe model perspective

In addition to those indices, insurance companies use catastrophe models to assess windstorm losses and determine the monetary damage, to which the public does not have access. These models are built on the principles of understanding hazard, exposure, and vulnerability components. The hazard component involves analyzing the severity of the event (windstorm) that typically includes historical event data. The exposure component refers to the assets (e.g., buildings, infrastructure, populations) that are at risk from the identified hazards. Catastrophe models integrate detailed geospatial and demographic data to quantify the exposure. The vulnerability component represents how susceptible the exposed assets are to damage or loss when a hazard event occurs. The vulnerability component includes the damage function, which defines the relationship between wind intensity and the resulting damage (Prahl et al., 2016). A damage function, which can take the form of either a power law, an exponential form, or an excess-over-threshold formulation, describes the non-linear relationship between the magnitude of a hazard and the average amount of damage (which can be monetary damage or any measurable quantity) inflicted on the specific items (such as buildings). Prahl's novel function challenges assumptions by introducing higher exponents in power-law curves. The use of these higher exponents shows a stronger increase in damage with higher wind speeds compared to previous models (e.g., Heneka et al., 2006; Prahl et al., 2012). This function captures the nonlinear relationship between wind speed and damage, providing a more accurate representation. As a result, it has improved predictive capabilities across a wider range of wind speeds.

Prior to the study of Prahl et al. (2016), Prahl et al. (2015) conducted an evaluation of storm damage functions to assess their performance. The evaluation revealed that the probabilistic models developed by Heneka et al. (2006) and Prahl et al. (2012) provide accurate predictions for losses from moderate to extreme storms. The model by Prahl et al. (2012) is preferred due to its broader applicability. However, the loss model proposed by Klawa and Ulbrich (2003) is recommended exclusively for extreme loss sce-

narios, as it demonstrates minimal bias and comparable errors to the probabilistic model developed by Prahl et al. (2012).

2.4. Seasonal clustering of windstorm losses

Over the North Atlantic, the extra-tropical cyclones typically occur as families, resulting in seasonal multi-windstorm losses (Bjerknes, 1922; Dacre and Pinto, 2020). Serial clustering of extra-tropical cyclones refers to the occurrence of multiple cyclones passing over a fixed location within a specific time frame. Generally, cyclone clustering is understood as a period during which a location experiences a high frequency of cyclones, occasionally resulting in significant cumulative impacts. The serial clustering of cyclones often occurs in regions on the flanks and at the exit of the North Atlantic cyclone track, thereby often resulting in substantial impacts on Europe due to these cyclones (Figure 2.6) (Dacre and Pinto, 2020). Prominent examples of serial clustering of European windstorms (storm names assigned by the German Weather Service) causing large economic losses include the December 1999 windstorm series with Anatol, Lothar, and Martin (Ulbrich et al., 2001), the January 2007 storms including Kyrill (Fink et al., 2009), the 2013/2014 UK-focused event (Kendon and McCarthy, 2015), and the February 2022 sequence of powerful windstorms, Ylenia, Zeynep, and Antonia (Mühr et al., 2022).

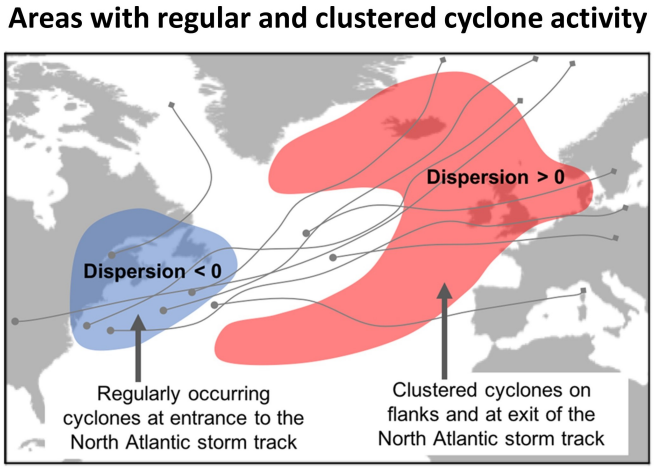

Figure 2.6.: The depicted regions in blue exhibit a regular occurrence of cyclones (underdispersion), whereas the red displays the region with clustered cyclone activity (overdispersion). The cyclone tracks are depicted in grey. The figure is reprinted from Figure 2 in Dacre and Pinto (2020), with copyright CC BY 4.0.

$$\Psi = \frac{\mathrm{Var}(N)}{\bar{N}} - 1 \tag{2.5}$$

From a meteorological perspective, clustering of cyclones is commonly assessed by examining the dispersion of cyclone statistics (Ψ), specifically the variance-to-mean ratio of monthly cyclone counts in

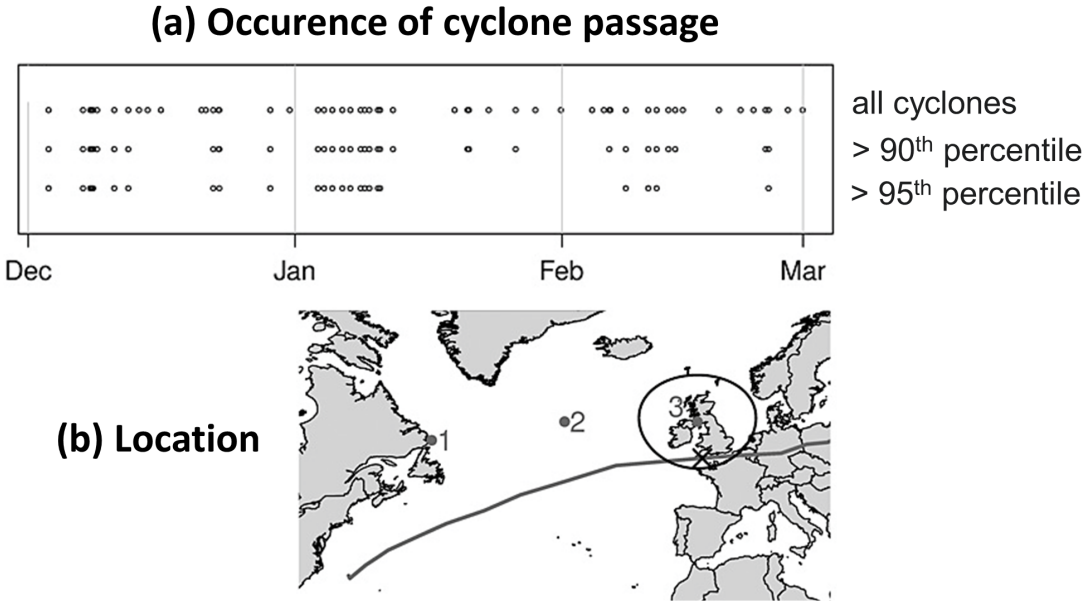

Figure 2.7.: (a) Cyclone passage occurrences within circular line 3 (December 1957 - February 1958) with the top row: all cyclones, the middle row: cyclones with core pressure above the 90th percentile, and the bottom row: cyclones with core pressure above the 95th percentile. (b) Location of circular line 3. The figure is reprinted from Figure 1 in Pinto et al. (2013). Copyright © 1999-2024 John Wiley & Sons, Inc or related companies. Used with permission.

certain areas (equation 2.5), to determine the temporal clustering (the occurrence of cyclone sequences within a defined time window) (Mailier et al., 2006). This idea is based on the hypothesis that cyclones occur randomly. In serial randomness, the number of events per time interval follows a Poisson distribution, with the average value over time equal to the variance. Thus, in dispersion statistics, serial clustering of cyclones occurs when the dispersion statistics are greater than 0. If the dispersion statistics are equal to zero, it indicates the occurrence of serial randomness of cyclones, meaning that the occurrence of one cyclone at any moment is independent of previous occurrences. On the other hand, if the dispersion is less than zero, it suggests that cyclones occur in a serially regular manner. Serial clustering of extra-tropical cyclones is typically more pronounced for stronger cyclones (Figure 2.7; Vitolo et al. 2009; Pinto et al. 2013).

Alternative approaches have been developed in order to assess the cumulative impact of serial cyclone clustering. The investigation of windstorm loss clustering was initially introduced by Karremann et al. (2014a), who approximated the data using a negative binomial distribution to estimate the deviation from a random Poisson distribution. In a subsequent study, Priestley et al. (2018) investigated this loss clustering on a seasonal basis using a different approach. They used terms commonly used in insurance, namely the maximum loss per season or Occurrence Exceedance Probability (OEP), and the total loss in a season or Annual Exceedance Probability (AEP). By quantifying the ratio between OEP and AEP, a large ratio suggests the presence of a single dominant event during the season, indicating no loss clustering.

Conversely, a small ratio indicates a season with loss clustering. However, the exact thresholds for what constitutes a "large" or "small" ratio have not been thoroughly explained. It is crucial to acknowledge that the frequency of multiple small cyclone events can exhibit an even or random distribution over time, which may not be identified as clustering based on metrics of dispersion statistics in the study conducted by Mailier et al. (2006). Therefore, whether a specific area or time frame exhibits clustering can vary depending on the metric being used (Dacre and Pinto, 2020).

2.5. Climate models

For climate studies, climate models are the representation of the climate system, by simulating the interactions among fundamental components of climate, including the atmosphere, oceans, land surface, and ice. Manabe and Wetherald introduced the first robust climate models in 1967, using radiative forcing as a measure to understand alterations in the Earth's energy balance from human and natural changes (Manabe and Wetherald, 1967; Forster, 2017). In the 1970s, Klaus Hasselmann focused on employing stochastic processes to tackle the random and unpredictable nature of climate variability, introducing a model that explains gradual climate shifts as the cumulative response to ongoing random influences from short-term "weather" disturbances (Hasselmann, 1976). The World Climate Research Programme (WCRP) initiated the Coupled Model Intercomparison Project (CMIP) starting in 1995 to coordinate and standardize general circulation model (GCM) simulations, with its findings used by the Intergovernmental Panel on Climate Change (IPCC) for assessment reports. For example, in 2004, the IPCC used the findings from CMIP3 (Meehl et al., 2007; Solomon et al., 2007), followed by CMIP5 in 2013 (Taylor et al., 2012; WG, 2013), and later incorporated the advancements of CMIP6 in 2021 (Eyring et al., 2016; Masson-Delmotte et al., 2021b) to address the limitations identified in CMIP5 (Stouffer et al., 2017).

Under CMIP3, CMIP5, and CMIP6, climate modeling groups use a common set of scenarios and protocols to allow direct comparison of results. CMIP3 uses the SRES (Special Report on Emissions Scenarios), which includes four scenario families—A1 (rapid growth, technological development), A2 (regional development, slower growth), B1 (global convergence, sustainability), and B2 (localized sustainability, moderate growth)—with further subdivisions in the A1 family based on energy assumptions (A1FI, A1B, A1T) (Nakićenović et al., 2000). In contrast, CMIP5 uses RCPs (Representative Concentration Pathways), which focus on greenhouse gas concentration pathways tied to radiative forcing (Van Vuuren et al., 2011). RCPs depict different trajectories of future GHG emissions and concentrations, characterized by their radiative forcing levels by 2100. There are four RCP scenarios from the low emission scenario to the highest emission scenario: RCP2.6, RCP4.5, RCP6.0, and RCP8.5. For example, the number 8.5 in RCP8.5 refers to a radiative forcing level of 8.5 watts per square meter (W/m²) by 2100, compared to pre-industrial levels. Considered the high-end scenario, RCP8.5 assumes high population

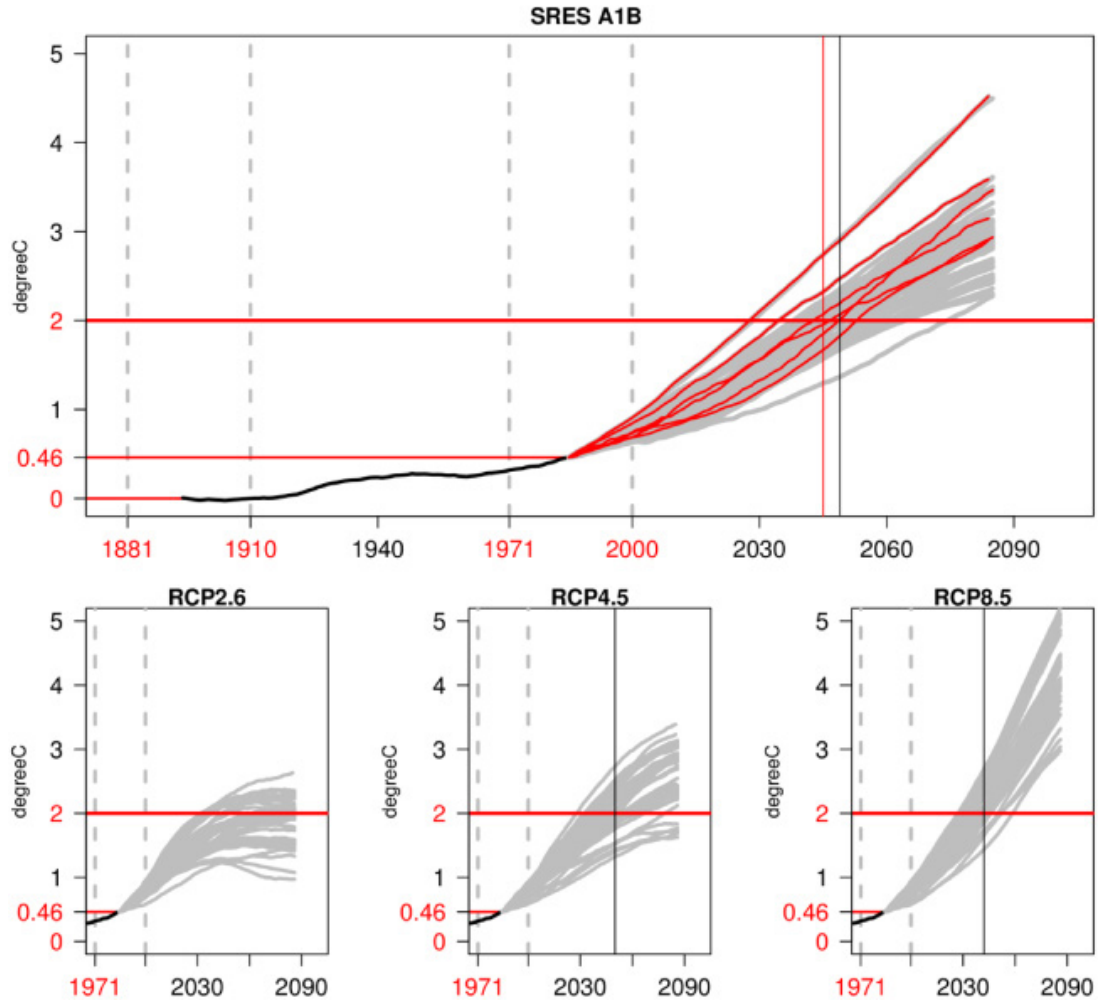

Figure 2.8.: The global mean temperature (30-year moving average) from 15 bias-corrected RCMs is shown in gray lines for the SRES A1B (moderate emissions) scenario (top panel, CMIP3) and RCP2.6, RCP4.5, and RCP8.5 scenarios (bottom panels, CMIP5). The horizontal black line in the top panel represents observed temperatures relative to pre-industrial levels. The vertical black lines are the median year when each CMIP3 (top panel) and CMIP5 (bottom panel) ensemble reaches +2°C. The vertical red line (top panel) marks the median year when reaching +2°C for the 6 main GCMs used to drive the RCMs in CMIP3. No black vertical line is shown for RCP2.6 because most simulations under this scenario remain below +2°C. The figure is reprinted from Figure 1 in Vautard et al. (2014), with copyright CC BY 3.0.

growth, increased energy demands, and continued reliance on fossil fuels, resulting in rising greenhouse gas emissions throughout the 21st century without significant mitigation efforts. Meanwhile, RCP2.6, the lowest emission scenario, represents an optimistic pathway with aggressive efforts to limit GHG emissions and minimize climate change impacts. Later in the CMIP6 study, the RCPs were substituted by the Shared Socio-economic Pathways (SSPs) (Riahi et al., 2017). The SSPs encompass not only GHG emissions but also socio-economic factors, thereby offering a more extensive foundation for climate modeling and projection.

When referring to the CMIP3, CMIP5, or CMIP6 models, it typically pertains to the output of General Circulation Models (GCMs), with low resolution (on average 100km for CMIP6, lower for previous CMIPs). GCMs are used to simulate the entire Earth's climate system, typically at coarse spatial resolutions that cover the entire globe (Manabe et al., 1975, 1979). These models provide valuable insights into large-scale climate patterns and global-scale climate change. To assess climate change between future and historical periods, it can be defined by the change under Global Warming Levels (GWLs) instead of using fixed time slices. This approach has the advantage of accurately estimating the change based on the warming level of each model, as different GCMs have different warming levels (Vautard et al., 2014; IMPACT2C Project, 2015). GWLs are defined as specific levels of global mean temperature increase relative to pre-industrial levels (Figure 2.8). The GWL periods are determined individually for each of the GCMs in the ensemble (Teichmann et al., 2018). GWLs vary across different GCMs owing to disparities in assumptions regarding future emissions, socioeconomic factors, and mitigation strategies in each individual model (Preuschmann et al., 2017). The commonly used GWLs are +2°C and +3°C, representing a projected increase of +2°C and +3°C in global temperature compared to pre-industrial levels. For example, the +2°C period is when the average global temperature over 30 years is 2°C higher than the temperature during the pre-industrial period (1881–1910). The study of GWL +2°C aligns with realistic near-future climate change scenarios (Kjellström et al., 2018) and is in line with the Paris Agreement's goal to limit global warming to below +2°C above pre-industrial levels (Schleussner et al., 2016). Studying GWL +3°C is relevant for exploring more extreme scenarios and gaining insights into long-term changes in the second half of the century (Raftery et al., 2017).

Investigating climate change with climate models requires using a multi-model ensemble approach (Tebaldi and Knutti, 2007). This approach is necessary because each climate model employs different settings and parameterizations, which can lead to varying responses to factors such as GHG concentrations, thereby introducing biases and uncertainties. Another source of uncertainty in climate models is extrapolating sensitivities from present to future conditions, as parameters crucial for simulating today's climate may not drive future changes, and the model is calibrated only for recent climate (Qian et al., 2016). To address those uncertainties, the IPCC report typically shows not only the best estimate of models but also the model spread (Pörtner et al., 2022). This is because each GCM provides statistically independent climate information and can represent structural uncertainty (Abramowitz et al., 2019). Using a multi-model ensemble of climate models is crucial as it helps understand the range of possible futures and provides more robust predictions.

Despite the capability of GCMs to project future climate change at a global scale, these models may not sufficiently capture local or regional-scale climate processes, including topographic effects, land-sea interactions, and regional weather patterns. Consequently, Regional Climate Models (RCMs) are required to focus on regional climate processes (Giorgi, 1990; Giorgi and Mearns, 1991). One such consortium

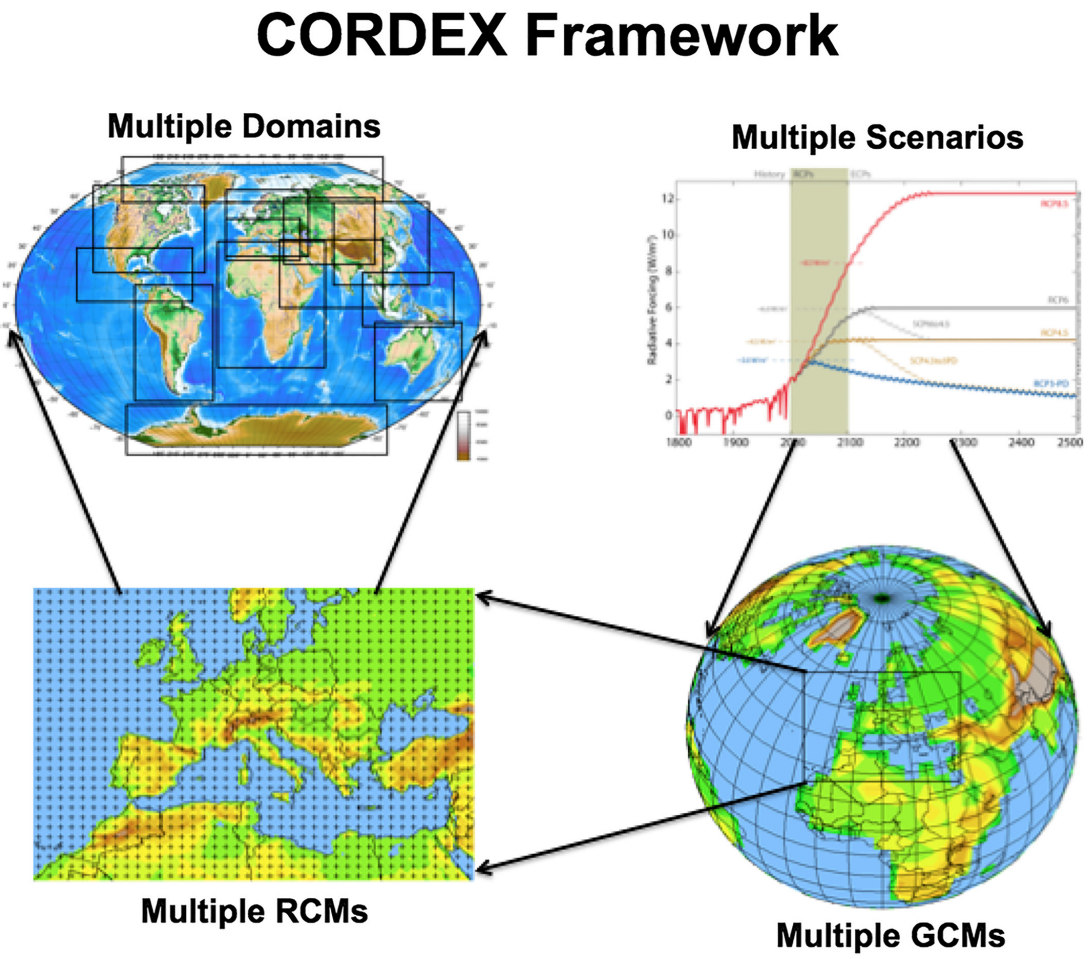

Figure 2.9.: Framework for the experiments within the Coordinated Regional Downscaling Experiment (CORDEX) with RCM stands for regional climate model, and GCM stands for general circulation model. The figure is reprinted from Figure 7 in Giorgi (2019). Copyright © 1999-2024 John Wiley & Sons, Inc. or related companies. Used with permission.

involved in creating RCMs is the EURO-CORDEX (Coordinated Regional Climate Downscaling Experiment) consortium (Figure 2.9). This consortium conducts downscaling for the European domain (Giorgi et al., 2009), transitioning from lower spatial resolution models, typically from GCMs, to higher resolution models to more accurately capture regional characteristics (Iles et al., 2020; Tapiador et al., 2020). In general, there are three approaches to downscaling: statistical-empirical methods, dynamical or nesting methods, and statistical-dynamical downscaling (SDD) (Hewitson and Crane, 1996; Wilby and Wigley, 1997; Fuentes and Heimann, 2000). The statistical-empirical methods are downscaling methods that use statistical relationships between large-scale atmospheric variables from GCMs and observed data for local climate variables. This method is computationally cheaper than running detailed RCMs, as it directly translates GCM outputs into local climate predictions. Dynamical downscaling uses boundary conditions from coarse-resolution GCMs to run high-resolution RCMs, refining large-scale climate processes. It projects these processes onto regional scales through physical climate simulations. The SDD combines statistical and dynamical downscaling methods. It begins by analyzing the outputs of the GCM

to identify various weather patterns. Instead of running the RCM continuously, it is run separately for each identified weather pattern. This approach reduces computational costs while capturing detailed regional climate features that are influenced by large-scale patterns. From the added value of downscaling in EURO-CORDEX, RCMs can better represent regional climate conditions. Previous studies have used the EURO-CORDEX wind dataset to investigate changes in wind speed (Michel and Sorteberg, 2023) and windstorms (Jung and Schindler, 2021; Outten and Sobolowski, 2021), as well as their potential implications for different sectors, particularly in the assessment of wind energy (Moemken et al., 2018; Bonanno et al., 2023).

2.6. Climate variability and change in European windstorms and losses

Climate variability refers to the fluctuations in the climate patterns across various time scales, ranging from months to decades, driven by natural sources and internal variability. On the other hand, climate change refers to the long-term changes in the climate system sustained over decades to centuries. Both climate variability and climate change play crucial roles in shaping the behavior of windstorms in Europe. They have the ability to influence the patterns and characteristics of windstorms by altering atmospheric circulation, varying windstorm frequency and intensity, as well as shifting storm tracks. These changes can lead to higher losses and societal impacts.

The historical windstorm data reveals significant variability, though it also shows a discernible trend (Figure 2.10). According to Feser et al. (2015), storminess over Northwestern Europe has shown a decrease from the late nineteenth century until the mid-1960s based on observational data. This was followed by an increase until the 1990s and then a subsequent decline, as indicated by reanalysis data. The rise in linear trends from 1960 to the mid-1990s is corroborated by the increase in the North Atlantic Oscillation (NAO) index. The NAO influences storm frequency in the North Atlantic-European region, showing positive correlations between NAO indices and winter storms in northern areas, but weaker or negative correlations in southern areas. A study conducted by Laurila et al. (2021) examines the trends and variability of wind speed in Europe and the North Atlantic region using the ERA5 reanalysis data (1979 - 2018), which is one of the most recent and widely used reanalysis datasets. Their results indicate that there are no clear linear trends in 10-meter wind speeds, but the analysis shows significant annual and decadal variability in wind speed patterns. Laurila et al. (2021) also highlighted that decadal 10-m wind speeds were stronger than average in Northern Europe during the 1990s and in Southern Europe during the 1980s and 2010s.

There is a growing body of literature that investigates the observed trends and frequency of extratropical cyclones in the Northern Hemisphere, using various datasets ranging from observations to reanalysis

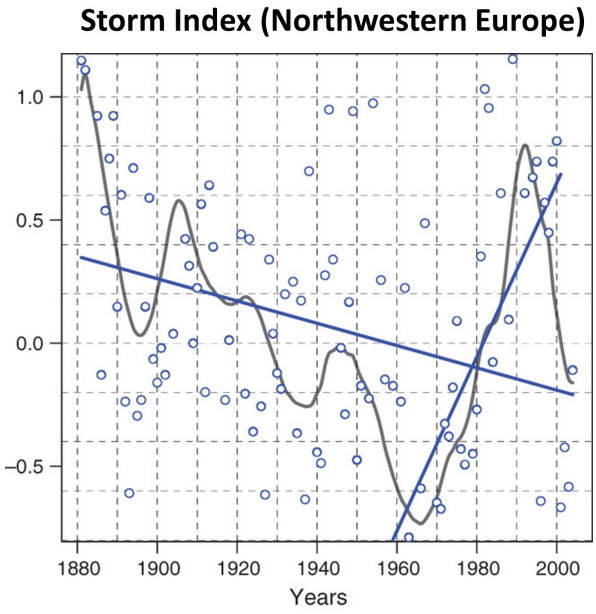

Figure 2.10.: The storm index is derived from geostrophic wind speed percentiles across Northwestern Europe, encompassing the British Isles, North Sea, and Norwegian Sea. The 95th percentiles of standardized geostrophic wind speed anomalies are denoted by the blue circles. The low-pass filtered data is represented by the gray curve. Additionally, the first blue line corresponds to the linear trends of the 95th percentiles for the period 1881-2004, obtained from station network datasets as documented in Alexandersson et al. (1998). The second blue line indicates the trends observed during the ERA-40 period (1957-2001). The figure is reprinted from Figure 2 in Feser et al. (2015).

data. However, it must be noted that the trends and frequency of extratropical cyclones are sensitive to the different sources of data. Thus, it is crucial to carefully consider these factors when interpreting trends and variability of storms using different datasets (Vautard et al., 2010; Krueger et al., 2013).

The general pattern of long-term changes in storm track density from the study by Priestley and Catto (2022), based on the latest CMIP6 GCMs, shows an eastward extension of the North Atlantic storm track toward Europe (Figure 2.11). This leads to a general increase in storm track density over Western and Central Europe, although the climate change signal among models is not robust. However, a decrease in storm track density over southern Europe is robust across all scenarios. This shift prompts an in-depth exploration of the underlying scientific mechanisms by which climate change influences the frequency and intensity of extratropical cyclones.

Further, we delve into the physical arguments through which climate change affects extratropical cyclones, specifically focusing on their structure and tracks in the Northern Hemisphere (Catto et al., 2019). Figure 2.12 displays the projected changes in cyclone structure, taking into account the uncertainty surrounding the influencing factors. These factors include the temperature gradients at the upper and lower levels, vertical temperature gradient, latent heating, precipitation, mean sea level pressure (MSLP), and

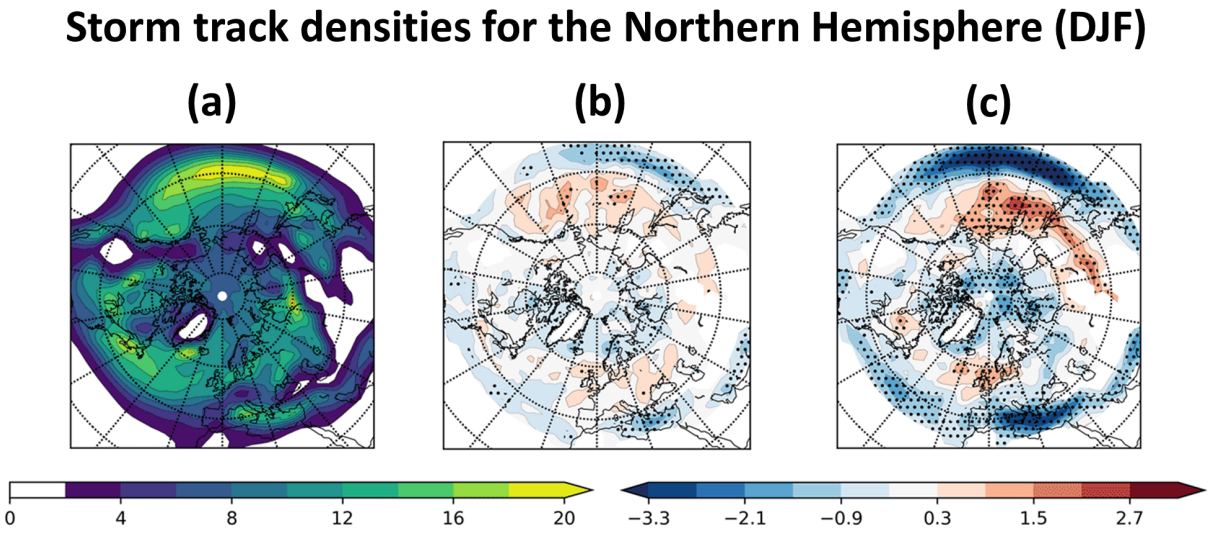

Figure 2.11.: Storm track density (a) during the historical period (1979–2014) from the CMIP6 multi-model ensemble and (b, c) projected changes for 2080–2100 under scenarios of (b) SSP1-26 (low emission) and (c) SSP5-85 (high emission) relative to the historical period, with stippling indicating over 80% model agreement on the sign of change. The figure is reprinted from Figure 2 (a, b, and e) in Priestley and Catto (2022), with copyright CC BY 4.0.

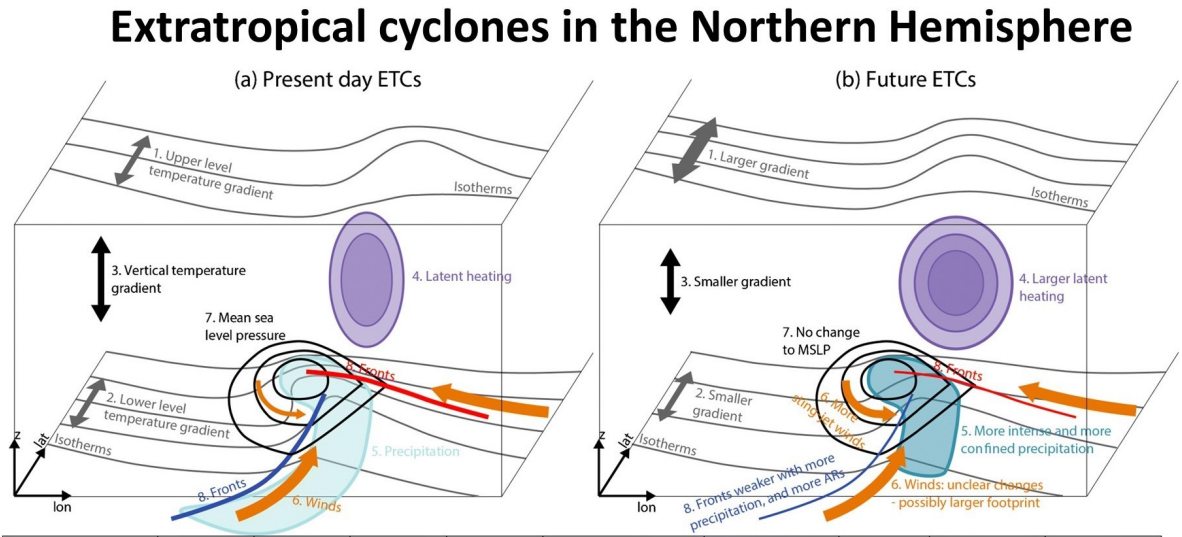

Feature	1	2	3	4	5 (intensity)	5 (extent)	6	7	8
Confidence	High	High	High	High	High	Low	Low	Medium	Low

Figure 2.12.: Schematic diagram illustrating projected alterations to extratropical cyclones in the Northern Hemisphere. The table presents the level of certainty regarding the change of each of the identified aspects depicted in the diagram, derived from the comprehensive examination of the scientific literature conducted. The figure is reprinted from Figure 2 in Catto et al. (2019), with copyright CC BY 4.0.

fronts. Regarding future predictions, there is a high level of confidence that the upper-level temperature gradient will increase. Conversely, the lower-level and vertical temperature gradients are expected to decrease, primarily due to polar amplification (a more rapid rate of warming in comparison to other

regions) in the Northern Hemisphere during winter (Wang et al., 2017). The larger upper-level temperature gradient and heightened atmospheric moisture are projected to contribute to increased latent heating (Ahmadi-Givi et al., 2004), consequently leading to more intense precipitation (high confidence). While it is anticipated that intensified precipitation may potentially enhance cyclone intensity, the exact extent and conditions under which this occurs remain uncertain, resulting in unclear changes (low confidence) in wind patterns. Additionally, there is medium confidence in the absence of changes in MSLP and low confidence in the alterations of fronts. Overall, although there are high-confidence expectations for certain changes, uncertainties persist regarding the interactions between various factors and their ultimate influence on extratropical cyclones. For the changes in storm track, according to the latest IPCC report (Pörtner et al., 2022), there is only low agreement on changes in extratropical cyclone track density in the North Atlantic and low agreement on a weakening of the Mediterranean storm track. In addition to the latest IPCC report, which shows an increase in extreme windstorms in Core Europe and a decrease in the Iberian Peninsula, it is clear that predicting future European windstorms is challenging due to regional differences. To conduct a comprehensive risk assessment at the regional level, it is important to deepen our understanding of regional climate patterns and utilize state-of-the-art regional climate models.

The changes in the intensity and frequency of extratropical cyclones result in corresponding variations in the impacts and damages associated with windstorms under projected climate conditions when compared to historical time periods. Previous studies have used general circulation model and regional climate model simulations to estimate future windstorm loss in Europe. It is projected that under future climate conditions from CMIP6 model ensembles, the windstorm losses in Northern and Central Europe will increase more than triple under a high emissions scenario SSP5-8.5 by 2100 (Little et al., 2023), while losses are projected to decrease from the selected CMIP6 ensemble across the remaining parts of Europe, including Poland (Severino et al., 2024). However, an opposing finding under a high emissions scenario RCP8.5 from the selected EURO-CORDEX model suggests a potential increase in projected windstorm losses over Poland (Gaska, 2023). These uncertainties, arising from disparities in climate models and scenarios, limitations in model resolution, and the representation of small-scale features, pose challenges in accurately estimating the future risk of European windstorms. Although there is uncertainty in climate models, particularly regarding the presence of variations in climate change signals among models, this uncertainty can offer valuable insights into a range of potential climate change scenarios.

3. Main research questions

This chapter outlines the main research questions of this thesis. The main objective is to investigate European windstorm losses under current and future climate conditions. First, historical losses from both meteorological and insurance perspectives are compared. Second, the study assesses regional changes in windstorm losses under various global warming levels (GWLs) compared to the historical period, using the EURO-CORDEX dataset. Finally, the seasonal loss clustering (indicating seasons with a large number of individual storms contributing to the total loss) under current and future climate conditions are examined. The findings, which directly address these objectives, are documented in Chapters 5 through 7.

The motivation for Chapter 5 stems from the limited studies comparing the effectiveness and accuracy of various methods for estimating windstorm losses, such as comparing the losses obtained from the simple Loss Index (LI) method that is commonly used by meteorologists and those from insurance companies. It is imperative to bridge the gap between the approaches commonly employed by scientists and those adopted by insurers. Doing so enables the evaluation of existing methods and facilitates enhancements for more accurate assessments of windstorm losses. This alignment fosters opportunities for improvement and refinement in loss estimation methods. Thus, in Chapter 5, the loss estimate from the LI method is compared with the loss from Aon Impact Forecasting's proprietary catastrophe models, which are not publicly accessible. This comparison aims to address the first main research question of the thesis:

Research question 1 :
How comparable are windstorm loss estimates between a meteorological loss index and a full insurance loss model ?

To answer the first research question, tests were conducted to assess how sensitive the LI method is to different meteorological input data, specifically ERA5 and ERA-Interim wind gust datasets. Following this, the loss estimates from the LI method are compared with those from Aon Impact Forecasting's proprietary catastrophe models to evaluate their alignment and accuracy in predicting windstorm losses.

While Chapter 5 focuses on windstorm losses observed in the past, Chapter 6 examines the possible impacts of climate change on European windstorm losses. There have been numerous studies investigating changes in European windstorm loss under climate change, using different GCMs and RCMs. However, to the best of our knowledge, no prior studies have employed RCMs derived from EURO-CORDEX to

comprehensively examine windstorm loss across the entire continent of Europe. Utilizing the EURO-CORDEX dataset presents the opportunity to attain more precise and geographically tailored insights, which are crucial for understanding the localized impacts of windstorms. Additionally, the utilization of EURO-CORDEX ensemble enables the examination of variations in windstorm losses across RCMs under GWLs +2°C and +3°C compared to the historical period. Thus, Chapter 6 addresses the second main research question of this thesis.

Research question 2 :
How does climate change affect windstorm losses across Europe based on a multi-model RCM ensemble ?

Before addressing the second main research question, the accuracy of wind gusts in the EURO-CORDEX dataset in the historical period is evaluated against reanalysis data. The added value of bias correction on EURO-CORDEX wind gust data is also examined. Subsequently, to understand the impact of climate change on windstorm losses, changes in windstorm intensity and frequency are investigated to determine how these factors influence the loss outcomes.

While the previous chapters cover windstorm losses in general, Chapter 7 focuses on the specific concern of multiple storms occurring per winter, leading to significant economic losses across Europe, a phenomenon referred to as seasonal loss clustering. The study of seasonal loss clustering is essential for insurers to meet Solvency II regulations in the EU, ensuring adequate capital for expected seasonal losses. A few studies have explored windstorm loss clustering at the country level and its changes under climate change, but without focusing on seasonal variations (Karremann et al., 2014a,b). Another study examined seasonal variations in windstorm loss clustering from an insurance perspective, but only under current climate (Priestley et al., 2018). These studies used lower-resolution reanalysis and climate model data, which may miss or misrepresent seasonal loss clustering, unlike higher-resolution data like ERA5 and EURO-CORDEX that better capture fine-scale variability and small-scale processes. In addition, the characteristics of high total seasonal losses (AEP) are not well understood, particularly in relation to seasonal loss clustering. To address these gaps, Chapter 7 investigates the third main research question of this thesis:

Research question 3 :
What are the characteristics of years with high total seasonal loss (AEP) in terms of seasonal loss clustering in a warming climate ?

To address research question 3, regional differences in seasonal loss clustering under the current climate are first explored from an insurance perspective using ERA5 data. Subsequently, changes in seasonal loss clustering under GWLs +2°C and +3°C, compared to the historical period, are analyzed using the EURO-CORDEX ensemble. The seasonal loss clustering is examined following the method in Priestley

et al. (2018), by analyzing the dominance of the maximum loss from a single event in a season (OEP) relative to the AEP through the ratio OEP/AEP.

By addressing these research questions, this study aims to provide further insights in this area of research. Firstly, comparing losses from the simple LI method and from the more complex insurance catastrophe model highlights the reliability and limitations of each approach, especially on how these approaches capture extreme or rare events. Secondly, investigating future changes in windstorm losses using the high-resolution EURO-CORDEX dataset provides more accurate and detailed regional projections, capturing fine-scale variations in windstorm intensity, frequency, and impact, thus enabling more precise risk assessments. Thirdly, understanding the characteristics of high AEP seasons in terms of seasonal loss clustering provides a clearer picture of the levels of clustering that drive large AEP seasons in a warming climate—an area that has not been thoroughly investigated in previous studies. Thus, this thesis offers valuable insights for the public and insurance companies in understanding windstorm losses under current and future climate conditions.

4. Data and methods

This chapter presents the data and methods used to obtain results from Chapter 5 to Chapter 7. This study estimates loss values from a meteorological perspective (LI) using reanalysis data and the EURO-CORDEX climate model for hazard components, combined with population density for exposure components, and compares historical loss data from LI with insurance loss data from PERILS and Aon Impact Forecasting's catastrophe model. Additionally, this chapter presents the methods used, including the calculation of losses from both meteorological and insurance perspectives, the return value analysis for investigating rare extreme losses, and the approach for examining seasonal loss clustering from an insurance perspective. Thus, this chapter lays a solid foundation for interpreting the results presented in the subsequent chapters.

4.1. Data

4.1.1. Reanalysis data

Reanalysis data are generated through data assimilation, which integrates observed data and model-based forecasts to estimate the conditions of the atmosphere, oceans, and other environmental factors (Parker, 2016). When observational data is sparse or missing, model-based forecasts help fill the gaps by simulating conditions using available data and physical laws, enabling a 3D reconstruction of weather in the past. In this study, the reanalysis data used for the extended winter period (ONDJFM) include ERA5 (Hersbach et al., 2020) and its predecessor ERA-Interim (Dee et al., 2011). From ERA5, post-processed wind gusts at 10 m height are utilized with hourly temporal and 30 km (0.25°) horizontal resolution for the period 1959-2021. From ERA-Interim, 10 m post-processed wind gust data are employed with 3-hourly temporal and 83 km (0.75°) horizontal resolution for the period 1979-2019. In both datasets, wind gusts are defined as the maximum 3-second wind at 10 m height following the definition of the World Meteorological Organization (WMO). The post-processed wind gust is the maximum gust computed in every time step using the standard deviation of the horizontal wind based on the similarity relation by Panofsky et al. (1977).

The use of reanalysis data aids in the comprehension of past weather and climate events. Among the several reanalysis datasets available, ERA5 and ERA-Interim are the preferred choices due to their high spatial resolution and extensive temporal coverage. In Chapter 5, reanalysis data (ERA5 and ERA-Interim) serve as inputs for the Loss Index (LI) methodology (section 4.2.1) to estimate windstorm

losses. Chapter 6 uses ERA5 reanalysis data (daily maximum wind gusts from 1976-2005, regridded to EURO-CORDEX resolution using conservative mapping) to correct biases in the EURO-CORDEX dataset (section 4.2.3). In Chapter 7, the original resolution of ERA5 data is used to investigate seasonal loss clustering of windstorms across Europe under current climate conditions (section 4.2.4).

4.1.2. Insurance data – PERILS

PERILS (www.perils.org) is a joint stock company, owned by ten shareholders from the insurance industry. It provides aggregated, anonymized insurance data for seven weather-related perils, including extratropical windstorms. PERILS receives data from insurance companies operating in its covered territories, including Europe, under a "Data Provider Agreement" that specifies data requirements, reporting schedules, processing procedures, and confidentiality protocols. Data provided to PERILS by insurance companies includes ultimate gross event loss and exposure data (sums insured) by country, CRESTA zone (insurance standard for geographical data; see www.cresta.org), and line of business (residential, commercial, industrial, agricultural, and motor hull), along with property premium data by country. PERILS receives this company data, anonymizes it, tests it for quality and completeness, and if deemed adequate, adds it to the existing data in the PERILS database. After receiving the data from insurance companies, PERILS uses it for estimating industry exposure and event losses. Industry exposure estimation evaluates the total insurance coverage across the market for a specific hazard, typically conducted before an event to determine the total insured value (TIV) at risk, using aggregated exposure data from companies and market property premiums. On the other hand, industry event loss estimation calculates the total losses incurred by the industry from a specific event, using aggregated company event loss data and market property premiums, and is typically performed after an event to determine the actual financial impact on the industry.

Insurance and reinsurance companies frequently rely on PERILS data as a point of reference for comprehending and quantifying windstorm losses. The provided loss figures represent the initial market losses at the time of the event. PERILS will only disclose loss information if a specific event has resulted in insured property losses exceeding a certain threshold (referred to as a 'Qualifying Event') in the covered territories. For extratropical windstorms in Europe, the loss threshold is established at EUR 500 million for events affecting the entire continent and EUR 300 million for events impacting individual countries, with values adjusted according to the currency exchange rate at the time of occurrence. Prior to September 2022, the PERILS loss threshold for extratropical windstorms in Europe was EUR 200 million for events that affected either the entire continent or individual countries. Generally, PERILS does not report any loss information for events that fall below these reporting thresholds. All storm losses listed in Table 4.2 are included in the PERILS event loss data, except for storms Daria, Erwin, Emma, Tappani, and

Isaias, which are excluded due to their time range or total loss value.

In Chapter 5, the final report of PERILS event loss data for extratropical windstorms is used, which includes aggregated loss data in euros. This study utilizes not only the PERILS event loss data but also the PERILS exposure data for the exposure component in the European Windstorm Model of Aon Impact Forecasting (Aon's IF Euro WS model) (section 4.2.2). The PERILS loss is compared to the loss from LI and the Aon's IF Euro WS model. For extratropical windstorms in Europe, PERILS provides data for markets in 12 countries: Belgium, Denmark, France, Germany, Ireland, Luxembourg, the Netherlands, the United Kingdom, Austria, Norway, and Sweden. The insurance data is supplied by PERILS on an annual subscription basis.

4.1.3. EURO-CORDEX dataset

To assess the potential impact of European windstorms in the future, we employ daily maximum surface wind gust data (12 km resolution) of 20 different general circulation model to regional climate model (GCM-RCM) chains of EURO-CORDEX. The ensemble comprises 20 members, specifically consisting of 4 RCMs, each of which is driven by 5 GCMs (Table 4.1). The simulations span the historical period (1976-2005) and the most extreme climate change scenario, specifically the RCP 8.5 scenario (2006-2100) under GWLs +2°C and +3°C. Our focus is on RCP8.5, which represents the highest emission scenario with no mitigation and anthropogenic radiative forcing of 8.5 W/m2 by 2100 (Riahi et al., 2011). We chose this scenario due to its alignment with current observed emissions (Schwalm et al., 2020). The period from 1976 to 2005 is widely recognized as a reference in climate studies, encompassing recent historical data in the late 20th and early 21st centuries (e.g., Zhu et al., 2020; Iyakaremye et al., 2021). The GWL periods (in Table 4.1) are defined individually for each of the 5 GCMs in the ensemble (Teichmann et al., 2018; Moemken et al., 2022), representing a projected increase of +2°C and +3°C in global temperature compared to pre-industrial levels. Employing EURO-CORDEX data offers several advantages, including high spatial resolution, regional specificity, and ensemble modeling (Jacob et al., 2014). This dataset provides highly detailed RCMs, enabling us to capture localized climate patterns and study their specific impacts and vulnerabilities. The use of a high-resolution 20-member ensemble helps us to assess the range of potential future climate scenarios and reduces uncertainties associated with a single model simulation. Before using the EURO-CORDEX dataset in Chapters 6 and 7, it is first bias-corrected using ERA5 reanalysis data. The bias correction method and results are detailed in Section 4.2.3.

Model consistency is used to evaluate the uncertainty and robustness of the climate change signals, following Jacob et al. (2014). Therefore, signals are defined as robust (non-robust) if more (less) than 66% of the ensemble members agree on the direction of change. This corresponds to 14 out of 20 ensemble

Table 4.1.: EURO-CORDEX (EUR-11) model chains (20 models) of daily maximum surface wind gust from the historical period (1976-2005) to future projection under RCP8.5 for GWLs +2°C and +3°C. Each GCM has 4 different RCMs. We use 1 ensemble member for each model that is r1i1p1, except for MPI-ESM-LR RACMO22E that is r12i1p1 (which depends on data availability). A-E (GCM) and 1-4 (RCM) correspond to the model codes employed in figures in appendix B. The table is reprinted from Table 1 in Alifdini et al. (2025), with copyright CC BY 4.0.

GWL +2°C	GWL +3°C	GCM	RCM
2029 – 2058	2052 – 2081	A. CNRM-CERFACS-CNRM-CM5 (Voldoire et al., 2013)	1. CLMcom-ETH-COSMO-crCLIM-v1-1 (Sørland et al., 2021)
2026 – 2055	2051 – 2080	B. ICHEC-EC-EARTH (Prodhomme et al., 2016)	2. KNMI-RACMO22E (Van Meijgaard et al., 2012)
2029 – 2058	2052 – 2081	C. MPI-M-MPI-ESM-LR (Giorgetta et al., 2013)	3. SMHI-RCA4 (Samuelsson et al., 2011)
2016 – 2045	2037 – 2066	D. MOHC-HadGEM2-ES (Martin et al., 2011)	4. MOHC-HadREM3-GA7-05 (Tucker et al., 2022)
2031 – 2060	2057 – 2086	E. NCC-NorESM1-M (Bentsen et al., 2013)	

members in this study.

4.2. Methods

4.2.1. Loss index

The Loss Index (LI) method outlined by Pinto et al. (2012) is employed to quantitatively measure the windstorm loss from a meteorological perspective (equation 4.1). In this study, the LI method computes windstorm losses using reanalysis data for current climate conditions and the bias-corrected EURO-CORDEX dataset for both current and future climate conditions.

$$LI_{\text{raw(area,24h)}} = \sum_{i=1}^{N}\sum_{j=1}^{M}\left(\left(\frac{v_{ij}}{v_{98ij}}\right)^3 \cdot I(v_{ij}, v_{98ij})\right) \cdot P_{ij} \cdot L_{ij} \tag{4.1}$$

where,

$$I(v_{ij}, v_{98_{ij}}) = \begin{cases} 1 & \text{if } v_{ij} > v_{98_{ij}} \\ 0 & \text{otherwise} \end{cases}$$

$$L_{ij} = \begin{cases} 0 & \text{if sea} \\ 1 & \text{if land} \end{cases}$$

N and M are the number of grid points. $v_{98\text{ij}}$ is the 98$^{\text{th}}$ percentile of daily maximum wind gust speed for each grid point. P_{ij} is the population density data for each grid point. By adopting the definition in

Karremann et al. (2014a), the v_{ij} is defined as the maximum wind gust within a 72-hour window (with LI calculation shifted every 6 hours) for the reanalysis data or as the maximum wind gust over a three-day period (with LI calculation shifted per 1-day window) for EURO-CORDEX, contingent upon the temporal resolution of the datasets. The LI calculation uses 2020 gridded population density data from the Centre for International Earth Science Information Network (CIESIN) at Columbia University, USA, with spatial resolutions of 5 km (for EURO-CORDEX wind data) or 30 km (for reanalysis wind data), and this data is regridded using conservative mapping to match the resolution of the wind gust dataset.

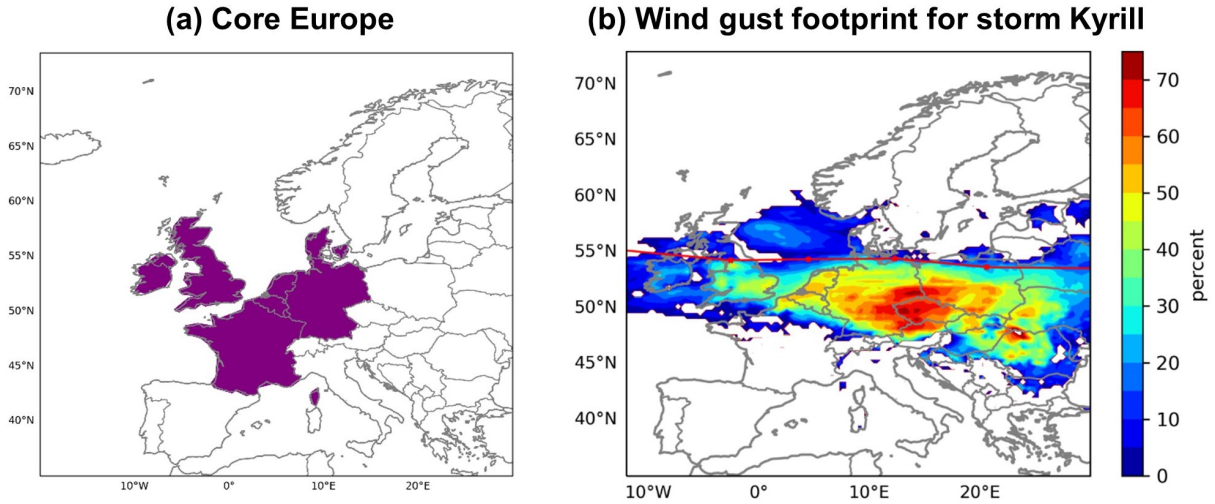

Figure 4.1.: (a) The group of countries within the Core Europe region (purple) as defined by (Pinto et al., 2012). (b) The footprint of windstorm Kyrill (2007), which significantly affected the Core Europe. Figure 4.1b is reprinted from Figure 1b in (Moemken et al., 2024a), with copyright CC BY 4.0.

In this study, the LI analysis primarily focuses on the Core Europe region, defined as a group of countries of Ireland, the United Kingdom, Belgium, the Netherlands, Luxembourg, Denmark, France, and Germany (Figure 4.1a). Core Europe was selected due to its heightened vulnerability to the substantial impacts of European windstorms, for example, as evidenced by the extensive and high-speed wind footprint of storm Kyrill in this region (Figure 4.1b). Consequently, insurance companies prioritize this region.

In Chapters 5 and 6, this study focuses on extreme storm events, considering only those with LI values above a certain threshold, which typically corresponds to an average of five storms per season (Pinto et al., 2012; Karremann et al., 2014a). It is important to note that this number does not represent an exact count of five storms per winter, but rather reflects the average number of storms per winter, independent of when they occur. Thus, Chapter 5 results in the top 205 LIs per dataset (LI ERA5 and LI ERA-Interim), calculated as 41 winters x 5 storms. For Chapter 6, LIs from 20 models across 29 winters in the historical period were compiled, identifying the top 2,900 LIs (29 winters x 20 models x 5 storms).

The threshold was set as the minimum value within these top 2,900 LIs, which was then used to evaluate changes in LIs and storm frequency under different GWLs relative to the historical period. In Chapter 7, LIs from those above a threshold were analyzed. For events above the threshold, the top 62 winters x 10 storms (for ERA5) and 580 winters x 10 storms (for EURO-CORDEX) were used. A threshold of 10 storms on average per season was chosen to capture more events, as using only 5 storms may result in low and insufficient LI values for several seasons, which is inadequate for investigating seasonal variations in loss clustering. Note that this involves the top storms based on LI values rather than exactly 10 storms per season.

In Chapter 5, the storm names associated with each LI value derived from reanalysis data are identified using weather charts from the Institut für Meteorologie at Freie Universität Berlin (Wetterkarte eV and Wetterdienst, 1999) (https://www.met.fu-berlin.de/wetterpate/archiv.html). However, this website only provides information on European windstorms from 1999. Thus, for the years prior to 1999, we refer to the websites of the Extreme Windstorm catalog (http://www.europeanwindstorms.org/cgi-bin/storms/storms.cgi) (Roberts et al., 2014).

Wind footprints were created from reanalysis data for Chapter 5, following the WMO guidelines and Haylock (2011). Thus, for each 72-hour period for a given grid point, when the maximum wind gust value ($v_{\max}$) exceeds the local 98$^{\text{th}}$ percentile (v_{98}), the footprint is defined in equation 4.2.

$$\text{wind gust footprint} = \left(\frac{v_{\max} - v_{98}}{v_{98}} \right) \times 100\%, \tag{4.2}$$

The corresponding cyclone tracks in Chapter 5 were derived following the tracking algorithm by Murray and Simmonds (1991) and Pinto et al. (2005). As an example, Figure 4.1b shows the footprint and cyclone track for windstorm Kyrill in January 2007 (Moemken et al., 2024a).

4.2.2. Aon Impact Forecasting European Windstorm Model

The European Windstorm Model of Aon Impact Forecasting (Aon's IF Euro WS model), implemented in ELEMENTS, Aon's loss modelling platform, is used (Aon, 2023; Moemken et al., 2024a). The model covers 22 countries in Western, Northern, and Central Europe. The aim of this catastrophe model is to provide a quantification of financial losses from windstorm risk in Europe. As partially discussed in Chapter 2 (section 2.3.2), the catastrophe model used in this study, the Aon's IF Euro WS model, estimates windstorm loss through three main components—hazard, vulnerability, and exposure—along with a financial component (Figure 4.2). The hazard component has two parts: a historical and a stochastic event set. The historical event set comprises 26 historical storms (see Table 4.2; Born et al., 2012), based on wind gust footprints built from weather station data. The stochastic event set covers 4,731 years of simulated events (Karremann et al., 2014a). The stochastic events represent physically consistent storm

events and are based on outputs of the ECHAM 5 general circulation model (Jungclaus et al., 2006). A combination of dynamical downscaling and statistical downscaling (Haas and Pinto, 2012) is used to produce the final high-resolution stochastic event set that is implemented in Aon's IF Euro WS model. The exposure component typically uses a combination of Aon's client data and the PERILS industry exposure database. The component comprises five lines of business: residential, commercial, industrial, agricultural, motor, and forestry (only Norway, Sweden, and Finland). For the purposes of this study, the exposure component only uses PERILS data from 2022. The vulnerability component is divided into Chance of Loss (COL) and Conditional Mean Damage Ratio (CMDR), thereby giving a more realistic view of loss than a single mean damage ratio. The COL is applied first, rating the probability of loss for a certain wind speed and a given building. If the building is determined to have suffered a loss, then the conditional damage ratio (CMDR) is applied. The vulnerability component of the model applies IF's proprietary damage curves to calculate the physical loss for each event at each insured location. Original limits and other policy conditions are then applied per event to calculate the gross loss and the net loss, thus obtaining the value of the insured loss in the financial component of the model.

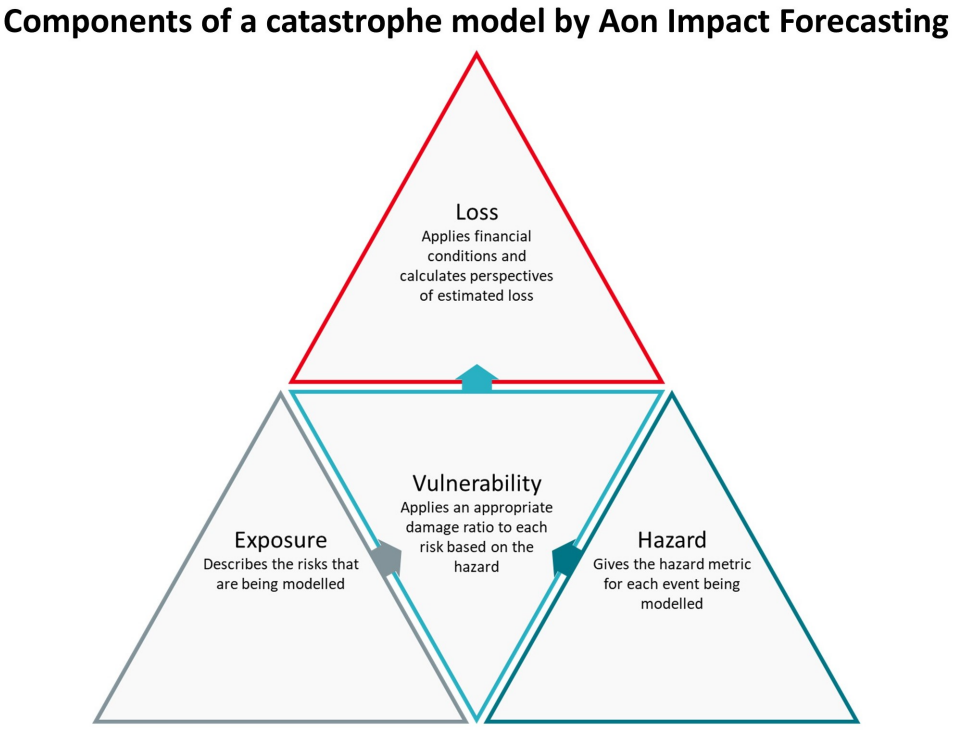

Figure 4.2.: Catastrophe model flow diagram of Aon Impact Forecasting (an insurance company). The figure is reprinted from Figure 2 in Supplementary File Part A of Moemken et al. (2024a), with copyright CC BY 4.0.

Table 4.2.: Historical event set of insured winter windstorms in Aon's IF Euro WS model in the period 1990-2020, including storm name and event date (as yyyy-mm-dd). The table is reprinted from Table S1 in Moemken et al. (2024a), with copyright CC BY 4.0.

Storm	Date
Daria	1990-01-25
Anatol	1999-12-03
Lothar	1999-12-26
Martin	1999-12-27
Jeanett	2002-10-27
Erwin	2005-01-07
Kyrill	2007-01-16
Emma	2008-03-01
Klaus	2009-01-24
Xynthia	2010-02-27
Tappani	2011-12-26
Christian	2013-10-26
Xaver	2013-12-04
Dirk	2013-12-23
Tini	2014-02-12
ElonFelix	2015-01-08
MikeNiklas	2015-03-31
Thomas	2017-02-23
Zeus	2017-03-06
Xavier(2017)	2017-10-06
Herwart	2017-10-29
Eleanor	2018-01-02
Friederike	2018-01-18
Isaias	2019-02-08
Eberhard	2019-03-10
Sabine	2020-02-09

Financial losses in the model are calculated using hazards, exposure, and vulnerability components, with the loss units dependent on the exposure data; if PERILS exposure data in euros is used, the losses will be in euros. In the ELEMENTS platform, loss calculations are performed by running a historic or stochastic model on an imported portfolio, with users setting output conditions like return periods for stochastic models. ELEMENTS uses random number generation to assign hazard values to each risk, drawing from model distributions. The model applies vulnerability functions to calculate the Ground Up (GU) loss by selecting a damage bin and applying its ratio to the Total Insured Value (TIV), then adjusts for financial conditions like deductibles to determine the Gross loss. In the historic model, the primary output is an Event Loss Table (ELT) that lists GU and gross losses per event, either as mean values or individual sample losses. In the stochastic model, the Occurrence Exceedance Probability (OEP) curve is generated by ranking the maximum annual losses from the ELT, while the Annual Exceedance Probability (AEP) curve is similarly created using total annual losses, with both curves calculated through frequency analysis and interpolation to determine losses at specific return periods. The loss that is used

in Chapter 5 is the loss from the historic model.

The Aon's IF Euro WS model is calibrated against insurance data, including PERILS data as the primary benchmark. For this reason, it is assumed that the model represents a market perspective of loss. A more detailed description of the model can be found in Supplementary Part A of the paper by Moemken et al. (2024a). For proprietary reasons, the comparison to LI is restricted to losses at the country level and normalized loss values. In Chapter 5, losses from Aon's IF Euro WS model are compared with those from LI (section 4.2.1) and the final event loss report from PERILS data (section 4.1.2) to provide a comprehensive view of losses from different perspectives.

4.2.3. Bias correction of wind gusts

The evaluation of the historical EURO-CORDEX simulations uncovered substantial biases for wind gusts compared to ERA5 (see Section 6.1.). Since these biases, especially the ones at the tail of the wind gust distribution, may influence the climate change signal for windstorm impacts, a bias correction is applied to the daily maximum wind gusts from the historical and RCP8.5 simulations. The aim is to improve accuracy and remove errors while additionally ensuring the coherence of the multi-model ensemble (Cannon et al., 2020).

Four different bias correction methods were tested, namely Normal Distribution Mapping, Empirical Quantile Mapping, Empirical Robust Quantile Mapping, and Quantile Mapping with Linear Transformation Function. A detailed description of the different methods can be found in Qian and Chang (2021). For the specific case in this study, the Empirical Quantile Mapping proved to be the most effective, as it successfully corrects the bias in the EURO-CORDEX ensemble, even for extreme wind gusts (values exceeding the 98th percentile).

The bias correction using Empirical Quantile Mapping is carried out by aligning the quantiles of the entire distribution of daily maximum surface wind gusts of EURO-CORDEX in the historical period with those derived from ERA5 reanalysis data (1976-2005) (Boé et al., 2007; Gudmundsson et al., 2012; Gudmundsson, 2016; Li et al., 2019). The empirical quantile mapping is a widely used bias correction method that here involves adjusting quantiles of EURO-CORDEX in the historical period to coincide with ERA5 quantiles, employing cumulative distribution functions (CDFs) and mapping climate model quantiles to ERA5 quantiles (equation 4.3).

$$x_{\text{CORDEX, hist corr}} = F^{-1}_{\text{ERA5}}\left(F_{\text{CORDEX, hist ori}}\left(x_{\text{CORDEX, hist ori}}\right)\right) \tag{4.3}$$

where:

- $x_{\text{CORDEX, hist corr}}$ is the bias-corrected model.
- F^{-1}_{ERA5} is the inverse CDF of the ERA5 data.
- $F_{\text{CORDEX, hist ori}}$ is the CDF of the original model data.
- $x_{\text{CORDEX, hist ori}}$ is the original model data.

For each grid point, the CDF of ERA5 reanalysis data and model data in the historical period (1976-2005) are initially computed at regularly spaced quantile levels (0, 0.01, 0.02, ..., 0.99, 1.00). Subsequently, linear interpolation is employed to derive quantile values for levels not explicitly listed. The correction function derived from the correction of the model in the historical period is applied to adjust future projection model data (Qian and Chang, 2021).

For this study, the ERA5 reanalysis data was chosen for the bias correction due to the limited number of available gridded observational wind gust data (Moemken et al., 2018; Michel and Sorteberg, 2023). ERA5 was selected because of its good representation of near-surface winds compared to other available reanalysis datasets (Ramon et al., 2019) and its high spatial resolution and recent data.

4.2.4. Seasonal loss clustering

The seasonal clustering of windstorm loss was estimated by calculating the ratio of OEP (Occurrence Exceedance Probability, representing the maximum LI in a season) to AEP (Annual Exceedance Probability, indicating the total LI in a season) (refer to equation 4.4) for each season (Priestley et al., 2018).

$$\frac{\text{OEP}}{\text{AEP}} \approx low \tag{4.4}$$

A lower ratio indicates the presence of multiple destructive windstorms within a season. Conversely, a higher ratio suggests that the season is dominated by a single large event, indicating that it is not a loss clustering season. How low and how high this OEP/AEP ratio is for seasonal loss clustering will be examined further in Chapter 7. Note that the clustering in this study is from an insurance perspective and does not analyze clustering in the meteorological sense (i.e., based on dispersion statistics) (Mailier et al., 2006; Karremann et al., 2014a,b).

4.2.5. Return value analysis

For the analysis of the rare extreme loss, the return value analysis is employed to obtain information regarding the recurrence interval of this rare extreme loss. The extensive EURO-CORDEX dataset allows

us to examine return levels for longer periods, with up to 580 winters available for analysis (20 models x 29 winters). The return value analysis is represented by the return level for the given return period in years. In Chapter 6, the return period refers to the average time between losses of a particular magnitude, while the return level represents the magnitude of the loss that is expected to be exceeded within a specified return period. Return value analysis is conducted both empirically and using Generalized Pareto Distribution (GPD) fitting (Coles et al., 2001; Lemos et al., 2020), with comparisons between empirical values and GPD fits to assess how well the theoretical GPD model matches the observed data.

In this analysis, only the most extreme LIs are used when the GPD fit reaches stability. Thresholds are first defined to determine the number of top LIs for the analysis by checking the mean excess, which is the average difference between LIs and the threshold when LIs exceed it (not shown). A linear pattern in the plot of thresholds versus mean excesses at higher threshold values indicates that excesses can be well-modeled by a GPD and that the mean excess function is stable in this range. For example, the stability of the GPD fit is reached using the top 81 LIs for Core Europe and top 90 LIs for Eastern Europe for each period. Since the same number of events is used for all periods, the threshold (u) differs between GWLs and the historical period; for the return value analysis, stability in top LIs across periods is ensured to allow for valid comparison.

Before fitting the GPD, the return value is first calculated empirically. Firstly, the top LIs are sorted in ascending order. Secondly, the probability of exceedance (p) is calculated using equation 4.5.

$$p = \frac{i}{n+1} \tag{4.5}$$

where i represents the rank of LI in ascending order. n is the number of top LIs. Thirdly, the empirical return period $\mathrm{RP_{emp}}$ is calculated using equation 4.6.

$$\mathrm{RP_{emp}} = \frac{1}{ny \times (1-p)} \tag{4.6}$$

where: *ny* is the block size, defined as the ratio of 580 winters to the number of top LIs. The empirical return level $\mathrm{RL_{emp}}$ for the given $\mathrm{RP_{emp}}$ is the value of each top LIs.

After calculating the empirical return period, the top LIs are fitted to the GPD, which models excesses over a threshold using the Peaks Over Threshold (POT) method, focusing on the tail of the distribution. The values of the return period for GPD were defined first ($\mathrm{RP_{GPD}}$), ranging from the minimum to the maximum $\mathrm{RP_{emp}}$ with a step size of 0.1. Afterwards, the Return Level for GPD fit ($\mathrm{RL_{GPD}}$) was com-

puted for each defined RP_{GPD} (equation 4.7).

$$RL_{GPD} = u + \frac{\sigma}{\xi}\left((RP_{GPD} \cdot ny)^{\xi} - 1\right) \tag{4.7}$$

where: σ represents the scale parameter and ξ represents the shape parameter, both of which are estimated using maximum likelihood estimation (MLE).

The confidence level of GPD is estimated using the delta method with an alpha of 0.05, corresponding to a 95% confidence interval. Following the fitting of the GPD to the top LIs, the goodness of fit was evaluated by comparing the sample distribution to the theoretical GPD fit using probability density functions, cumulative distribution functions, and quantile-quantile and probability-probability plots (not shown).

To examine the recurrence interval of seasonal loss clustering in Chapter 7, this study conducts the return value analysis using only empirical methods, as the focus is not on rare extreme events but on the seasonal variation of loss clustering. This analysis uses OEP, AEP, and the OEP/AEP ratio, employing the same method as in Chapter 6, with the following modifications:

- The RL_{emp} corresponds to OEP, AEP, and their ratio OEP/AEP.

- The time series of OEP, AEP, and their ratio OEP/AEP are utilized, with 62 data points (ERA5) and 580 data points (EURO-CORDEX), or one datum per winter.

- For the OEP/AEP ratio in the first step, the ratio values are sorted in ascending order based on the AEP values.

- n equal to 62 (ERA5) and 580 (EURO-CORDEX)

- ny equal to 1

5. Insurance loss model vs meteorological loss index - How comparable are their loss estimates for European windstorms?

Large parts of this chapter are based on :
Moemken, J., Alifdini*, I., Ramos, A. M., Georgiadis, A., Brocklehurst, A., Braun, L., and Pinto, J. G. 2024a. Insurance loss model vs. meteorological loss index – how comparable are their loss estimates for European windstorms?, Nat. Hazards Earth Syst. Sci., 24, 3445–3460. https://doi.org/10.5194/nhess-24-3445-2024.*
**These authors contributed equally to this work*

This chapter aims to address the research gaps and questions outlined in Chapter 3. Firstly, the sensitivity of loss estimates of the Loss Index (LI) to different meteorological input data was analyzed. Secondly, the windstorm loss estimate from LI was compared to that from an insurance loss model. With this aim, the LI by Pinto et al. (2012) in the adaptation of Karremann et al. (2014a) is calculated using ERA5 (Hersbach et al., 2020) and its predecessor ERA-Interim (Dee et al., 2011). In a second step, the loss estimates from LI are compared to the output of an insurance loss (catastrophe) model for a set of historical European windstorms. Here, for the first time in a scientific study, the European Windstorm Model of Aon Impact Forecasting (in the following Aon's IF Euro WS model) is used. The differences and similarities were analyzed, focusing on the loss values and storm rankings of individual events. The study is restricted to 11 European countries covered by the model (see Figure 5.1) and the extended winter season October–March (ONDJFM).

This chapter is organized as follows: Section 5.1 focuses on the sensitivity of LI to different reanalysis datasets, while Section 5.2 presents the comparison between LI and Aon's IF Euro WS model. Section 5.3 concludes this chapter with a summary and discussion of results.

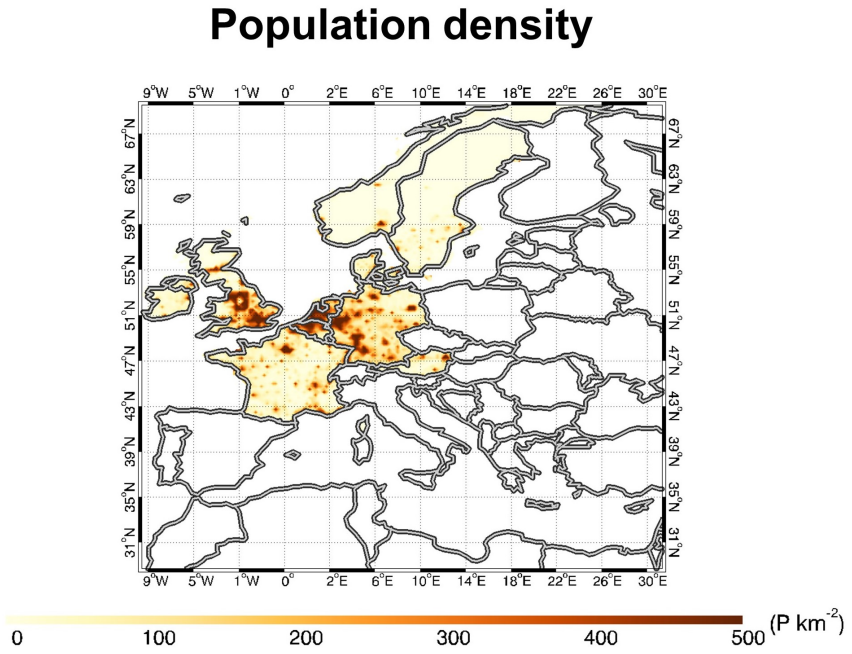

Figure 5.1.: Population density for 2020 was derived from CIESIN for the 11 countries covered in this study. The figure is reprinted from Figure 1a in Moemken et al. (2024a), with copyright CC BY 4.0.

5.1. Comparison between ERA5 and ERA-Interim

First, the sensitivity of the LI to meteorological input data is analyzed. To this end, the ERA5 and ERA-Interim datasets are compared with regard to wind gusts, which serve as the relevant input variable for the LI. Subsequently, both datasets are employed to derive the LI for the study domain, and the results are compared in relation to storm loss and storm ranking.

5.1.1. Wind gust climatology

The 98th and 99.9th percentiles of daily maximum wind gust are compared between ERA5 and ERA-Interim. The percentiles are calculated for the winter half year ONDJFM for 1979-2019, the period common to both datasets. Figure 5.2 shows both percentiles for ERA5 (left) and ERA-Interim (middle), as well as the absolute difference between the datasets (right). For the 98th percentile (Figure 5.2, upper row), both datasets show a similar spatial pattern: For most of Europe, the 98th percentile ranges between 16 and 30 m/s, with the highest values over the North and Baltic Sea and the British Isles. Except for Sweden and the Baltic region, values are in general higher for ERA5 compared to ERA-Interim. Differences reach the highest values (over 4 m/s) over mountainous regions like the Alps, the Pyrenees, and the Scandinavian mountains, while they are in the range of 2 m/s for Core Europe. This suggests a slight shift towards higher gust speeds in the wind gust distribution of ERA5 compared to ERA-Interim for large parts of Central Europe. For the 99.9th percentile (Figure 5.2, lower row), differences between the

datasets are larger for all of Europe– not only in terms of magnitude but also regarding the spatial pattern. This confirms the overall shift in the wind gust distribution but also indicates a longer tail of the wind gust distribution for ERA5 over continental Europe. Differences result most likely from the different ECMWF model version used for the reanalysis and the overall better representation of resolution and physical processes in the ERA5 setup (see Hersbach et al. (2020) for detailed information).

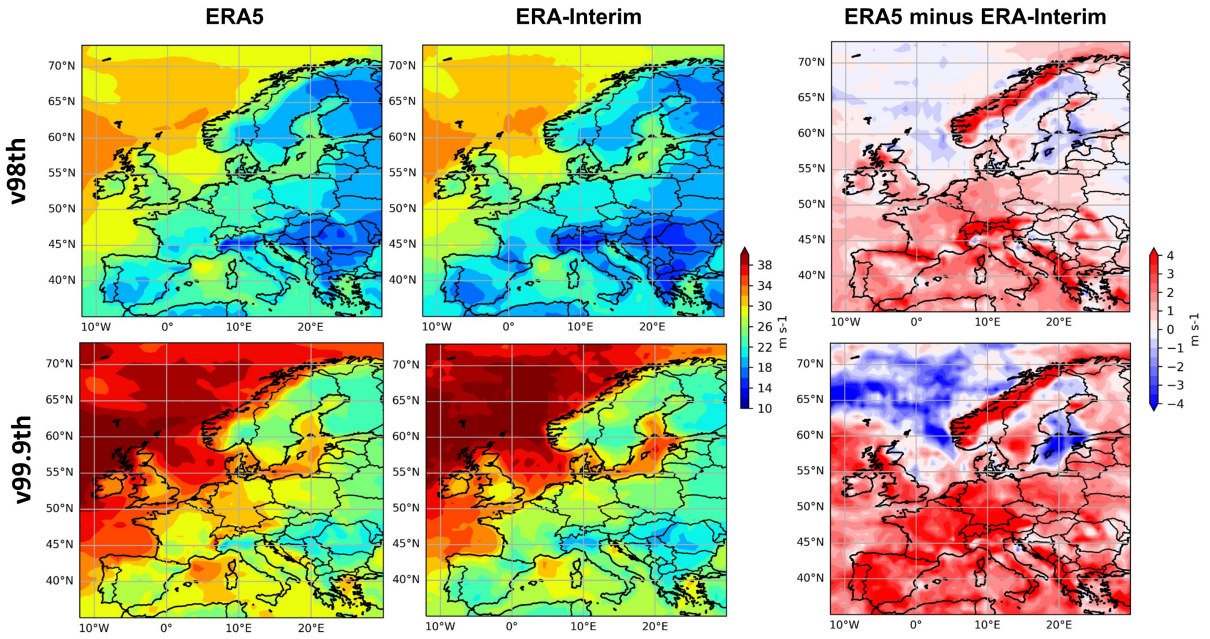

Figure 5.2.: 98th percentile (upper row) and 99.9th percentile (lower row) of daily maximum wind gust for the winter half year (ONDJFM) for the period 1979-2019 derived from ERA5 (left) and ERA Interim (middle). Difference between ERA5 minus ERA Interim (right). The figures (a-c) are reprinted from Figure 2 in Moemken et al. (2024a), with copyright CC BY 4.0.

5.1.2. Storm losses and storm ranking

In the next step, the loss values and the storm ranking for the 20 common most extreme storms (Top 20) in the period 1979-2019 are compared. The Top20 storms are derived separately for each country as well as for Core Europe. The storm list for Core Europe can be found in Appendix Tables A.1 and A.2. Figure 5.3 presents the comparison of normalized loss values derived from LI ERA5 (x-axis) and LI ERA-Interim (y-axis) for four different regions/countries, namely Core Europe, the United Kingdom, Germany, and France. For most events and countries, the datasets show comparable normalized losses. Moreover, the ratio between extreme storms with high losses to extreme storms with moderate losses is similar in both datasets. This is confirmed by the fact that most events are grouped closely around the linear regression line. Only storm Irina (October 2002) is classified as an outlier for the UK, i.e., that the difference in loss value is large based on the Inter-Quartile Range (IQR; Dodge (2008)). The large differ-

ence between ERA5 and ERA-Interim for storm Irina can be explained by looking at the storm footprint (Figure A.1): It is overall flatter in ERA5 compared to ERA-Interim. This is particularly the case for the UK, where the mean wind gust over land is 12.1 m/s for ERA5 and 24.6 m/s for ERA-Interim. Therefore, the LI for storm Irina is higher in ERA-Interim due to the cumulative effect (summation of v/v98; see Section 2.3.1).

When comparing the original loss values (Appendix Figure A.2), the values based on ERA5 are approximately 10 times larger than those for ERA-Interim. The most obvious reason is the higher spatial resolution of ERA5 compared to ERA-Interim (roughly 3 times higher): As LI sums over all grid points with wind gusts above the 98^{th} percentile, a higher number of grid points results in an overall higher value of LI. This is confirmed by a sensitivity study, in which we re-gridded ERA5 data to the coarser ERA-Interim resolution before calculating LI (Appendix Figure A.3). After re-gridding, LI ERA5 and LI ERA-Interim are in the same order of magnitude, while the overall behaviour/order of storms does not change (cp. Figures A.2 and A.3). The main reason for the remaining differences between LI ERA5 and LI ERA-Interim is most likely the shift towards higher gust speeds and the longer tail in the wind gust distribution of ERA5 compared to ERA-Interim, as discussed in Section 5.1.1.

The comparison of storm ranks between LI ERA5 and LI ERA-Interim is presented in Figure 5.4. Differences are generally larger than for the loss values. This is confirmed both by a higher number of outlier storms in individual countries such as France and by an overall larger spread of events along the linear regression line.

In general, LI ERA5 and LI ERA-Interim show a good agreement. This is supported by overall high Spearman's rank correlation coefficients (Spearman, 1904; Dodge, 2008), which we computed to quantify and map the differences between the datasets across countries. In addition to the value of Spearman's rank correlation, which measures the strength and direction of the relationship, we use the R^2 of Spearman's rank correlation that indicates the proportion of variance in the ranks of one variable that is predictable from the ranks of the other variable. For most countries, the correlations between LI ERA5 and LI ERA-Interim exceed 0.5, thereby confirming the good agreement between the datasets (Figure 5.5). Moreover, more than half of the countries have R^2 values above 0.40, indicating that more than 40% of the variance in the ranks of LI ERA5 is explained by the variance in the ranks of the LI ERA-Interim (Table 5.1). Based on these results, we focus only on LI ERA5 in the following chapter in order to benefit from the higher spatial and temporal resolution and the more recent data.

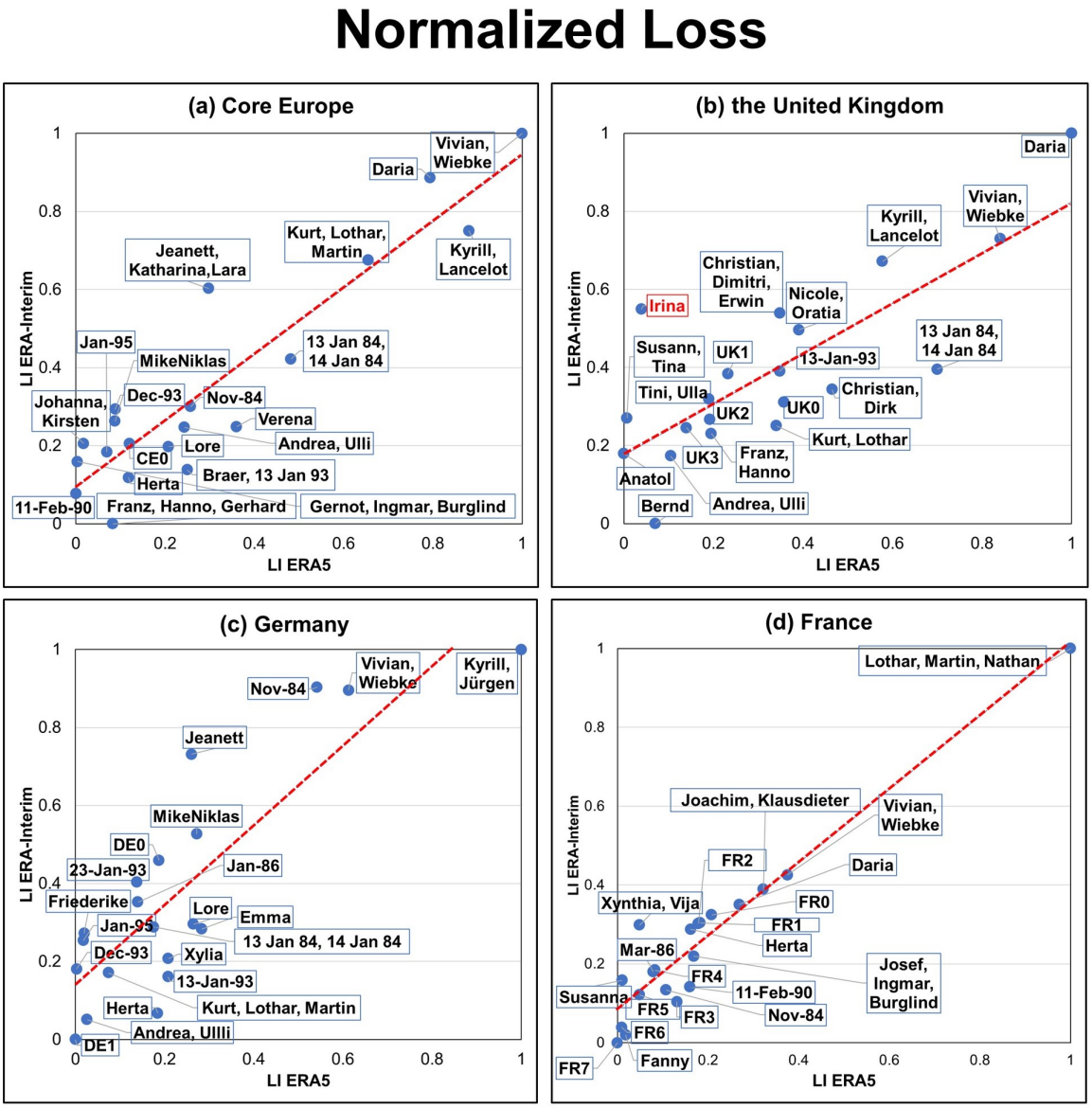

Figure 5.3.: Comparison of normalized loss values based on LI ERA5 (x-axis) and LI ERA Interim (y-axis). Depicted are the common 20 most extreme storms in the period 1979-2019 for (a) Core Europe, (b) the United Kingdom, (c) Germany, and (d) France. Corresponding storm names to each data point are marked with a blue line. Storms without a formal name are named based on the region (e.g. CE for Core Europe) and the loss value (starting from zero for storms with highest loss). The red dashed line denotes the linear regression line. Outlier storms based on the IQR method (see section 5.1.2) are marked in red. The figure is reprinted from Figure 3 in Moemken et al. (2024a), with copyright CC BY 4.0.

5.2. Comparison of loss estimates from LI ERA5 and Aon's IF Euro WS model

In the second part of this study, the output from Aon's IF Euro WS model is compared to LI ERA5, with a focus on normalized losses and storm ranks at the country level. PERILS loss data is also used for comparison. The analysis is based on Aon's historical event set of insured storms in the period 1990-2020 (see Table 4.2). Thus, the number of common storms between Aon's IF Euro WS model and LI

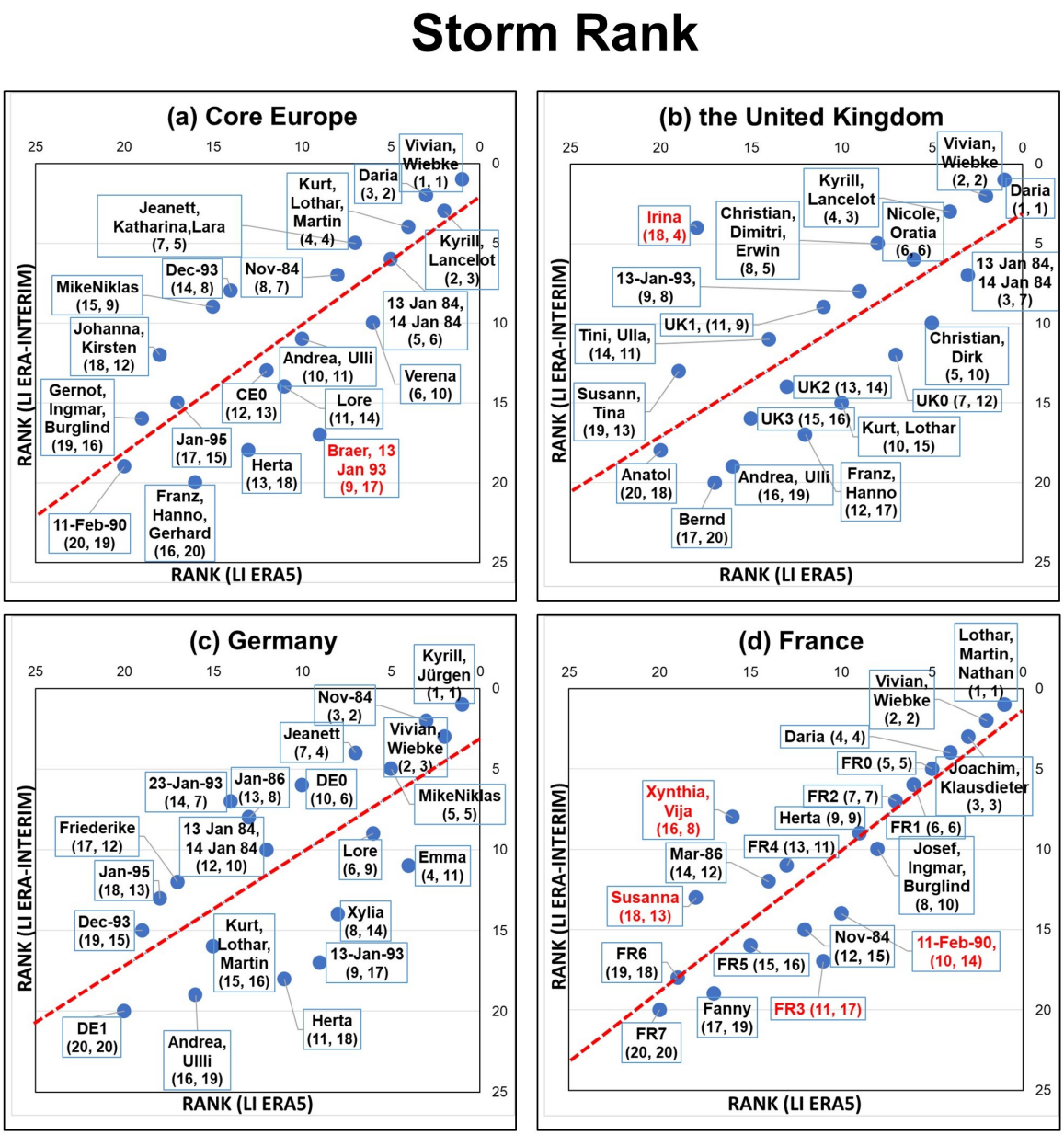

Figure 5.4.: Same as Figure 5.3, but for the comparison of storm ranks. The values in brackets indicate the rank (first value ERA5, second value ERA Interim). The figure is reprinted from Figure 4 in Moemken et al. (2024a), with copyright CC BY 4.0.

ERA5 can differ in the individual countries (see Table 5.1 and Appendix Figure A.4). Please note that some events cannot be clearly separated based on LI ERA5 (e.g., Lothar and Martin; see Figure 5.3 and Table A.1), while they are single events in Aon's IF Euro WS model. In these cases, the same LI value is assigned to both storm events for the comparison between LI ERA5 and Aon's IF Euro WS model.

Table 5.1.: Explained variance (R^2) of Spearman's rank correlation coefficient between LI ERA5 and LI ERA-Interim (2nd column), LI ERA5 and Aon's IF Euro WS model (3rd column), LI ERA5 and PERILS (4th column), and Aon's IF Euro WS model and PERILS (last column). The number of common storms per country is indicated in brackets. The table is reprinted from Table 5.1 in Moemken et al. (2024a), with copyright CC BY 4.0.

Region	LI ERA5 vs ERA-Interim	LI ERA5 vs Aon's IF Euro WS	LI ERA5 vs PERILS	Aon's IF Euro WS vs PERILS
Core Europe	0.65 [20]	0.52 [23]	0.26 [17]	0.57 [19]
Austria	0.43 [20]	0.75 [15]	1.0 [4]	1.0 [4]
Belgium	0.62 [20]	0.22 [21]	0.09 [11]	0.66 [11]
Denmark	0.25 [20]	0.41 [15]	0.49 [5]	0.14 [6]
France	0.79 [20]	0.6 [17]	0.56 [10]	0.54 [11]
Germany	0.5 [20]	0.57 [23]	0.33 [15]	0.47 [15]
Ireland	0.37 [20]	0.2 [19]	0.49 [5]	0.64 [5]
Luxembourg	0.64 [20]	0.26 [15]	0.07 [6]	0.43 [6]
Netherlands	0.2 [20]	0.64 [21]	0.68 [11]	0.7 [11]
Norway	0.29 [20]	0.4 [9]	0.25 [3]	1.0 [3]
Sweden	0.51 [20]	0.23 [13]	1.0 [4]	0.16 [4]
United Kingdom	0.49 [20]	0.36 [20]	0.44 [13]	0.7 [13]

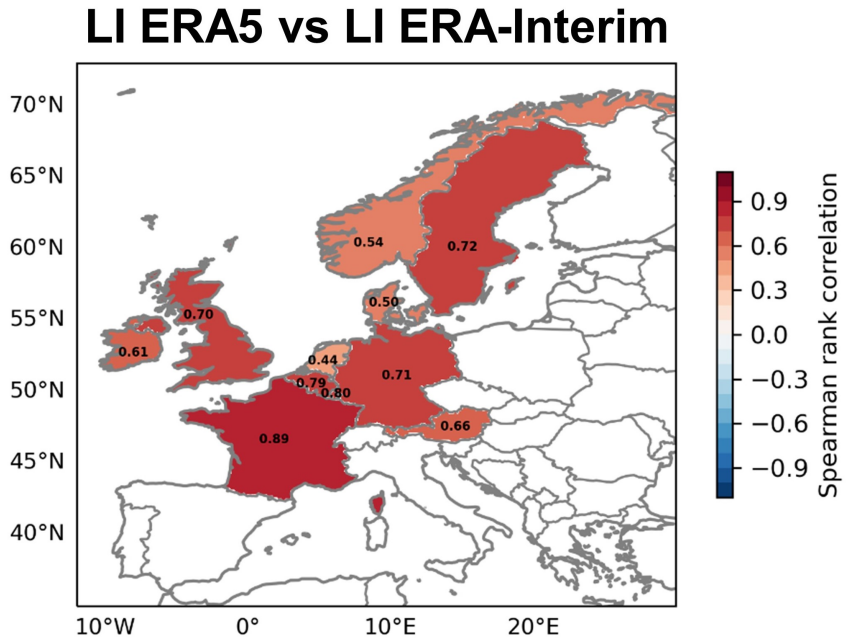

Figure 5.5.: Spearman's rank correlation coefficient at the country level for LI ERA5 vs. LI ERA-Interim. The ranking is based on common storms per country. The figure is reprinted from Figure 5 in Moemken et al. (2024a), with copyright CC BY 4.0.

5.2.1. Case study – Storm Sabine

First, one case study is analysed in detail, namely storm Sabine that hit Europe in February 2020. The normalized losses (relative ranking) and storm ranks (ordinal ranking) are compared at the country level, additionally including PERILS as a reference (Figure 5.6). All three datasets agree with regard to the

region affected by the storm, which closely follows Sabine's cyclone track (black line and dots in the left column of Figure 5.6). However, the normalized loss values can differ significantly in the three datasets. Values are generally higher for LI ERA5 for all countries, except for Norway, where all datasets show the same normalized loss. Aon's IF Euro WS model and PERILS show a good agreement in terms of the relative ranking of storm Sabine in the different countries. In terms of the ordinal ranking (Figure 5.6, lower row), Sabine is among the Top 6 storms in all three datasets. However, while the ranking for Aon's IF Euro WS model and PERILS differs by no more than one position, differences are larger between LI ERA5 and Aon's IF Euro WS model/PERILS and can reach up to five positions, e.g., for the UK. In general, the agreement/disagreement between LI ERA5 on one hand and Aon's IF Euro WS model/PERILS on the other hand is different for each country, and systematic differences are not apparent. Nevertheless, the results suggest that LI ERA5 might have difficulties in clearly distinguishing individual storms from one another, i.e. that the loss values of the most extreme events are too close together. This will be examined in more detail in the following sections.

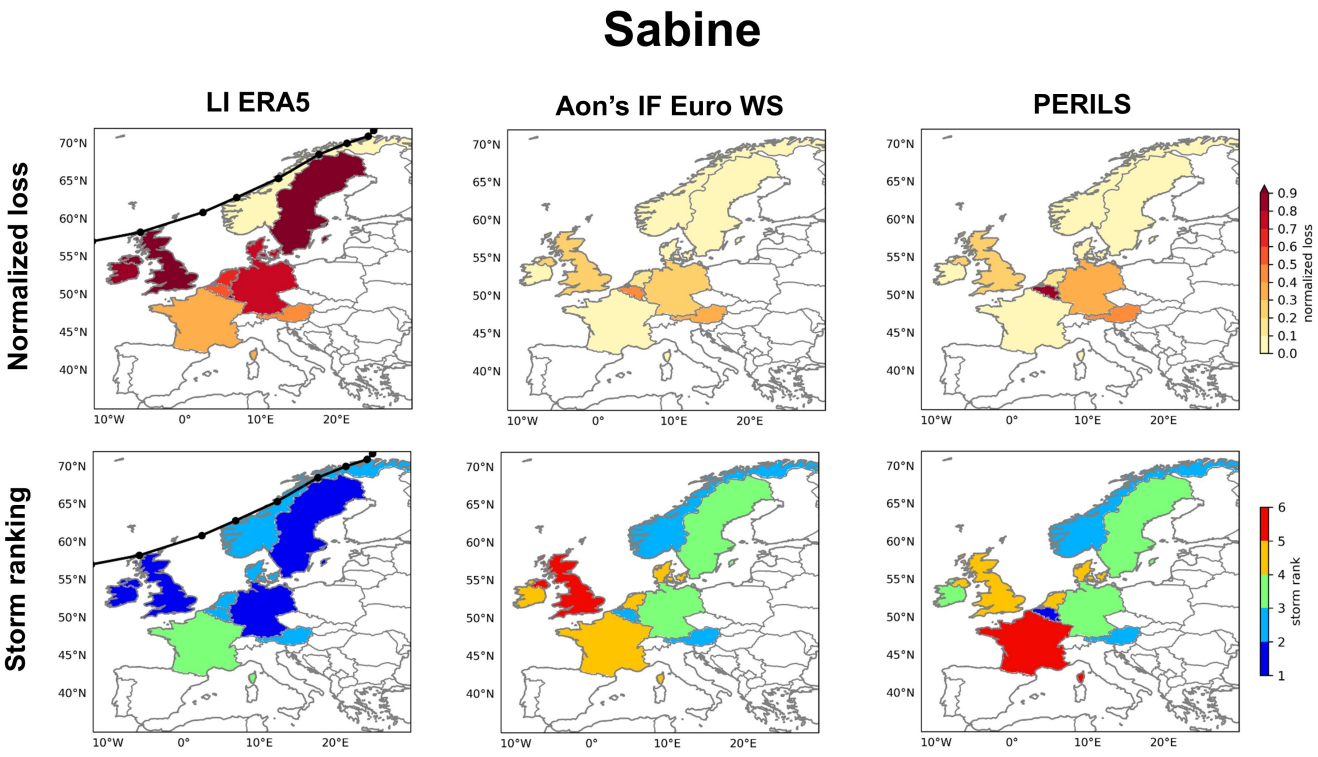

Figure 5.6.: Normalized losses (upper row) and storm ranking (lower row) at the country level for storm Sabine in February 2020. Losses are derived from LI ERA5 (left), Aon's IF Euro WS model (middle), and PERILS (right). The black line and dots in the left column denote the cyclone track derived from ERA5 using the tracking algorithm of Pinto et al. (2005). Losses are only shown for the 11 countries covered by Aon. The ranking is based on common storms per country (see Table 5.1). The figure is reprinted from Figure 6 in Moemken et al. (2024a), with copyright CC BY 4.0.

5.2.2. Windstorm loss

In this section, we compare the normalized loss values derived from Aon's IF Euro WS model (x-axis) and LI ERA5 (y-axis) for all common storms for four different regions/countries: Core Europe, the United Kingdom, Germany, and France (Figure 5.7). In general, the two datasets reveal large differences. Only individual storm events like Daria in January 1990 or Kyrill in January 2007 show comparable normalized losses. This is supported by a rather large spread of storm events along the regression line (Figure 5.7). Nevertheless, only a small number of storms are identified as outliers based on the IQR method– for example, Sabine in Core Europe or Martin in France. For LI ERA5, the range of loss values is quite similar between larger regions like Core Europe and smaller regions (individual countries). Aon's IF Euro WS model, on the other hand, reveals a different range of loss values for different regions. Within individual regions, Aon's IF Euro WS model shows a clear distinction between extreme "high loss" storm events such as Daria and those events with "moderate" losses (e.g., Isaias). Normalized loss values between those events can differ by a factor of up to 1000 for single countries. This distinction is less pronounced in LI ERA5 (see e.g., Figure 5.7b), where the individual storm events are closer together and usually differ by a factor of less than 100 in terms of their respective normalized loss. Such differences are not uncommon when comparing loss datasets (Moemken et al., 2024b).

In a sensitivity study, we tested whether the differences between LI ERA5 and Aon's IF Euro WS model result from the different event definitions– 72-hour periods vs. 24-hour periods. With this aim, we calculated LI ERA5 for running 24-hour windows. The comparison of normalized loss values is shown in Appendix Figure A.5 (see Figure A.6 for storm ranks). Overall, we find no systematic reduction in the differences between LI ERA5 and Aon's IF Euro WS model when using 24-hour windows instead of 72-hour windows. For some storms and/or countries, differences decrease with a shorter event definition (e.g., for Germany), while for others they increase (e.g., Core Europe). Moreover, the number of common storm events decreases with a shorter event definition for LI ERA5 (not shown).

5.2.3. Storm ranking

LI ERA5 and Aon's IF Euro WS model are also compared in terms of storm ranks for the common most extreme storms per country. Figure 5.8 shows this comparison for Core Europe, the UK, Germany, and France. As for the normalized losses, rather large differences between the datasets are observed, though less pronounced. Most events show rank differences in the range of zero to three positions. Only in the case of individual storms, such as Klaus in Core Europe or Martin in Germany, can rank differences reach up to 16 positions. These events are also marked as outliers based on the IQR method.

Figure 5.7.: Comparison of normalized loss values between Aon's IF Euro WS model (x-axis) and LI ERA5 (y-axis). Depicted are the common most extreme storms for the period 1990-2020 for (a) Core Europe, (b) the United Kingdom, (c) Germany, and (d) France. A logarithmic scale is used for the axes. The red dashed line denotes the logarithmic regression. Outlier storms based on the IQR method are marked in red. Please note the different scales. The figure is reprinted from Figure 7 in Moemken et al. (2024a), with copyright CC BY 4.0.

Finally, the Spearman's rank correlation coefficients (Figure A.6) and the corresponding explained variance (R^2; Table 5.1) are compared, again including PERILS as a reference. Figure A.6 displays the correlation coefficients for each country, providing a clear depiction of the agreement or disagreement between LI ERA5, Aon's IF Euro WS model, and PERILS. For most parts of Central Europe, LI ERA5 and Aon's IF Euro WS model show a high agreement, with correlation values reaching up to 0.86 for

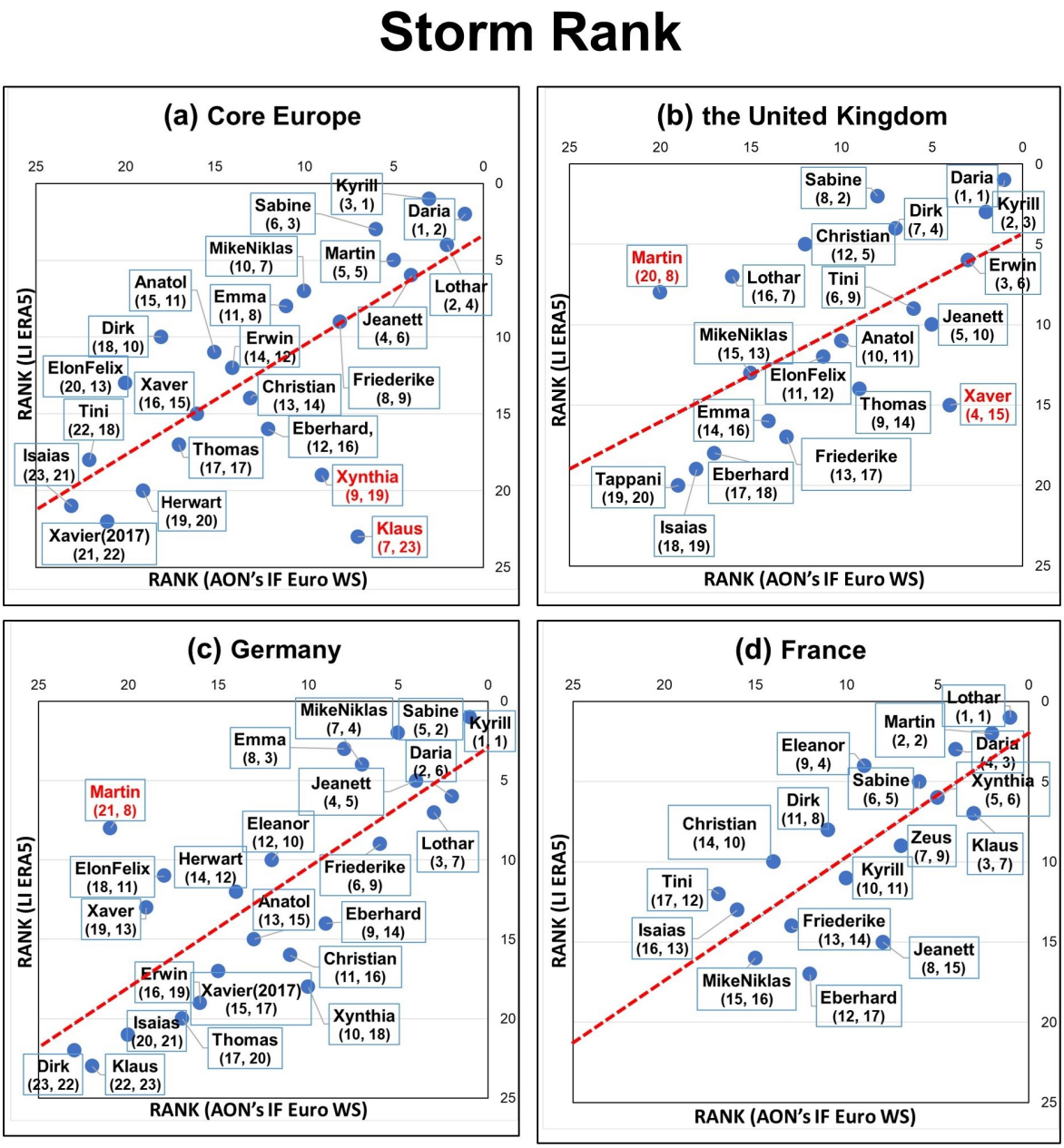

Figure 5.8.: Same as Figure 5.7, but for the comparison of storm ranks. The values in brackets indicate the rank (first value Aon's model, second value ERA5). The figure is reprinted from Figure 8 in Moemken et al. (2024a), with copyright CC BY 4.0.

Austria. Lower correlations with values below 0.5 and therefore larger differences can be found for Ireland, Belgium, and Sweden. The correlation pattern between LI ERA5 and PERILS looks similar, with overall lower values. Only the perfect anti-correlation for Sweden and the perfect correlation for Austria are striking. However, these values could be due to the small sample of common storms (see Appendix Figure A.4) and should therefore be viewed with caution. The comparison of Aon's IF Euro WS model and PERILS reveals mostly high correlation coefficients, ranging between 0.69 for Germany and 1.0 for

Austria and Norway. In terms of the explained variance, Austria exhibits the highest R^2 value when comparing LI ERA5 against Aon's IF Euro WS model and PERILS (Table 5.1). This result suggests that for Austria, over 70% of the variation in the ranks of loss from one dataset can be explained by the variation in the ranks of the other loss values. Due to the small sample of common events in some countries, some correlation values in this comparison should also be treated with care.

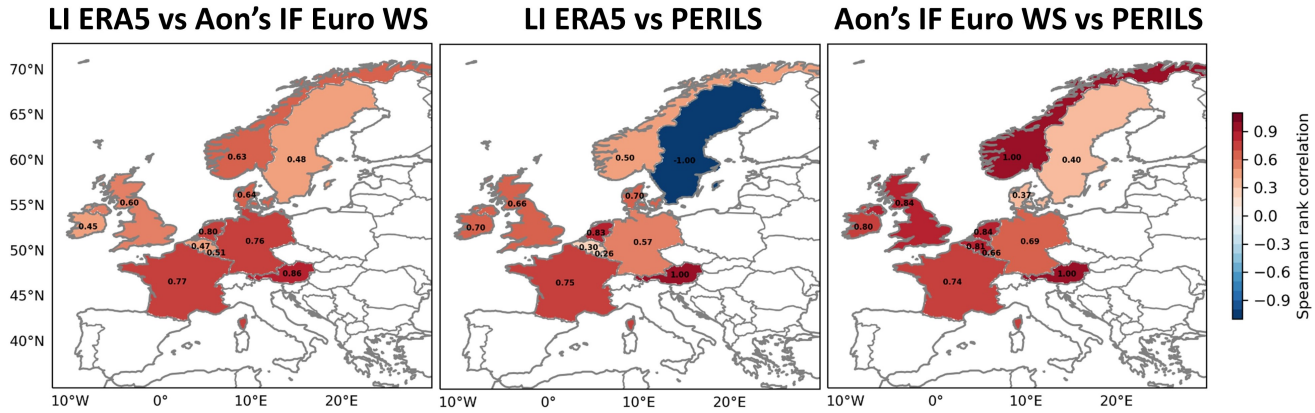

Figure 5.9.: Spearman's rank correlation coefficient at the country level for LI ERA5 vs Aon's IF Euro WS model (left), LI ERA5 vs PERILS (middle), and Aon's IF Euro WS model vs PERILS (right). The ranking is based on common storms per country (see Table 5.1 and Appendix Figure A.4). The figure is reprinted from Figure 9 in Moemken et al. (2024a), with copyright CC BY 4.0.

5.3. Summary and discussion

In this study, estimated windstorm losses over Europe from the meteorological loss index (LI) and the catastrophe windstorm model of Aon Impact Forecasting, used in insurance, were compared. Furthermore, the sensitivity of LI to the meteorological input data was tested by using both ERA5 and its predecessor, ERA-Interim. The main results can be summarized as follows:

Section 5.1. Comparison between ERA5 and ERA-Interim

- LI values for ERA5 are roughly 10 times higher than for ERA-Interim due to ERA5's higher spatial resolution, with the wind gust distribution in ERA5 shifted towards higher values and a longer tail.

- Regarding normalized losses and storm ranks, LI ERA5 and LI ERA-Interim show comparable behavior for Core Europe, with Spearman's rank correlation mostly ranging between 0.61 (Ireland) and 0.89 (France).

Section 5.2. Comparison of loss estimates from LI ERA5 and Aon's IF Euro WS model

- LI ERA5 shows overall lower normalized loss values compared to Aon's IF Euro WS model, with storm ranks generally comparable for most of Core Europe (correlations between 0.45 and 0.8).

- Aon's IF Euro WS model reveals a clearer distinction between high and moderate impact events, with insured loss differences of 3 orders of magnitude (e.g., Daria vs Isaias in the UK), compared to 1 to 1.5 orders of magnitude in LI ERA5.

- The catastrophe model shows a clear regional dependency of loss values, while this regional dependence is less pronounced in LI ERA5.

In previous studies, LI has been calculated and analysed for a variety of reanalysis datasets with different spatial and temporal resolutions: ERA-40 with 1.125° and 6-hourly resolution in Pinto et al. (2012), NCEP with 1.875° and 6-hourly resolution in Karremann et al. (2014a), or ERA-Interim with 0.75° and 6-hourly resolution in Priestley et al. (2018). In line with the findings of this study, those studies show that the magnitude of LI is sensitive to the spatial resolution of the underlying dataset. Nevertheless, they all agree on the general (regional) behaviour of LI. Another reason for the different LI values for ERA5 compared to ERA-Interim is a slight shift towards higher gust speeds and a longer tail in the wind gust distribution of ERA5. This is in line with Minola et al. (2020), who compared wind gust data from ERA-Interim and ERA5 with observational data across Sweden. They find an overall better agreement between observations and ERA5, although some discrepancies persist in regions with complex topography. It is therefore concluded that the recent ERA5 dataset is adequate for comparison to the insurance model in the second part of this study.

One reason for the differences between the meteorological index and the catastrophe model of Aon Impact Forecasting is their different methodological design: First, Aon's IF Euro WS model uses a 1-day window for the loss calculation, while LI ERA5 is based on 72-hour windows. Thus, Aon's IF Euro WS model is better able to separate storm events in short succession (like Lothar and Martin in December 1999). A sensitivity study demonstrated that using a 24-hour event definition for LI ERA5 does not lead to a systematic reduction in the differences between LI ERA5 and Aon's IF Euro WS model (Section 5.2.2). Therefore, the 72-hour event definition was retained in LI ERA5. This has several advantages: The entire windstorm footprint can be captured (Hewson and Neu, 2015). Additionally, the 72-hour event definition corresponds to a definition often used in reinsurance treaties (the so-called 72-hour clause; Klawa and Ulbrich, 2003; Karremann et al., 2014a) . Finally, the correlations between LI ERA5 and Aon's IF Euro WS model are higher when using 72-hour windows, especially for Core Europe. Another methodological difference is the consideration of different risk components. LI ERA5 only includes the hazard component and an estimate for the exposure component, while Aon's IF Euro WS model additionally includes a sophisticated engineering-based vulnerability component that takes, e.g., building resistance, loss frequency due to quasi-random effects, and local societal adaptations into account.

Aside from that, this study reveals some shortcomings of the two approaches. As all meteorological indices, LI relies upon the quality of both the underlying wind data and the impact function used for the calculation of loss. In the specific case of LI, the initial index was developed and evaluated for Germany by Klawa and Ulbrich (2003), employing insurance data of Munich Re and GDV ("Gesamtverband der Deutschen Versicherer e.V."). In a follow-up study, Karremann et al. (2014b) were able to demonstrate that the chosen 98^{th} percentile is an appropriate threshold to identify extreme storm events over Central and Western Europe. Nevertheless, they also point out that the 98^{th} percentile might be too low for Southeastern Europe, the Mediterranean, and Scandinavia. For these regions, Karremann et al. (2014b) suggest the use of a fixed, reasonable threshold below which losses are improbable. Moreover, the usage of present-day population density as a proxy for exposure levels might lead to an overestimation of loss values (Koks and Haer, 2020). Furthermore, LI depends on the used gust data. The ERA5 wind gust data we use here is based on the parameterization approach by Panofsky et al. (1977). While this approach performs well in flat terrain, it is sensitive to the local parameterization of the roughness length (Born et al., 2012; van den Brink, 2019). Finally, the LI index is missing a detailed damage component. The applied cubic relation tries to mimic the non-linear response of buildings to wind gusts. However, compared to the market perspective of Aon's IF Euro WS model, LI ERA5 seems to struggle with capturing this non-linearity, especially for the high-impact events at the tail of the gust spectrum. In some extreme cases, certain exposures (e.g., greenhouses, timber building, or agricultural buildings) may have vulnerability functions approximating a step-function. Various studies tested different formulations of meteorological indices, also considering different exponents (e.g., Klawa and Ulbrich, 2003; Pinto et al.,

2012; Prahl et al., 2015; Gliksman et al., 2023). All these studies agree that the performance of the different indices depends on the underlying event set. For some events, formulations with higher exponents seem to estimate windstorm losses better, while for other events, the cubic relationship provides results that are more realistic. In this sense, no formulation clearly outperforms the others. Aon's IF Euro WS model, on the other hand, includes no information on non-insured market loss. Additionally, insurance data in general depend on the insurance coverage and policy in single countries. Both factors might result in an overrepresentation of windstorms that hit countries with high market coverage Moemken et al. (2024b).

This study is the first to compare a comprehensive, proprietary insurance windstorm model with a simplified meteorological loss index. Due to the proprietary nature of the full insurance model, this study focuses on a simple and straightforward comparison between these two methods rather than a more detailed analysis. Overall, results of this study suggest that the loss distribution in LI is not steep enough, and accordingly, the tail is too short, leading to an underestimation of high-impact windstorms compared to the market perspective derived from the insurance catastrophe model. Nonetheless, LI is an effective index precisely because of its simplicity since it only considers wind gust and population density. Although it cannot be used to price a storm (due to the missing vulnerability information), it is suitable for estimating the impacts and rank events. The first comparison between a meteorological index and a full commercial windstorm model could serve as a reference for future studies focusing on the development and improvement of both storm loss models and storm severity indices.

6. Future changes of European windstorm losses in EURO-CORDEX simulations

Large parts of this chapter are based on:
Alifdini, I., Moemken, J., Ramos, A. M., and Pinto, J. G. 2025. Future Changes of European Windstorm Losses in EURO-CORDEX Simulations. Tellus A: Dynamic Meteorology and Oceanography, 77(1), 20–37. https://doi.org/10.16993/tellusa.4094.

Based on the research gaps and research questions outlined in Chapter 3, this chapter aims to address two primary objectives. Firstly, this chapter aims to assess how accurately wind gusts in EURO-CORDEX datasets reflect the present windstorm climate compared to ERA5 reanalysis data and to evaluate the effectiveness of bias correction in EURO-CORDEX using ERA5 as a reference. Secondly, it assesses how climate change, under the Representative Concentration Pathways (RCP) 8.5 scenario at varying global warming levels (GWLs), affects European windstorm frequency, intensity, and associated losses (LI). This chapter focuses on countries in Core Europe, Eastern Europe, and additional analyzed countries (Figure 6.1)

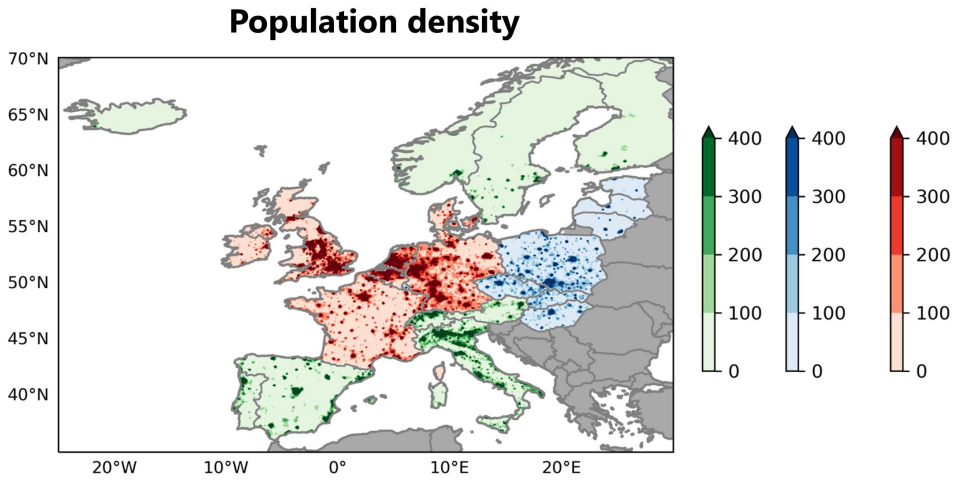

Figure 6.1.: Population density (P km^{-2}) for the year 2020 with Core Europe in red, Eastern Europe in blue, all other analyzed countries in green, and non-considered countries in grey. The figure is reprinted from Figure 1 in Alifdini et al. (2025), with copyright CC BY 4.0.

Section 6.1 focuses on the comparison between the EURO-CORDEX wind gust data and reanalysis data and the bias correction. The possible changes in frequency and intensity of windstorm losses in a warmer

climate and associated uncertainties are described in Section 6.2. Finally, Section 6.3 provides a summary of the results and a detailed discussion.

6.1. Evaluation of historical simulations

The quality of the historical simulations in representing the current wind gust climate over Europe was evaluated by comparing them with ERA5 reanalysis. To accomplish this, wind gusts in the historical period of the EURO-CORDEX ensemble (29 winters, 1976-2005) were used with the corresponding winters from ERA5 reanalysis data. The findings presented here are expressed in terms of the ensemble mean bias of the mean and the 98th percentile of daily maximum wind gust.

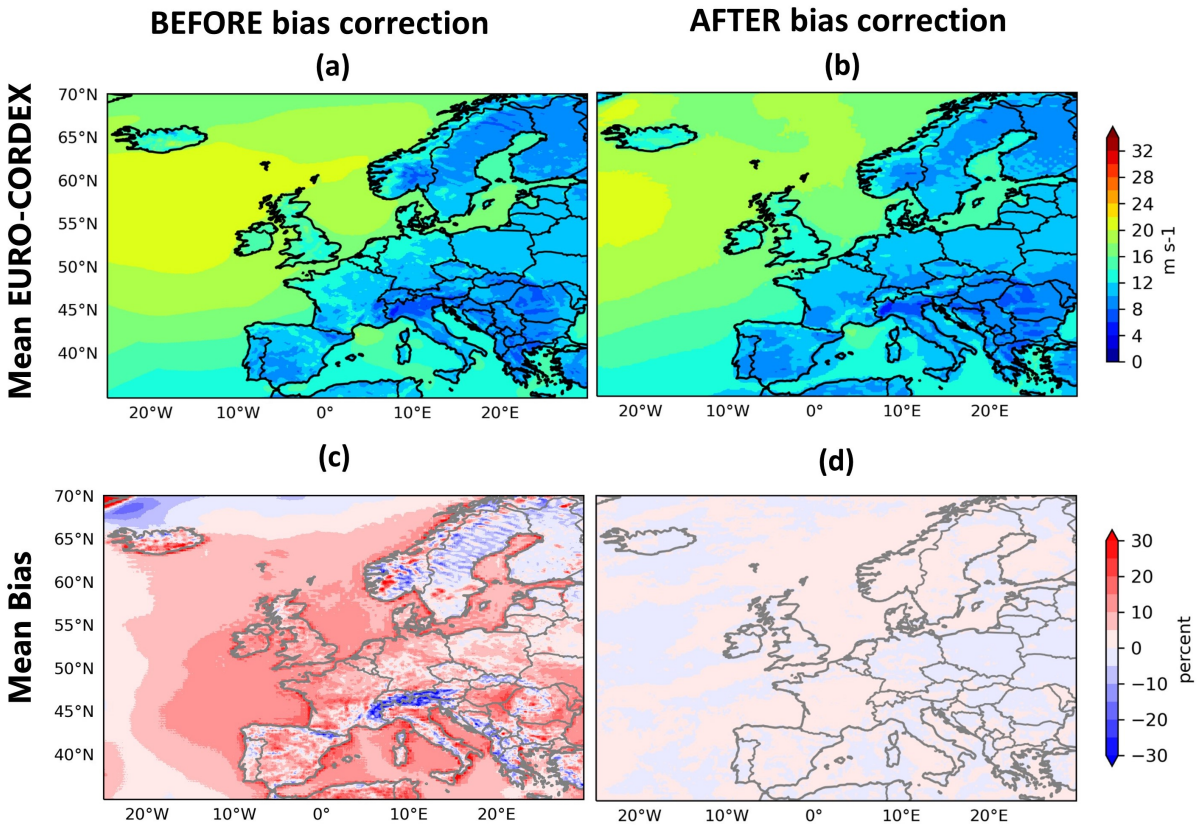

Figure 6.2.: (a-b) Mean of daily maximum wind gust (ms^{-1}) for the ensemble mean of the EURO-CORDEX historical simulations (1976-2005) before bias correction (a) and after bias correction using Empirical Quantile Mapping (b). (c-d) Difference between the EURO-CORDEX ensemble mean and ERA5 (%). The figure is reprinted from Figure 2 in Alifdini et al. (2025), with copyright CC BY 4.0.

Focusing on the mean of daily maximum wind gust, results show in general stronger wind gust in the EURO-CORDEX ensemble mean compared to ERA5, except for mountainous regions such as Scandinavia, the Alps, or the Pyrenees, where the bias is generally negative (Figure 6.2a, c). Some re-

gions in Europe present a positive bias higher than 20% (e.g., Iceland, coastal regions of the Mediterranean). When looking at particular RCM-GCM combinations, HadREM3-GA7-05 and RACMO22E have stronger mean wind gusts compared to ERA5 in most of Western and Central Europe (Appendix Figure B.2). For the 98th percentile, a positive bias is generally seen for the Iberian Peninsula, Southern France, and Eastern Europe (Figure 6.3a, c). However, the 98th percentile of wind gust shows a negative bias when compared with ERA5 over Central Europe, including the Alps. In terms of wind gusts over the ocean, it is evident that the EURO-CORDEX ensemble exhibits a strong positive bias when compared with ERA5. When looking at individual ensemble members (Appendix Figure B.3), a strong positive bias is found in wind patterns for RCA4 across all GCMs. All other RCM-GCM combinations agree on the less windy patterns over Central Europe. The bias from the RCA4 model is dominant across all GCMs, while in other models, it is unclear if the bias comes primarily from the GCM or the RCM.

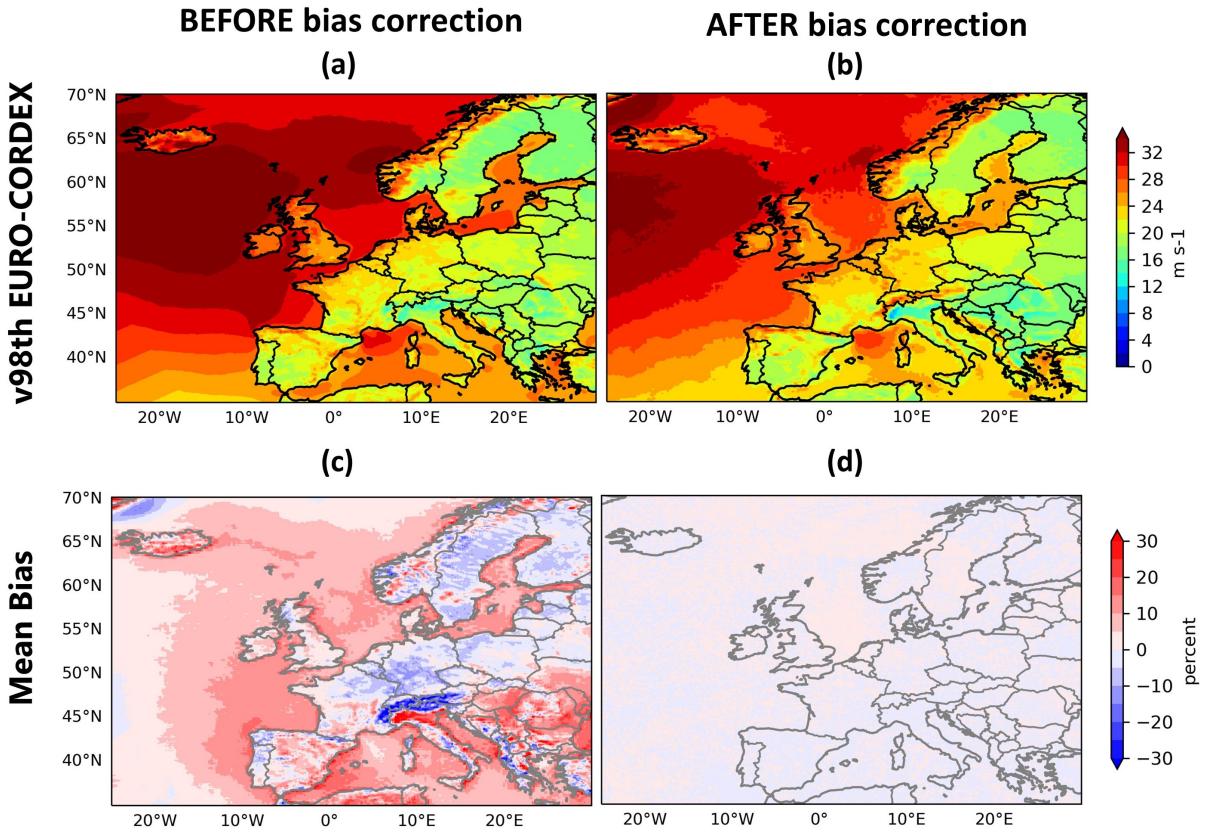

Figure 6.3.: Same as Figure 6.2, but for the 98th percentile of daily maximum wind gusts. The figure is reprinted from Figure 3 in Alifdini et al. (2025), with copyright CC BY 4.0.

Considering these results, the historical simulations of the EURO-CORDEX ensemble exhibit substantial biases of wind gusts when compared to ERA5 reanalysis, in particular for the RCA4 RCM. Since the bias is considerably high in some regions of Europe, a bias correction was conducted using Empirical Quantile Mapping (see Section 4.2.3.) of both current and future windstorm climates in EURO-CORDEX

before analyzing changes in windstorm loss.

After using Empirical Quantile Mapping, the bias between the historical EURO-CORDEX simulations and ERA5 are computed again. The corrected models were found to have much reduced biases in the mean of daily maximum wind gust (Figure 6.2b, d) ranging between -5% and +5%. Regarding the most extreme wind gusts (98^{th} percentile), the bias correction performed well (lower/higher than ± 5%), even in areas that are characterized by elevated topography, such as the Alps or the Pyrenees (Figure 6.3b, d). In this study of maximum wind gust, bias correction is very useful in reducing the bias not only for the mean but also for the extremes. Finally, the bias correction substantially reduces the bias over all 20 ensemble members when compared with ERA5 (Figures B.4, B.5), even for RCA4 where the highest bias was occurring.

6.2. Changes under future climate conditions

The potential changes in European windstorm loss under future climate conditions are evaluated. For this study, the bias correction method applied does not alter the climate change signal (see Figure B.6). The method primarily adjusts the intensity of climate change signals without substantially altering their spatial patterns in most areas, thereby ensuring alignment with observed data and enhancing the reliability of future projections. The analysis focuses on changes in windstorm intensity, windstorm frequency, windstorm related losses, and rare extreme events. The latter two are of particular interest for the insurance industry for determining premium values for windstorm risk in the context of climate change.

6.2.1. Changes in windstorm intensity

In the first step, changes in windstorm intensity were investigated. This was done in terms of changes in wind gust speed above the (historical) 98^{th} percentile. Figure 6.4 shows the ensemble mean of the historical windstorm intensity and the projected changes for GWL2 and GWL3, respectively. Areas with robust signals (Section 4.1.3) are marked with diagonal lines. The climate change signals of the individual ensemble members are shown in Appendix Figures B.7 and B.8, respectively.

For the GWL2, the ensemble mean projects a decrease in windstorm intensity for the Mediterranean, the UK, and mountainous regions on the continent (Figure 6.4b). Strongest and mostly robust trends are found for the Iberian Peninsula, with changes of up to -20%. For Eastern Europe, the Baltic Sea, and parts of Core Europe, the ensemble mean projects a slight, though non-robust increase for the GWL2, with trends mostly below 5%. The signals do not appear to be dominated by an individual GCM or RCM, as can be seen from the individual ensemble members in Figure B.7.

Climate change signals increase in magnitude and robustness for GWL3 (Figure 6.4c). The decreasing trends in windstorm intensity over the Iberian Peninsula now reach up to -30% in the ensemble mean and spread further towards France. The positive, but still non-robust signals over Eastern Europe also intensify and can reach up to 20% locally. Again, the individual ensemble members exhibit very different spatial patterns that do not indicate a clear dominance of a single GCM or RCM (Figure B.8).

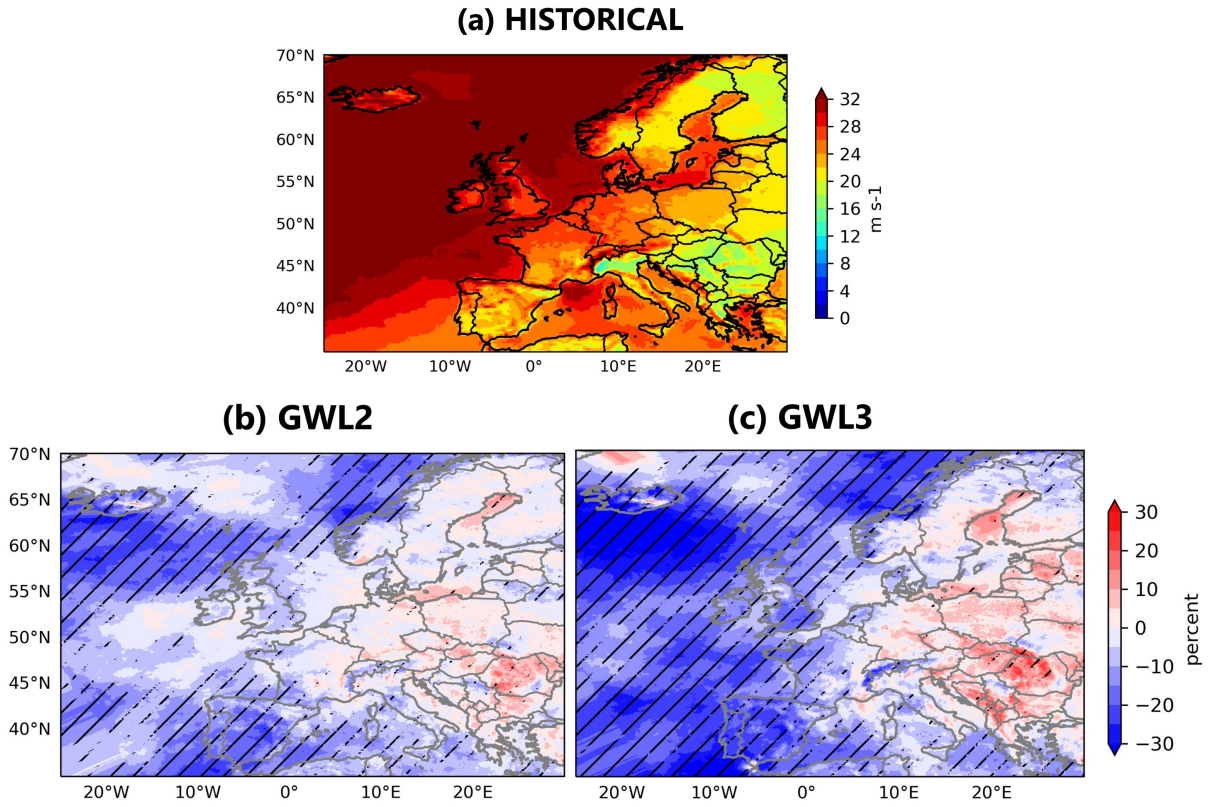

Figure 6.4.: (a) Windstorm intensity (ms^{-1}), shown as wind gust speed above the 98th percentile, derived from the EURO-CORDEX ensemble mean for the historical period (1976-2005). Changes in windstorm intensity (%) compared to the historical period for the ensemble mean of (b) GWL2 and (c) GWL3. Black diagonal lines indicate robust climate change signals, meaning that 14 or more ensemble members agree on the sign of change. The figure is reprinted from Figure 4 in Alifdini et al. (2025), with copyright CC BY 4.0.

6.2.2. Changes in windstorm frequency

Next, changes in windstorm frequency were analyzed, which refers to changes in the number of storms in the 29 winters of the GWL periods compared with the 29 winters of the historical period. For the GWL2 (Figure 6.5a), the EURO-CORDEX ensemble mean projects a slight decrease in storm frequency (less than 10%) for Core Europe, with robust signals in Ireland and the Netherlands. In Eastern Europe, the projected changes are non-robust and mostly negative. Only Austria, Hungary, and Slovakia show slight positive trends (smaller than 3%) in the ensemble mean. Largest changes in windstorm frequency

are projected for the Iberian Peninsula and Iceland, with negative trends of up to 16%.

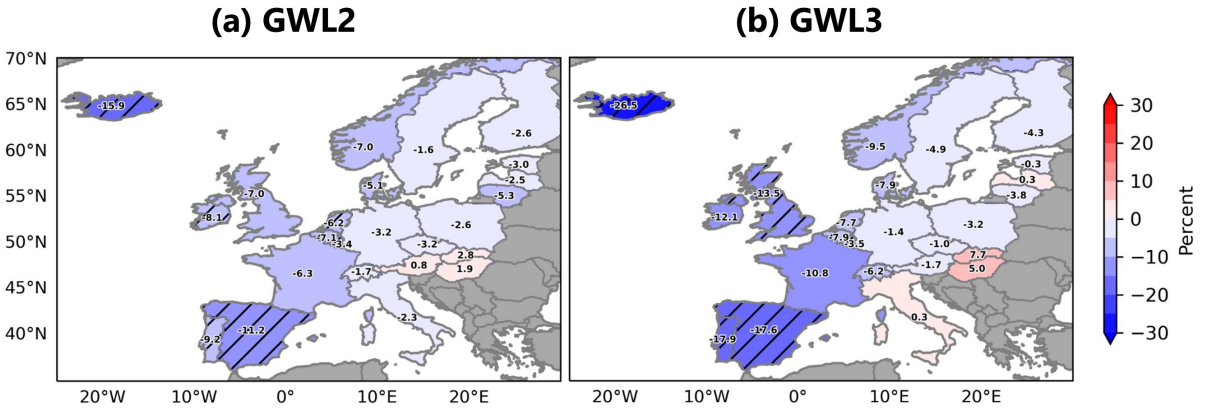

Figure 6.5.: Changes in windstorm frequency (%) compared to the historical period for the ensemble mean for (a) GWL2 and (b) GWL3. Black diagonal lines indicate robust climate change signals, meaning that 14 or more ensemble members agree on the sign of change. The figure is reprinted from Figure 5 in Alifdini et al. (2025), with copyright CC BY 4.0.

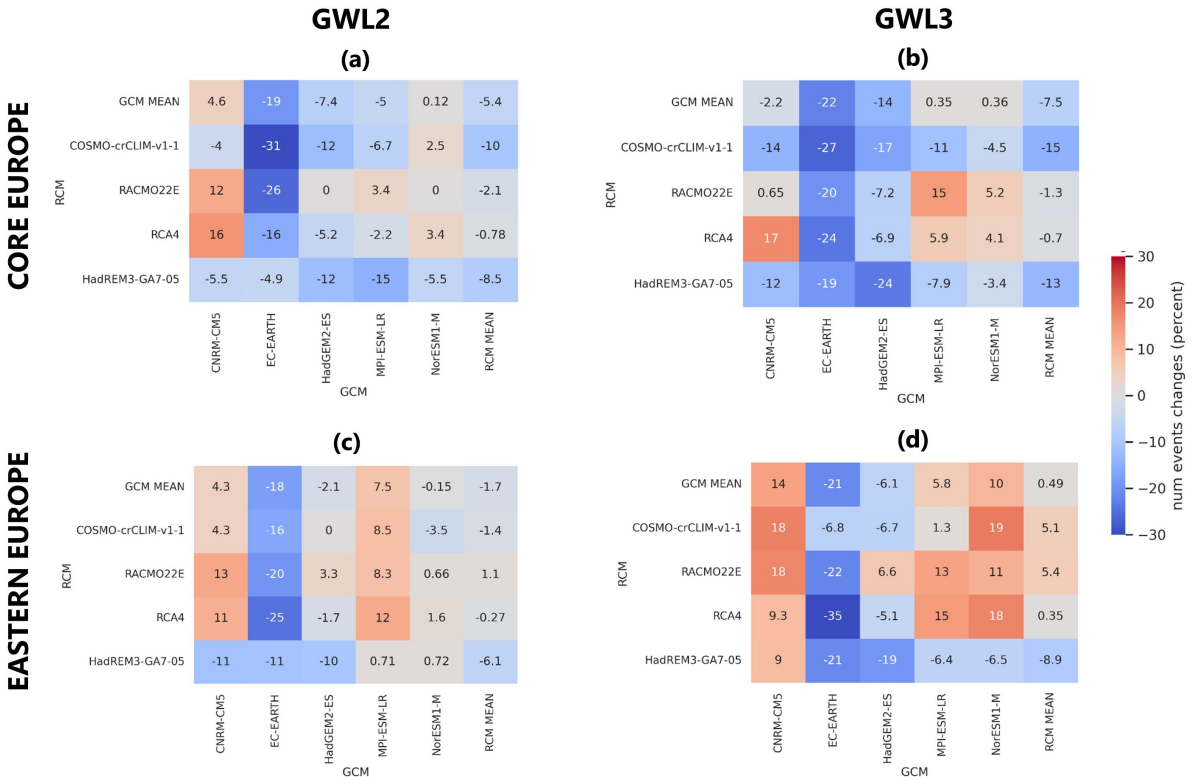

Figure 6.6.: Changes in windstorm frequency (%) compared to the historical period for the individual ensemble members derived for Core Europe (upper row) and Eastern Europe (lower row) for (a) GWL2, and (b) GWL3. For each matrix, rows represent RCMs and columns GCMs. The RCM (GCM) mean is depicted in the last column (first row). The figure is reprinted from Figure 6 in Alifdini et al. (2025), with copyright CC BY 4.0.

As for the windstorm intensity, changes are more pronounced for a GWL3 (Figure 6.5b). The ensemble mean projects negative trends for most parts of Europe. The only exceptions are Italy, Hungary, Slovakia, and Latvia, where the windstorm intensity can increase by up to 8% (non-robust). Largest (and robust) changes are again found for the Iberian Peninsula and Iceland, where the decrease in storm intensity can reach up to 26.5%.

For the individual ensemble members, all simulations driven by EC-EARTH show a strong decrease in storm frequency (up to 31% for single members and more than 15% in the GCM mean) for Core Europe and Eastern Europe in both GWLs (Figure 6.6). The same can be seen for most of the individual countries (Appendix Figure B.9, model code B). The climate change signals for all other RCM-GCM combinations are generally less pronounced and often do not exhibit a clear pattern. For example, the trends within one RCM (like RCA4) may vary for different GCMs (and vice versa). Moreover, for some ensemble members, trends may change in sign from one GWL to another as for the COSMO-CLM simulation driven by NorESM1-M. This applies both to the larger regions of Core and Eastern Europe (Figure 6.6) and to individual countries (Figure B.9).

6.2.3. Changes in windstorm losses

Changes in windstorm losses were analyzed by examining the top 2900 storm events from the historical period and using their minimum LI values as threshold to study changes in LI under future climate conditions (Section 4.2.1.). While a fixed number of events per ensemble member was not used but rather a focus on the most extreme events in the whole ensemble, the applied bias correction assures that, overall, all 20 ensemble members contribute equally to the historical event set (Figure B.1). For the GWLs, the total number of events and the contribution of the individual RCM-GCM combinations are changing, with the CNRM-CM5 simulations (EC-EARTH simulations) contributing more (less) to the event set of most extreme storms (Figure B.1). The following will focus on the total LI, summed over all storms in the event set (historical and GWLs, respectively).

Under a global warming of +2°, the ensemble mean projects a small (less than 10%) and non-robust decrease of LI for Core Europe (Figure 6.7b). The only exception is Germany, with a slight increase in LI (not significant). In Eastern Europe, trends are mostly positive (though non-robust) with values up to 8%. Largest (and robust) climate change signals can be found for Iceland and the Iberian Peninsula, where the negative trend in storm loss exceeds 20%. For the +3° GWL, changes are more pronounced in many European countries (Figure 6.7c). Exceptions are Germany, Austria, and some of the Baltic states, where the trends in LI are projected to change sign. For Core Europe, all countries show a decrease in LI in the ensemble mean, with largest (more than 15%) and robust trends for the UK. On the other hand, all countries in Eastern Europe show an increase in LI in the ensemble mean (non-robust). Overall, pro-

jected changes in LI are comparatively small under both GWLs, with values seldomly exceeding 15%. The only exceptions are the Iberian Peninsula and Iceland, where a decrease of almost 30% is projected under the GWL3.

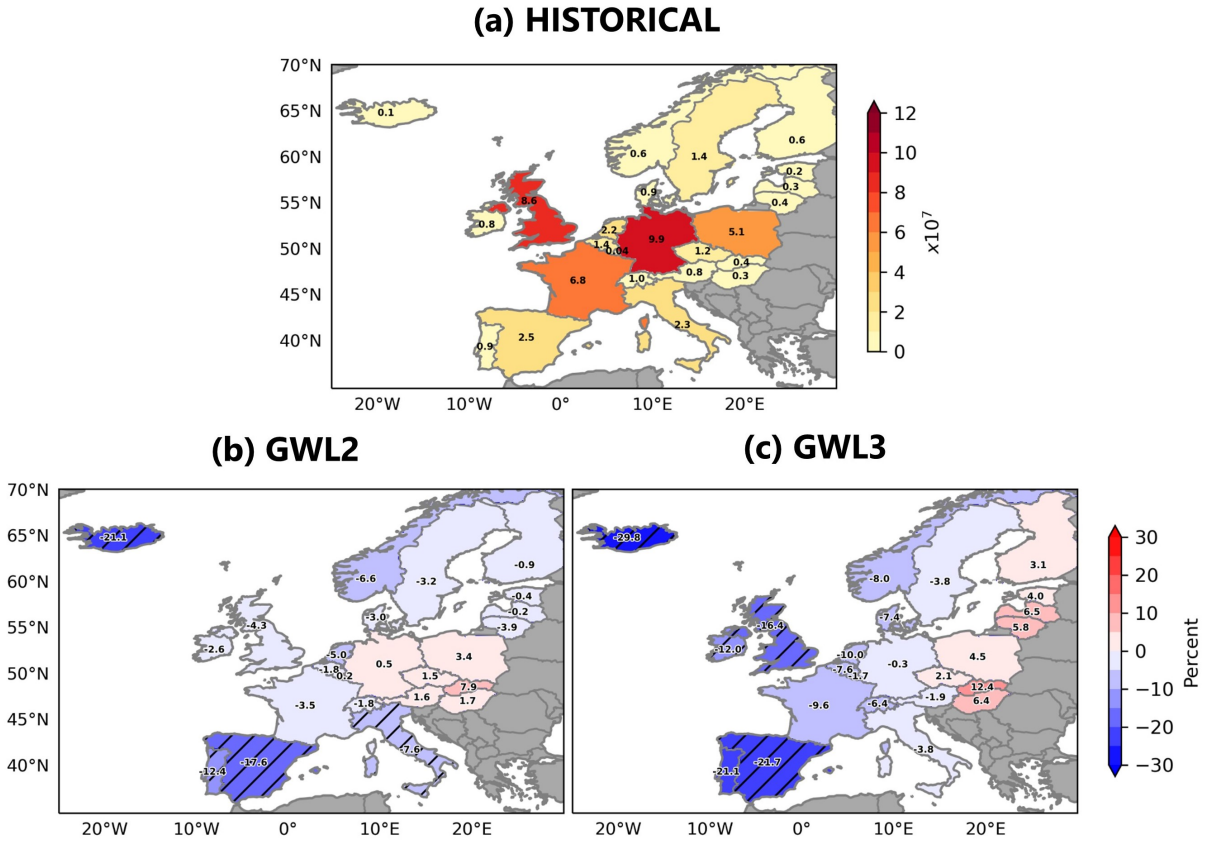

Figure 6.7.: (a) Windstorm loss, shown as total LI, derived from the EURO-CORDEX ensemble mean for the historical period (1976-2005). Changes in windstorm loss (%) compared to the historical period for the ensemble mean for (b) GWL2, and (c) GWL3. Black diagonal lines indicate robust climate change signals, meaning that 14 or more ensemble members agree on the sign of change. The figure is reprinted from Figure 7 in Alifdini et al. (2025), with copyright CC BY 4.0.

The analysis of the various ensemble members (Figure 6.8) reveals a strong decrease in LI for all EC-EARTH-simulations for Core Europe, Eastern Europe, and most individual countries (Figure B.10). This decrease can be found under both GWLs with values reaching up to 36% and agrees well to the projected changes in windstorm frequency (Section 6.2.2). On the other hand, most simulations driven by CNRM-CM5 show a strong increase in LI, with values reaching up to 45% for Eastern Europe (Figure 6.8e, f). The other RCM-GCM combinations mostly agree on increasing LI for Eastern Europe under both GWLs, with overall lower values (1-25%) and no clear dominance of a single GCM or RCM.

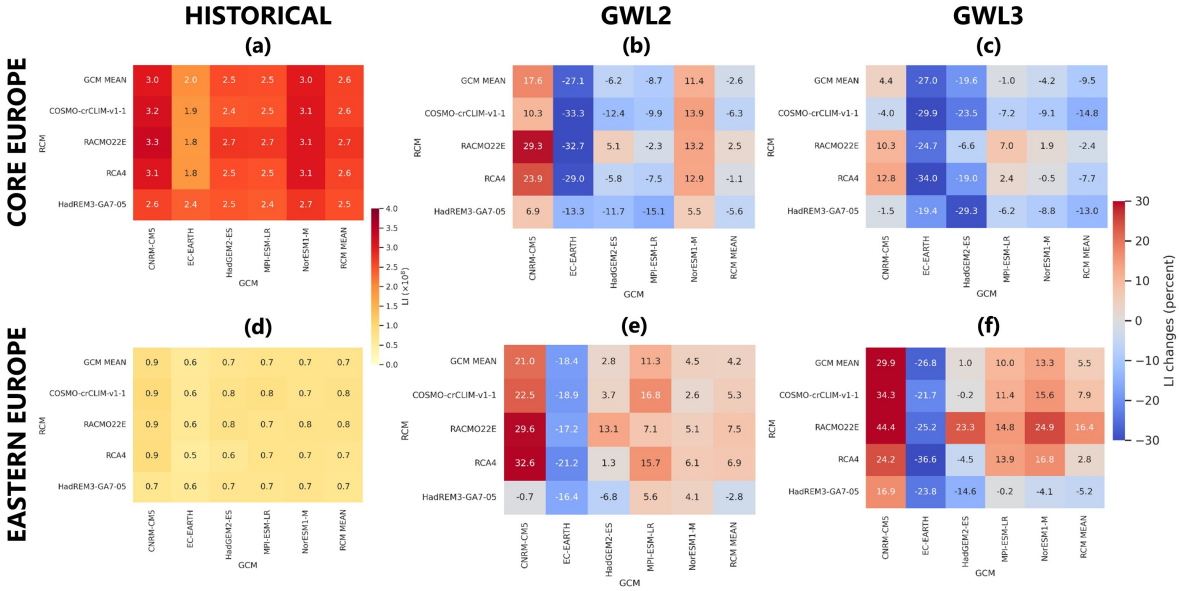

Figure 6.8.: Windstorm loss derived for Core Europe (a) and Eastern Europe (d) for the individual ensemble members for the historical period (1976-2005). Changes in windstorm loss (%) compared to the historical period for the individual ensemble members for (b,e) GWL2, and (c,f) GWL3. For each matrix, rows represent RCMs and columns GCMs. The RCM (GCM) mean is depicted in the last column (first row). The figure is reprinted from Figure 8 in Alifdini et al. (2025), with copyright CC BY 4.0.

6.2.4. Changes in rare extreme loss events

In the final step, changes in rare extreme loss events at different return levels and return periods were analyzed. This is particularly crucial for insurance companies, as they have to determine appropriate premiums for those rare extreme events to have sufficient funds to cover claims. This part of the study focused on Core Europe and Eastern Europe instead of individual countries to ensure more reliable and stable GPD fits (Section 4.2.5), but single countries are also discussed. Based on the stability of the scale and shape parameters of the GPD fit (see Section 4.2.5), the top 81 events for Core Europe and the top 90 events for Eastern Europe were used.

For Core Europe (Figure 6.9a), the return period for rare extreme loss events is projected to shorten across all return levels for the GWL2 (blue curve). This indicates that rare extreme losses are expected to occur more frequently compared to the historical period (green curve). For example, a loss value corresponding to a 50-yr return period under historical climate conditions is projected to occur about every 33 years for a global warming of 2°C. Under the GWL3 (red curve), on the contrary, results show a strong overlap with the distribution for the historical period (green curve), and even a small lengthening of the return period. A historical loss value corresponding to a 50-yr return period, for instance, is estimated to occur every 58 years for the GWL3. The changes in rare extreme loss events for Core Europe are primarily influenced by extreme events in individual countries. A detailed analysis of Core Europe countries (Figures 6.9c,e and B.11) reveals that while, for example, Ireland and the UK do not show a

significant change of return periods, these changes are clear for Germany and France, which also show shorter return periods for GWL3 than GWL2. Nevertheless, there is large uncertainty and thus no clear climate change signal for rare extreme events is found for Core Europe.

The results are more consistent for Eastern Europe (Figure 6.9b). For both GWLs, a shortening of return periods compared to current climate conditions is projected. Changes are more pronounced for the GWL2 than for the GWL3. For example, a 50-year event in the historical period will become a 19-year event under the GWL2 and a 28-year event under the GWL3, respectively. Considering the individual countries (Figures 6.9d,f and B.12), the shortening of return periods is observed for most of the individual countries, some with more (e.g. Poland, Latvia), some with less clarity or hardly any signal (e.g. Hungary). But together with the analysis for the countries in Core Europe, it appears that the signal generally becomes clearer the further east we look. Overall, the differing patterns of rare extreme loss between Core Europe and Eastern Europe highlight regional variations. Furthermore, there is no evidence that a GWL3 results in more frequent or severe rare extreme loss events than a GWL2.

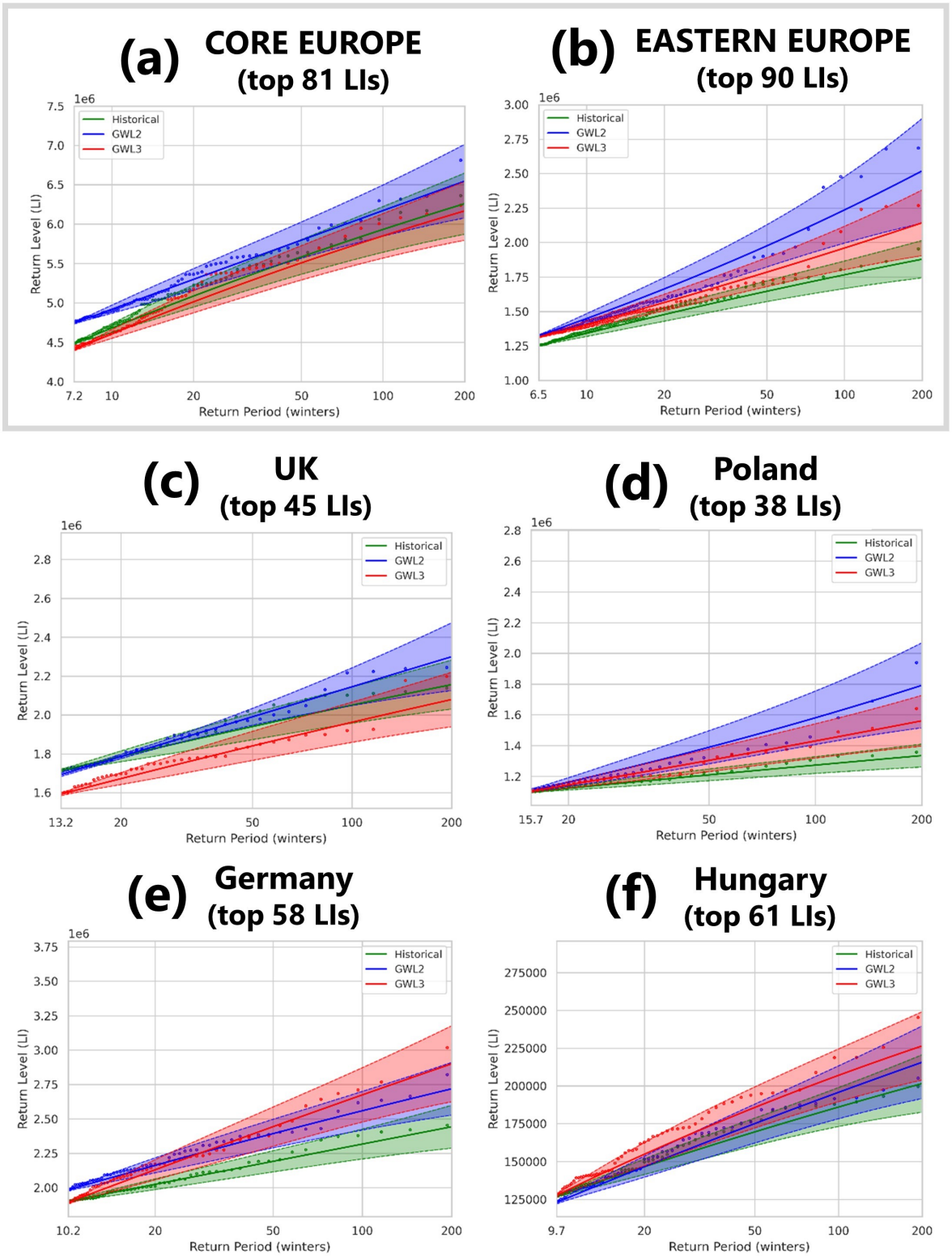

Figure 6.9.: Return periods of the most extreme loss events derived for (a) Core Europe and (b) Eastern Europe for the historical period (green), the GWL2 (blue), and the GWL3 (red). The dots represent the empirical values, the solid lines show the GPD fit, and the dashed lines represent the upper and lower bounds of the 95% confidence interval. Same as (a) and (b), but for countries belonging to Core Europe (c,e) and Eastern Europe (d,f). The number of top LIs used in these figures are based on the stability of the scale and shape parameters of the GPD fit. The figure is reprinted from Figure 9 in Alifdini et al. (2025), with copyright CC BY 4.0.

6.3. Summary and discussion

This study analyzed potential impacts of climate change on windstorm losses in Europe. With this aim, the simple meteorological storm severity index named loss index (LI; after Pinto et al., 2012), was applied to a large EURO-CORDEX multi-model ensemble. 10 m wind gust speed was bias-corrected using an Empirical Quantile Mapping approach. Climate change signals were estimated for two global warming levels relative to pre-industrial conditions (+2°C and +3°C) using RCP8.5 scenario simulations. The main results are:

Section 6.1. Evaluation of historical simulations

- The historical EURO-CORDEX simulations show substantial biases in 10 m wind gust compared to ERA5 reanalysis data. The largest biases occur over regions with complex topography and for simulations with the RCA4 model.

- These biases were considerably eased with the Empirical Quantile Mapping bias correction.

Section 6.2. Changes under future climate conditions

- The ensemble mean projections reveal an increase in windstorm intensity for most parts of continental Core and Eastern Europe in future decades, while a decrease is found for the Iberian Peninsula. Changes are more pronounced under GWL3.

- The windstorm frequency is projected to decrease under future climate conditions for large parts of Europe. Largest and robust changes are found for the Iberian Peninsula, Iceland (both GWLs), and the UK (GWL3).

- Regarding windstorm loss, climate change signals are comparatively small and mostly non-robust overall, with negative trends for Core Europe and positive trends for Eastern Europe.

- The return periods of the most extreme loss events are projected to shorten for Eastern Europe independent of the GWL, while no clear and consistent trends are found for Core Europe as a whole.

- The EURO-CORDEX projections reveal large uncertainties in the sign and the magnitude of change, resulting in mostly non-robust climate change signals. Trends vary across the individual GCM-RCM chains without a clear dominance of a single GCM or RCM.

The evaluation of the EURO-CORDEX models was performed by comparing the historical EURO-CORDEX daily maximum wind gusts with ERA5 reanalysis. Ideally, observational (gridded) wind gust should be used for the comparison with the historical period. To the best of our knowledge, no such gridded observational wind gust dataset is available, as E-OBS only accounts for daily mean wind speed. The ERA5 reanalysis was therefore used due to its generally good representation of near-surface winds (e.g. Ramon et al., 2019; Molina et al., 2021). However, ERA5 shows the lowest wind speed

over mountainous regions (Laurila et al., 2021) and underestimates wind gusts over mountains in Sweden compared to observations (Minola et al., 2020). This underestimation can be attributed to ERA5's wind gust parametrization, which does not accurately account for the elevation-dependent in the turbulent contribution. Nevertheless, ERA5 performs better than ERA-Interim, showing a closer agreement with observations for both wind speed and wind gust (Minola et al., 2020). Since no gridded wind gust data is available that serves as a better reference than ERA5, ERA5 was used for bias correction. The data was corrected by means of Empirical Quantile Mapping, the EURO-CORDEX ensemble presented a substantial bias in 10 m wind gust. This method corrects not only the mean and variance but the whole distribution (Themeßl et al., 2011). The bias-corrected model presented reduced climatological mean bias in spatial patterns and intensities.

The consideration of the EURO-CORDEX models allowed a quantification of the changes of European windstorm losses and examine their uncertainty and robustness. Here, the RCP8.5 scenario was chosen due to its larger availability in EURO-CORDEX and because GWL3 is not reached in some ensemble members for RCP4.5. Given that the changes are scenario dependent (Masson-Delmotte et al., 2021a), including a second, more moderate scenario (e.g., RCP4.5) would provide a better assessment of the uncertainties of changes. Very recently, the improved framework for CMIP6-CORDEX simulations has been issued (Katragkou et al., 2024), and CMIP6 downscaling experiments are now under way, considering the recent Shared Socio-economic Pathways (SSPs) and aerosol forcing. Future studies should include a comparison between SSPs and RCPs and investigate possible differences for European windstorms.

Changes in windstorm-related impacts in Europe have been studied not only from a global climate projection perspective (e.g. Pinto et al., 2007; Little et al., 2023) but also using regional climate simulations (e.g. Michel and Sorteberg, 2023; Bloomfield et al., 2023). Our results show an increase in windstorm intensity and a simultaneous decrease in frequency (thus fewer but more intense storms) for large parts of continental Europe. For the UK and the Iberian Peninsula, both windstorm intensity and frequency are projected to decrease. However, and in line with Spinoni et al. (2020) and Michel and Sorteberg (2023), the climate change signals are subtle, often not significant, and have a large uncertainty.

The results of this study at the regional scale can also be discussed in the context of changes in the large-scale atmospheric conditions in future decades. The representation of the Northern Hemisphere storm tracks under future climate change has been evaluated in climate model simulations from Phases 3, 5, and 6 of the Coupled Model Intercomparison Project (CMIP) by Harvey et al. (2020). They found consistent wintertime changes in the spatial patterns of the multi-model ensembles in CMIP3, CMIP5, and CMIP6- a weakening on the northern flank of the North Atlantic storm track and an extension towards Europe. This agrees with our results at the regional scale, showing an increase in windstorm intensity

over Eastern Europe. More recently, Priestley and Catto (2022) show that extra-tropical cyclone numbers are projected to decrease globally in winter when analyzing the CMIP6 models, in line with previous studies (e.g. Ulbrich et al., 2009). Moreover, Priestley and Catto (2022), describe an extension of the North Atlantic storm track into Europe in all scenarios, with an increase in extreme windstorms identified for the North Sea region (see also Pinto et al., 2009; Pinto et al., 2012). These assessments are thus all consistent with the present study.

The current results also have implications for the mid- and long-time planning of the insurance companies. While Moemken et al. (2024a) provided evidence that LI tends to underestimate high-impact events compared with an insurance catastrophe model, they highlight the overall effectiveness of LI to estimate windstorm impacts. Combined with current results, this information might help insurance companies to implement a climate change component in their catastrophe models and potentially even to consider different future pathways. Given the regional differences and subtleties in the results, a region-specific approach, tailored to the particular conditions of each area, could be important to quantify windstorm impacts in the forthcoming decades.

7. Seasonal loss clustering in a warming climate

The primary goal of this chapter is to investigate the characteristics of high total loss per winter (AEP) in terms of seasonal loss clustering to address research question 3 (Chapter 3). The aim is to provide a better understanding of high AEP seasons and the degree of seasonal loss clustering (OEP/AEP ratio) that leads to them. To achieve this, regional differences in seasonal loss clustering are first explored to understand how it varies across regions in Europe. This chapter discusses three key aspects: firstly, introducing the historical record of seasonal loss and examining its impact on seasonal loss clustering; secondly, exploring regional variations in seasonal loss clustering through distribution and return value analysis; and lastly, investigating the characteristics of high AEP seasons and the possible role of climate change.

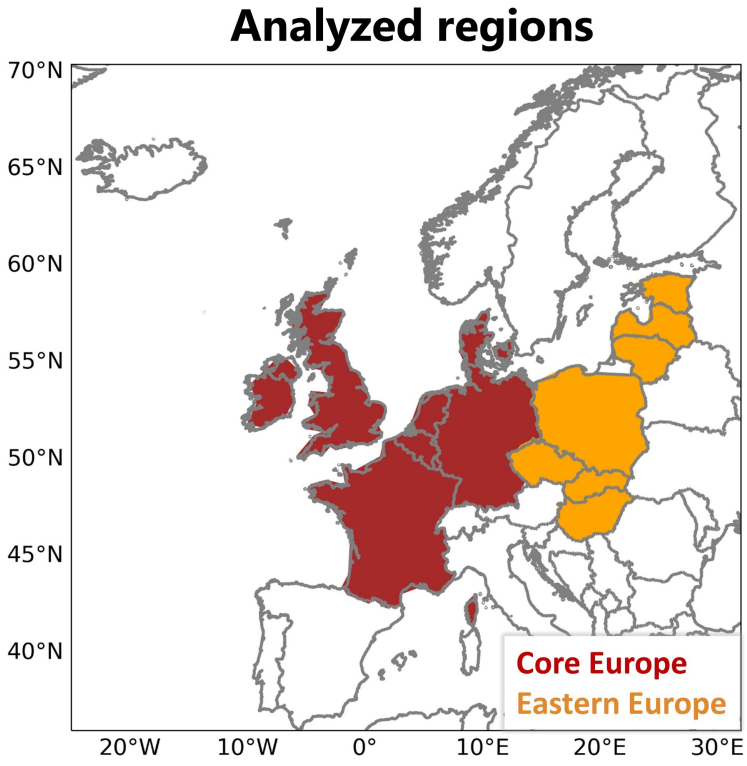

Figure 7.1.: Regions were grouped in order to identify seasonal loss clustering. The following regions were considered: Core Europe (red) and Eastern Europe (orange).

To examine seasonal loss clustering, the focus is on two regions: Core Europe and Eastern Europe. This selection is based on the typical market portfolios used in the insurance industry and the distinct geographic and economic divisions that define the European insurance market (Figure 7.1). Core Europe,

highly susceptible to multiple windstorms each season, is the primary focus of this investigation. While Eastern Europe is historically primarily affected by floods and summer storms as the main risks, windstorm is an important secondary peril, and insurance is increasingly interested in assessing risks in this region. Moreover, chapter 6 shows that most countries in Eastern Europe experience higher losses under GWLs compared to the historical period, which is why this region is also included in this study. By distinguishing Core and Eastern Europe, insights can be gained into the regionalised impacts of seasonal loss clustering of windstorms, potentially identifying unique risk factors or vulnerabilities.

Section 7.1 examines seasonal loss clustering during the historical period using ERA5 reanalysis data, focusing on the historical record of seasonal loss clustering, regional variations in OEP (maximum loss per winter), AEP, the OEP/AEP ratio, and the relationships among these variables. This section also analyses the characteristics of high AEP seasons. Section 7.2 discusses the impact of climate change on seasonal loss clustering using the EURO-CORDEX ensemble. Finally, section 7.3 provides a summary and discussion of the findings.

7.1. Seasonal loss clustering in the historical period

7.1.1. Historical record and relationship analysis

Given its geographical location, Europe is often affected by windstorms, resulting in significant seasonal losses, both in terms of maximum (OEP) and cumulative (AEP) losses (Figures 7.2, 7.3). For instance, during the winter of 1989/1990, Core Europe experienced a series of storms that caused a substantial AEP of 5 million and a substantial OEP of 700K, resulting in an OEP/AEP ratio of 0.14 (Figure 7.2). Similarly, Eastern Europe experienced high AEP values that winter, with an OEP/AEP ratio of 0.2. Priestley et al. (2018) defines a season with loss clustering as having a low OEP/AEP ratio, while a season dominated by a single event has a high ratio. Based on this reasoning, the 1989/1990 season can be seen as an example of seasonal loss clustering, where multiple storms contribute to the total loss, leading to a low OEP/AEP ratio. In contrast, the winter of 1984/1985 had a lower AEP, and the OEP/AEP ratio was much higher—around 0.82 for Core Europe and 0.6 for Eastern Europe. This indicates that a single storm dominated the total seasonal loss in those regions for this winter. The comparison highlights regional differences in the OEP/AEP ratio: seasons with loss clustering (multiple storms) have a low OEP/AEP ratio, while seasons dominated by a single event have a high OEP/AEP ratio. At the outset, seasonal loss clustering is investigated based on the definition of Priestley et al. (2018), noting that the details will be further explored in a later subsection (7.1.3).

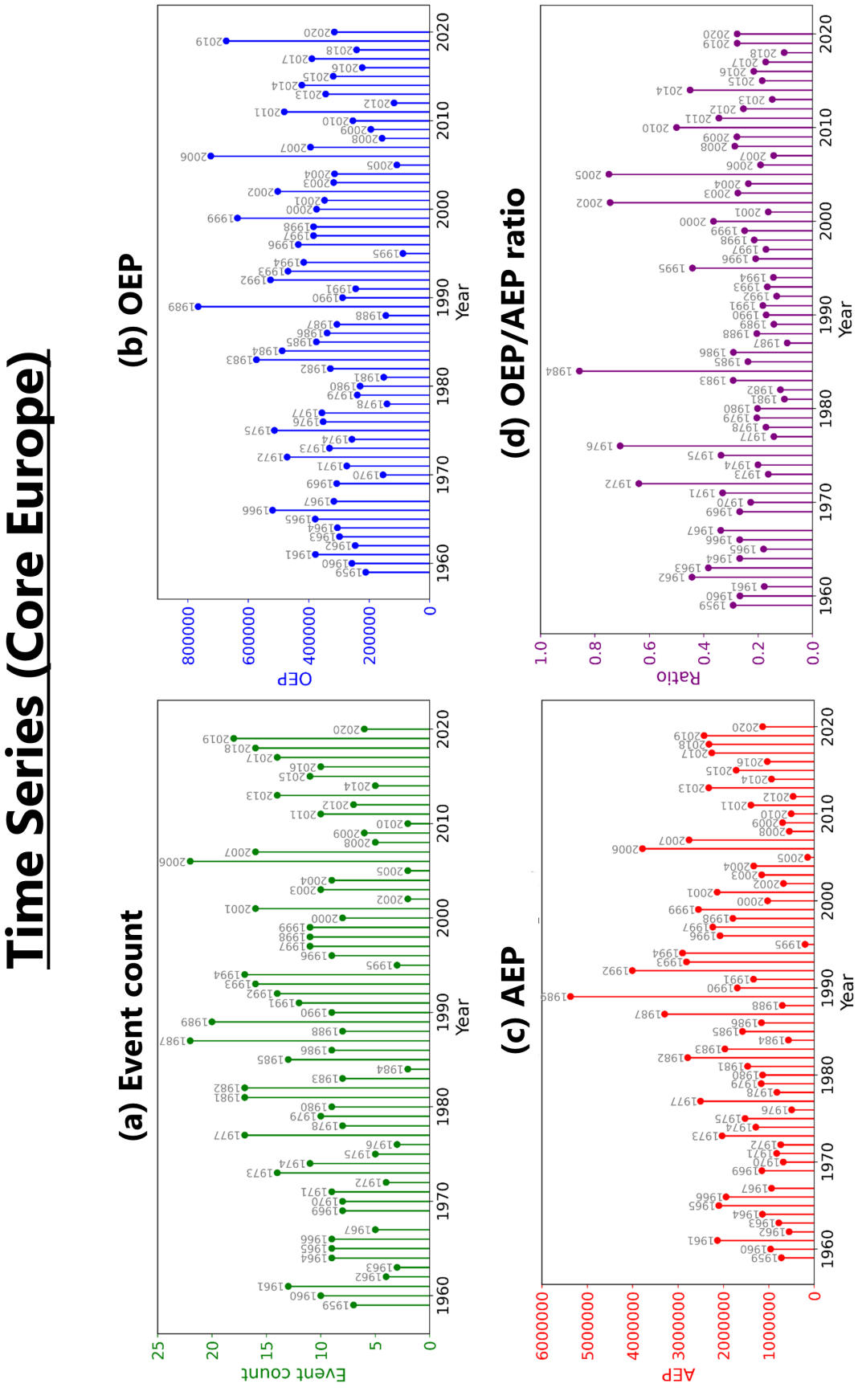

Figure 7.2.: Time series of (a) event count, (b) OEP, (c) AEP, and (d) the OEP/AEP ratio using ERA5 (1959-2021) for Core Europe. The OEP (maximum LI) and AEP (total LI) are calculated based on the LI values for each winter, with the year representing the start of each winter season where the LI value exceeds the threshold.

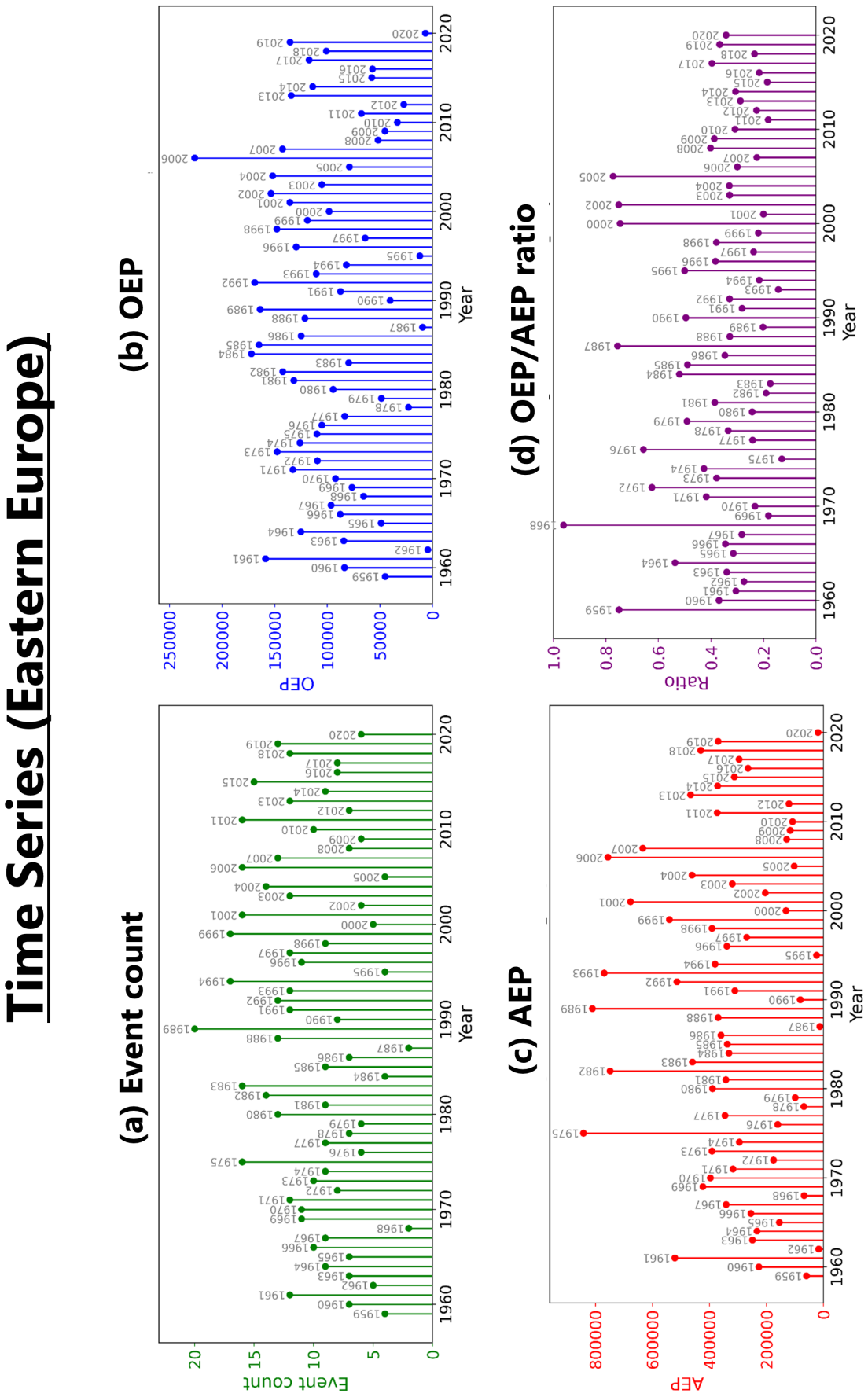

Figure 7.3.: Same as Figure 7.2, but for Eastern Europe.

To better understand the relationship between seasonal loss values and seasonal loss clustering, the relationships among OEP, AEP, and the OEP/AEP ratio are explored. For Core Europe (Figure 7.4), OEP and AEP show a moderate correlation (0.60), indicating that higher AEP is generally associated with higher OEP. A stronger correlation (0.88) exists between storm count and AEP, indicating that more storms tend to result in significantly higher aggregate losses. The OEP/AEP ratio shows a strong negative correlation with both AEP (-0.76) and storm count (-0.85). This means that seasons with a lower OEP/AEP ratio tend to have high AEP values and multiple storms. OEP shows a very weak relationship with the OEP/AEP ratio (-0.03) and event count (0.30), suggesting no or only a small link between OEP, event count, or loss clustering. The results above indicate that while an increase in storms leads to higher cumulative losses and greater loss clustering, OEP does not show a clear or predictable pattern based on loss clustering. Similarly, the relationships for Eastern Europe follow a similar pattern, though the magnitudes of the correlations vary slightly (Figure C.1).

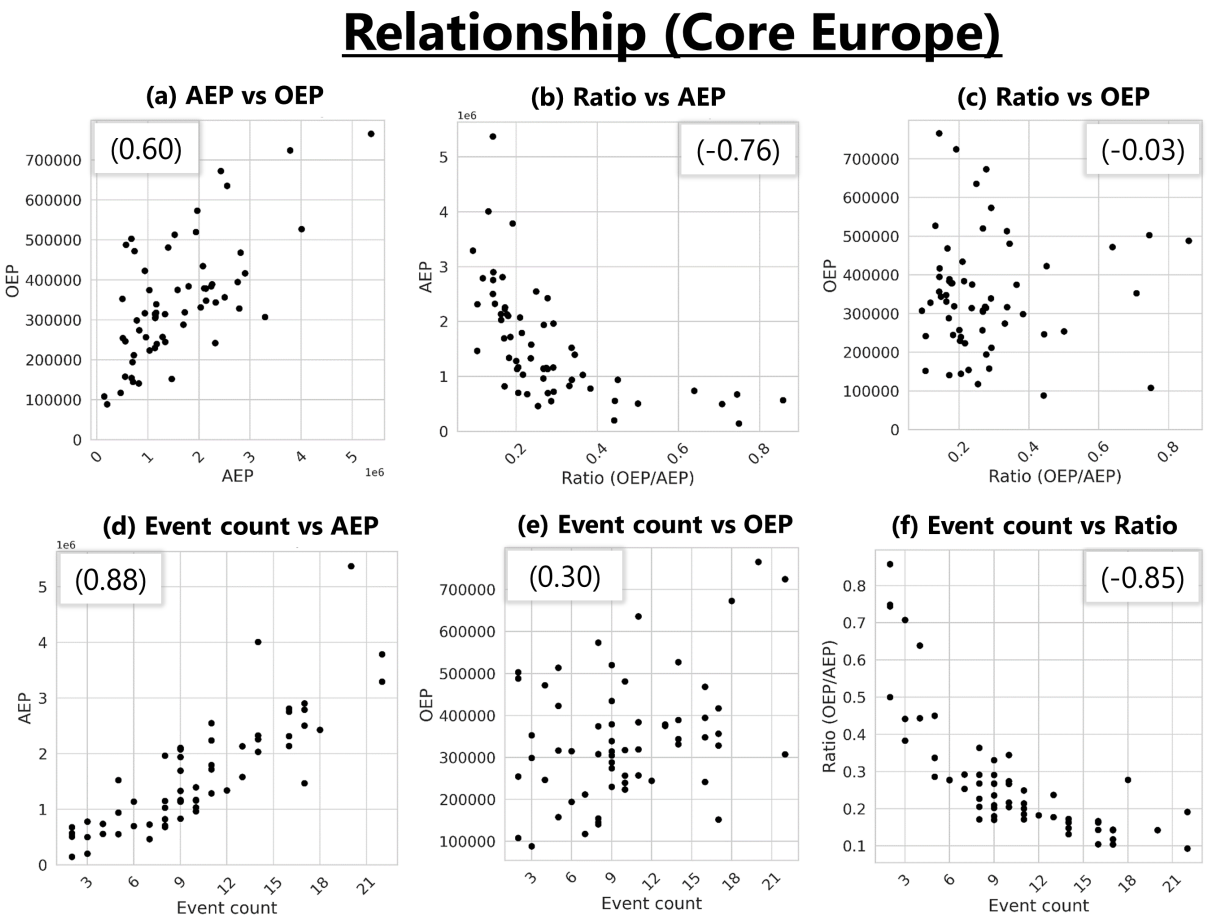

Figure 7.4.: Scatterplots between AEP, OEP, the OEP/AEP ratio, and event count for Core Europe using LI ERA5 (1959-2021). One point represents 1 winter. The number in parentheses is the Spearman's rank correlation coefficient.

7.1.2. Regional variability

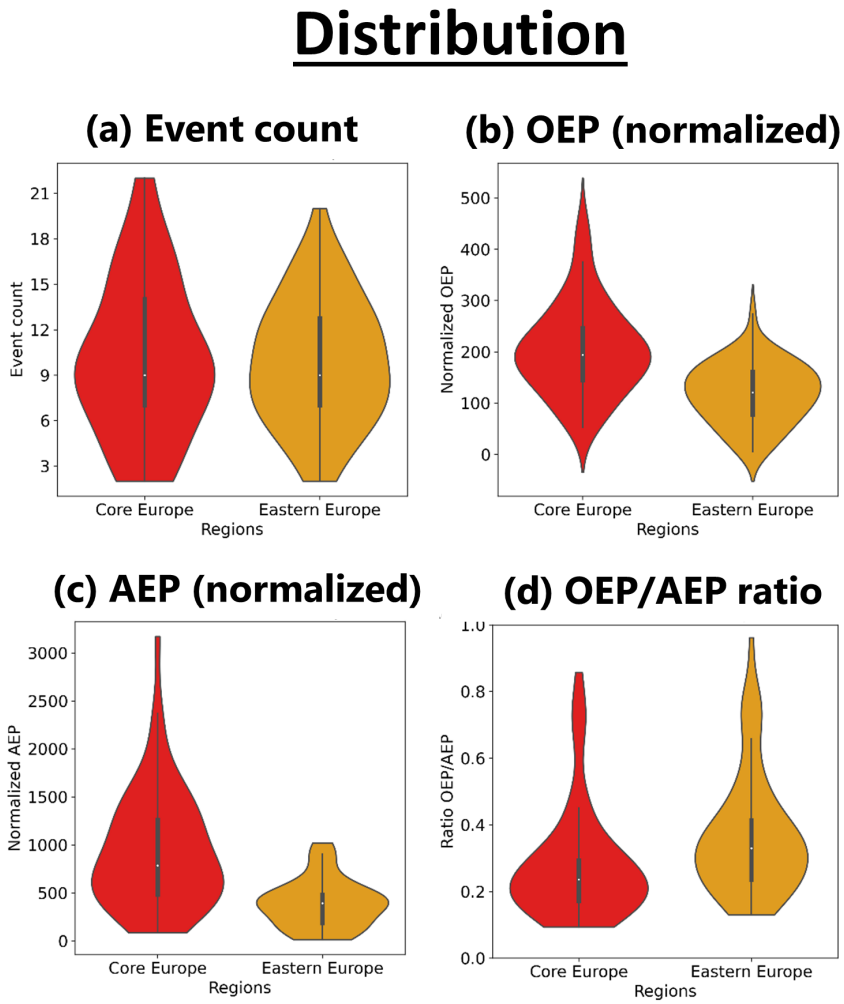

Figure 7.5.: Violin plots of (a) event count, (b) OEP (normalized), (c) AEP (normalized), and (d) the OEP/AEP ratio calculated using the original OEP and AEP values from LI ERA5 data (1959-2021) for Core Europe (red) and Eastern Europe (orange). Figures (b) and (c) are normalized by the number of grids in each region.

The distribution and range of storm counts, OEP, AEP, and the OEP/AEP ratio were analyzed using violin plots to visualize their patterns and variability (Figure 7.5). In Core Europe, the storm count plot (Fig. 7.5a) is narrower and reaches higher numbers compared to Eastern Europe, indicating more frequent storms in Core Europe. All regions show a unimodal distribution (one clear peak) for OEP (Fig. 7.5b), but Core Europe has a higher median, about 25% larger than Eastern Europe, with its maximum OEP value 40% larger than Eastern Europe's highest. For AEP (Fig. 7.5c), both regions have a single peak, but Core Europe's distribution is negatively skewed (extends toward lower values), while Eastern Europe's is more symmetrical. Moreover, the median AEP in Core Europe is 85% higher, and the maximum AEP is 250% higher than in Eastern Europe. The results above indicate that Core Europe experiences more frequent and severe storms, leading to higher losses (OEP and AEP) compared to Eastern Europe. The OEP/AEP ratio (Fig. 7.5d) for both regions is negatively skewed, with wider plots at lower levels, in-

dicating that winter seasons with multiple clustered storms are more common than winter seasons with a single dominant storm. Core Europe shows a wider distribution at these lower levels, suggesting that seasonal loss clustering is more prevalent in this region.

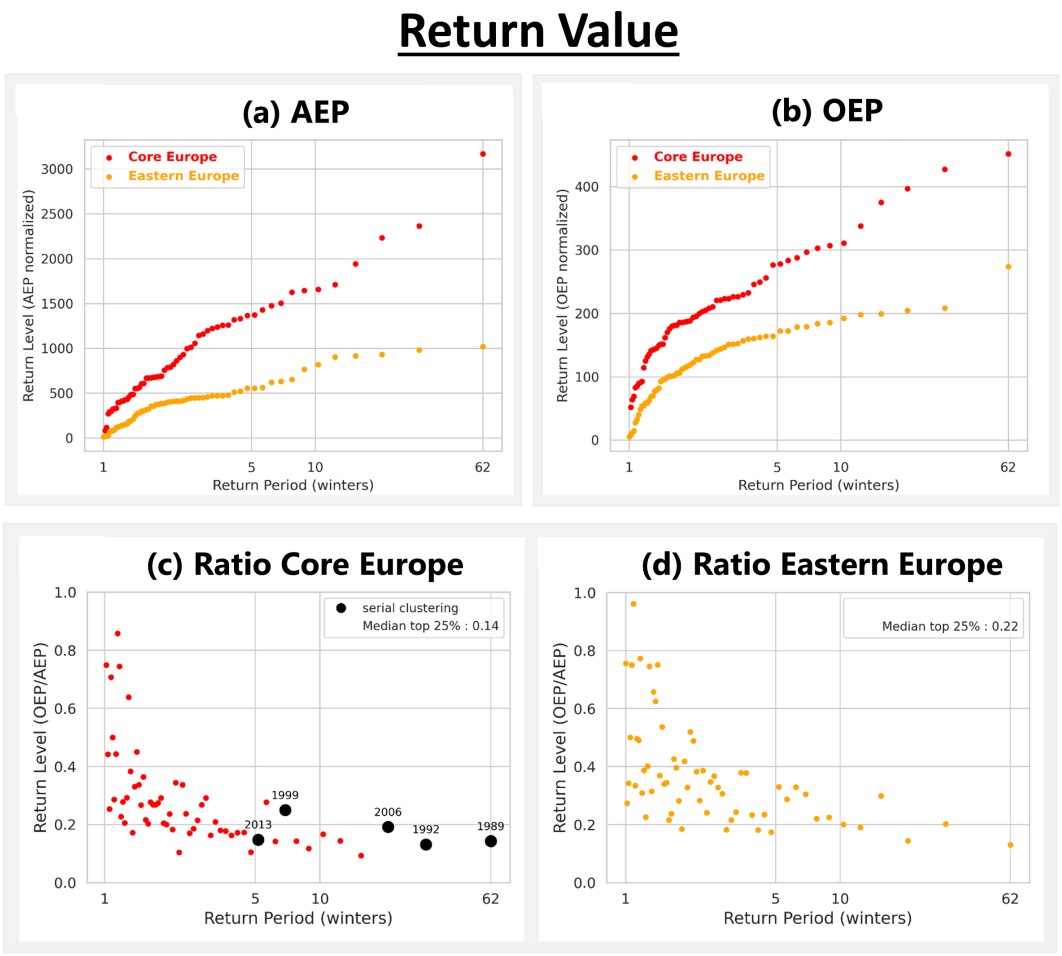

Figure 7.6.: Empirical return values of (a) normalized AEP and (b) normalized OEP from LI ERA5 (1959-2021), with values normalized by the number of grids in each region. The empirical return value of the OEP/AEP ratio, ranked by AEP values, for Core Europe (c) and Eastern Europe (d). In (c,d), the minimum return period corresponds to the smallest AEP, and the maximum to the largest. In Figure (c), black dots indicate the first year of winter seasons with serial clustering of windstorms based on Pinto et al. (2014). The "median top 25%" in the legend refers to the median of the OEP/AEP ratio for the winters with the highest AEP values, specifically the top 25% (15 out of 62 winters). The red dot represents Core Europe, and the orange dot represents Eastern Europe. Each point corresponds to one winter.

A comparison of normalized AEP, OEP, and the OEP/AEP ratio distributions, represented as return periods, was conducted to assess the susceptibility of each region to various levels of seasonal losses and identify seasonal loss clustering patterns (Figure 7.6). AEP and OEP values are normalized by the number of grid points in each region to ensure comparisons between Core and Eastern Europe purely reflect the influence of wind and population density, independent of regional size. As expected, Core Europe displays shorter return periods for AEP and OEP compared to Eastern Europe. For example, a 3-year

AEP in Core Europe takes 10 years to occur in Eastern Europe, while a 10-year OEP in Eastern Europe happens every 2 years in Core Europe (Figure 7.6 a,b). The OEP/AEP ratio plot shows that the low ratio mainly occurs at higher return periods linked to large AEPs (Figure 7.6 c,d). In Core Europe, the low OEP/AEP ratio is prominent during winters with serial windstorm events, such as 1989/1990 and 1992/1993 (Pinto et al., 2014). These winters, with high AEP values and low OEP/AEP ratios (below 0.3), show that multiple windstorms can lead to large AEPs, driving clustered seasonal losses. Seasonal loss clustering arising from multiple windstorms in Core Europe is most pronounced in the 25% most severe winters (15 out of 62).

Although specific studies on serial windstorm clustering in Eastern Europe are lacking, storm tracks from Core Europe often reach into the northern part of Eastern Europe during serial windstorm clustering seasons (Roberts et al., 2014). Furthermore, positive dispersion statistics of storm counts suggest the presence of serial windstorm clustering in the northern part of Eastern Europe (Priestley et al., 2018). Consequently, this study focuses on the top 25% of winters with the largest AEP to identify years of significant seasonal loss clustering in both Core and Eastern Europe. A lower mean of the OEP/AEP ratio in Core Europe than in Eastern Europe for the top 25% of winters indicates that Core Europe experiences more frequent windstorm events that cumulatively contribute to the total seasonal losses than Eastern Europe.

7.1.3. Characteristics of high AEP season

To refine the definition of seasonal loss clustering from Priestley et al. (2018), which does not specify what qualifies as a "low" or "high" OEP/AEP ratio, seasons with the top 25% AEP are used to explore this. The investigation begins by examining the characteristics of these high AEP seasons (Figure 7.7). The first characteristic found is that the high AEP values for the top 25% AEP seasons in Core and Eastern Europe are primarily due to many storms contributing to the total loss, indicating a low OEP/AEP ratio, and not because of a very large OEP. The second characteristic observed for Core Europe is that 80% of the seasons in the top 25% AEP have an OEP/AEP ratio below the first tercile of OEP/AEP climatology, while only 20% have an OEP/AEP ratio from the first to second terciles. Therefore, it can be inferred that the first tercile of the climatology of the OEP/AEP ratio can be used as a threshold to categorize a season as having seasonal loss clustering, as it accounts for 80% of the seasons. The use of the first tercile is justified because it effectively captures the lower range of OEP/AEP ratios, where seasonal loss clustering is most prevalent. By applying the same definition of seasonal loss clustering threshold, Eastern Europe has fewer seasons with seasonal loss clustering (67%) compared to Core Europe (80%). Since no top 25% AEP seasons exceed the second tercile of the OEP/AEP ratio climatology, seasons with ratios above this tercile are classified as non-clustering seasons. Meanwhile, seasons with an OEP/AEP

ratio from the 1st to 2nd tercile are categorized as neutral seasons, where both loss clustering and single event-dominant seasons may occur.

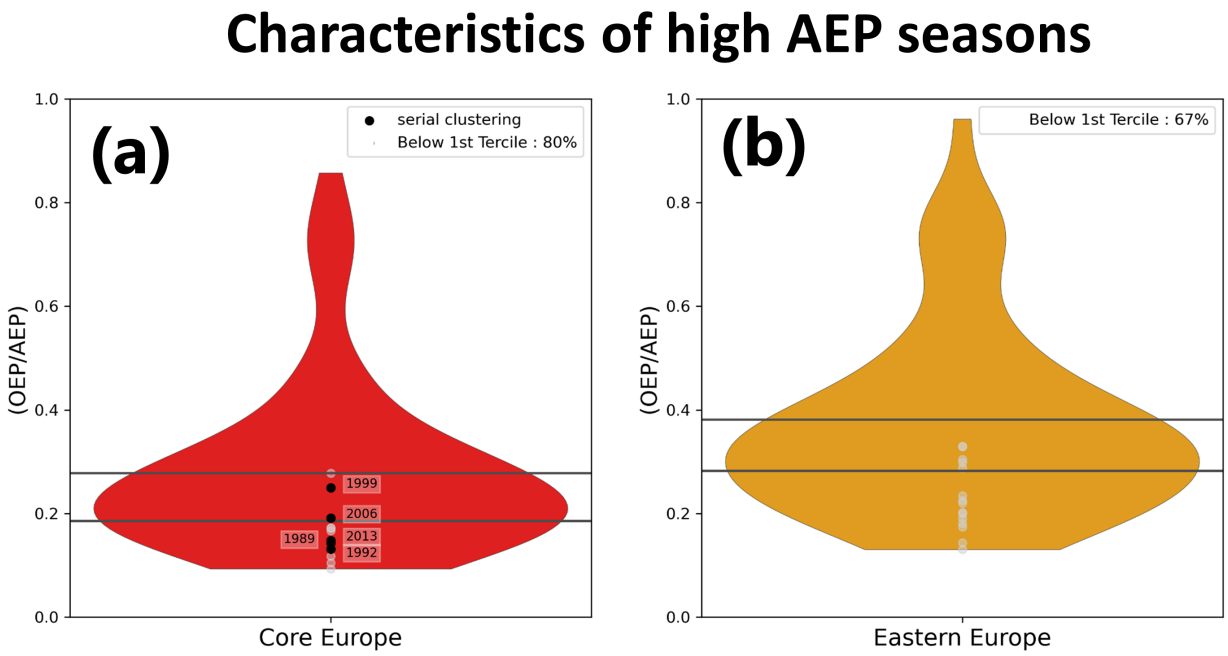

Figure 7.7.: The violin plot of the OEP/AEP ratio (all winters from 1959-2021) for (a) Core Europe and (b) Eastern Europe. The bottom and upper solid gray horizontal lines represent the 1st (33.33%) and 2nd (66.66%) terciles of the OEP/AEP ratio climatology. The gray and black dots indicate the OEP/AEP ratios for the top 25% of AEP. The black dots with labeled years represent seasons where serial clustering windstorms occur, based on Pinto et al. (2014), with the years indicating the first year of the full winter season. The percentage (below the 1st tercile) refers to the proportion of seasons in the top 25% AEP that fall below the 1st tercile of the OEP/AEP ratio climatology for each region.

The reason for using terciles as a threshold in the OEP/AEP ratio for loss clustering is that they offer more flexibility in handling data variability compared to quartiles or percentiles, which are more sensitive to outliers (Campbell, 2021). Terciles divide the data into three groups, making them less affected by extreme values. By using terciles, the focus can remain on general patterns in the OEP/AEP ratio without being overly influenced by outliers that do not reflect the overall trend. In this study, terciles divided the seasons into three distinct categories (clustering, neutral, and non-clustering), providing clear and simple categorizations that can be directly used for further analysis.

7.2. Seasonal loss clustering under climate change

This section investigates the possible impact of climate change on AEP, OEP, and the OEP/AEP ratio to assess shifts in the likelihood of seasonal loss clustering. The return periods of AEP and OEP are shown for Core and Eastern Europe (Figure 7.8). In Core Europe, the general pattern shows that under GWL3, large AEPs are less frequent because it takes longer to reach them. However, under GWL2, large AEP

seasons happen more frequently as they occur in shorter time spans. For OEP, the overall changes in Core Europe are minimal, but large OEP seasons happen slightly more often under GWL2 with shorter return periods. In contrast, Eastern Europe shows a more pronounced shift, with large AEPs and OEPs occurring more frequently under both GWLs compared to the historical period. The results above suggest that the impact of GWLs on AEP in Core Europe is unclear, as large AEPs are less frequent under GWL3 but more frequent under GWL2. In contrast, Eastern Europe clearly faces an increased risk of severe AEPs and OEPs under both GWLs.

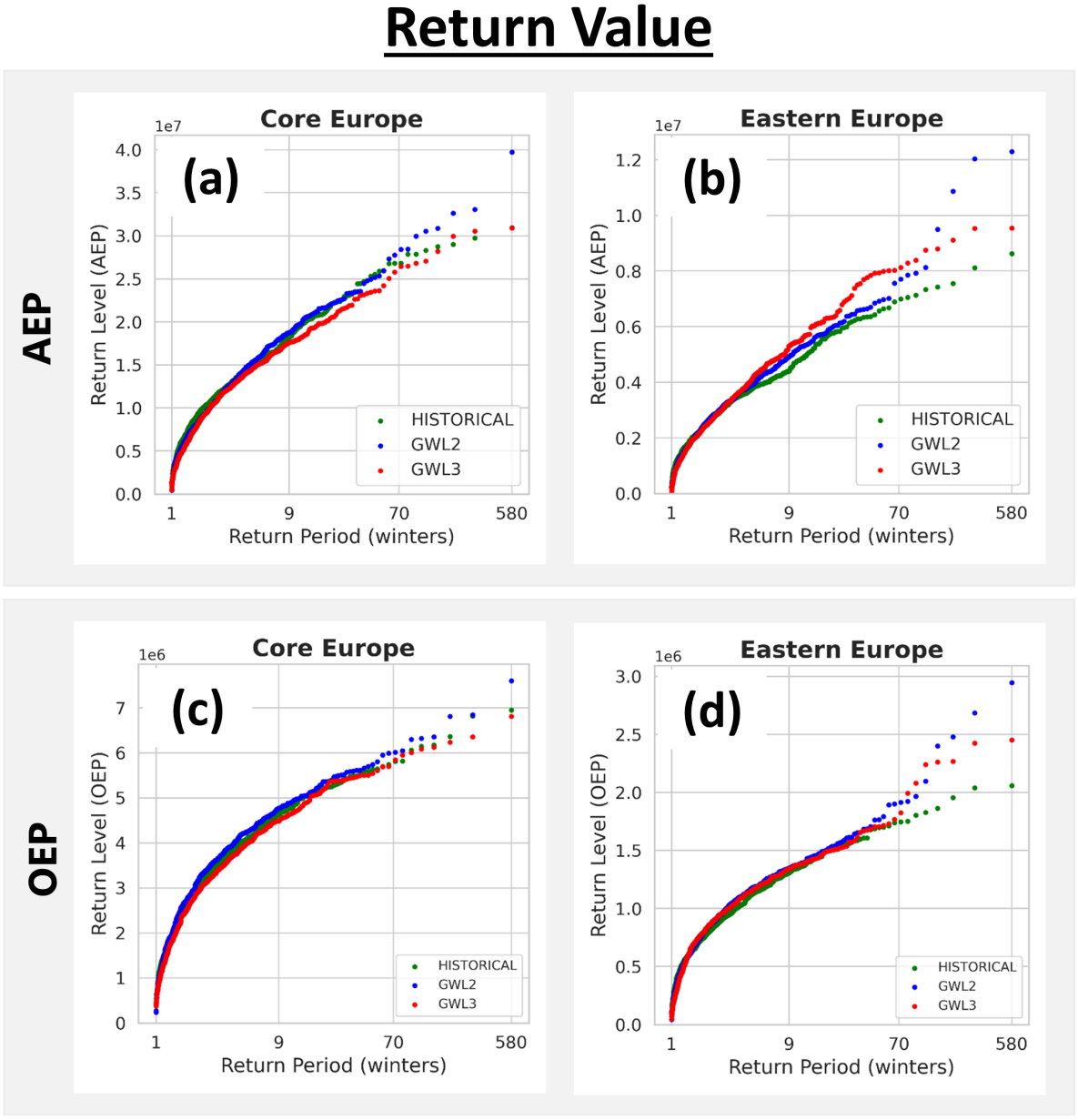

Figure 7.8.: Empirical return values of AEP (upper row) and OEP (lower row) from LI (EURO-CORDEX ensemble) for (a,c) Core Europe and (b,d) Eastern Europe are shown for the historical period (green), GWL2 (blue), and GWL3 (red). Each point represents one winter.

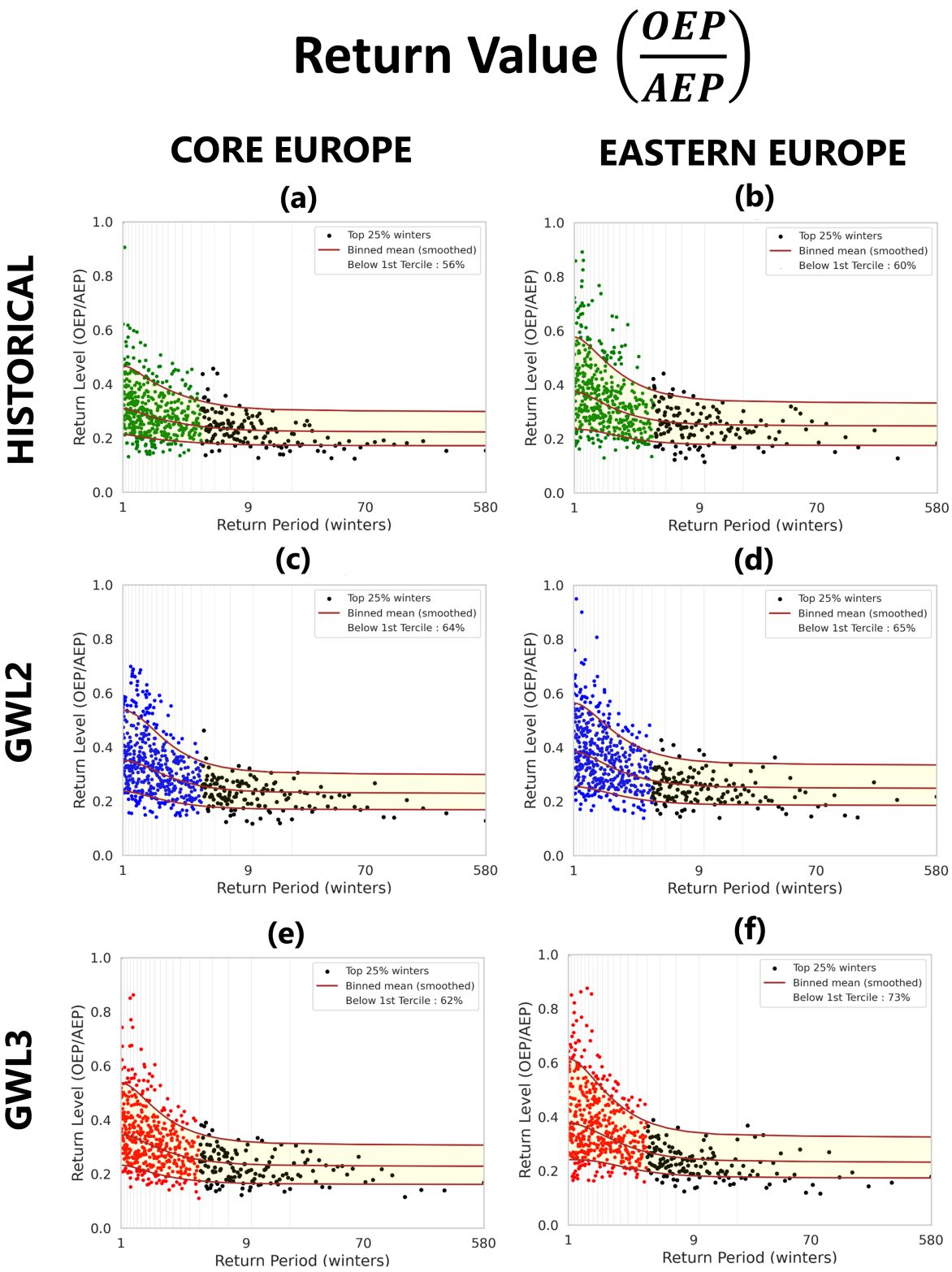

Figure 7.9.: Empirical return values of the OEP/AEP ratio from the EURO-CORDEX ensemble, ranked by AEP value, are shown from the historical period to GWLs for (a,c,e) Core Europe and (b,d,f) Eastern Europe. The OEP/AEP ratio at the minimum return period corresponds to the smallest AEP, while the ratio at the maximum return period corresponds to the largest AEP. The thin vertical gray lines represent the bin sizes for every 5% density of the data. The solid brown lines represent the averages of OEP/AEP within each bin, smoothed using Gaussian smoothing, which reduces noise by averaging nearby points with more weight: the bottom 25% of values (lower line), the middle 50% of values (middle line), and the top 25% of values (upper line). The percentage (below the 1st tercile) represents the proportion of seasons in the top 25% AEP that have an OEP/AEP ratio below the 1st tercile (33.33%) of the OEP/AEP ratio climatology for each period.

The overall patterns in the OEP/AEP ratio under GWLs, compared to the historical period, remain generally consistent (Figure 7.9). In other words, seasons with low OEP/AEP ratios (loss clustering seasons) are associated with high AEP values. The model ensemble shows a large spread in the OEP/AEP ratio, making it difficult to identify clear differences between GWLs and the historical period. Similarly, for the top 25% of winters with the highest AEP—where serial windstorm clustering was previously observed in ERA5 data—the overall changes are generally small. When applying the clustering definition using a threshold based on the 1st tercile of OEP/AEP climatology (Section 7.1.3), both regions show an increase in the percentage of loss clustering seasons under GWLs compared to the historical period, with a slightly larger climate change signal in Eastern Europe than in Core Europe. This might be due to the more zonal storm tracks, which extend further east under future climate, as previously observed in other climate model data (e.g., Pinto et al. 2013; Harvey et al. 2020). However, it must be noted that bias and uncertainty are observed, as the historical period shows slightly more loss clustering in Eastern Europe (60%) than in Core Europe (56%), which is not in agreement with the expected pattern in the real world, where Core Europe typically shows more loss clustering seasons than Eastern Europe (as previously shown in ERA5 data). This discrepancy is attributed to the large spread in the EURO-CORDEX ensemble. To summarize, the EURO-CORDEX successfully identifies the overall pattern of the OEP/AEP ratio, where low OEP/AEP ratios correspond to large AEP seasons. However, the model doesn't accurately represent the seasonal loss clustering due to the large spread in the model ensemble.

7.3. Summary and discussion

The investigation of the regional variation in seasonal loss clustering under the current climate, as well as the changes under GWLs compared to the historical period, was conducted. The key findings of this chapter are summarized below:

Section 7.1. Seasonal loss clustering under historical period

- Seasonal loss clustering is common in seasons with an OEP/AEP ratio below the first tercile of the OEP/AEP climatology for seasons having the top 25% of AEP values, with clustering occurring more frequently in Core Europe than in Eastern Europe.

- Both AEP and OEP values in Core Europe are larger, with shorter return periods compared to Eastern Europe.

Section 7.2. Seasonal loss clustering under climate change

- The EURO-CORDEX successfully captures the overall OEP/AEP ratio pattern, where a low ratio corresponds to large AEP seasons. For Core and Eastern Europe, an increase in the number of seasons with seasonal loss clustering was observed under both GWLs compared to the historical period. However, bias and uncertainty remain, as the model failed to accurately represent seasonal loss clustering under the historical period.

- The impact of GWLs on seasonal loss value in Core Europe remains unclear, whereas Eastern Europe faces a clear increase in the risk of severe AEPs and OEPs under both GWLs.

Consistent with the study of Priestley et al. (2018), this study reveals a clear positive relationship between AEP and OEP, where higher AEP values are consistently associated with higher OEP values. Unlike Priestley et al. (2018), which found that seasons with large AEP could result from either low or high OEP/AEP ratio, this study demonstrates that large AEP values consistently indicate low OEP/AEP ratio across datasets. Despite this difference, both studies agree that OEP/AEP ratios cannot reliably predict OEP patterns due to the irregularity and variability of losses from single events, whereas AEP is more predictable. Additionally, this study highlights that winter seasons with serial windstorm clustering (Leckebusch et al., 2007; Pinto et al., 2014) consistently rank among the highest AEP values, which has not been explored in the previous study.

The differences between this study and Priestley et al. (2018) likely stem from the threshold of loss value used to calculate OEP and AEP and the differences in datasets used. First, in terms of the loss value threshold, Priestley et al. (2018) calculated the OEP/AEP ratio using all events, whereas this study only considers events above a certain threshold. The drawback of using all events is that in seasons with many storms but relatively small extreme losses, the loss distribution is more evenly spread. This can result

in a low OEP/AEP ratio, classifying the season as loss clustering with a high AEP. However, since the storms are relatively small, this may be less relevant for insurance companies. This approach makes the OEP/AEP ratio more sensitive to smaller extreme events. Second, Priestley et al. (2018) shows that the OEP/AEP ratio pattern varies across datasets when using all events. However, this study finds that when using events above a certain threshold, the general pattern of the OEP/AEP ratio, sorted by AEP values, is similar between the ERA5 and EURO-CORDEX datasets, with high AEP consistently corresponding to a low ratio. This suggests that the relationship between OEP/AEP ratio and AEP is relatively robust and not highly sensitive to the specific dataset, at least when extreme events are considered. The robust relationship found in this study could also arise from using a higher-resolution dataset. Thus, the threshold-based approach might provide a more stable and consistent measure of loss clustering across different datasets, allowing for more reliable comparisons between them.

This study examined regional differences in seasonal loss clustering from an insurance perspective. Results show that seasonal loss clustering is more frequent in Core Europe than in Eastern Europe, as reflected by a lower OEP/AEP ratio and shorter return periods for both AEP and OEP in Core Europe. This is attributed to Core Europe's proximity to the North Atlantic storm track, which leads to a higher frequency and intensity of multiple storms occurring within a season (Dacre and Pinto, 2020). In contrast, Eastern Europe, situated further downstream, experiences weaker, less frequent storm clusters and longer return periods. Thus, Core Europe's location and exposure to key meteorological drivers make it more susceptible to seasonal loss clustering, thereby shortening the return periods for AEP and OEP.

This study examined how climate change affects AEP and OEP, highlighting differences between Core and Eastern Europe under various GWLs in comparison to the historical period. In Core Europe, the impacts of climate change on extreme AEP are mixed: return periods shorten under GWL2 but lengthen under GWL3, suggesting that risk levels vary with warming intensity. Meanwhile, OEP remains relatively stable. In contrast, Eastern Europe shows consistently shorter return periods for both AEP and OEP across all GWLs, implying a clear and predictable increase in risk compared to historical baselines. The results of this study for seasonal loss (AEP and OEP) are consistent with Alifdini et al. (2025) (Chapter 6), which identified differing changes in rare extreme losses between Core and Eastern Europe from the same EURO-CORDEX dataset. Core Europe shows no clear climate change signal for rare extreme events, while Eastern Europe displays more consistent changes, with projected shortening of return periods under GWLs compared to historical climate conditions. The shortening of return periods for AEP and OEP in Eastern Europe may be associated with the eastward extension of North Atlantic storm tracks, as noted by Ulbrich et al. (2009) and Harvey et al. (2020). In addition, Karremann et al. (2014a) demonstrated that the combination of increased individual loss events and loss clustering in a warmer climate would result in significantly shorter return periods for storm series impacting Europe.

In addition to evaluating the impact of climate change on AEP and OEP, changes in the OEP/AEP ratio are examined to understand how climate change may influence seasonal loss clustering. Findings indicate no significant differences in the overall patterns of OEP/AEP ratio under GWLs compared to historical periods. This aligns with the results in Chapter 6, that climate change has a modest impact on storm frequency and intensity in these regions, with projected changes varying across models. Similarly, Economou et al. (2015) observed only small and inconsistent changes in serial windstorm clustering using dispersion statistics across CMIP5 models, in line with the minimal changes in the overall patterns of the OEP/AEP ratio identified in this study. In addition, Economou et al. (2015) shows that changes in windstorm clustering are difficult to observe in the CMIP5 ensemble due to the large spread in the model. This is also observed in the EURO-CORDEX dataset, which downscales from CMIP5, where the large spread in the model ensemble makes it challenging to draw robust conclusions about the impact of climate change on seasonal loss clustering. The loss clustering observed in this study differs from the findings of Karremann et al. (2014b), who analyzed loss clustering by focusing on top events with dispersion statistics (Mailier et al., 2006) and a negative binomial distribution (Wilks, 2006), without examining OEP and AEP variability per winter. Different methods offer different perspectives on windstorm clustering, which can lead to varying results (Dacre and Pinto, 2020).

The regional differences in seasonal loss clustering and the impacts of climate change can provide valuable insights for insurance and reinsurance companies in adjusting premiums and capital allocation strategies. For instance, in Eastern Europe, where return periods for AEP and OEP are shortening under GWLs, premiums in the long term may need to rise to reflect the increased risk of multiple storms. Moreover, it is important for insurers to update catastrophe models to incorporate regional changes in seasonal loss clustering by utilizing higher-resolution climate model data to enhance risk predictions. Traditional catastrophe models may not adequately capture the shifts in AEP and OEP identified in this study, particularly under varying GWLs. By integrating more accurate climate data into their models, insurers can better anticipate future shifts in storm clustering and minimize the financial impact of extreme storm series.

This study has some shortcomings. First, to build upon this preliminary analysis of changes in seasonal loss clustering, further study is necessary to investigate potential shifts in storm tracks under various GWLs using EURO-CORDEX data, allowing for a more comprehensive comparison of clustering from multiple viewpoints. Second, it would be beneficial to explore seasonal loss clustering using larger climate model ensemble (Karwat et al., 2024). Nevertheless, the outcomes of this study provide valuable insights for insurance companies, aiding in the exploration of potential changes in seasonal loss clustering under climate change and facilitating informed decisions regarding premiums.

8. Discussion and conclusions

The main goal of this thesis is to investigate the impact of European windstorms under both current and future climate conditions by considering different perspectives. Examining these windstorms in such contexts is crucial due to the significant damage they cause to infrastructure, property, and natural environments. Chapter 5 establishes the foundation by comparing the meteorological loss index (LI) method with the insurance loss model, providing key insights into windstorm losses from different perspectives. Chapter 6 expands the analysis by investigating changes in LI using EURO-CORDEX datasets, offering a clear picture of how climate change affects windstorm loss over time. Chapter 7 builds on this by examining seasonal loss clustering under both current and future climate conditions, exploring how the dominance of single vs multiple events for the total seasonal loss may evolve in future decades. This chapter presents an overview and key findings of each chapter, followed by a discussion, outlook, and overall conclusions of the thesis.

8.1. Overview and key findings

8.1.1. Insurance loss model vs. meteorological loss index

In Chapter 5, windstorm loss estimates from the LI method were compared with those from Aon Impact Forecasting's proprietary catastrophe model, which are not publicly available. Comparing the LI (which uses wind gust speed and population as a proxy with traditional insurance loss models (based on hazard, exposure, and vulnerability) provides valuable insights into the trade-offs between simplicity and accuracy while also validating the reliability and robustness of loss estimates from different perspectives. This process also aids in identifying areas that can be improved upon and facilitates informed decision-making within the insurance industry. Prior to comparing with the insurance model, the sensitivity of the LI method was first evaluated using two different reanalysis datasets: ERA5 and ERA-Interim. The general behavior of the LI is largely similar when using ERA5 or ERA-Interim. In Chapter 5, the main aim is to address the first research question of this thesis:

Research question 1 : How comparable are windstorm loss estimates from a meteorological loss index and a full insurance loss model ?
Compared to Aon's IF Euro WS model, the LI tends to underestimate high-impact storms; however, it is well-suited for ranking events, and thus remains a simple and effective tool to estimate losses from the meteorological perspective.

8.1.2. Future changes in European windstorm losses

In Chapter 6, the investigation of the changes in windstorm losses under different global warming levels (GWLs), in comparison to historical periods, was conducted utilizing the EURO-CORDEX dataset. Using EURO-CORDEX provides more precise and location-specific insights, which are essential for understanding the local impact of windstorms under climate change. These insights help insurance companies better anticipate and manage risks, supporting greater stability in financial markets. The main aim of Chapter 6 is to address the second research question of this thesis :

Research question 2 : How does climate change affect windstorm losses across Europe based on a multi-model RCM ensemble ?
The projected changes in windstorm losses are small and mostly non-robust, with generally small negative trends for Core Europe and small positive trends for Eastern Europe. For the most extreme loss events, the model ensemble projects shorter return periods for Eastern Europe regardless of the GWLs, while no clear trends emerge for Core Europe.

8.1.3. Seasonal loss clustering in a warming climate

In Chapter 7, for the first time, the seasonal loss clustering of windstorms was investigated from insurance perspectives under both current and future climate conditions. This study is crucial for insurance companies, as multiple extreme windstorms in a season can lead to significant economic losses, underscoring the need for adequate capital reserves to cover such risks. Chapter 7 mainly aims to address the third research question of this thesis:

Research question 3 : What are the characteristics of years with high AEP in terms of seasonal loss clustering in a warming climate ?
For high AEP seasons (top 25% AEP), seasonal loss clustering is prevalent in seasons with an OEP/AEP ratio below the first tercile of the OEP/AEP climatology, indicating a dominance of multiple windstorms for this season. This effect is more prevalent in Core Europe than in Eastern Europe. Under climate change, the number of seasons with seasonal loss clustering increases, with a slightly larger increase in Eastern Europe compared to Core Europe. However, bias and uncertainty exist, as the models fail to accurately represent seasonal loss clustering during the historical period due to the large spread in the model ensemble.

8.2. Discussion

This section highlights the key lessons from the three chapters and explores how the results contribute to advancing the understanding of windstorm losses by connecting the findings across the three chapters (Table 8.1). Furthermore, this section addresses the challenges and limitations encountered in the study and identifies potential areas for future research. The discussion highlights three key aspects: the use of the Loss Index (LI) to estimate windstorm loss, the insurance implications of the findings, and the impact of variations in the datasets employed. These insights provide a deeper understanding of the research gaps that can be addressed and improved upon in the future.

First, the uses of LI to estimate windstorm loss have been implemented from Chapter 5 to Chapter 7. In Chapter 5, the analysis explored losses from two perspectives: the LI perspective and the insurance viewpoint. Although the LI method cannot be used for pricing insurance storms, our results show that it remains an effective index and can be widely used in scientific communities for estimating impacts and ranking storm events due to its simplicity of computation. Therefore, Chapters 6 and 7 use the LI method to study the impact of climate change on windstorm losses, including seasonal loss clustering. A key advantage of the LI method, as highlighted in Chapter 7, is its ability to effectively capture the link between seasons with high AEP and seasonal loss clustering. This connection was not as well represented in Priestley et al. (2018). However, the LI formulation introduces some limitations. Because it involves cubing the ratio of the maximum wind gust to the 98th percentile of daily maximum wind gusts (Pinto et al., 2012), even a small bias in wind data can result in significant variations in LI values. For instance, in Chapters 6 and 7, minor errors in the EURO-CORDEX climate model can lead to large discrepancies in LI estimates. Given the sensitivity of LI to errors in climate models, bias correction, and the combination of outputs from multiple models, as demonstrated in Chapters 6 and 7, can help reduce uncertainty and yield more reliable estimates.

Table 8.1.: A Summary of insights from each result chapters and conclusions drawn from the overall findings.

Topic	Chapter 5	Chapter 6	Chapter 7	Conclusion
Effectiveness of LI	LI is a simple and effective method for storm loss ranking.	Small model biases can significantly affect LI values and windstorm losses.	LI well captures loss clustering, with high AEP values linked to loss clustering.	LI is effective for storm ranking and loss clustering, but small model biases can significantly impact its values.
Insurance implications	The Aon IF model distinguishes loss values across levels, but a comparison with other insurance models is needed.	The bias-corrected high-resolution EURO-CORDEX dataset can be used to update the hazard component in insurance models.	The large spread in climate model data makes it challenging for insurers to detect future changes in loss clustering.	Insurers should compare their catastrophe models with others and use higher-resolution climate models to improve regional loss assessments and windstorm pricing.
Dataset impact	Varying data resolutions using the same wind gust parameterization show minimal impact on the overall storm loss ranking.	Biases in GCMs, RCMs (downscaling process), and wind gust parameterization contribute to uncertainty in loss estimates.	Different datasets exhibit similar overall seasonal loss clustering patterns, likely due to bias correction.	Different resolutions of data have little effect on loss patterns, but climate model biases potentially introduce uncertainty in estimates.

The second area concerns the implications for insurance, highlighting what insurance companies need to improve in their catastrophe models to better prepare for the risks of windstorm losses under climate change (Pielke et al., 1999; Rose and Huyck, 2016). In Chapter 5, the insurance loss model from Aon Impact Forecasting performs better when discerning losses across different storm intensities, compared to the LI. However, to further evaluate the performance of Aon's IF Euro WS model, it would be valuable to compare it with other insurance models, although the absence of a universally accepted "ground truth" for loss values complicates such assessments (Moemken et al., 2024b). Although PERILS collects reported windstorm loss data from multiple insurers to provide industry-wide insights for European events, helping insurers validate their loss values, it does not compare the catastrophe model settings used by different insurers.

Comparing windstorm losses across multiple insurance companies is valuable for several reasons. For example, do catastrophe models tend to underestimate losses in high-risk areas or overestimate them? Even though there is a lack of a definitive "truth" or reference model, as catastrophe models are based on probabilistic simulations of extreme events, cross-model comparisons across multiple insurance companies can help identify patterns or discrepancies. Insurance companies use different catastrophe models, each

with distinct methodologies, assumptions, and data sources (Mitchell-Wallace et al., 2017). In addition, these companies have different portfolios (residential, commercial, and industrial), and this influences how they use catastrophe models (Grossi et al., 2005). A study comparing windstorm losses from catastrophe models across insurance companies would reveal key differences in hazard assumptions, exposure data, and vulnerability curves—areas often obscured by the "black box" nature of these models (Khanduri and Morrow, 2003; Dumm et al., 2008; Black et al., 2018). Comparing these assumptions across insurers would reveal how sensitive models are to different parameters, helping identify which variables drive the most significant variations in loss estimates. Such a comparative study could also evaluate how well insurers align with regulatory standards for solvency and risk management (Parliament, 2009), particularly in the context of seasonal loss clustering, as discussed in Chapter 7. Additionally, with the growing importance of climate change and emerging risks, understanding how different companies assess these risks through catastrophe models could have far-reaching implications for the future of the insurance industry.

One major challenge for insurers is estimating possible changes in windstorm losses due to climate change, which remains highly uncertain (Little et al., 2023; Severino et al., 2024; Jaison et al., 2024). The uncertainty in the impact of climate change on windstorm loss makes it more difficult to accurately assess the potential impact of these events, resulting in challenges in setting appropriate pricing for insurance companies (Déroche, 2023). This underscores the need for insurance companies to update their catastrophe models by incorporating more refined climate models. For example, the bias-corrected EURO-CORDEX wind gust data from this study (Chapter 6) can be used to update the hazard component in insurance catastrophe models (Chapter 5), enabling direct application in the industry for assessing windstorm loss changes in pricing. By using more refined climate models, insurers can better discern the premiums for windstorm losses across different European countries, as these models are better equipped to capture regional wind differences. For instance, this study has shown that there is a difference in the climate change signal of windstorm losses (Chapters 6 , 7) between Central and Eastern Europe. Insurance companies could take this into account, as the thresholds for premiums across different countries in Europe should vary accordingly. Furthermore, employing an ensemble of models allows insurers to predict the probability of windstorm losses across a range of scenarios.

Third, the results of this study discuss the impact of using different datasets in windstorm loss assessments. Chapter 5 emphasizes the importance of understanding how variations in data resolution can influence these loss estimates, although these datasets use the same wind gust parameterization. The results show that while the general behavior of storm ranking and the order of normalized loss remain largely unchanged, the magnitude of loss is influenced by resolution, with higher resolution data yielding larger LI values compared to lower resolution data due to the LI formulation. This leads to the following inquiry: What is the impact of different wind gust parameterizations on loss estimates? The

impact could lead to more pronounced effects on loss values and storm rankings, as different wind gust parameterizations can cause variations in the magnitude of wind gust speeds (Sheridan, 2011; Born et al., 2012; Kurbatova et al., 2018). A previous study by Born et al. (2012) showed that different wind gust parameterizations can significantly influence wind gust speed estimates across diverse terrains; thus, refining these methods to incorporate topographical effects is essential for improving prediction accuracy. Different parameterizations for wind gusts can introduce variability into model outputs, as wind gusts are influenced by terrain, land-sea contrast, and atmospheric turbulence, all of which are challenging to simulate precisely (Sheridan, 2011, 2018). However, in Chapter 7, the general behavior of seasonal loss clustering based on the AEP value does not differ significantly from the behavior in ERA5. This may be because the EURO-CORDEX data was bias-corrected using ERA5 data.

In addition to the impact of different wind gust parameterizations mentioned above, the impacts of downscaling in climate models are also discussed. Chapter 6 shows that different GCMs and RCMs in the EURO-CORDEX data can exhibit varying patterns of climate change signals. However, it remains unclear whether these patterns originate from the GCMs or RCMs. The bias and uncertainty in EURO-CORDEX wind gust data may arise from the uncertainty in GCMs, as RCM data is downscaled from GCM data to create higher-resolution models (Vautard et al., 2021; Wohland, 2022; Michel and Sorteberg, 2023). Additional uncertainty can also come from the performance of different wind gust parameterizations (Born et al., 2012). Both GCMs and RCMs require parameterizations to represent smaller-scale phenomena like wind gusts, which may vary based on the method used. This means that both the inherent uncertainty in the GCM/RCM chain and the variability in how wind gusts are parameterized contribute to the overall uncertainty in wind gust predictions in regional climate models. Another challenge is selecting GCMs for downscaling, ensuring they are both robust (perform reasonably well) and independent (not overly similar to each other), as their ability to simulate climate conditions varies by season, region, and climate variables such as wind (Zhang et al., 2024). Otherwise, the scarcity of historical data—due to the relative rarity of windstorm events and their regional variability—limits the ability to calibrate and validate climate models against recorded windstorm losses (Della-Marta et al., 2010). Recent efforts, including comparisons of historical climate models with high-resolution reanalysis datasets like ERA5 (chapter 6) and optimizing wind downscaling techniques (Ekström et al., 2015), have started to address some of these issues. However, gaps remain in verifying wind conditions, especially in regions with few observations, and all datasets, including observations, have biases that add uncertainty to climate models (Kotlarski et al., 2019).

The main challenge in estimating future changes in windstorm losses lies in the uncertainty surrounding how climate change will impact storm tracks, storm characteristics, and wind patterns (e.g., Catto et al. 2019). These factors are still not fully understood, yet they are crucial in determining future windstorm risks (Masson-Delmotte et al., 2021a; Pörtner et al., 2022; Lee et al., 2023). This increased uncertainty

could also lead to higher reinsurance costs, as reinsurers may raise prices to account for the added financial risks of unpredictable events. The use of CMIP6 (the latest GCMs available), along with Shared Socioeconomic Pathways (SSP) scenarios, allows for a comprehensive analysis of the future impacts of windstorm losses on society by incorporating potential socioeconomic changes. However, even when using the CMIP6 model, there is still a large uncertainty and spread in windstorm loss changes in different models (Little et al., 2023; Severino et al., 2024). The large uncertainty in CMIP6 must be carefully considered when downscaling climate models for the ongoing CMIP6-CORDEX project (Katragkou et al., 2024). While large uncertainty in climate models offers a range of possible scenarios, excessive uncertainty can hinder policy-making and delay responses to climate risks. Therefore, it is thus of crucial importance to improve our climate models so that they can better capture the regional condition. Current high-resolution model data, such as convection-permitting climate model simulations that explicitly simulate convective processes at spatial scales of a few kilometers or less, can help address this challenge (Prein et al., 2015; Lucas-Picher et al., 2021; Takayabu et al., 2022). However, obtaining data from these simulations can be difficult due to the significant computational resources required to run them, given the high resolution and complexity of the models. The use of EURO-CORDEX data can capture the regional characteristics, but it has biases, and there is a large uncertainty between different models, as we have discussed in Chapter 6.

8.3. Concluding remarks

This study provides several contributions to a better understanding of windstorm losses under both current and future climate conditions, incorporating a comparative analysis of these losses from different perspectives. In Chapter 5, the Loss Index (LI) method, which is widely used within the scientific community, is contrasted with the windstorm loss models employed by an insurance company. The findings show that while both methodologies provide valuable insights, the LI method, although not suitable for determining storm pricing, is effective for estimating impacts and ranking events. Building upon this analysis, Chapter 6 and Chapter 7 extend the examination using LI to future climate projections utilizing the EURO-CORDEX dataset, revealing minimal changes in windstorm losses and the general patterns of OEP/AEP ratio (and thus the role of multiple storms per season) across most regions in Europe.

In Chapter 5, different methodologies yield varying loss estimates, underscoring the importance of methodological choices in accurately capturing windstorm losses, particularly for rare extreme events. Further research is needed to assess how these methodological choices introduce biases and affect loss estimates. This includes comparing loss estimates from other insurance models, which may vary in their hazard, exposure, and vulnerability components. To enhance the accuracy of loss estimates, finer-resolution hazard maps are essential for capturing windstorm characteristics at regional scales. Addition-

ally, creating synthetic events—hypothetical scenarios of rare or unprecedented windstorms—can help test the robustness of catastrophe models and assess their ability to predict potential losses in extremely rare events (Becker, 2019; Welker et al., 2021).

The impact of climate change on windstorm losses remains uncertain due to low agreement and large spread across climate models, highlighting the need for further investigation using higher-resolution climate models. With the growing number of machine learning and AI technologies in recent years, by using these technologies, we may be able to achieve more accurate or at least faster estimates of windstorm projections (Huntingford et al., 2019; Eyring et al., 2024; Lewis et al., 2024). The investigation on the characteristics of seasonal loss clustering presents additional challenges due to the limited historical records of clustered events. This issue can be addressed through stochastic simulations that generate synthetic seasonal scenarios of clustered windstorm events (Wang, 2008; Sharkey et al., 2020; Tsoi, 2024), the consideration of large datasets like LAERTES-EU (Ehmele et al., 2020, 2022), and the use of other large ensembles (e.g., Karwat et al. 2024) to extract physically consistent windstorm datasets. Such approaches enable insurers to explore a broader range of extreme clustered storm scenarios that may be underrepresented in historical data, allowing for a more thorough investigation of their impact on seasonal loss clustering.

To address these challenges, it is essential to continue fostering public and private partnerships that promote collaboration among insurers, academics, and policymakers. The outcomes of this study could serve as a valuable reference for the public, academic communities, and the insurance industry, which rely on accurate loss forecasting and risk management to estimate windstorm losses under both current and future climate conditions.

A. Appendix for Chapter 5

Table A.1.: List of top 20 storms from ERA5 for 1979-2019 for Core Europe. Information includes the storm name, storm rank, event period and value of Loss Index (LI). Shown are only the common 20 most extreme storms with ERA Interim. The table is reprinted from Table S2 in Moemken et al. (2024a), with copyright CC BY 4.0.

Rank	Storm name	Start date	End date	LI
1	Vivian, Wiebke	1990-02-26	1990-02-28	769794.9
2	Kyrill, Lancelot	2007-01-18	2007-01-20	724570.7
3	Daria	1990-01-25	1990-01-28	691602.4
4	Kurt, Lothar, Martin	1999-12-23	1999-12-26	639103.5
5	13 Jan 84, 14 Jan 84	1984-01-12	1984-01-15	573311.1
6	Verena	1993-01-12	1993-01-15	527002.6
7	Jeanett, Katharina, Lara	2002-10-25	2002-10-28	503317.0
8	Nov 84	1984-11-22	1984-11-24	487979.3
9	Braer, 13 Jan 93	1993-01-11	1993-01-14	485094.7
10	Andrea, Ulli	2012-01-03	2012-01-05	482571.3
11	Lore	1994-01-25	1994-01-28	468993.4
12	CE1	1997-02-24	1997-02-26	435918.6
13	Herta	1990-02-01	1990-02-04	435159.4
14	Dec-93	1993-12-08	1993-12-11	423932.7
15	Mike, Niklas	2015-03-29	2015-03-31	423640.9
16	Franz, Hanno, Gerhard	2007-01-10	2007-01-13	421784.4
17	Jan-95	1995-01-21	1995-01-24	416758.5
18	Johanna, Kirsten	2008-03-10	2008-03-12	396952.7
19	Gernot, Ingmar, Burglind	2018-01-01	2018-01-03	391770.7
20	11 Feb 90	1990-02-11	1990-02-14	390314.1

Table A.2.: Same as Table A.1, but for ERA Interim. The table is reprinted from Table S3 in Moemken et al. (2024a), with copyright CC BY 4.0.

Rank	Storm name	Start date	End date	LI
1	Vivian, Wiebke	1990-02-26	1990-03-01	81503.9
2	Daria	1990-01-25	1990-01-28	76591.4
3	Kyrill, Lancelot	2007-01-18	2007-01-20	70723.7
4	Kurt, Lothar, Martin	1999-12-25	1999-12-27	67481.7
5	Jeanett, Katharina, Lara	2002-10-25	2002-10-28	64321.1
6	13 Jan 84, 14 Jan 84	1984-01-12	1984-01-15	56511.3
7	Nov 84	1984-11-22	1984-11-25	51238.6
8	Dec-93	1993-12-08	1993-12-11	50957.0
9	Mike, Niklas	2015-03-29	2015-03-31	49616.4
10	Verena	1993-01-12	1993-01-15	49027.0
11	Andrea, Ulli	2012-01-03	2012-01-06	48946.2
12	Johanna, Kirsten	2008-03-10	2008-03-13	47165.6
13	CE1	1997-02-24	1997-02-26	47125.3
14	Lore	1994-01-25	1994-01-28	46779.8
15	Jan-95	1995-01-21	1995-01-24	46234.1
16	Gernot, Ingmar, Horst, Burglind	2018-01-01	2018-01-04	45150.2
17	13 Jan 93	1993-01-11	1993-01-14	44229.0
18	Herta	1990-02-01	1990-02-04	43373.9
19	11 Feb 90	1990-02-11	1990-02-14	41585.6
20	Franz, Hanno, Gerhard	2007-01-10	2007-01-13	38258.8

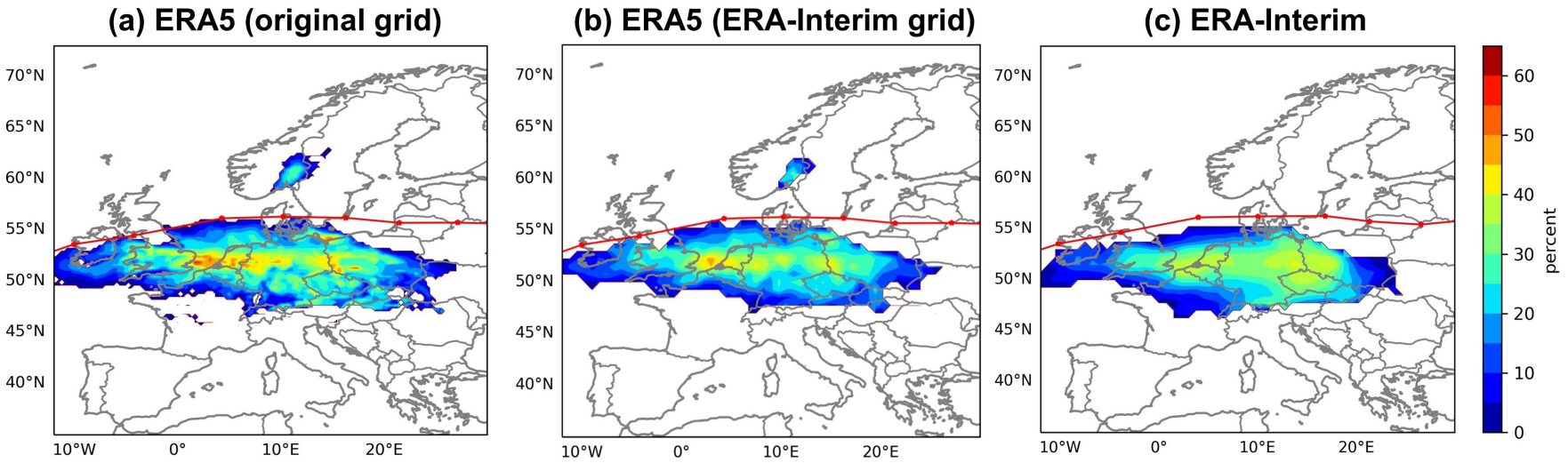

Figure A.1.: Wind gust footprint for storm Irina in October 2002 based on ERA5 (a), ERA5 re gridded to the ERA Interim grid (b), and ERA Interim (c). Shown is the largest exceedance (in percent) of the 98th percentile of daily maximum wind gust within 72 hours. The red line and dots denote the cyclone track derived from ERA5 (a, b) and ERA Interim (c) using the tracking algorithm of (Pinto et al., 2005). The figure is reprinted from Figure S1 in Moemken et al. (2024a), with copyright CC BY 4.0.

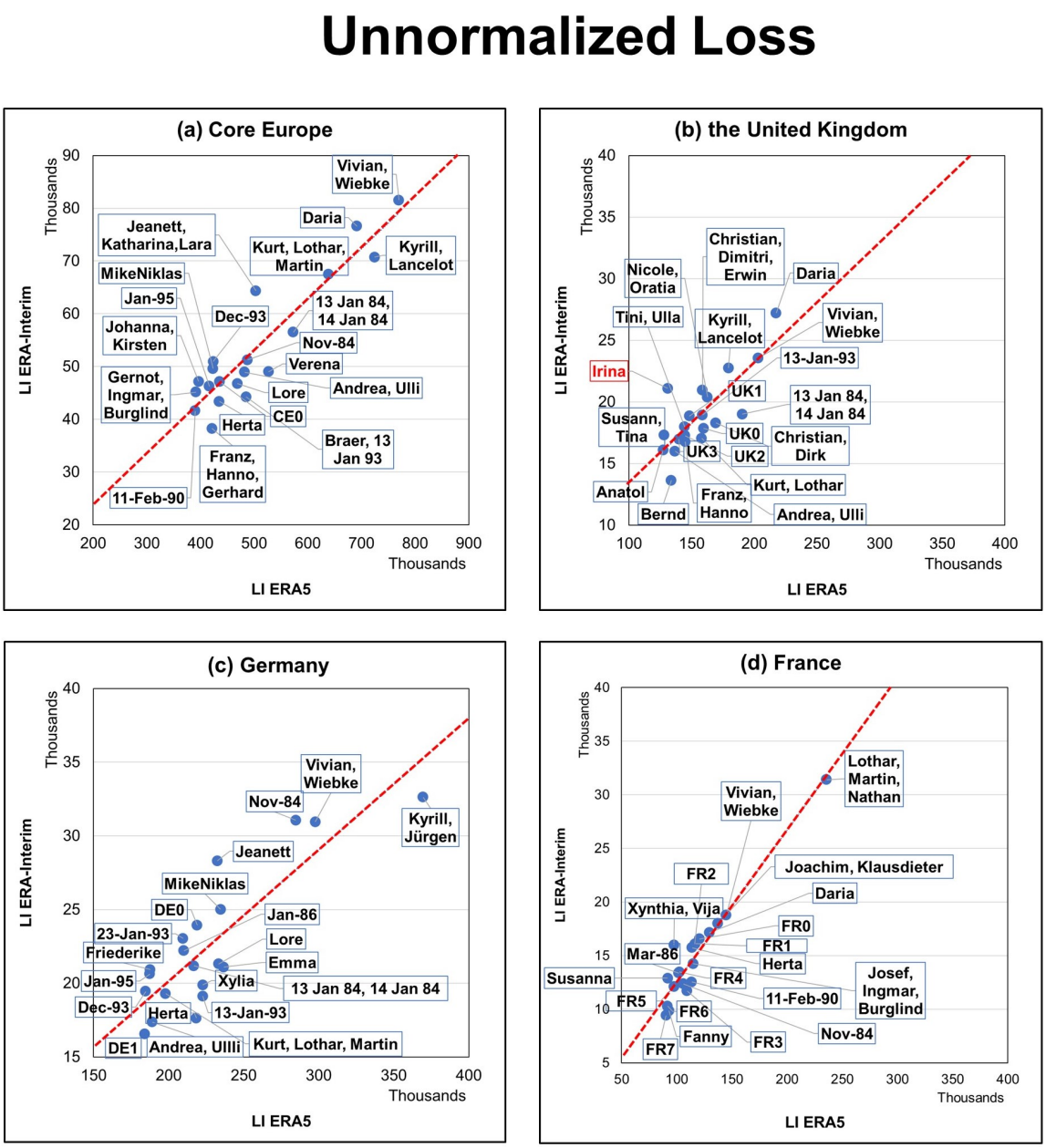

Figure A.2.: Comparison of loss values (in thousands) based on LI ERA5 (x axis) and LI ERA Interim (y axis). Depicted are the common 20 most extreme storms in the period 1979-2019 for (a) Core Europe, (b) the United Kingdom, (c) Germany, and (d) France. Corresponding storm names to each data point are marked with a blue line. Storms without a formal name are named based on the region (e.g. CE for Core Europe) and the loss value (starting for zero for storm with highest loss). The red dashed line denotes the linear regression line. Outlier storms based on the IQR method (see section 3.2) are marked in red. Please note the different scales. The figure is reprinted from Figure S2 in Moemken et al. (2024a), with copyright CC BY 4.0.

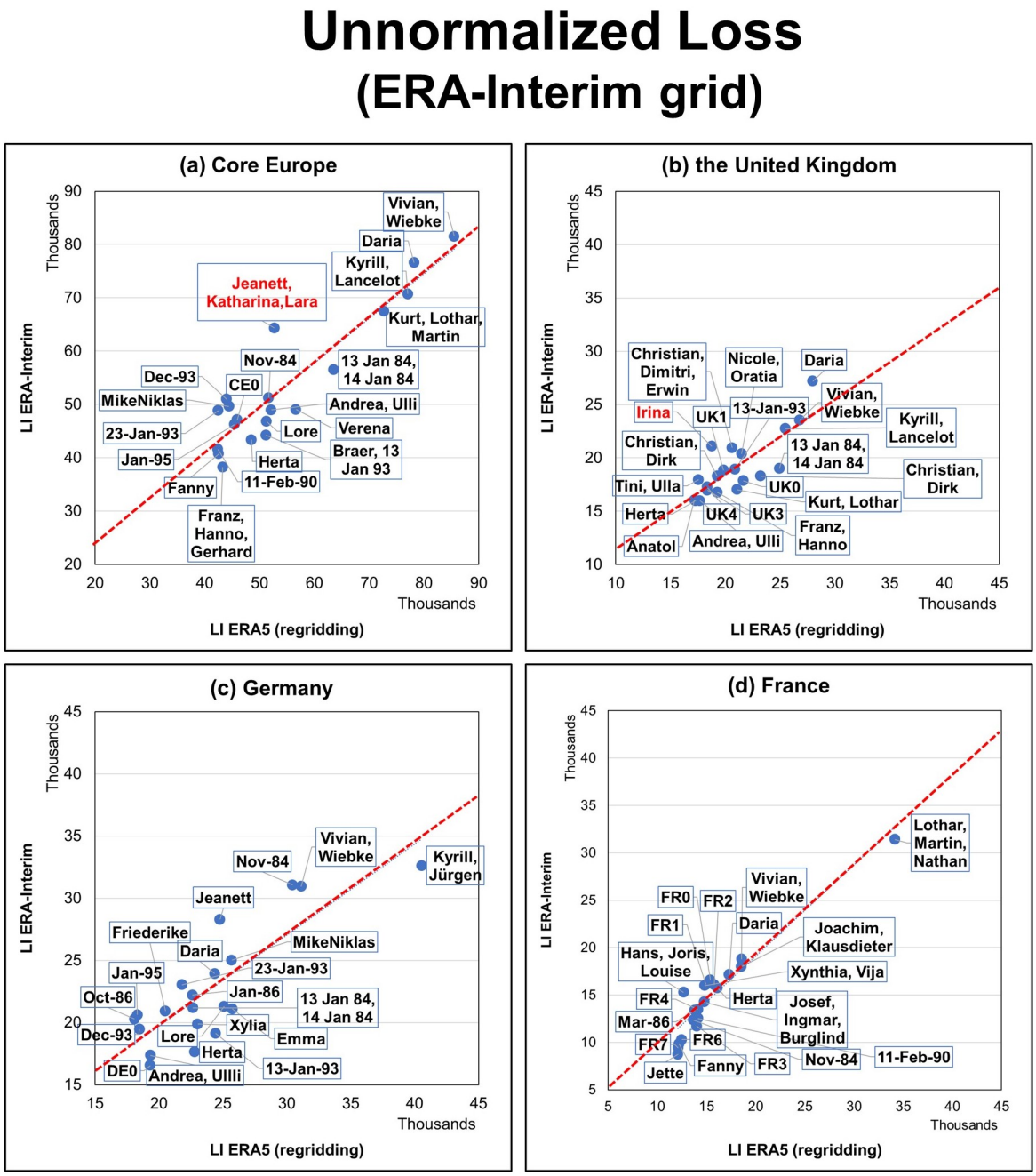

Figure A.3.: Comparison of loss values (in thousands) based on LI ERA5 (x axis) and LI ERA Interim (y axis). Depicted are the common 20 most extreme storms in the period 1979-2019 for (a) Core Europe, (b) the United Kingdom, (c) Germany, and (d) France. Corresponding storm names to each data point are marked with a blue line. Storms without a formal name are named based on the region (e.g. CE for Core Europe) and the loss value (starting for zero for storm with highest loss). The red dashed line denotes the linear regression line. Outlier storms based on the IQR method (see section 3.2) are marked in red. Please note that LI ERA5 is calculated from ERA5 gust data re gridded to the ERA Interim grid. Please note the different scales. The figure is reprinted from Figure S3 in Moemken et al. (2024a), with copyright CC BY 4.0.

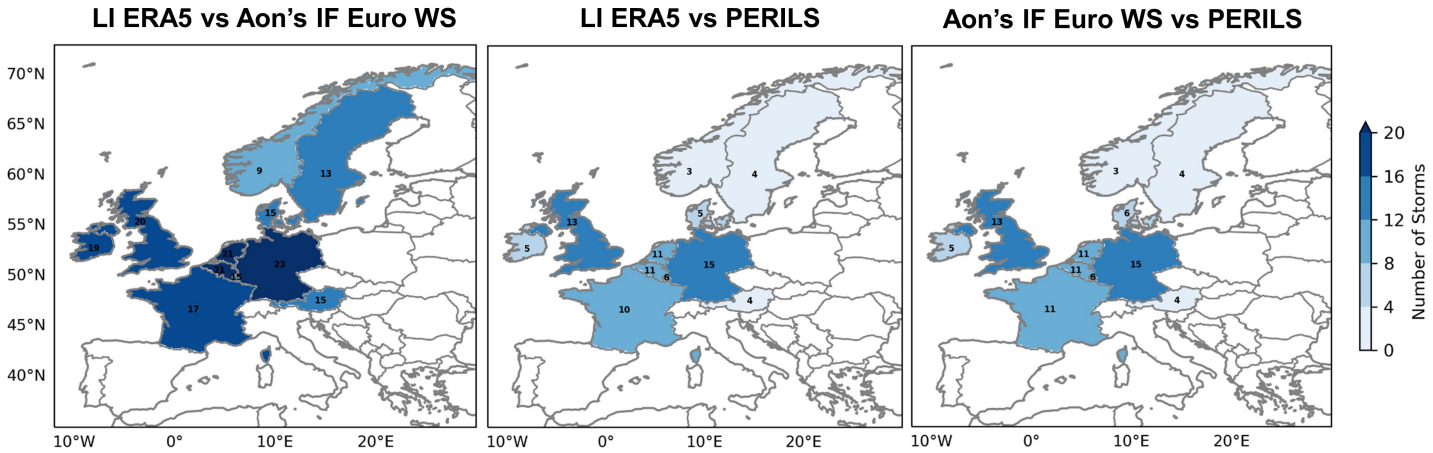

Figure A.4.: Number of common storms per country for LI ERA5 vs Aon's IF Euro WS model (left), LI ERA5 vs PERILS (middle), and Aon's IF Euro WS model vs PERILS (right). The figure is reprinted from Figure S4 in Moemken et al. (2024a), with copyright CC BY 4.0.

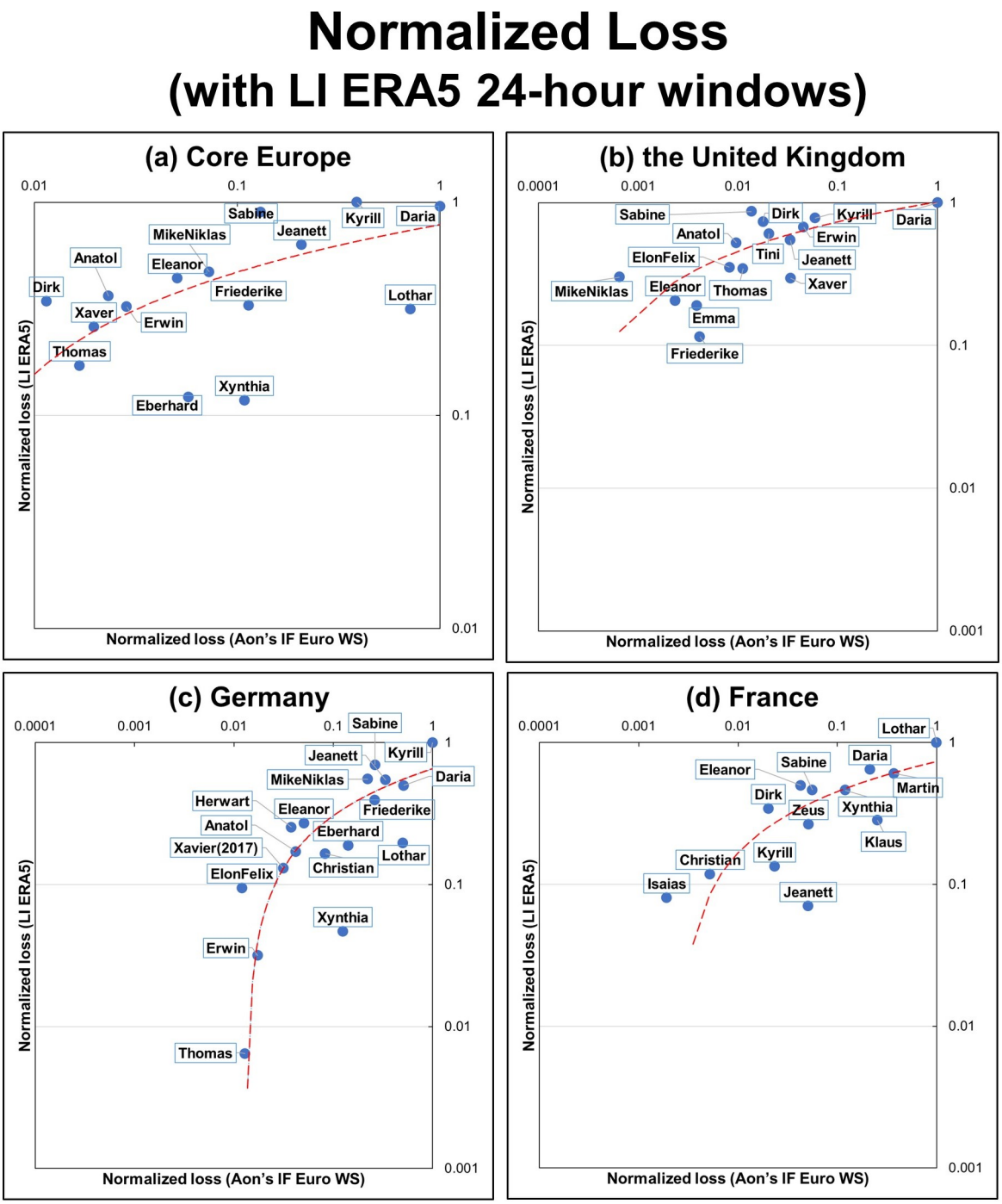

Figure A.5.: Comparison of normalized loss values between Aon's IF Euro WS model (x axis) and LI ERA5 (y axis). Depicted are the common most extreme storms for the period 1990-2020 for (a) Core Europe, (b) the United Kingdom, (c) Germany, and (d) France. A logarithmic scale is used for the axes. The red dashed line denotes the logarithmic regression. Outlier storms based on the IQR method are marked in red. LI ERA5 is calculated for 24 hour windows. Please note the different scales. The figure is reprinted from Figure S5 in Moemken et al. (2024a), with copyright CC BY 4.0.

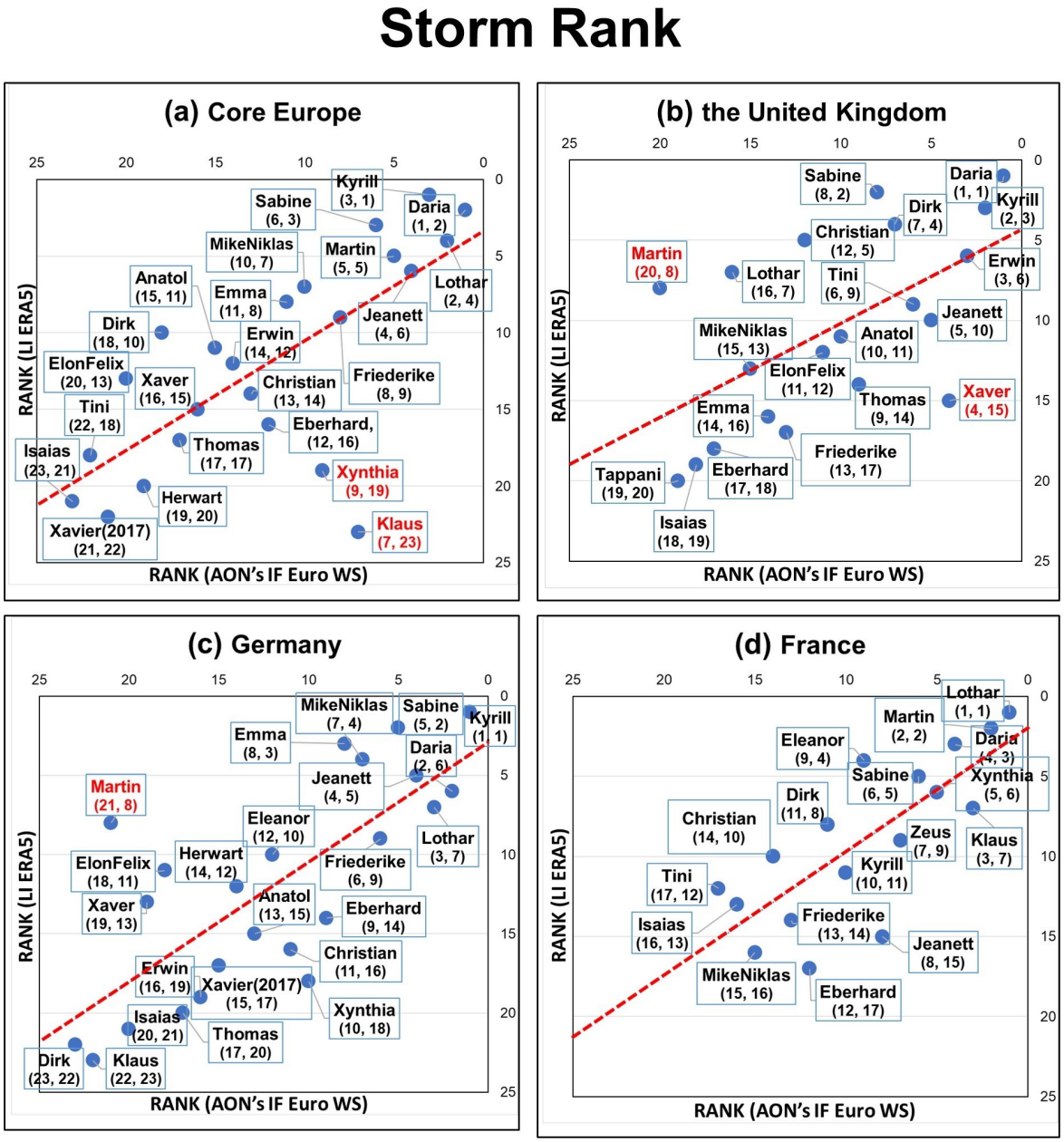

Figure A.6.: Same as Figure A.5, but for the comparison of storm ranks. The values in brackets indicate the rank (first value Aon's model, second value ERA5). The figure is reprinted from Figure S6 in Moemken et al. (2024a), with copyright CC BY 4.0.

B. Appendix for Chapter 6

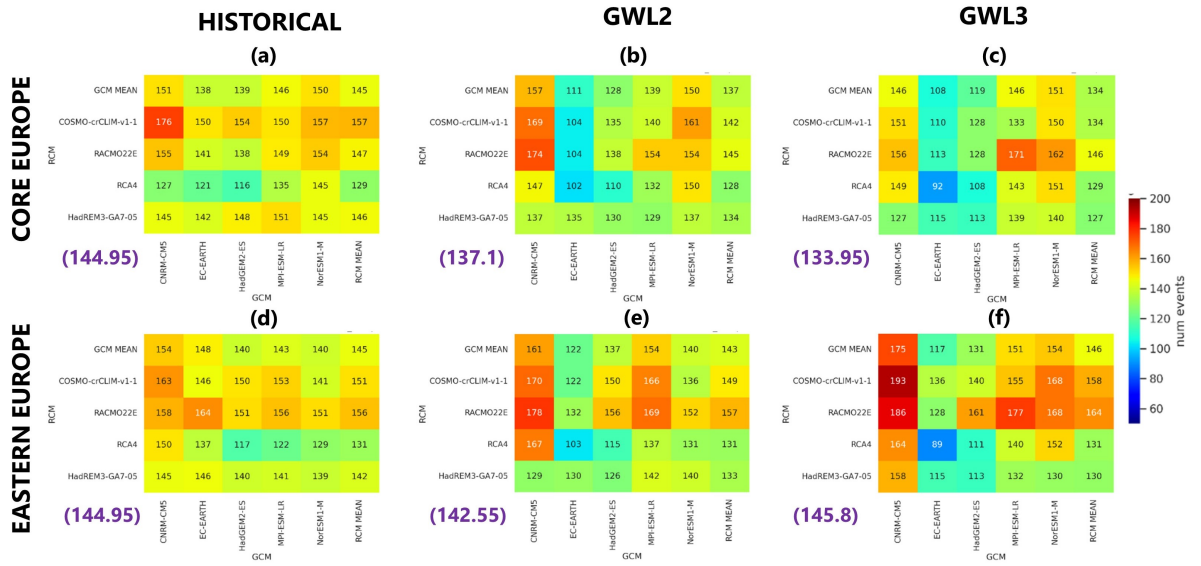

Figure B.1.: Number of storm events for the individual EURO-CORDEX ensemble members for (a, d) the historical period (b, e) GWL2 and (c, f) GWL3. The ensemble mean is given in purple. The threshold for the selection of events is the minimum LI value for the top 2900 events in the historical period (Section 2.2.2). The figure is reprinted from Figure S1 in Alifdini et al. (2025), with copyright CC BY 4.0.

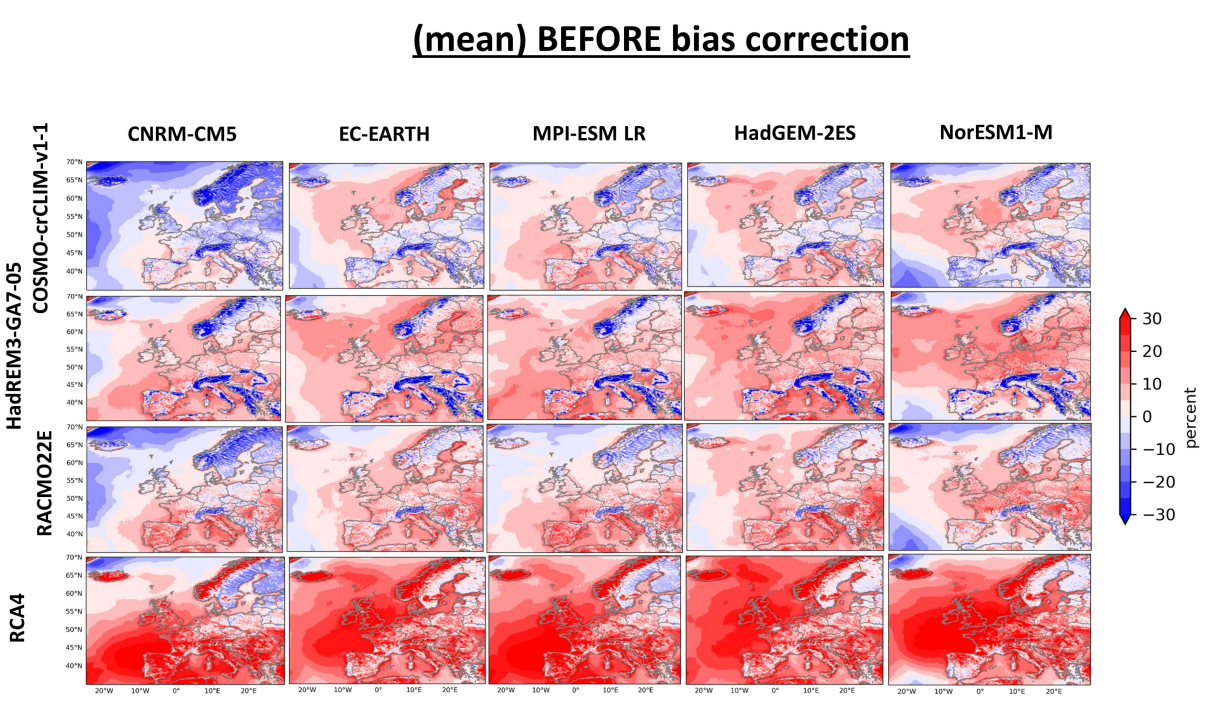

Figure B.2.: Difference in the mean of daily maximum wind gust between the EURO-CORDEX historical simulations (1976-2005) and ERA5 (%) for the individual GCM-RCM chains. The figure is reprinted from Figure S2 in Alifdini et al. (2025), with copyright CC BY 4.0.

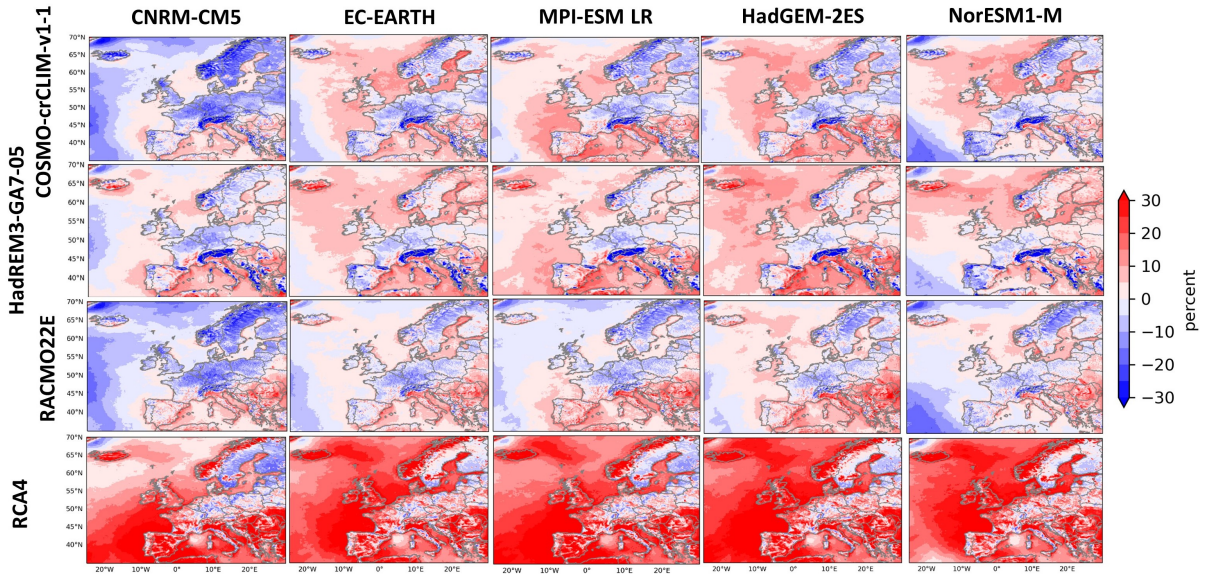

Figure B.3.: Same as Figure B.2, but for the 98th percentile of daily maximum wind gust. The figure is reprinted from Figure S3 in Alifdini et al. (2025), with copyright CC BY 4.0.

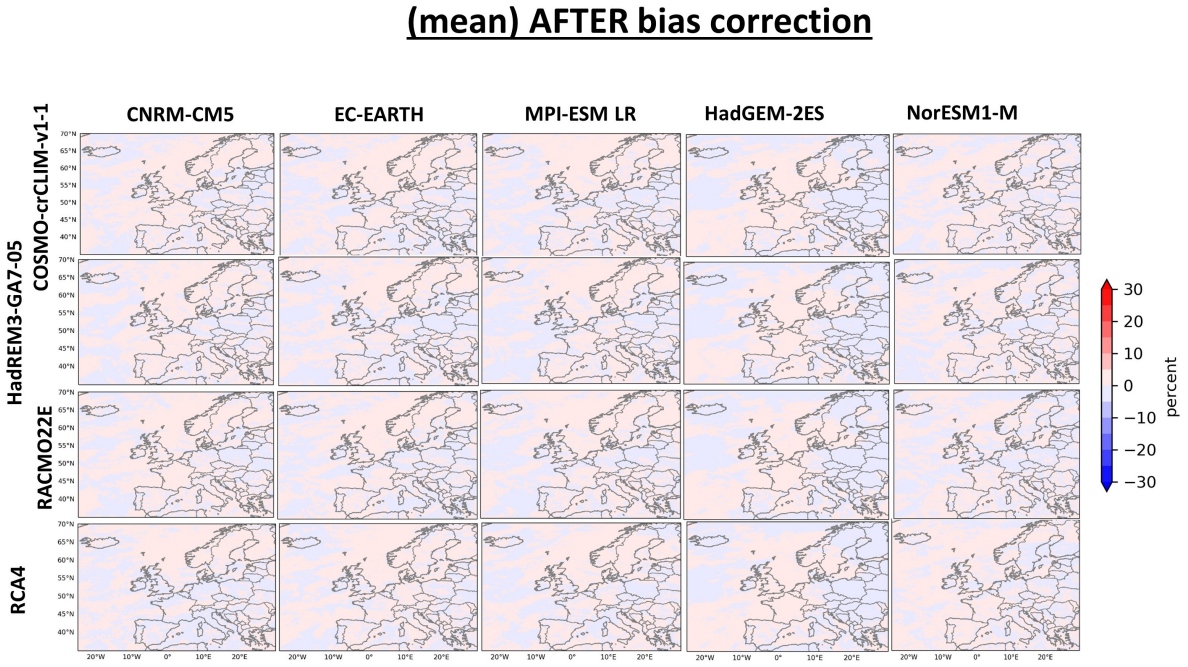

Figure B.4.: Difference in the mean of daily maximum wind gust between the EURO-CORDEX historical simulations (1976-2005) and ERA5 (%) for the individual GCM-RCM chains after bias correction. The figure is reprinted from Figure S4 in Alifdini et al. (2025), with copyright CC BY 4.0.

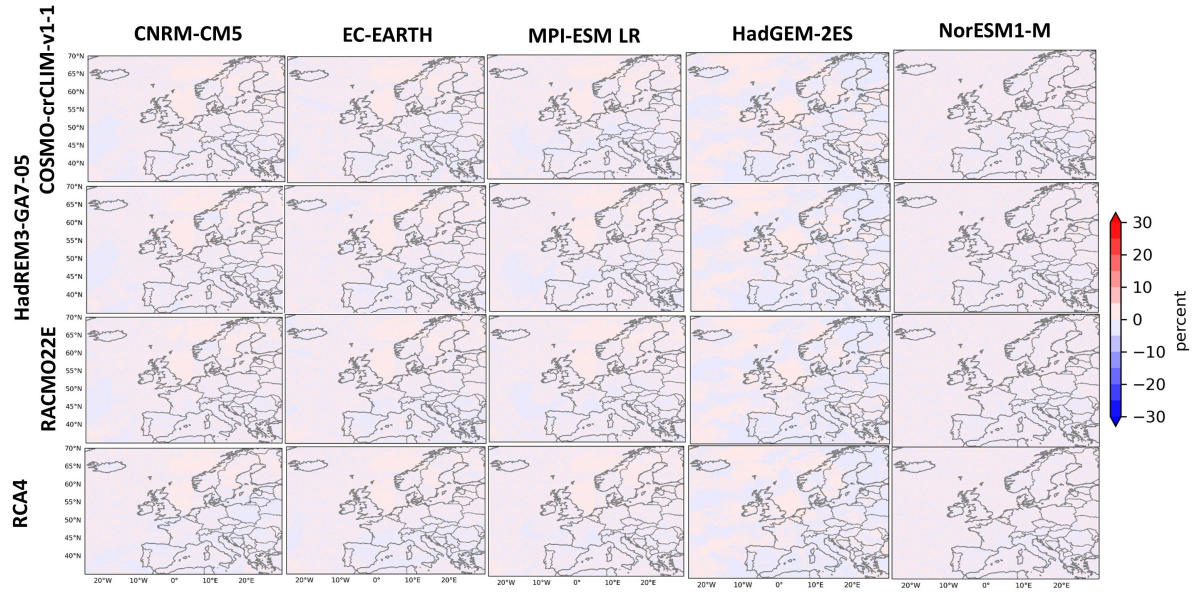

Figure B.5.: Same as Figure B.4, but for the 98th percentile of daily maximum wind gust. The figure is reprinted from Figure S5 in Alifdini et al. (2025), with copyright CC BY 4.0.

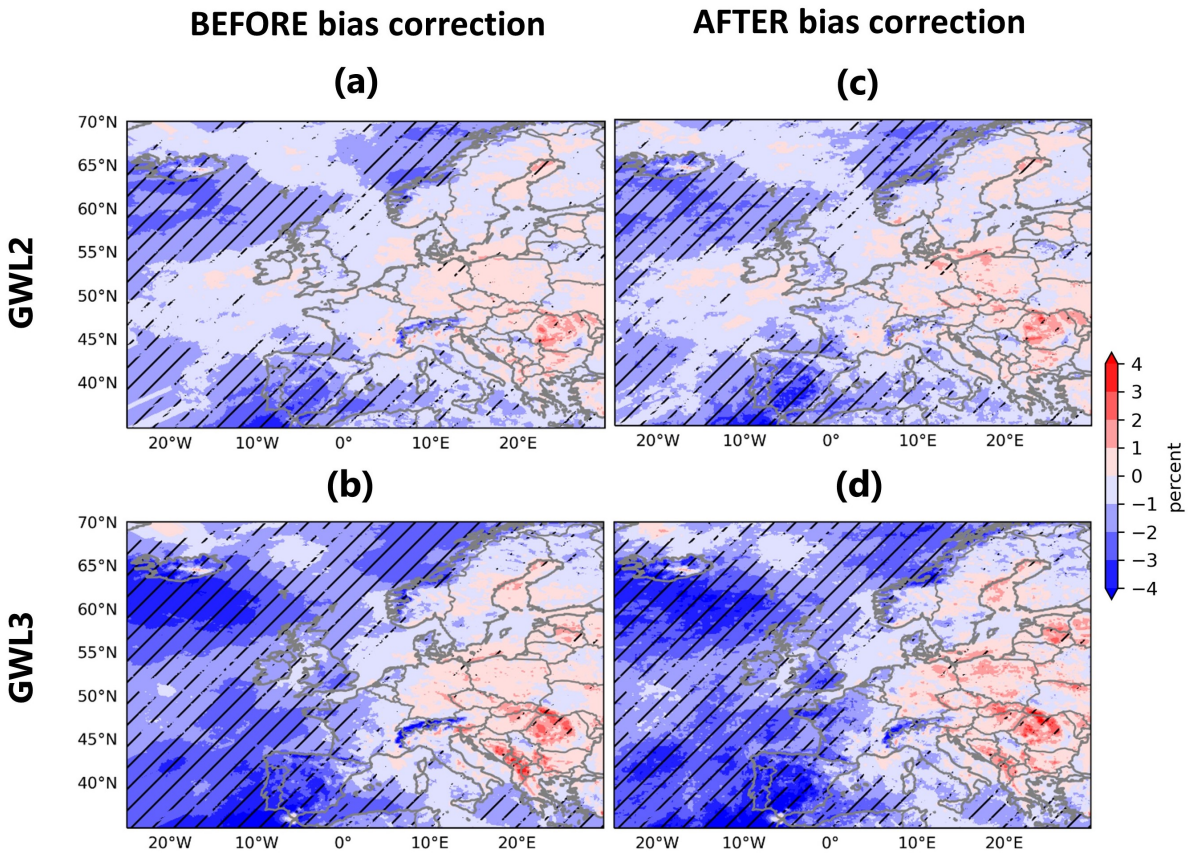

Figure B.6.: Mean differences (20 models) of the 98th percentile of daily maximum wind gust EURO-CORDEX RCP8.5 minus historical period ONDJFM. Slashes denote agreement among over 14 models on difference sign. Note: In this figure, changes are calculated using the 98th percentile for each historical, GWL2, and GWL3. The figure is reprinted from Figure S6 in Alifdini et al. (2025), with copyright CC BY 4.0.

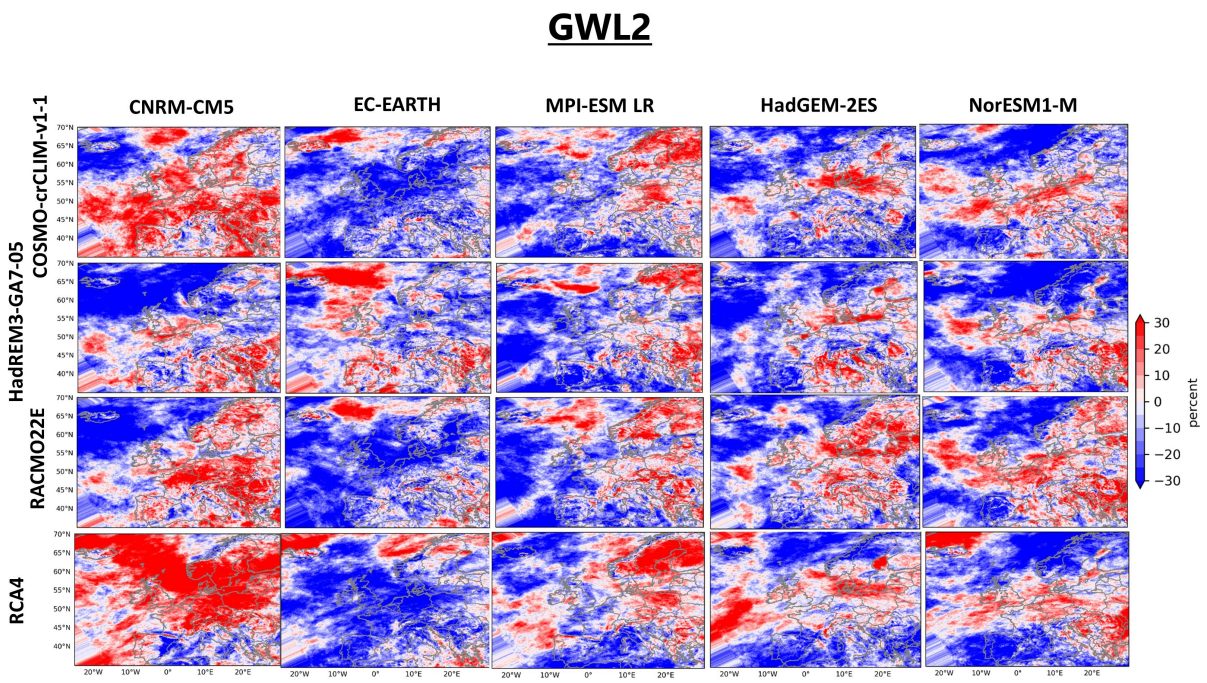

Figure B.7.: Changes in windstorm intensity (%) compared to the historical period for the individual EURO-CORDEX ensemble members for the GWL2. The figure is reprinted from Figure S7 in Alifdini et al. (2025), with copyright CC BY 4.0.

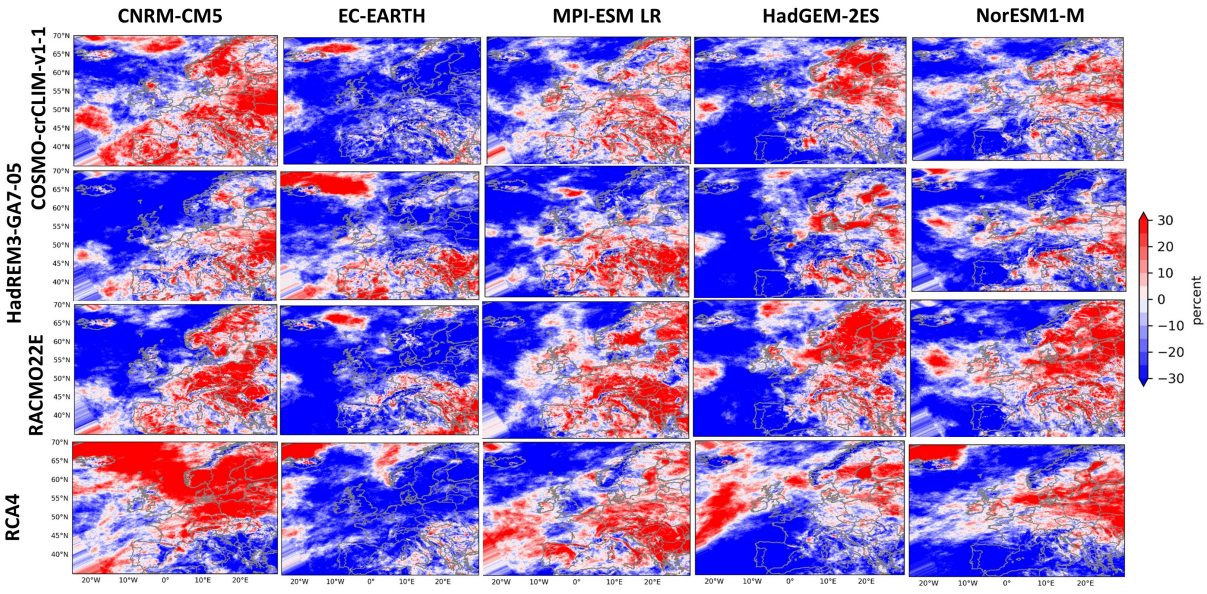

Figure B.8.: Same as Figure B.7, but for the GWL3. The figure is reprinted from Figure S8 in Alifdini et al. (2025), with copyright CC BY 4.0.

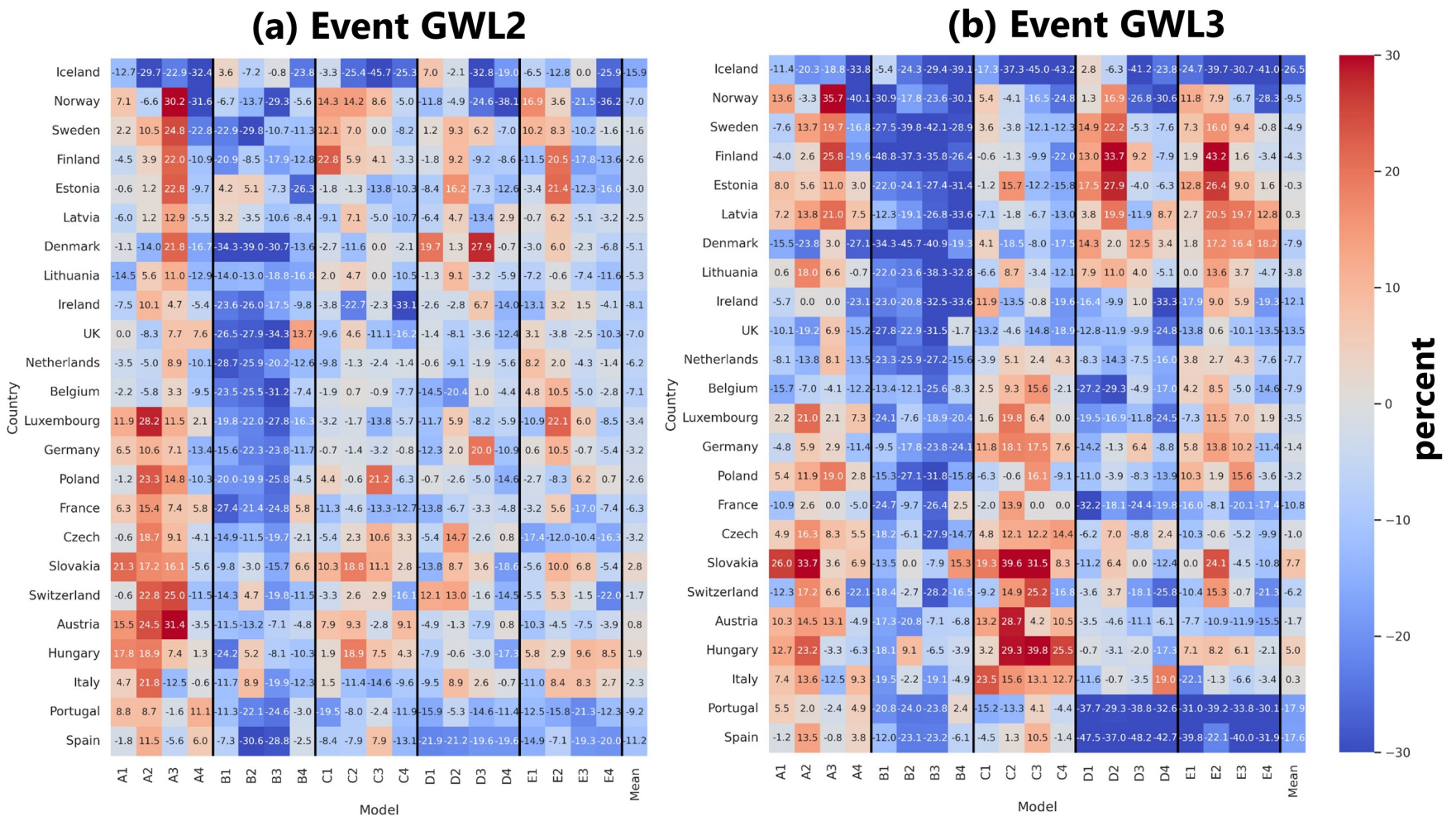

Figure B.9.: Changes in windstorm frequency (%) compared to the historical period for the various ensemble members derived for the individual countries for (a) GWL2 and (b) GWL3. For each matrix, rows represent countries and columns represent GCM-RCM pairs. The ensemble mean is depicted in the last column. The model code can be derived from Table 4.1. The figure is reprinted from Figure S9 in Alifdini et al. (2025), with copyright CC BY 4.0.

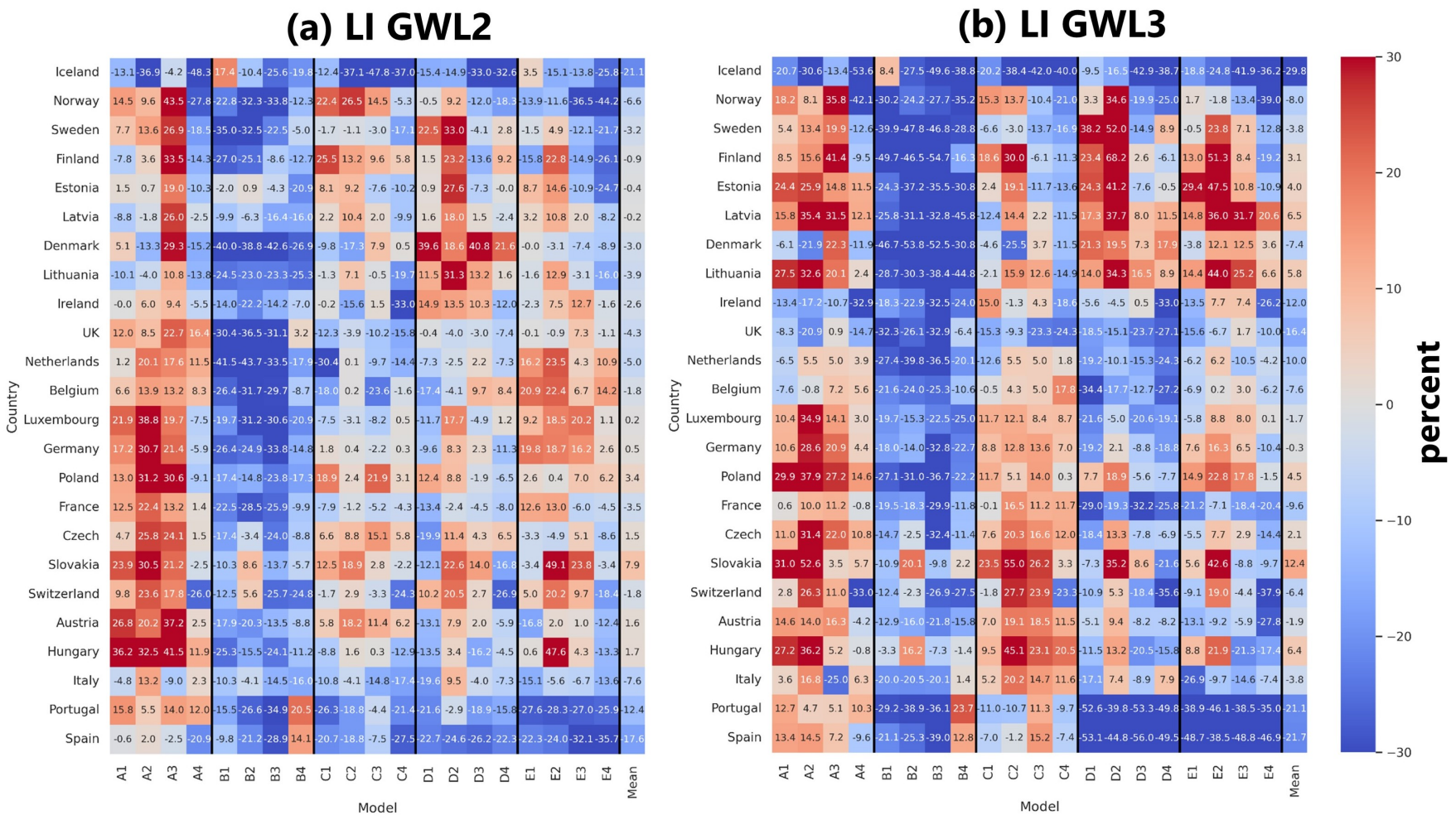

Figure B.10.: Same as Figure B.9, but for changes in windstorm loss (%). The figure is reprinted from Figure S10 in Alifdini et al. (2025), with copyright CC BY 4.0.

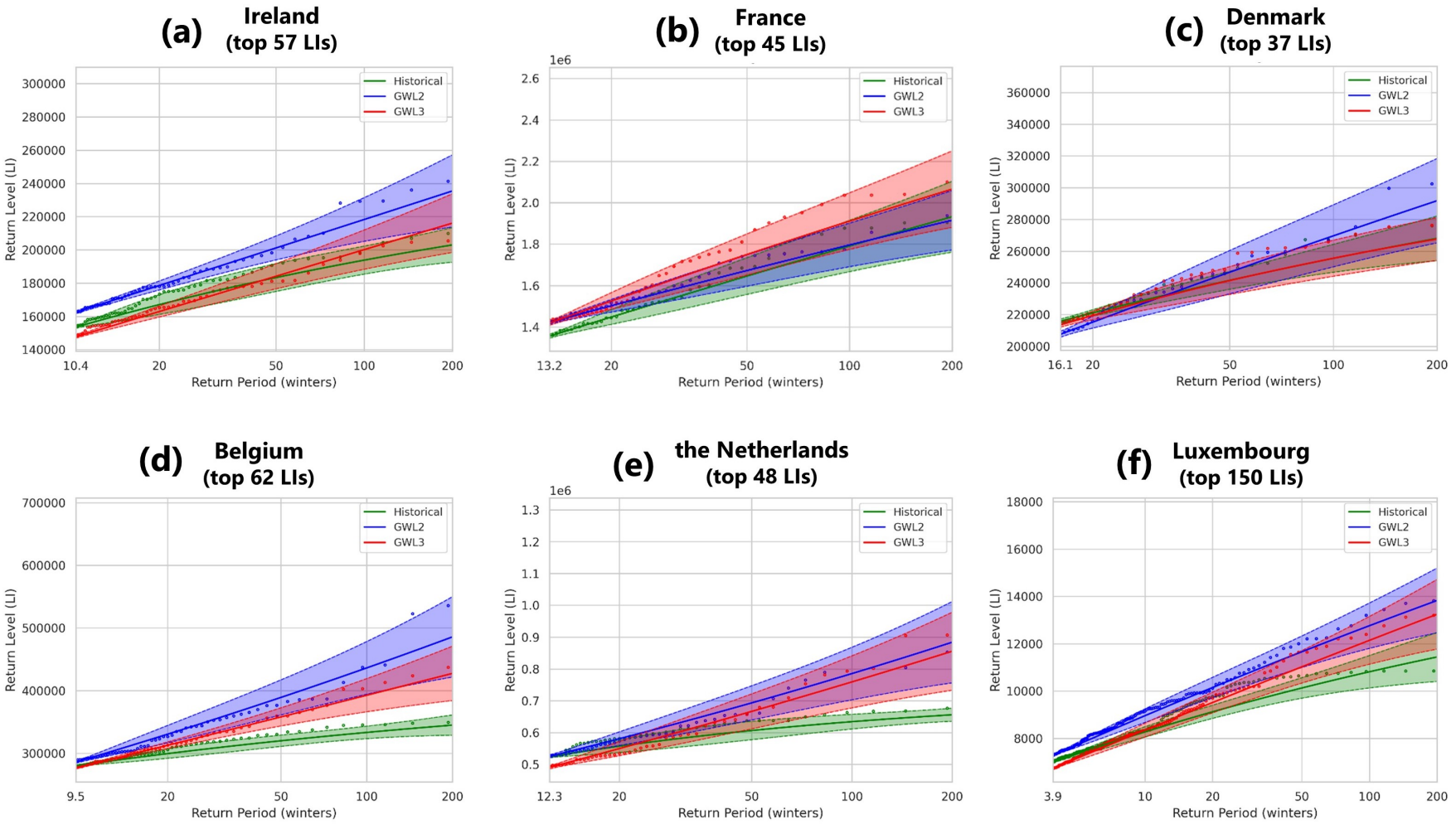

Figure B.11.: Return periods of the most extreme loss events for countries in Core Europe not shown in Figure 6.9 are presented for the historical period (green), GWL2 (blue), and GWL3 (red). The dots represent empirical values, the solid lines show the GPD fit, and the dashed lines represent the upper and lower bounds of the 95% confidence interval. The figure is reprinted from Figure S11 in Alifdini et al. (2025), with copyright CC BY 4.0.

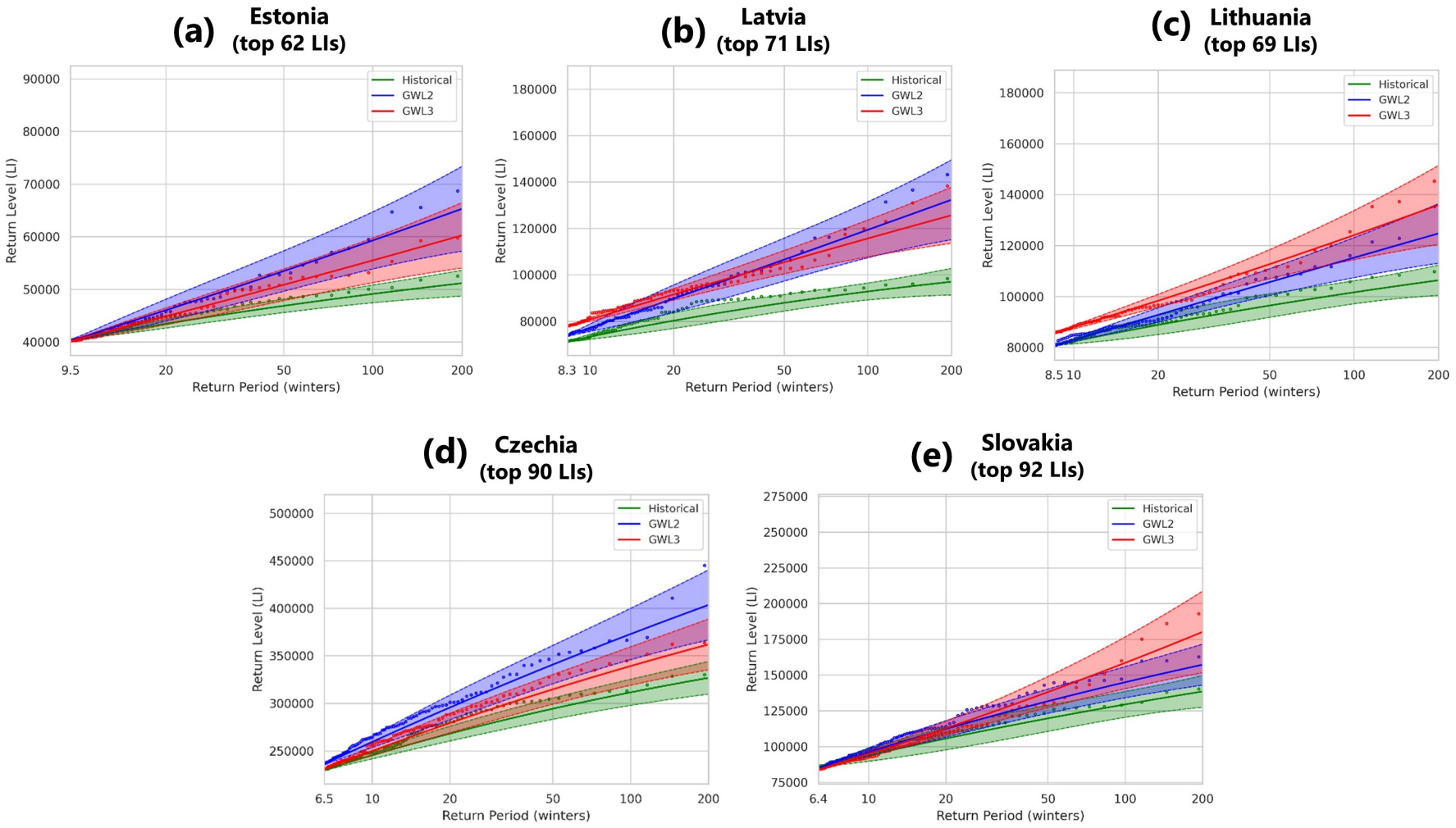

Figure B.12.: Same as Figure B.11, but for countries in Eastern Europe that are not shown in Figure 6.9. The figure is reprinted from Figure S12 in Alifdini et al. (2025), with copyright CC BY 4.0.

C. Appendix for Chapter 7

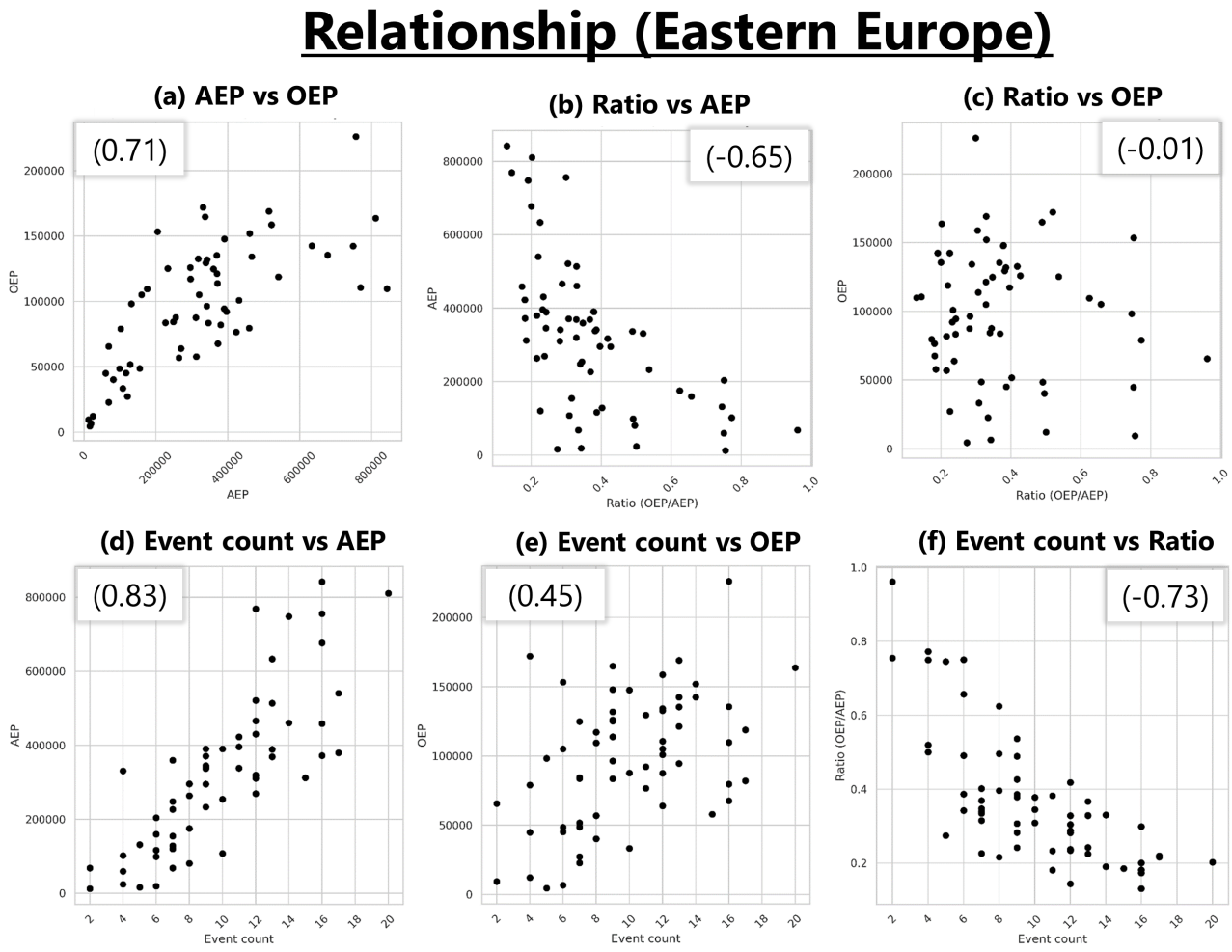

Figure C.1.: Same as Figure 7.4, but for Eastern Europe.

D. Bibliography

, 2022: Gust. Glossary of Meteorology, URL http://glossary.ametsoc.org/wiki/gust.

Abramowitz, G., N. Herger, E. Gutmann, D. Hammerling, R. Knutti, M. Leduc, R. Lorenz, R. Pincus, and G. A. Schmidt, 2019: Esd reviews: Model dependence in multi-model climate ensembles: Weighting, sub-selection and out-of-sample testing. *Earth System Dynamics*, **10 (1)**, 91–105.

Ahmadi-Givi, F., G. Graig, and R. Plant, 2004: The dynamics of a midlatitude cyclone with very strong latent-heat release, qj roy. meteor. soc., 130, 295–323.

Alexandersson, H., T. Schmith, K. Iden, and H. Tuomenvirta, 1998: Long-term variations of the storm climate over nw europe. *The Global atmosphere and ocean system*, **6 (2)**, 97–120.

Alifdini, I., J. Moemken, A. M. Ramos, and J. G. Pinto, 2025: Future changes of european windstorm losses in euro-cordex simulations. *Tellus A: Dynamic Meteorology and Oceanography*, **77 (1)**, 20–37.

Aon, 2023: Impact forecasting – transparent and customizable catastrophe models and platform. URL https://assets.aon.com/-/media/files/aon/capabilities/reinsurance/aon-impact-forecasting.pdf, last accessed: 23 November 2023.

Aon, 2023: Weather, Climate and Catastrophe Insight. https://www.aon.com/getmedia/f34ec133-3175-406c-9e0b-25cea768c5cf/20230125-weather-climate-catastrophe-insight.pdf, last accessed: 04 October 2023.

Becker, B. D., 2019: Draft metaxa set: A new synthetic european windstorm event set. Tech. rep., Tech. rep., Met Office.

Bentsen, M., I. Bethke, J. B. Debernard, T. Iversen, A. Kirkevåg, Ø. Seland, H. Drange, C. Roelandt, I. A. Seierstad, C. Hoose, et al., 2013: The norwegian earth system model, noresm1-m–part 1: description and basic evaluation of the physical climate. *Geoscientific Model Development*, **6 (3)**, 687–720.

Berz, G. and A. Smolka, 1988: Windstorm hazard and insurance. *Journal of Wind Engineering and Industrial Aerodynamics*, **30 (1-3)**, 191–203.

Bjerknes, J., 1919: On the structure of moving cyclones. *Monthly Weather Review*, **47 (2)**, 95–99.

———, 1922: Life cycle of cyclones and the polar front theory of atmospheric circulation. *Geofys. Publ.*, **3**, 1–18.

Black, R., A. Tsanakas, A. D. Smith, M. B. Beck, I. D. Maclugash, J. Grewal, L. Witts, N. Morjaria, R. Green, and Z. Lim, 2018: Model risk: illuminating the black box. *British Actuarial Journal*, **23**, e2.

Bloomfield, H., J. Hillier, A. Griffin, A. Kay, L. C. Shaffrey, F. Pianosi, R. James, D. Kumar, A. Champion, and P. Bates, 2023: Co-occurring wintertime flooding and extreme wind over europe, from daily to seasonal timescales. *Weather and Climate Extremes*, **39**, 100 550.

Bloomfield, H., L. Shaffrey, K. Hodges, and P. Vidale, 2018: A critical assessment of the long-term changes in the wintertime surface arctic oscillation and northern hemisphere storminess in the era20c reanalysis. *Environmental Research Letters*, **13 (9)**, 094 004.

Boé, J., L. Terray, F. Habets, and E. Martin, 2007: Statistical and dynamical downscaling of the seine basin climate for hydro-meteorological studies. *International Journal of Climatology: A Journal of the Royal Meteorological Society*, **27 (12)**, 1643–1655.

Bonanno, R., F. Viterbo, and R. G. Maurizio, 2023: Climate change impacts on wind power generation for the italian peninsula. *Regional Environmental Change*, **23 (1)**, 15.

Born, K., P. Ludwig, and J. G. Pinto, 2012: Wind gust estimation for mid-european winter storms: towards a probabilistic view. *Tellus A: Dynamic Meteorology and Oceanography*, **64 (1)**, 17 471.

Brasseur, O., 2001: Development and application of a physical approach to estimating wind gusts. *Monthly Weather Review*, **129 (1)**, 5–25.

Bui, H. and T. Spengler, 2021: On the influence of sea surface temperature distributions on the development of extratropical cyclones. *Journal of the Atmospheric Sciences*, **78 (4)**, 1173–1188.

Businger, S. and J. A. Businger, 2001: Viscous dissipation of turbulence kinetic energy in storms. *Journal of the atmospheric sciences*, **58 (24)**, 3793–3796.

Campbell, M. J., 2021: *Statistics at square one*. John Wiley & Sons.

Cannon, A. J., C. Piani, and S. Sippel, 2020: Bias correction of climate model output for impact models. *Climate Extremes and Their Implications for Impact and Risk Assessment*, Elsevier, 77–104.

Catto, J., 2016: Extratropical cyclone classification and its use in climate studies. *Reviews of Geophysics*, **54 (2)**, 486–520.

Catto, J. L., D. Ackerley, J. F. Booth, A. J. Champion, B. A. Colle, S. Pfahl, J. G. Pinto, J. F. Quinting, and C. Seiler, 2019: The future of midlatitude cyclones. *Current Climate Change Reports*, **5**, 407–420.

Clark, P. A. and S. L. Gray, 2018: Sting jets in extratropical cyclones: a review. *Quarterly Journal of the Royal Meteorological Society*, **144 (713)**, 943–969.

Coles, S., J. Bawa, L. Trenner, and P. Dorazio, 2001: *An introduction to statistical modeling of extreme values*, Vol. 208. Springer.

Dacre, H. F. and J. G. Pinto, 2020: Serial clustering of extratropical cyclones: A review of where, when and why it occurs. *NPJ Climate and Atmospheric Science*, **3 (1)**, 48.

Dee, D. P., S. M. Uppala, A. J. Simmons, P. Berrisford, P. Poli, S. Kobayashi, U. Andrae, M. Balmaseda, G. Balsamo, d. P. Bauer, et al., 2011: The era-interim reanalysis: Configuration and performance of the data assimilation system. *Quarterly Journal of the royal meteorological society*, **137 (656)**, 553–597.

Della-Marta, P. M., M. A. Liniger, C. Appenzeller, D. N. Bresch, P. Köllner-Heck, and V. Muccione, 2010: Improved estimates of the european winter windstorm climate and the risk of reinsurance loss using climate model data. *Journal of Applied Meteorology and Climatology*, **49 (10)**, 2092–2120.

Déroche, M.-S., 2023: Invited perspectives: An insurer's perspective on the knowns and unknowns in natural hazard risk modelling. *Natural hazards and earth system sciences*, **23 (1)**, 251–259.

Deutscher Wetterdienst (DWD), 2017: 10 jahre kyrill - stärkste sturmflut seit 1953. `https://www.dwd.de/DE/presse/pressemitteilungen/DE/2017/20170111_10jahrekyrill_news.html`, accessed: June 30, 2024.

Dodge, Y., 2008: *The concise encyclopedia of statistics*. Springer Science & Business Media.

Donat, M. G., T. Pardowitz, G. Leckebusch, U. Ulbrich, and O. Burghoff, 2011: High-resolution refinement of a storm loss model and estimation of return periods of loss-intensive storms over germany. *Natural Hazards and Earth System Sciences*, **11 (10)**, 2821–2833.

Dorland, C., R. S. Tol, and J. P. Palutikof, 1999: Vulnerability of the netherlands and northwest europe to storm damage under climate change. *Climatic change*, **43**, 513–535.

Dumm, R. E., M. E. Johnson, and M. M. Simons, 2008: Inside the black box: Evaluating and auditing hurricane loss models. *Journal of Insurance Regulation*, **27 (2)**.

Durst, C., 1960: Wind speeds over short periods of time. *Meteor. Mag*, **89 (1056)**, 181–187.

Economou, T., D. B. Stephenson, J. Pinto, L. Shaffrey, and G. Zappa, 2015: Serial clustering of extratropical cyclones in a multi-model ensemble of historical and future simulations. *Quarterly Journal of the Royal Meteorological Society*, **141 (693)**, 3076–3087.

Edwards, P. N., 2011: History of climate modeling. *Wiley Interdisciplinary Reviews: Climate Change*, **2 (1)**, 128–139.

Ehmele, F., L.-A. Kautz, H. Feldmann, Y. He, M. Kadlec, F. D. Kelemen, H. S. Lentink, P. Ludwig, D. Manful, and J. G. Pinto, 2022: Adaptation and application of the large laertes-eu regional climate model ensemble for modeling hydrological extremes: a pilot study for the rhine basin. *Natural Hazards and Earth System Sciences*, **22 (2)**, 677–692.

Ehmele, F., L.-A. Kautz, H. Feldmann, and J. G. Pinto, 2020: Long-term variance of heavy precipitation across central europe using a large ensemble of regional climate model simulations. *Earth System Dynamics*, **11 (2)**, 469–490.

Ekström, M., M. R. Grose, and P. H. Whetton, 2015: An appraisal of downscaling methods used in climate change research. *Wiley Interdisciplinary Reviews: Climate Change*, **6 (3)**, 301–319.

Eyring, V., S. Bony, G. A. Meehl, C. A. Senior, B. Stevens, R. J. Stouffer, and K. E. Taylor, 2016: Overview of the coupled model intercomparison project phase 6 (cmip6) experimental design and organization. *Geoscientific Model Development*, **9 (5)**, 1937–1958.

Eyring, V., W. D. Collins, P. Gentine, E. A. Barnes, M. Barreiro, T. Beucler, M. Bocquet, C. S. Bretherton, H. M. Christensen, K. Dagon, et al., 2024: Pushing the frontiers in climate modelling and analysis with machine learning. *Nature Climate Change*, **14 (9)**, 916–928.

Feser, F., M. Barcikowska, O. Krueger, F. Schenk, R. Weisse, and L. Xia, 2015: Storminess over the north atlantic and northwestern europe—a review. *Quarterly Journal of the Royal Meteorological Society*, **141 (687)**, 350–382.

Feser, F., B. Rockel, H. von Storch, J. Winterfeldt, and M. Zahn, 2011: Regional climate models add value to global model data: a review and selected examples. *Bulletin of the American Meteorological Society*, **92 (9)**, 1181–1192.

Fink, A. H., T. Brücher, V. Ermert, A. Krüger, and J. G. Pinto, 2009: The european storm kyrill in january 2007: synoptic evolution, meteorological impacts and some considerations with respect to climate change. *Natural Hazards and Earth System Sciences*, **9 (2)**, 405–423.

Foley, A., 2010: Uncertainty in regional climate modelling: A review. *Progress in Physical Geography*, **34 (5)**, 647–670.

Forster, P., 2017: Half a century of robust climate models. *Nature*, **545 (7654)**, 296–297.

Fuentes, U. and D. Heimann, 2000: An improved statistical-dynamical downscaling scheme and its application to the alpine precipitation climatology. *Theoretical and Applied Climatology*, **65**, 119–135.

Gaska, J., 2023: Climate change and windstorm losses in poland in the twenty-first century. *Environmental Hazards*, **22 (2)**, 99–115.

Giorgetta, M. A., J. Jungclaus, C. H. Reick, S. Legutke, J. Bader, M. Böttinger, V. Brovkin, T. Crueger, M. Esch, K. Fieg, et al., 2013: Climate and carbon cycle changes from 1850 to 2100 in mpi-esm simulations for the coupled model intercomparison project phase 5. *Journal of Advances in Modeling Earth Systems*, **5 (3)**, 572–597.

Giorgi, F., 1990: Simulation of regional climate using a limited area model nested in a general circulation model. *Journal of Climate*, **3 (9)**, 941–963.

———, 2019: Thirty years of regional climate modeling: where are we and where are we going next? *Journal of Geophysical Research: Atmospheres*, **124 (11)**, 5696–5723.

Giorgi, F., C. Jones, G. R. Asrar, et al., 2009: Addressing climate information needs at the regional level: the cordex framework. *World Meteorological Organization (WMO) Bulletin*, **58 (3)**, 175.

Giorgi, F. and L. O. Mearns, 1991: Approaches to the simulation of regional climate change: a review. *Reviews of geophysics*, **29 (2)**, 191–216.

Gliksman, D., P. Averbeck, N. Becker, B. Gardiner, V. Goldberg, J. Grieger, D. Handorf, K. Haustein, A. Karwat, and F. Knutzen, 2023: A european perspective on wind and storm damage–from the meteorological background to index-based approaches to assess impacts. *Natural Hazards and Earth System Sciences*, **23**, 2171–2201.

Grossi, P., H. Kunreuther, and D. Windeler, 2005: An introduction to catastrophe models and insurance. *Catastrophe modeling: A new approach to managing risk*, Springer, 23–42.

Gudmundsson, L., 2016: *qmap: Statistical transformations for post-processing climate model output*. R package version 1.0-4.

Gudmundsson, L., J. B. Bremnes, J. E. Haugen, and T. Engen-Skaugen, 2012: Downscaling rcm precipitation to the station scale using statistical transformations–a comparison of methods. *Hydrology and Earth System Sciences*, **16 (9)**, 3383–3390.

Haas, R. and J. G. Pinto, 2012: A combined statistical and dynamical approach for downscaling large-scale footprints of european windstorms. *Geophysical Research Letters*, **39 (23)**.

Hanna, E. and T. E. Cropper, 2017: North atlantic oscillation. *Oxford Research Encyclopedia of Climate Science*.

Harvey, B., P. Cook, L. Shaffrey, and R. Schiemann, 2020: The response of the northern hemisphere storm tracks and jet streams to climate change in the cmip3, cmip5, and cmip6 climate models. *Journal of Geophysical Research: Atmospheres*, **125 (23)**, e2020JD032 701.

Hasselmann, K., 1976: Stochastic climate models part i. theory. *tellus*, **28 (6)**, 473–485.

Haylock, M., 2011: European extra-tropical storm damage risk from a multi-model ensemble of dynamically-downscaled global climate models. *Natural Hazards and Earth System Sciences*, **11 (10)**, 2847–2857.

Heneka, P., T. Hofherr, B. Ruck, and C. Kottmeier, 2006: Winter storm risk of residential structures–model development and application to the german state of baden-württemberg. *Natural Hazards and Earth System Sciences*, **6 (5)**, 721–733.

Hersbach, H., B. Bell, P. Berrisford, S. Hirahara, A. Horányi, J. Muñoz-Sabater, J. Nicolas, C. Peubey, R. Radu, D. Schepers, et al., 2020: The era5 global reanalysis. *Quarterly Journal of the Royal Meteorological Society*, **146 (730)**, 1999–2049.

Hewitson, B. C. and R. G. Crane, 1996: Climate downscaling: techniques and application. *Climate Research*, **7 (2)**, 85–95.

Hewson, T. D. and U. Neu, 2015: Cyclones, windstorms and the imilast project. *Tellus A: Dynamic Meteorology and Oceanography*, **67 (1)**, 27 128.

Hodges, K., 1995: Feature tracking on the unit sphere. *Monthly Weather Review*, **123 (12)**, 3458–3465.

Hodges, K. I., 1994: A general method for tracking analysis and its application to meteorological data. *Monthly Weather Review*, **122 (11)**, 2573 – 2586, URL `https://journals.ametsoc.org/view/journals/mwre/122/11/1520-0493_1994_122_2573_agmfta_2_0_co_2.xml`.

Holton, J. R. and G. J. Hakim, 2012: *An introduction to dynamic meteorology*. Academic press.

Huntingford, C., E. S. Jeffers, M. B. Bonsall, H. M. Christensen, T. Lees, and H. Yang, 2019: Machine learning and artificial intelligence to aid climate change research and preparedness. *Environmental Research Letters*, **14 (12)**, 124 007.

Iles, C. E., R. Vautard, J. Strachan, S. Joussaume, B. R. Eggen, and C. D. Hewitt, 2020: The benefits of increasing resolution in global and regional climate simulations for european climate extremes. *Geoscientific Model Development*, **13 (11)**, 5583–5607.

IMPACT2C Project, 2015: The +2 °c global warming period concept. `https://www.atlas.impact2c.eu/en/about/about-impact2c-web-atlas/2-c-global-warming-period-concept/`, accessed: 2024-07-19.

Iyakaremye, V., G. Zeng, and G. Zhang, 2021: Changes in extreme temperature events over africa under 1.5 and 2.0 c global warming scenarios. *International Journal of Climatology*, **41 (2)**, 1506–1524.

Jacob, D., J. Petersen, B. Eggert, A. Alias, O. B. Christensen, L. M. Bouwer, A. Braun, A. Colette, M. Déqué, G. Georgievski, et al., 2014: Euro-cordex: new high-resolution climate change projections for european impact research. *Regional environmental change*, **14**, 563–578.

Jaison, A., C. Michel, A. Sorteberg, and Ø. Breivik, 2024: Projections of windstorms damages under changing climate and demography for norway. *Environmental Research: Climate*, **3 (4)**, 045 006.

Jardine, A., K. Selby, and D. Higgins, 2023: A multidisciplinary investigation of storms ciara and dennis, february 2020. *International journal of disaster risk reduction*, **90**, 103 657.

Jung, C. and D. Schindler, 2021: Does the winter storm-related wind gust intensity in germany increase under warming climate?–a high-resolution assessment. *Weather and Climate Extremes*, **33**, 100 360.

Jungclaus, J. H., N. Keenlyside, M. Botzet, H. Haak, J.-J. Luo, M. Latif, J. Marotzke, U. Mikolajewicz, and E. Roeckner, 2006: Ocean circulation and tropical variability in the coupled model echam5/mpi-om. *Journal of climate*, **19 (16)**, 3952–3972.

Kaidor, 2013: Earth global circulation. `https://commons.wikimedia.org/wiki/File:Earth_Global_Circulation_-_en.svg`, based on: NASA depiction of Earth global atmospheric circulation.

Karremann, M., J. Pinto, P. Von Bomhard, and M. Klawa, 2014a: On the clustering of winter storm loss events over germany. *Natural Hazards and Earth System Sciences*, **14 (8)**, 2041–2052.

Karremann, M. K., J. G. Pinto, M. Reyers, and M. Klawa, 2014b: Return periods of losses associated with european windstorm series in a changing climate. *Environmental Research Letters*, **9 (12)**, 124 016.

Karwat, A., C. L. Franzke, J. G. Pinto, S.-S. Lee, and R. Blender, 2024: Northern hemisphere extratropical cyclone clustering in era5 reanalysis and the cesm2 large ensemble. *Journal of Climate*, **37 (4)**, 1347–1365.

Katragkou, E., S. Sobolowski, C. Teichmann, F. Solmon, V. Pavlidis, D. Rechid, P. Hoffmann, J. Fernandez, G. Nikulin, and D. Jacob, 2024: Delivering an improved framework for the new generation of cmip6-driven euro-cordex regional climate simulations. *Bulletin of the American Meteorological Society*, **105 (6)**, E962–E974.

Kendon, M. and M. McCarthy, 2015: The uk's wet and stormy winter of 2013/2014. *Weather*, **70 (2)**, 40–47.

Khanduri, A. and G. Morrow, 2003: Vulnerability of buildings to windstorms and insurance loss estimation. *Journal of wind engineering and industrial aerodynamics*, **91 (4)**, 455–467.

Kjellström, E., G. Nikulin, G. Strandberg, O. B. Christensen, D. Jacob, K. Keuler, G. Lenderink, E. van Meijgaard, C. Schär, S. Somot, et al., 2018: European climate change at global mean temperature increases of 1.5 and 2 c above pre-industrial conditions as simulated by the euro-cordex regional climate models. *Earth System Dynamics*, **9 (2)**, 459–478.

Klawa, M. and U. Ulbrich, 2003: A model for the estimation of storm losses and the identification of severe winter storms in germany. *Natural Hazards and Earth System Sciences*, **3 (6)**, 725–732.

Knutti, R. and J. Sedláček, 2013: Robustness and uncertainties in the new cmip5 climate model projections. *Nature climate change*, **3 (4)**, 369–373.

Koks, E. and T. Haer, 2020: A high-resolution wind damage model for europe. *Scientific reports*, **10 (1)**, 6866.

Kotlarski, S., P. Szabó, S. Herrera, O. Räty, K. Keuler, P. M. Soares, R. M. Cardoso, T. Bosshard, C. Pagé, F. Boberg, et al., 2019: Observational uncertainty and regional climate model evaluation: a pan-european perspective. *International Journal of Climatology*.

Krueger, O., F. Schenk, F. Feser, and R. Weisse, 2013: Inconsistencies between long-term trends in storminess derived from the 20cr reanalysis and observations. *Journal of Climate*, **26 (3)**, 868–874.

Krueger-Krusche, M., 2007: Sturmschaden berlin kyrill. Wikimedia Commons, URL `https://commons.wikimedia.org/wiki/File:Sturmschaden_Berlin_Kyrill_01.jpg`, accessed: 2024-10-09.

Kurbatova, M., K. Rubinstein, I. Gubenko, and G. Kurbatov, 2018: Comparison of seven wind gust parameterizations over the european part of russia. *Advances in Science and Research*, **15**, 251–255.

Lamb, H. and K. Frydendahl, 1991: *Historic storms of the north sea, British Isles and Northwest Europe*. Cambridge University Press.

Laurila, T. K., V. A. Sinclair, and H. Gregow, 2021: Climatology, variability, and trends in near-surface wind speeds over the north atlantic and europe during 1979–2018 based on era5. *International Journal of Climatology*, **41 (4)**, 2253–2278.

Leckebusch, G., D. Renggli, and U. Ulbrich, 2008: Development and application of an objective storm severity measure for the northeast atlantic region. *Meteorologische Zeitschrift*, **17 (5)**, 575–587.

Leckebusch, G. C., U. Ulbrich, L. Fröhlich, and J. G. Pinto, 2007: Property loss potentials for european midlatitude storms in a changing climate. *Geophysical Research Letters*, **34 (5)**.

Lee, H., K. Calvin, D. Dasgupta, G. Krinner, A. Mukherji, P. Thorne, C. Trisos, J. Romero, P. Aldunce, K. Barret, et al., 2023: Ipcc, 2023: Climate change 2023: Synthesis report, summary for policymakers. contribution of working groups i, ii and iii to the sixth assessment report of the intergovernmental panel on climate change [core writing team, h. lee and j. romero (eds.)]. ipcc, geneva, switzerland.

Lemos, I. P., A. M. G. Lima, and M. A. V. Duarte, 2020: thresholdmodeling: A python package for modeling excesses over a threshold using the peak-over-threshold method and the generalized pareto distribution. *Journal of Open Source Software*, **5 (46)**, 2013.

Lewis, J. I., A. Toney, and X. Shi, 2024: Climate change and artificial intelligence: assessing the global research landscape. *Discover Artificial Intelligence*, **4 (1)**, 1–12.

Li, D., J. Feng, Z. Xu, B. Yin, H. Shi, and J. Qi, 2019: Statistical bias correction for simulated wind speeds over cordex-east asia. *Earth and Space Science*, **6 (2)**, 200–211.

Little, A. S., M. D. Priestley, and J. L. Catto, 2023: Future increased risk from extratropical windstorms in northern europe. *Nature Communications*, **14 (1)**, 4434.

Lucas-Picher, P., D. Argüeso, E. Brisson, Y. Tramblay, P. Berg, A. Lemonsu, S. Kotlarski, and C. Caillaud, 2021: Convection-permitting modeling with regional climate models: Latest developments and next steps. *Wiley Interdisciplinary Reviews: Climate Change*, **12 (6)**, e731.

Mailier, P. J., D. B. Stephenson, C. A. Ferro, and K. I. Hodges, 2006: Serial clustering of extratropical cyclones. *Monthly weather review*, **134 (8)**, 2224–2240.

Manabe, S., K. Bryan, and M. Spelman, 1979: A global ocean-atmosphere climate model with seasonal variation for future studies of climate sensitivity. *Dynamics of Atmospheres and Oceans*, **3 (2-4)**, 393–426.

Manabe, S., K. Bryan, and M. J. Spelman, 1975: A global ocean-atmosphere climate model. part i. the atmospheric circulation. *Journal of Physical Oceanography*, **5 (1)**, 3–29.

Manabe, S. and R. T. Wetherald, 1967: Thermal equilibrium of the atmosphere with a given distribution of relative humidity. *Journal of the Atmospheric Sciences*, **24 (3)**, 241–259.

Martin, G. M., N. Bellouin, W. J. Collins, I. D. Culverwell, P. R. Halloran, S. C. Hardiman, T. J. Hinton, C. D. Jones, R. E. McDonald, A. J. McLaren, F. M. O'Connor, M. J. Roberts, J. M. Rodriguez, S. Woodward, M. J. Best, M. E. Brooks, A. R. Brown, N. Butchart, C. Dearden, S. H. Derbyshire, I. Dharssi, M. Doutriaux-Boucher, J. M. Edwards, P. D. Falloon, N. Gedney, L. J. Gray, H. T. Hewitt, M. Hobson, M. R. Huddleston, J. Hughes, S. Ineson, W. J. Ingram, P. M. James, T. C. Johns, C. E. Johnson, A. Jones, C. P. Jones, M. M. Joshi, A. B. Keen, S. Liddicoat, A. P. Lock, A. V. Maidens, J. C. Manners, S. F. Milton, J. G. L. Rae, J. K. Ridley, A. Sellar, C. A. Senior, I. J. Totterdell, A. Verhoef, P. L. Vidale, and A. Wiltshire, 2011: The hadgem2 family of met office unified model climate configurations. *Geoscientific Model Development*, **4**, 723–757, URL `https://doi.org/10.5194/gmd-4-723-2011`, martin et al.

Masson-Delmotte, V., P. Zhai, A. Pirani, S. Connors, C. Péan, S. Berger, N. Caud, Y. Chen, L. Goldfarb, M. Gomis, M. Huang, K. Leitzell, E. Lonnoy, J. Matthews, T. Maycock, T. Waterfield, O. Yelekçi, R. Yu, and B. Zhou, 2021a: Summary for policymakers. *Climate Change 2021: The Physical Science Basis. Contribution of Working Group I to the Sixth Assessment Report of the Intergovernmental Panel on Climate Change*, Masson-Delmotte, V., P. Zhai, A. Pirani, S. Connors, C. Péan, S. Berger,

N. Caud, Y. Chen, L. Goldfarb, M. Gomis, M. Huang, K. Leitzell, E. Lonnoy, J. Matthews, T. Maycock, T. Waterfield, O. Yelekçi, R. Yu, and B. Zhou, Eds., Cambridge University Press, Cambridge, United Kingdom and New York, NY, USA, 3–32.

Masson-Delmotte, V., P. Zhai, A. Pirani, S. L. Connors, C. Péan, S. Berger, N. Caud, Y. Chen, L. Goldfarb, M. Gomis, et al., 2021b: Climate change 2021: the physical science basis. *Contribution of working group I to the sixth assessment report of the intergovernmental panel on climate change*, **2 (1)**, 2391.

Meehl, G. A., C. Covey, T. Delworth, M. Latif, B. McAvaney, J. F. Mitchell, R. J. Stouffer, and K. E. Taylor, 2007: The wcrp cmip3 multimodel dataset: A new era in climate change research. *Bulletin of the American meteorological society*, **88 (9)**, 1383–1394.

Michel, C. and A. Sorteberg, 2023: Future projections of euro-cordex raw and bias-corrected daily maximum wind speeds over scandinavia. *Journal of Geophysical Research: Atmospheres*, **128 (6)**, e2022JD037 953.

Minola, L., F. Zhang, C. Azorin-Molina, A. S. Pirooz, R. Flay, H. Hersbach, and D. Chen, 2020: Near-surface mean and gust wind speeds in era5 across sweden: towards an improved gust parametrization. *Climate Dynamics*, **55 (3)**, 887–907.

Mitchell-Wallace, K., M. Jones, J. Hillier, and M. Foote, 2017: *Natural catastrophe risk management and modelling: A practitioner's guide*. John Wiley & Sons.

Moemken, J., I. Alifdini, A. M. Ramos, A. Georgiadis, A. Brocklehurst, L. Braun, and J. G. Pinto, 2024a: Insurance loss model vs meteorological loss index–how comparable are their loss estimates for european windstorms? *Natural Hazards and Earth System Sciences Discussions*, **2024**, 1–19.

Moemken, J., B. Koerner, F. Ehmele, H. Feldmann, and J. G. Pinto, 2022: Recurrence of drought events over iberia. part ii: Future changes using regional climate projections. *Tellus*, **74 (1)**, 262.

Moemken, J., G. Messori, and J. G. Pinto, 2024b: Windstorm losses in europe–what to gain from damage datasets. *Weather and Climate Extremes*, 100661.

Moemken, J., M. Reyers, H. Feldmann, and J. G. Pinto, 2018: Future changes of wind speed and wind energy potentials in euro-cordex ensemble simulations. *Journal of Geophysical Research: Atmospheres*, **123 (12)**, 6373–6389.

Molina, M. O., C. Gutiérrez, and E. Sánchez, 2021: Comparison of era5 surface wind speed climatologies over europe with observations from the hadisd dataset. *International Journal of Climatology*, **41 (10)**, 4864–4878.

Mühr, B., L. Eisenstein, J. G. Pinto, P. Knippertz, S. Mohr, and M. Kunz, 2022: Winter storm series: Ylenia, zeynep, antonia (int: Dudley, eunice, franklin) february 2022 (nw and central europe). Tech. rep., Technical Report No.

MunichRe, 1993: Winterstürme in europa. *Publication of the Munich Re, Ordering Number*.

Murray, R. and I. Simmonds, 1991: A numerical scheme for tracking cyclone centres from digital data. part ii: application to january and july general circulation model simulations. *Australian Meteorological Magazine*, **39**, 167–180.

Nakićenović, N. et al., 2000: *Emission Scenarios, A Special Report of Working Group III of the Intergovernmental Panel on Climate Change*. Cambridge University Press, New York, 599 pp.

Neu, U., M. G. Akperov, N. Bellenbaum, R. Benestad, R. Blender, R. Caballero, A. Cocozza, H. F. Dacre, Y. Feng, K. Fraedrich, et al., 2013: Imilast: A community effort to intercompare extratropical cyclone detection and tracking algorithms. *Bulletin of the American Meteorological Society*, **94 (4)**, 529–547.

Outten, S. and S. Sobolowski, 2021: Extreme wind projections over europe from the euro-cordex regional climate models. *Weather and Climate Extremes*, **33**, 100 363.

Palter, J. B., 2015: The role of the gulf stream in european climate. *Annual review of marine science*, **7**, 113–137.

Palutikof, J. and A. Skellern, 1991: Storm severity over britain, a report to commercial union general insurance, climatic research unit. *University of East Anglia, Norwich, United Kingdom*.

Panofsky, H. A. and J. A. Dutton, 1984: Atmospheric turbulence. models and methods for engineering applications. *New York: Wiley*.

Panofsky, H. A., H. Tennekes, D. H. Lenschow, and J. Wyngaard, 1977: The characteristics of turbulent velocity components in the surface layer under convective conditions. *Boundary-Layer Meteorology*, **11**, 355–361.

Parker, W. S., 2016: Reanalyses and observations: What's the difference? *Bulletin of the American Meteorological Society*, **97 (9)**, 1565–1572.

Parliament, E., 2009: Directive 2009/138/ec of the european parliament and of the council of 25 november 2009 on the taking-up and pursuit of the business of insurance and reinsurance (solvency ii) (recast). *Official Journal of the European Union L*, **337**, 11.

Pielke, R., C. W. Landsea, R. T. Musulin, and M. Downton, 1999: Evaluation of catastrophe models using a normalized historical record: Why it is needed and how to do it. *Journal of Insurance Regulation*, **18 (2)**, 177–194.

Pinto, J., T. Spangehl, U. Ulbrich, and P. Speth, 2005: Sensitivities of a cyclone detection and tracking algorithm: Individual tracks and climatology. *Meteorologische Zeitschrift - METEOROL Z*, **14**.

Pinto, J. G., N. Bellenbaum, M. K. Karremann, and P. M. Della-Marta, 2013: Serial clustering of extratropical cyclones over the north atlantic and europe under recent and future climate conditions. *Journal of geophysical research: Atmospheres*, **118 (22)**, 12–476.

Pinto, J. G., E. Fröhlich, G. Leckebusch, and U. Ulbrich, 2007: Changing european storm loss potentials under modified climate conditions according to ensemble simulations of the echam5/mpi-om1 gcm. *Natural Hazards and Earth System Sciences*, **7 (1)**, 165–175.

Pinto, J. G., I. Gómara, G. Masato, H. F. Dacre, T. Woollings, and R. Caballero, 2014: Large-scale dynamics associated with clustering of extratropical cyclones affecting western europe. *Journal of Geophysical Research: Atmospheres*, **119 (24)**, 13–704.

Pinto, J. G., M. K. Karremann, K. Born, P. M. Della-Marta, and M. Klawa, 2012: Loss potentials associated with european windstorms under future climate conditions. *Climate Research*, **54 (1)**, 1–20.

Pinto, J. G., S. Zacharias, A. H. Fink, G. C. Leckebusch, and U. Ulbrich, 2009: Factors contributing to the development of extreme north atlantic cyclones and their relationship with the nao. *Climate dynamics*, **32**, 711–737.

Pörtner, H.-O., D. C. Roberts, E. S. Poloczanska, K. Mintenbeck, M. Tignor, A. Alegría, M. Craig, S. Langsdorf, S. Löschke, V. Möller, et al., 2022: Ipcc, 2022: Summary for policymakers.

Prahl, B., D. Rybski, J. Kropp, O. Burghoff, and H. Held, 2012: Applying stochastic small-scale damage functions to german winter storms. *Geophysical Research Letters*, **39 (6)**.

Prahl, B. F., D. Rybski, M. Boettle, and J. P. Kropp, 2016: Damage functions for climate-related hazards: Unification and uncertainty analysis. *Natural Hazards and Earth System Sciences*, **16 (5)**, 1189–1203.

Prahl, B. F., D. Rybski, O. Burghoff, and J. P. Kropp, 2015: Comparison of storm damage functions and their performance. *Natural Hazards and Earth System Sciences*, **15 (4)**, 769–788.

Prein, A. F., W. Langhans, G. Fosser, A. Ferrone, N. Ban, K. Goergen, M. Keller, M. Tölle, O. Gutjahr, F. Feser, et al., 2015: A review on regional convection-permitting climate modeling: Demonstrations, prospects, and challenges. *Reviews of geophysics*, **53 (2)**, 323–361.

Preuschmann, S., A. Hänsler, L. Kotova, N. Dürk, W. Eibner, C. Waidhofer, C. Haselberger, and D. Jacob, 2017: The impact2c web-atlas–conception, organization and aim of a web-based climate service product. *Climate services*, **7**, 115–125.

Priestley, M. D. and J. L. Catto, 2022: Future changes in the extratropical storm tracks and cyclone intensity, wind speed, and structure. *Weather and Climate Dynamics*, **3 (1)**, 337–360.

Priestley, M. D., H. F. Dacre, L. C. Shaffrey, S. Schemm, and J. G. Pinto, 2020: The role of secondary cyclones and cyclone families for the north atlantic storm track and clustering over western europe. *Quarterly Journal of the Royal Meteorological Society*, **146 (728)**, 1184–1205.

Priestley, M. D. K., H. F. Dacre, L. C. Shaffrey, K. I. Hodges, and J. G. Pinto, 2018: The role of serial european windstorm clustering for extreme seasonal losses as determined from multi-centennial simulations of high-resolution global climate model data. *Natural Hazards and Earth System Sciences*, **18 (11)**, 2991–3006, URL `https://nhess.copernicus.org/articles/18/2991/2018/`.

Prodhomme, C., F. Doblas-Reyes, O. Bellprat, and E. Dutra, 2016: Impact of land-surface initialization on sub-seasonal to seasonal forecasts over europe. *Climate Dynamics*, **47**, 919–935.

Pörtner, H.-O., D. Roberts, M. Tignor, E. Poloczanska, K. Mintenbeck, A. Alegría, M. Craig, S. Langsdorf, S. Löschke, V. Möller, A. Okem, and B. Rama, (Eds.) , 2022: *Climate Change 2022: Impacts, Adaptation, and Vulnerability. Contribution of Working Group II to the Sixth Assessment Report of the Intergovernmental Panel on Climate Change*. Cambridge University Press, Cambridge, UK and New York, NY, USA, 3056 pp.

Qian, W. and H. H. Chang, 2021: Projecting health impacts of future temperature: a comparison of quantile-mapping bias-correction methods. *International journal of environmental research and public health*, **18 (4)**, 1992.

Qian, Y., C. Jackson, F. Giorgi, B. Booth, Q. Duan, C. Forest, D. Higdon, Z. J. Hou, and G. Huerta, 2016: Uncertainty quantification in climate modeling and projection. *Bulletin of the American Meteorological Society*, **97 (5)**, 821–824.

Raftery, A. E., A. Zimmer, D. M. Frierson, R. Startz, and P. Liu, 2017: Less than 2 c warming by 2100 unlikely. *Nature climate change*, **7 (9)**, 637–641.

Ramon, J., L. Lledó, V. Torralba, A. Soret, and F. J. Doblas-Reyes, 2019: What global reanalysis best represents near-surface winds? *Quarterly Journal of the Royal Meteorological Society*, **145 (724)**, 3236–3251.

Riahi, K., S. Rao, V. Krey, C. Cho, V. Chirkov, G. Fischer, G. Kindermann, N. Nakicenovic, and P. Rafaj, 2011: Rcp 8.5—a scenario of comparatively high greenhouse gas emissions. *Climatic change*, **109**, 33–57.

Riahi, K., D. P. Van Vuuren, E. Kriegler, J. Edmonds, B. C. O'neill, S. Fujimori, N. Bauer, K. Calvin, R. Dellink, O. Fricko, et al., 2017: The shared socioeconomic pathways and their energy, land use, and greenhouse gas emissions implications: An overview. *Global environmental change*, **42**, 153–168.

Roberts, J., A. Champion, L. Dawkins, K. Hodges, L. Shaffrey, D. Stephenson, M. Stringer, H. Thornton, and B. Youngman, 2014: The xws open access catalogue of extreme european windstorms from 1979 to 2012. *Natural Hazards and Earth System Sciences*, **14 (9)**, 2487–2501.

Rose, A. and C. K. Huyck, 2016: Improving catastrophe modeling for business interruption insurance needs. *Risk analysis*, **36 (10)**, 1896–1915.

Samuelsson, P., C. G. Jones, U. Will´ En, A. Ullerstig, S. Gollvik, U. Hansson, E. Jansson, C. Kjellstro¨ M, G. Nikulin, and K. Wyser, 2011: The rossby centre regional climate model rca3: model description and performance. *Tellus A: Dynamic Meteorology and Oceanography*, **63 (1)**, 4–23.

Schleussner, C.-F., J. Rogelj, M. Schaeffer, T. Lissner, R. Licker, E. M. Fischer, R. Knutti, A. Levermann, K. Frieler, and W. Hare, 2016: Science and policy characteristics of the paris agreement temperature goal. *Nature Climate Change*, **6 (9)**, 827–835.

Schultz, D. M., L. F. Bosart, B. A. Colle, H. C. Davies, C. Dearden, D. Keyser, O. Martius, P. J. Roebber, W. J. Steenburgh, H. Volkert, et al., 2019: Extratropical cyclones: A century of research on meteorology's centerpiece. *Meteorological monographs*, **59**, 16–1.

Schultz, D. M. and D. Keyser, 2021: Antecedents for the shapiro–keyser cyclone model in the bergen school literature. *Bulletin of the American Meteorological Society*, **102 (2)**, E383–E398.

Schultz, D. M. and G. Vaughan, 2011: Occluded fronts and the occlusion process: A fresh look at conventional wisdom. *Bulletin of the American Meteorological Society*, **92 (4)**, 443–466.

Schulz, J.-P., 2008: Revision of the turbulent gust diagnostics in the cosmo model. *COSMO Newsletter*, **8**, 17–22.

Schwalm, C. R., S. Glendon, and P. B. Duffy, 2020: Rcp8. 5 tracks cumulative co2 emissions. *Proceedings of the National Academy of Sciences*, **117 (33)**, 19 656–19 657.

Schwierz, C., P. Köllner-Heck, E. Zenklusen Mutter, D. N. Bresch, P.-L. Vidale, M. Wild, and C. Schär, 2010: Modelling european winter wind storm losses in current and future climate. *Climatic change*, **101**, 485–514.

Severino, L. G., C. M. Kropf, H. Afargan-Gerstman, C. Fairless, A. J. de Vries, D. I. Domeisen, and D. N. Bresch, 2024: Projections and uncertainties of winter windstorm damage in europe in a changing climate. *Natural Hazards and Earth System Sciences*, **24 (5)**, 1555–1578.

Shapiro, M. A. and D. Keyser, 1990: *Fronts, jet streams and the tropopause*. Springer.

Sharkey, P., J. A. Tawn, and S. J. Brown, 2020: Modelling the spatial extent and severity of extreme european windstorms. *Journal of the Royal Statistical Society Series C: Applied Statistics*, **69 (2)**, 223–250.

Shaw, T. A., M. Baldwin, E. A. Barnes, R. Caballero, C. I. Garfinkel, Y.-T. Hwang, and A. Voigt, 2016: Storm track processes and the opposing influences of climate change. *Nature Geoscience*, **9 (9)**, 656–664.

Sheridan, P., 2011: *Review of techniques and research for gust forecasting and parameterisation*. Met Office Exeter, UK.

———, 2018: Current gust forecasting techniques, developments and challenges. *Advances in Science and Research*, **15**, 159–172.

Sinclair, M. R., 1994: An objective cyclone climatology for the southern hemisphere. *Monthly Weather Review*, **122 (10)**, 2239 – 2256, URL `https://journals.ametsoc.org/view/journals/mwre/122/10/1520-0493_1994_122_2239_aoccft_2_0_co_2.xml`.

Solomon, S., D. Qin, M. Manning, Z. Chen, M. Marquis, K. B. Averyt, M. Tignor, and H. L. Miller, (Eds.) , 2007: *Climate Change 2007: The Physical Science Basis*. Cambridge University Press, Cambridge, UK and New York, USA, URL `https://www.ipcc.ch/report/ar4/wg1/`.

Sørland, S. L., R. Brogli, P. K. Pothapakula, E. Russo, J. Van de Walle, B. Ahrens, I. Anders, E. Buchignani, E. L. Davin, M.-E. Demory, et al., 2021: Cosmo-clm regional climate simulations in the coordinated regional climate downscaling experiment (cordex) framework: a review. *Geoscientific Model Development*, **14 (8)**, 5125–5154.

Spearman, C., 1904: The proof and measurement of association between two things. *The American journal of psychology*, **15 (1)**, 72–101.

Spinoni, J., G. Formetta, L. Mentaschi, G. Forzieri, L. Feyen, et al., 2020: Global warming and windstorm impacts in the eu. *Luxembourg: Publications Office of the European Union, doi*, **10**, 039 014.

Stouffer, R. J., V. Eyring, G. A. Meehl, S. Bony, C. Senior, B. Stevens, and K. Taylor, 2017: Cmip5 scientific gaps and recommendations for cmip6. *Bulletin of the American Meteorological Society*, **98 (1)**, 95–105.

Takayabu, I., R. Rasmussen, E. Nakakita, A. Prein, H. Kawase, S.-I. Watanabe, S. A. Adachi, T. Takemi, K. Yamaguchi, Y. Osakada, et al., 2022: Convection-permitting models for climate research. *Bulletin of the American Meteorological Society*, **103 (1)**, E77–E82.

Tapiador, F. J., A. Navarro, R. Moreno, J. L. Sánchez, and E. García-Ortega, 2020: Regional climate models: 30 years of dynamical downscaling. *Atmospheric Research*, **235**, 104 785.

Tarbuck, E. J. and F. K. Lutgens, 2013: *The atmosphere: an introduction to meteorology*. Prentice Hall.

Taylor, K. E., R. J. Stouffer, and G. A. Meehl, 2012: An overview of cmip5 and the experiment design. *Bulletin of the American meteorological Society*, **93 (4)**, 485–498.

Tebaldi, C. and R. Knutti, 2007: The use of the multi-model ensemble in probabilistic climate projections. *Philosophical transactions of the royal society A: mathematical, physical and engineering sciences*, **365 (1857)**, 2053–2075.

Teichmann, C., K. Bülow, J. Otto, S. Pfeifer, D. Rechid, K. Sieck, and D. Jacob, 2018: Avoiding extremes: benefits of staying below+ 1.5 c compared to+ 2.0 c and+ 3.0 c global warming. *Atmosphere*, **9 (4)**, 115.

Thalla, O. and S. C. Stiros, 2018: Wind-induced fatigue and asymmetric damage in a timber bridge. *Sensors*, **18 (11)**, 3867.

Themeßl, M. J., A. Gobiet, and A. Leuprecht, 2011: Empirical-statistical downscaling and error correction of daily precipitation from regional climate models. *International Journal of Climatology*, **31 (10)**, 1530–1544.

Thompson, D. W. and J. M. Wallace, 2000: Annular modes in the extratropical circulation. part i: Month-to-month variability. *Journal of climate*, **13 (5)**, 1000–1016.

Tsoi, E. Y. C., 2024: Using generative models to produce realistic populations of the united kingdom windstorms. *arXiv preprint arXiv:2409.10696*.

Tucker, S. O., E. J. Kendon, N. Bellouin, E. Buonomo, B. Johnson, and J. M. Murphy, 2022: Evaluation of a new 12 km regional perturbed parameter ensemble over europe. *Climate Dynamics*, **58 (3)**, 879–903.

Ulbrich, U., A. Fink, M. Klawa, and J. G. Pinto, 2001: Three extreme storms over europe in december 1999. *Weather*, **56 (3)**, 70–80.

Ulbrich, U., G. C. Leckebusch, and J. G. Pinto, 2009: Extra-tropical cyclones in the present and future climate: a review. *Theoretical and applied climatology*, **96**, 117–131.

van den Brink, H. W., 2019: An effective parametrization of gust profiles during severe wind conditions. *Environmental Research Communications*, **2 (1)**, 011 001.

Van Meijgaard, E., L. Van Ulft, G. Lenderink, S. De Roode, E. L. Wipfler, R. Boers, and R. van Timmermans, 2012: *Refinement and application of a regional atmospheric model for climate scenario calculations of Western Europe*. KVR 054/12, KvR.

Van Vuuren, D. P., J. Edmonds, M. Kainuma, K. Riahi, A. Thomson, K. Hibbard, G. C. Hurtt, T. Kram, V. Krey, J.-F. Lamarque, et al., 2011: The representative concentration pathways: an overview. *Climatic change*, **109**, 5–31.

Vautard, R., J. Cattiaux, P. Yiou, J.-N. Thépaut, and P. Ciais, 2010: Northern hemisphere atmospheric stilling partly attributed to an increase in surface roughness. *Nature geoscience*, **3 (11)**, 756–761.

Vautard, R., A. Gobiet, S. Sobolowski, E. Kjellström, A. Stegehuis, P. Watkiss, T. Mendlik, O. Landgren, G. Nikulin, C. Teichmann, et al., 2014: The european climate under a 2 c global warming. *Environmental Research Letters*, **9 (3)**, 034 006.

Vautard, R., N. Kadygrov, C. Iles, F. Boberg, E. Buonomo, K. Bülow, E. Coppola, L. Corre, E. van Meijgaard, R. Nogherotto, et al., 2021: Evaluation of the large euro-cordex regional climate model ensemble. *Journal of Geophysical Research: Atmospheres*, **126 (17)**, e2019JD032 344.

Vitolo, R., D. B. Stephenson, I. M. Cook, and K. Mitchell-Wallace, 2009: Serial clustering of intense european storms. *Meteorologische Zeitschrift*, **18 (4)**, 411–424.

Voldoire, A., E. Sanchez-Gomez, D. Salas y Mélia, B. Decharme, C. Cassou, S. Sénési, S. Valcke, I. Beau, A. Alias, M. Chevallier, et al., 2013: The cnrm-cm5. 1 global climate model: description and basic evaluation. *Climate dynamics*, **40**, 2091–2121.

Walker, E., D. M. Mitchell, and W. J. Seviour, 2020: The numerous approaches to tracking extratropical cyclones and the challenges they present. *Weather*, **75 (11)**, 336–341.

Wang, J., H.-M. Kim, and E. K. Chang, 2017: Changes in northern hemisphere winter storm tracks under the background of arctic amplification. *Journal of Climate*, **30 (10)**, 3705–3724.

Wang, L., 2008: *Stochastic modeling and simulation of transient events*. University of Notre Dame.

Welker, C., T. Röösli, and D. N. Bresch, 2021: Comparing an insurer's perspective on building damages with modelled damages from pan-european winter windstorm event sets: a case study from zurich, switzerland. *Natural Hazards and Earth System Sciences*, **21 (1)**, 279–299.

Wetterkarte eV, B. and D. Wetterdienst, 1999: Berliner wetterkarte. *Institut für Meteorologie der Freien Universität Berlin*.

WG, I., 2013: The physical science basis. *Contribution of working group I to the fifth assessment report of the intergovernmental panel on climate change*, **1535**.

Wilby, R. L. and T. M. Wigley, 1997: Downscaling general circulation model output: a review of methods and limitations. *Progress in physical geography*, **21 (4)**, 530–548.

Wilks, D. S., 2006: *Statistical methods in the atmospheric sciences*. Academic press.

Wohland, J., 2022: Process-based climate change assessment for european winds using euro-cordex and global models. *Environmental Research Letters*, **17 (12)**, 124 047.

World Meteorological Organization, 2014: *Measurement of Surface Wind*. World Meteorological Organisation, Geneva, Switzerland, URL `https://library.wmo.int/doc_num.php?explnum_id=10100`, in Guide to Meteorological Instruments and Methods of Observation (2017 Update).

Zhang, M.-Z., Z. Xu, Y. Han, and W. Guo, 2024: Evaluation of cmip6 models toward dynamical downscaling over 14 cordex domains. *Climate Dynamics*, **62 (6)**, 4475–4489.

Zhu, S., F. Ge, Y. Fan, L. Zhang, F. Sielmann, K. Fraedrich, and X. Zhi, 2020: Conspicuous temperature extremes over southeast asia: seasonal variations under 1.5 c and 2 c global warming. *Climatic Change*, **160**, 343–360.

E. List of Figures

1.1 Impacts of windstorm Kyrill in January 2007. (a) The satellite image of windstorm Kyrill from Meteosat-8 RGB at 12 PM on January 18, 2007. (b) Storm Kyrill 2007 damaged cars in Berlin-Lichterfelde after the heavy storm. The figure (a) is reprinted from the press release by Deutscher Wetterdienst (DWD) (2017), with ©Deutscher Wetterdienst/EUMETSAT (used with permission). Figure (b) is reprinted from Krueger-Krusche (2007) under ©CC BY-SA 3.0 Unported. 1

2.1 Global wind circulation. The figure is reprinted from Kaidor (2013), via Wikimedia Commons. Copyright ©CC BY-SA 3.0 6

2.2 Conceptual models of (a) Norwegian cyclone and (b) Shapiro-Keyser cyclone depict lower-tropospheric geopotential height and fronts (top) and lower-tropospheric potential temperature (bottom). In the top panels, blue indicates the cold front, red represents the warm front, and violet denotes the occluded front. The cyclone center, denoted as 'L,' progresses through stages separated by approximately 6 to 24 hours, with the distance from 'L' to the outermost contour in stage IV being 1000 km. The figures are reprinted from Figures 2 and 12 in Schultz and Vaughan (2011). © American Meteorological Society. Used with permission. 7

2.3 Cyclone track density (cyclone days per winter) for the most intense 10% of cyclones, derived from NCEP reanalysis data (1958–1998). The figure is reprinted from Figure 4a in Pinto et al. (2009). Copyright © CC BY-NC 2.0 8

2.4 Windstorm conceptual model of extratropical cyclone in the Northern Hemisphere, illustrating (a) the track of the cyclone (represented by a black dotted line) and the storm footprints caused by the warm jet (yellow), sting jet (red), and cold jet (orange). (b) The phases of the cyclone's life cycle, depicting the development of fronts and isobars, as well as the formation of jets. The small green dots represent a minor frontal wave, the orange dots represent a frontal wave cyclone, and the black dots represent a barotropic low. (c) The temporal evolution of the jets, displaying the corresponding wind gust magnitudes from phase 1 to 7. The dashed blue line represents the most rapid deepening, while the solid blue arrow indicates the maximum depth of the cyclone. This figure is reprinted from Figures 1 in Hewson and Neu (2015), with copyright CC BY 4.0. 9

2.5 The Wind Gust Estimate (WGE) method by Brasseur (2001) employs the utilization of turbulent kinetic energy (TKE) averaged over a specified depth within the boundary layer to determine the estimates of wind gust. The figures are reprinted from Figure 4 in Brasseur (2001). © American Meteorological Society. Used with permission. 12
2.6 The depicted regions in blue exhibit a regular occurrence of cyclones (underdispersion), whereas the red displays the region with clustered cyclone activity (overdispersion). The cyclone tracks are depicted in grey. The figure is reprinted from Figure 2 in Dacre and Pinto (2020), with copyright CC BY 4.0. 16
2.7 (a) Cyclone passage occurrences within circular line 3 (December 1957 - February 1958) with the top row: all cyclones, the middle row: cyclones with core pressure above the 90th percentile, and the bottom row: cyclones with core pressure above the 95th percentile. (b) Location of circular line 3. The figure is reprinted from Figure 1 in Pinto et al. (2013). Copyright © 1999-2024 John Wiley & Sons, Inc or related companies. Used with permission. 17
2.8 The global mean temperature (30-year moving average) from 15 bias-corrected RCMs is shown in gray lines for the SRES A1B (moderate emissions) scenario (top panel, CMIP3) and RCP2.6, RCP4.5, and RCP8.5 scenarios (bottom panels, CMIP5). The horizontal black line in the top panel represents observed temperatures relative to pre-industrial levels. The vertical black lines are the median year when each CMIP3 (top panel) and CMIP5 (bottom panel) ensemble reaches +2°C. The vertical red line (top panel) marks the median year when reaching +2°C for the 6 main GCMs used to drive the RCMs in CMIP3. No black vertical line is shown for RCP2.6 because most simulations under this scenario remain below +2°C. The figure is reprinted from Figure 1 in Vautard et al. (2014), with copyright CC BY 3.0. 19
2.9 Framework for the experiments within the Coordinated Regional Downscaling Experiment (CORDEX) with RCM stands for regional climate model, and GCM stands for general circulation model. The figure is reprinted from Figure 7 in Giorgi (2019). Copyright © 1999-2024 John Wiley & Sons, Inc. or related companies. Used with permission. 21
2.10 The storm index is derived from geostrophic wind speed percentiles across Northwestern Europe, encompassing the British Isles, North Sea, and Norwegian Sea. The 95^{th} percentiles of standardized geostrophic wind speed anomalies are denoted by the blue circles. The low-pass filtered data is represented by the gray curve. Additionally, the first blue line corresponds to the linear trends of the 95^{th} percentiles for the period 1881-2004, obtained from station network datasets as documented in Alexandersson et al. (1998). The second blue line indicates the trends observed during the ERA-40 period (1957-2001). The figure is reprinted from Figure 2 in Feser et al. (2015). Copyright © 1999-2024 John Wiley & Sons, Inc. or related companies. Used with permission. 23

2.11 Storm track density (a) during the historical period (1979–2014) from the CMIP6 multi-model ensemble and (b, c) projected changes for 2080–2100 under scenarios of (b) SSP1-26 (low emission) and (c) SSP5-85 (high emission) relative to the historical period, with stippling indicating over 80% model agreement on the sign of change. The figure is reprinted from Figure 2 (a, b, and e) in Priestley and Catto (2022), with copyright CC BY 4.0. 24
2.12 Schematic diagram illustrating projected alterations to extratropical cyclones in the Northern Hemisphere. The table presents the level of certainty regarding the change of each of the identified aspects depicted in the diagram, derived from the comprehensive examination of the scientific literature conducted. The figure is reprinted from Figure 2 in Catto et al. (2019), with copyright CC BY 4.0. 24

4.1 (a) The group of countries within the Core Europe region (purple) as defined by (Pinto et al., 2012). (b) The footprint of windstorm Kyrill (2007), which significantly affected the Core Europe. Figure 4.1b is reprinted from Figure 1b in (Moemken et al., 2024a), with copyright CC BY 4.0. 35
4.2 Catastrophe model flow diagram of Aon Impact Forecasting (an insurance company). The figure is reprinted from Figure 2 in Supplementary File Part A of Moemken et al. (2024a), with copyright CC BY 4.0. 37

5.1 Population density for 2020 was derived from CIESIN for the 11 countries covered in this study. The figure is reprinted from Figure 1a in Moemken et al. (2024a), with copyright CC BY 4.0. 44
5.2 98^{th} percentile (upper row) and 99.9^{th} percentile (lower row) of daily maximum wind gust for the winter half year (ONDJFM) for the period 1979-2019 derived from ERA5 (left) and ERA Interim (middle). Difference between ERA5 minus ERA Interim (right). The figures (a-c) are reprinted from Figure 2 in Moemken et al. (2024a), with copyright CC BY 4.0. 45
5.3 Comparison of normalized loss values based on LI ERA5 (x-axis) and LI ERA Interim (y-axis). Depicted are the common 20 most extreme storms in the period 1979-2019 for (a) Core Europe, (b) the United Kingdom, (c) Germany, and (d) France. Corresponding storm names to each data point are marked with a blue line. Storms without a formal name are named based on the region (e.g. CE for Core Europe) and the loss value (starting from zero for storms with highest loss). The red dashed line denotes the linear regression line. Outlier storms based on the IQR method (see section 5.1.2) are marked in red. The figure is reprinted from Figure 3 in Moemken et al. (2024a), with copyright CC BY 4.0. 47

5.4 Same as Figure 5.3, but for the comparison of storm ranks. The values in brackets indicate the rank (first value ERA5, second value ERA Interim). The figure is reprinted from Figure 4 in Moemken et al. (2024a), with copyright CC BY 4.0. 48
5.5 Spearman's rank correlation coefficient at the country level for LI ERA5 vs. LI ERA-Interim. The ranking is based on common storms per country. The figure is reprinted from Figure 5 in Moemken et al. (2024a), with copyright CC BY 4.0. 49
5.6 Normalized losses (upper row) and storm ranking (lower row) at the country level for storm Sabine in February 2020. Losses are derived from LI ERA5 (left), Aon's IF Euro WS model (middle), and PERILS (right). The black line and dots in the left column denote the cyclone track derived from ERA5 using the tracking algorithm of Pinto et al. (2005). Losses are only shown for the 11 countries covered by Aon. The ranking is based on common storms per country (see Table 5.1). The figure is reprinted from Figure 6 in Moemken et al. (2024a), with copyright CC BY 4.0. 50
5.7 Comparison of normalized loss values between Aon's IF Euro WS model (x-axis) and LI ERA5 (y-axis). Depicted are the common most extreme storms for the period 1990-2020 for (a) Core Europe, (b) the United Kingdom, (c) Germany, and (d) France. A logarithmic scale is used for the axes. The red dashed line denotes the logarithmic regression. Outlier storms based on the IQR method are marked in red. Please note the different scales. The figure is reprinted from Figure 7 in Moemken et al. (2024a), with copyright CC BY 4.0. . 52
5.8 Same as Figure 5.7, but for the comparison of storm ranks. The values in brackets indicate the rank (first value Aon's model, second value ERA5). The figure is reprinted from Figure 8 in Moemken et al. (2024a), with copyright CC BY 4.0. 53
5.9 Spearman's rank correlation coefficient at the country level for LI ERA5 vs Aon's IF Euro WS model (left), LI ERA5 vs PERILS (middle), and Aon's IF Euro WS model vs PERILS (right). The ranking is based on common storms per country (see Table 5.1 and Appendix Figure A.4). The figure is reprinted from Figure 9 in Moemken et al. (2024a), with copyright CC BY 4.0. 54

6.1 Population density (P km^{-2}) for the year 2020 with Core Europe in red, Eastern Europe in blue, all other analyzed countries in green, and non-considered countries in grey. The figure is reprinted from Figure 1 in Alifdini et al. (2025), with copyright CC BY 4.0. . . 59
6.2 (a-b) Mean of daily maximum wind gust (ms^{-1}) for the ensemble mean of the EURO-CORDEX historical simulations (1976-2005) before bias correction (a) and after bias correction using Empirical Quantile Mapping (b). (c-d) Difference between the EURO-CORDEX ensemble mean and ERA5 (%). The figure is reprinted from Figure 2 in Alifdini et al. (2025), with copyright CC BY 4.0. 60

6.3 Same as Figure 6.2, but for the 98th percentile of daily maximum wind gusts. The figure is reprinted from Figure 3 in Alifdini et al. (2025), with copyright CC BY 4.0. 61
6.4 (a) Windstorm intensity (ms^{-1}), shown as wind gust speed above the 98th percentile, derived from the EURO-CORDEX ensemble mean for the historical period (1976-2005). Changes in windstorm intensity (%) compared to the historical period for the ensemble mean of (b) GWL2 and (c) GWL3. Black diagonal lines indicate robust climate change signals, meaning that 14 or more ensemble members agree on the sign of change. The figure is reprinted from Figure 4 in Alifdini et al. (2025), with copyright CC BY 4.0. . . 63
6.5 Changes in windstorm frequency (%) compared to the historical period for the ensemble mean for (a) GWL2 and (b) GWL3. Black diagonal lines indicate robust climate change signals, meaning that 14 or more ensemble members agree on the sign of change. The figure is reprinted from Figure 5 in Alifdini et al. (2025), with copyright CC BY 4.0. . . 64
6.6 Changes in windstorm frequency (%) compared to the historical period for the individual ensemble members derived for Core Europe (upper row) and Eastern Europe (lower row) for (a) GWL2, and (b) GWL3. For each matrix, rows represent RCMs and columns GCMs. The RCM (GCM) mean is depicted in the last column (first row). The figure is reprinted from Figure 6 in Alifdini et al. (2025), with copyright CC BY 4.0. 64
6.7 (a) Windstorm loss, shown as total LI, derived from the EURO-CORDEX ensemble mean for the historical period (1976-2005). Changes in windstorm loss (%) compared to the historical period for the ensemble mean for (b) GWL2, and (c) GWL3. Black diagonal lines indicate robust climate change signals, meaning that 14 or more ensemble members agree on the sign of change. The figure is reprinted from Figure 7 in Alifdini et al. (2025), with copyright CC BY 4.0. 66
6.8 Windstorm loss derived for Core Europe (a) and Eastern Europe (d) for the individual ensemble members for the historical period (1976-2005). Changes in windstorm loss (%) compared to the historical period for the individual ensemble members for (b,e) GWL2, and (c,f) GWL3. For each matrix, rows represent RCMs and columns GCMs. The RCM (GCM) mean is depicted in the last column (first row). The figure is reprinted from Figure 8 in Alifdini et al. (2025), with copyright CC BY 4.0. 67
6.9 Return periods of the most extreme loss events derived for (a) Core Europe and (b) Eastern Europe for the historical period (green), the GWL2 (blue), and the GWL3 (red). The dots represent the empirical values, the solid lines show the GPD fit, and the dashed lines represent the upper and lower bounds of the 95% confidence interval. Same as (a) and (b), but for countries belonging to Core Europe (c,e) and Eastern Europe (d,f). The number of top LIs used in these figures are based on the stability of the scale and shape parameters of the GPD fit. The figure is reprinted from Figure 9 in Alifdini et al. (2025), with copyright CC BY 4.0. 69

7.1 Regions were grouped in order to identify seasonal loss clustering. The following regions were considered: Core Europe (red) and Eastern Europe (orange). 73
7.2 Time series of (a) event count, (b) OEP, (c) AEP, and (d) the OEP/AEP ratio using ERA5 (1959-2021) for Core Europe. The OEP (maximum LI) and AEP (total LI) are calculated based on the LI values for each winter, with the year representing the start of each winter season where the LI value exceeds the threshold. 75
7.3 Same as Figure 7.2, but for Eastern Europe. 76
7.4 Scatterplots between AEP, OEP, the OEP/AEP ratio, and event count for Core Europe using LI ERA5 (1959-2021). One point represents 1 winter. The number in parentheses is the Spearman's rank correlation coefficient. 77
7.5 Violin plots of (a) event count, (b) OEP (normalized), (c) AEP (normalized), and (d) the OEP/AEP ratio calculated using the original OEP and AEP values from LI ERA5 data (1959-2021) for Core Europe (red) and Eastern Europe (orange). Figures (b) and (c) are normalized by the number of grids in each region. 78
7.6 Empirical return values of (a) normalized AEP and (b) normalized OEP from LI ERA5 (1959-2021), with values normalized by the number of grids in each region. The empirical return value of the OEP/AEP ratio, ranked by AEP values, for Core Europe (c) and Eastern Europe (d). In (c,d), the minimum return period corresponds to the smallest AEP, and the maximum to the largest. In Figure (c), black dots indicate the first year of winter seasons with serial clustering of windstorms based on Pinto et al. (2014). The "median top 25%" in the legend refers to the median of the OEP/AEP ratio for the winters with the highest AEP values, specifically the top 25% (15 out of 62 winters). The red dot represents Core Europe, and the orange dot represents Eastern Europe. Each point corresponds to one winter. 79
7.7 The violin plot of the OEP/AEP ratio (all winters from 1959-2021) for (a) Core Europe and (b) Eastern Europe. The bottom and upper solid gray horizontal lines represent the 1st (33.33%) and 2nd (66.66%) terciles of the OEP/AEP ratio climatology. The gray and black dots indicate the OEP/AEP ratios for the top 25% of AEP. The black dots with labeled years represent seasons where serial clustering windstorms occur, based on Pinto et al. (2014), with the years indicating the first year of the full winter season. The percentage (below the 1st tercile) refers to the proportion of seasons in the top 25% AEP that fall below the 1st tercile of the OEP/AEP ratio climatology for each region. 81
7.8 Empirical return values of AEP (upper row) and OEP (lower row) from LI (EURO-CORDEX ensemble) for (a,c) Core Europe and (b,d) Eastern Europe are shown for the historical period (green), GWL2 (blue), and GWL3 (red). Each point represents one winter. 82

7.9 Empirical return values of the OEP/AEP ratio from the EURO-CORDEX ensemble, ranked by AEP value, are shown from the historical period to GWLs for (a,c,e) Core Europe and (b,d,f) Eastern Europe. The OEP/AEP ratio at the minimum return period corresponds to the smallest AEP, while the ratio at the maximum return period corresponds to the largest AEP. The thin vertical gray lines represent the bin sizes for every 5% density of the data. The solid brown lines represent the averages of OEP/AEP within each bin, smoothed using Gaussian smoothing, which reduces noise by averaging nearby points with more weight: the bottom 25% of values (lower line), the middle 50% of values (middle line), and the top 25% of values (upper line). The percentage (below the 1st tercile) represents the proportion of seasons in the top 25% AEP that have an OEP/AEP ratio below the 1st tercile (33.33%) of the OEP/AEP ratio climatology for each period. . 83

A.1 Wind gust footprint for storm Irina in October 2002 based on ERA5 (a), ERA5 re gridded to the ERA Interim grid (b), and ERA Interim (c). Shown is the largest exceedance (in percent) of the 98th percentile of daily maximum wind gust within 72 hours. The red line and dots denote the cyclone track derived from ERA5 (a, b) and ERA Interim (c) using the tracking algorithm of (Pinto et al., 2005). The figure is reprinted from Figure S1 in Moemken et al. (2024a), with copyright CC BY 4.0. 99

A.2 Comparison of loss values (in thousands) based on LI ERA5 (x axis) and LI ERA Interim (y axis). Depicted are the common 20 most extreme storms in the period 1979-2019 for (a) Core Europe, (b) the United Kingdom, (c) Germany, and (d) France. Corresponding storm names to each data point are marked with a blue line. Storms without a formal name are named based on the region (e.g. CE for Core Europe) and the loss value (starting for zero for storm with highest loss). The red dashed line denotes the linear regression line. Outlier storms based on the IQR method (see section 3.2) are marked in red. Please note the different scales. The figure is reprinted from Figure S2 in Moemken et al. (2024a), with copyright CC BY 4.0. 100

A.3 Comparison of loss values (in thousands) based on LI ERA5 (x axis) and LI ERA Interim (y axis). Depicted are the common 20 most extreme storms in the period 1979-2019 for (a) Core Europe, (b) the United Kingdom, (c) Germany, and (d) France. Corresponding storm names to each data point are marked with a blue line. Storms without a formal name are named based on the region (e.g. CE for Core Europe) and the loss value (starting for zero for storm with highest loss). The red dashed line denotes the linear regression line. Outlier storms based on the IQR method (see section 3.2) are marked in red. Please note that LI ERA5 is calculated from ERA5 gust data re gridded to the ERA Interim grid. Please note the different scales. The figure is reprinted from Figure S3 in Moemken et al. (2024a), with copyright CC BY 4.0. 101

A.4 Number of common storms per country for LI ERA5 vs Aon's IF Euro WS model (left), LI ERA5 vs PERILS (middle), and Aon's IF Euro WS model vs PERILS (right). The figure is reprinted from Figure S4 in Moemken et al. (2024a), with copyright CC BY 4.0. 102
A.5 Comparison of normalized loss values between Aon's IF Euro WS model (x axis) and LI ERA5 (y axis). Depicted are the common most extreme storms for the period 1990-2020 for (a) Core Europe, (b) the United Kingdom, (c) Germany, and (d) France. A logarithmic scale is used for the axes. The red dashed line denotes the logarithmic regression. Outlier storms based on the IQR method are marked in red. LI ERA5 is calculated for 24 hour windows. Please note the different scales. The figure is reprinted from Figure S5 in Moemken et al. (2024a), with copyright CC BY 4.0. 103
A.6 Same as Figure A.5, but for the comparison of storm ranks. The values in brackets indicate the rank (first value Aon's model, second value ERA5). The figure is reprinted from Figure S6 in Moemken et al. (2024a), with copyright CC BY 4.0. 104

B.1 Number of storm events for the individual EURO-CORDEX ensemble members for (a, d) the historical period (b, e) GWL2 and (c, f) GWL3. The ensemble mean is given in purple. The threshold for the selection of events is the minimum LI value for the top 2900 events in the historical period (Section 2.2.2). The figure is reprinted from Figure S1 in Alifdini et al. (2025), with copyright CC BY 4.0. 105
B.2 Difference in the mean of daily maximum wind gust between the EURO-CORDEX historical simulations (1976-2005) and ERA5 (%) for the individual GCM-RCM chains. The figure is reprinted from Figure S2 in Alifdini et al. (2025), with copyright CC BY 4.0. 106
B.3 Same as Figure B.2, but for the 98th percentile of daily maximum wind gust. The figure is reprinted from Figure S3 in Alifdini et al. (2025), with copyright CC BY 4.0. 106
B.4 Difference in the mean of daily maximum wind gust between the EURO-CORDEX historical simulations (1976-2005) and ERA5 (%) for the individual GCM-RCM chains after bias correction. The figure is reprinted from Figure S4 in Alifdini et al. (2025), with copyright CC BY 4.0. 107
B.5 Same as Figure B.4, but for the 98th percentile of daily maximum wind gust. The figure is reprinted from Figure S5 in Alifdini et al. (2025), with copyright CC BY 4.0. 107
B.6 Mean differences (20 models) of the 98th percentile of daily maximum wind gust EURO-CORDEX RCP8.5 minus historical period ONDJFM. Slashes denote agreement among over 14 models on difference sign. Note: In this figure, changes are calculated using the 98th percentile for each historical, GWL2, and GWL3. The figure is reprinted from Figure S6 in Alifdini et al. (2025), with copyright CC BY 4.0. 108

B.7 Changes in windstorm intensity (%) compared to the historical period for the individual EURO-CORDEX ensemble members for the GWL2. The figure is reprinted from Figure S7 in Alifdini et al. (2025), with copyright CC BY 4.0. 109
B.8 Same as Figure B.7, but for the GWL3. The figure is reprinted from Figure S8 in Alifdini et al. (2025), with copyright CC BY 4.0. 109
B.9 Changes in windstorm frequency (%) compared to the historical period for the various ensemble members derived for the individual countries for (a) GWL2 and (b) GWL3. For each matrix, rows represent countries and columns represent GCM-RCM pairs. The ensemble mean is depicted in the last column. The model code can be derived from Table 4.1. The figure is reprinted from Figure S9 in Alifdini et al. (2025), with copyright CC BY 4.0. 110
B.10 Same as Figure B.9, but for changes in windstorm loss (%). The figure is reprinted from Figure S10 in Alifdini et al. (2025), with copyright CC BY 4.0. 111
B.11 Return periods of the most extreme loss events for countries in Core Europe not shown in Figure 6.9 are presented for the historical period (green), GWL2 (blue), and GWL3 (red). The dots represent empirical values, the solid lines show the GPD fit, and the dashed lines represent the upper and lower bounds of the 95% confidence interval. The figure is reprinted from Figure S11 in Alifdini et al. (2025), with copyright CC BY 4.0. . 112
B.12 Same as Figure B.11, but for countries in Eastern Europe that are not shown in Figure 6.9. The figure is reprinted from Figure S12 in Alifdini et al. (2025), with copyright CC BY 4.0. 113

C.1 Same as Figure 7.4, but for Eastern Europe. 115

F. List of Tables

4.1 EURO-CORDEX (EUR-11) model chains (20 models) of daily maximum surface wind gust from the historical period (1976-2005) to future projection under RCP8.5 for GWLs +2°C and +3°C. Each GCM has 4 different RCMs. We use 1 ensemble member for each model that is r1i1p1, except for MPI-ESM-LR RACMO22E that is r12i1p1 (which depends on data availability). A-E (GCM) and 1-4 (RCM) correspond to the model codes employed in figures in appendix B. The table is reprinted from Table 1 in Alifdini et al. (2025), with copyright CC BY 4.0. 34

4.2 Historical event set of insured winter windstorms in Aon's IF Euro WS model in the period 1990-2020, including storm name and event date (as yyyy-mm-dd). The table is reprinted from Table S1 in Moemken et al. (2024a), with copyright CC BY 4.0. 38

5.1 Explained variance (R^2) of Spearman's rank correlation coefficient between LI ERA5 and LI ERA-Interim (2nd column), LI ERA5 and Aon's IF Euro WS model (3rd column), LI ERA5 and PERILS (4th column), and Aon's IF Euro WS model and PERILS (last column). The number of common storms per country is indicated in brackets. The table is reprinted from Table 5.1 in Moemken et al. (2024a), with copyright CC BY 4.0. 49

8.1 A Summary of insights from each result chapters and conclusions drawn from the overall findings. 92

A.1 List of top 20 storms from ERA5 for 1979-2019 for Core Europe. Information includes the storm name, storm rank, event period and value of Loss Index (LI). Shown are only the common 20 most extreme storms with ERA Interim. The table is reprinted from Table S2 in Moemken et al. (2024a), with copyright CC BY 4.0. 97

A.2 Same as Table A.1, but for ERA Interim. The table is reprinted from Table S3 in Moemken et al. (2024a), with copyright CC BY 4.0. 98

Acknowledgments

"Keep learning for life, because learning has no limits." — (BJ Habibie)

This inspiring quote from Indonesia's third president has guided my academic journey, reinforcing my belief that learning knows no bounds. As I conclude this chapter, I am thankful for the knowledge gained and the chance to contribute to my field.

First and foremost, I express my heartfelt gratitude to my supervisor, Prof. Joaquim Pinto, for the invaluable opportunity to pursue my PhD within the EDIPI project and for insightful discussions. I thank Prof. Andreas H. Fink for taking over the co-supervision of my PhD thesis. Moreover, I am extremely grateful to Dr. Julia Moemken for her co-supervision throughout my PhD and Dr. Alexandre Ramos, who joined as a co-supervisor midway through my PhD. Special thanks to Prof. Gabrielle Messouri, the EDIPI project leader, for facilitating my research travels across Europe.

I extend my sincere appreciation to Dr. Alexandro Georgiadis, my principal supervisor at Aon Impact Forecasting, for providing me with a remarkable opportunity to conduct research within an insurance company. I am also grateful to Dr. Aidan Brocklehurst, Lukas Braun, and their team for their support and warm welcome during my research stay at Aon Impact Forecasting in Prague. Furthermore, I thank Prof. Rodrigo Caballero and Aleksa Stankovic for their support during my secondment at MISU. My time in Stockholm was enriching, and I am thankful for their guidance and the opportunity to collaborate.

I also thank my colleagues from IMKTRO KIT: Dr. Ting-Chen Chen for preparing the cyclone track data, Dr. Jisesh Sethunadh for discussions on LI calculations, Federico Stainoh for his suggestions on statistical analysis methods in my first paper, Hendrik Feldmann for insights on EURO-CORDEX data in my second paper, and Ines Dillerup and Dr. Julia Moemken for reviewing the German version of the abstract of this thesis.

My deepest gratitude goes to my parents, Mama and Papa, whose unwavering support has been a constant source of strength throughout my PhD journey. To my beloved Mama in heaven, thank you for all the love and support you gave me during the ups and downs of my PhD journey while you were still here. I hope you're smiling proudly, just as you did before, knowing your daughter has fulfilled her dream and graduated with a PhD. I miss you every day, and I carry your strength and guidance with me always.